MICROFLUIDIC CANCER CELL ISOLATION SYSTEM USING MAGNETIC NANOPARTICLE HYBRIDS AND ADVANCED INTERDIGITATED ELECTRODE TECHNOLOGY

Dishant Mahendru

MSc (by research)

The University of York

Electronics

September 2010

ABSTRACT

For the past decade in the biomedical engineering industry, extensive research has been conducted in improving magnetic sensing technologies for cell isolation systems. These technologies, through the popular biomarkers, i.e. DNA, RNA, proteins, antibodies, have already been implemented in clinical diagnosis and/or prognosis [4]. An example of a successful commercial product is *Invitrogen's Dynabeads® Technology* [39].

Magnetic cell isolation technologies have been evolving slowly mainly due to the complexity of the cancers, the short number of successful cancer biomarkers, and the ethics of magnetic nanoparticles in in-vivo cancer therapy. However, in-vitro cancer therapy is becoming attractive.

This thesis explains the research and development of a microfluidic cancer cell isolation system, which together magnetically separates and destroys cancer cells through hyperthermia of MWNTs.

The full year was been spent on literature review, designing the microfluidic system, training fabrication and characterization techniques, fabricating component 1 through photolithography, and characterizing surface smoothness and height variation, through atomic force microscopy, and confirming size specifications and detecting electrode rigidity, through scanning electron microscopy. The project is currently being patented due to the uniqueness of the in-vitro cancer therapy concept.

AFM confirmed the electrode heights to be approximately 25 nm ± 3 nm, for all three samples, and random variations of surface electrode smoothness from ± 5-10 nm. This concluded how the uneven distribution of SiO_2 layer affected the height and smoothness of the electrodes.

SEM confirmed decent size specifications for mask design 2 and 5, as they followed the desired size specifications in the design process. However, mask design 4 ended up with electrodes, twice the width of the desired size, that could have been a result of diffraction or mask complexity which thereafter affected the evaporated material.

TABLE OF CONTENTS

LIST OF TABLES

LIST OF FIGURES

LIST OF ACRONYMS AND ABBREVIATIONS

AFM	Atomic Force Microscopy
BLM	Bilayer Lipid Membranes
CFM	Chemical Force Microscopy
CNT	Carbon NanoTubes
CVD	Chemical Vapour Deposition
CCD	Charge-Coupled Device
CECVD	Catalyst Enhanced Chemical Vapor Deposition
CMRI	Cellular Magnetic Resonance Imaging
CRT	Cathode Ray Tube
DI	DeIonized
DWNT	Double-Wall NanoTubes
EB	Electron Beam
EDAX	Energy Dispersive X-ray Analysis
EDC	1-Ethyl-3-[3-Dimethylaminopropyl]Carbodiimide hydrochloride
FIB	Focused Ion Beam
FESEM	Field Emission Scanning Electron Microscopy
LOAC	Lab On A Chip
MFM	Magnetic Force Microscopy
MRI	Magnetic Resonance Imaging
MWNT	Multi-Wall NanoTubes
NIR	Near InfraRed
NP	NanoParticle
PL	PhotoLuminescence
POC	Point Of Care
QD	Quantum Dot
R&D	Research and Development
SAM	Self-Assembled Mono- and multi-layers
SEM	Scanning Electron Microscopy
SPM	Scanning Probe Microscopy
SPNP	SuperParamagnetic NanoParticle
SPQD	SuperParamagnetic Quantum Dot
SQUID	Superconducting QUantum Interference Device
STM	Scanning Tunneling Microscopy
SWNT	Single-Wall NanoTubes
TEM	Transmission Electron Microscopy

XPS	X-ray Photoelectron Spectroscopy
XRD	X-Ray Diffraction

ACKNOWLEDGMENTS

I would like to give my thanks and innermost gratitude to a number of people who helped me with my project, by spending their time and effort from their usual activities.

Without their assistance, guidance, advice and help, I wouldn't be where I am with the project right now.

I enjoyed every second of this wonderful experience and would like to thank the following for sharing it with me:

Dr. Yongbing Xu
(Supervisor)

Dr. Iain Will
(Technical and Research Manager)

Mr. Malcolm Law
(Experimental Officer)

Mr. Jonathon Cremer
(Experimental Officer)

Mr. Xuefeung Hu
(Research Student)

Dr. Daxin Niu
(Research Student)

Ms. Wen Zhang
(Research Student)

Mr. Tsong Lu
(Research Student)

Ms. Ann Ding
(Research Student)

I also would like to thank my family and friends for their interest and support towards the project.

"Be the change you want to see in the world."
Mahatma Gandhi *(1869-1948)*

AUTHOURS DECLARATION

I declare that this thesis is solely my own work and has not previously been published or submitted for any other degree or award.

Dishant Mahendru

1. INTRODUCTION

1.1. FOCUS ON CARBON NANOTUBES IN CANCER RESEARCH

Sumio Iijima in 1992 first discovered CNTs through the careful examination of using a carbon cathode in the arc-discharge process for the fabrication of fullerenes. Since then CNTs have been classified as a revolutionary nanomaterial and have acquired the status as one of the futures building blocks.

For the past decade, research has been improving the synthesis of CNTs, and fully exploring the nanomaterials properties to its maximum potential. Discovering the CNTs unique electronic, mechanical and thermal properties, has led to a huge improvement in the semiconductor industry. The use of CNTs in the biomedical, bionanotechnology and bionanomedicine industry has been a recent interest which has sparked a whole new area of research.

A lot of research has been conducted on the applications of CNTs in diagnostics and therapeutics of dreadful diseases, i.e. cancer which has approximately *10 million cases every year* [5]. Researchers are hoping to replace current treatments of cancer: surgery, radiation and chemotherapy, with therapies focusing on directly targeting cancerous cells without affecting the normal ones. A lot of research, between the physical sciences and engineering, has been focusing on the complexity and functionality of combining popular biomarkers, i.e. DNA, RNA, proteins, antibodies with CNTs for cancer therapeutics, i.e. transportation systems, drug carriers, diagnostics and prognostics. A lot of papers have successfully published the potential uses of CNTs to treat several types of cancer with minimal or no toxic effects to normal cells.

However, these types of technologies are evolving slowly due to the complexity of cancers, the lack of successful cancer biomarkers, and the ethics of using CNTs in in-vivo cancer therapies, which currently pose problems of insolubility, inefficient distribution, lack of selectivity and toxicity. However, this is the reason why using this nanoparticles in in-vitro cancer therapy is becoming attractive.

1.2. FOCUS ON SUPERPARAMAGNETIC NANOPARTICLES IN CANCER RESESARCH

SPNP's consist of iron oxide particles/magnetite (Fe_3O_4) particles that are less than 15 nm in diameter. Currently being one of the more popular commercial superparamagnetic nanoparticles (SPNP's), these have been used as contrasting agents for MRI. Its main quality, paramagnetism, has been used in magnetic drug targeting for cancer therapeutics. Electromagnetic fields localize SPNP's to targeted sites, such as tumour cells and sources. As SPNP's are functionalized with a specified biomarker to form bio-composites, anti-cancer drugs can then delivered to the correct cancer cell or source. Research has also shown that when under the influence of an alternating field, these SPNP's experience Brownian relaxation. This is when heat is generated by the rotation of particles in the field. In order to reach high critical temperatures, which could destroy cells of micron size, concentrations of 0.01% to 0.1% iron oxide particles are needed for thermal ablation, which is very hard to achieve.

Another main quality of SPNP's is easy functionalization with other nanomaterials and nanoparticles, to create more effective hybrid technologies for specified applications.

1.3. FOCUS ON QUANTUM DOTS IN CANCER RESEARCH

Cellular imaging and tracking is an important clinical necessity used in deciding on appropriate cancer therapy. Current imaging techniques, i.e. ultrasound, x-ray, radionuclide imaging, MRI and computer tomography, have been used for cancer screening and detection of metastasis.

Nevertheless, there are two major limitations to current imaging techniques. Firstly, these are not sensitive enough to detect small numbers of malignant cells in both the primary or metastatic sites. Secondly, specific cancer cell surface markers, which are crucial for targeting in cancer therapeutics and diagnostics, cannot be detected using current imaging techniques. The solution to these limitations lies on improving current imaging techniques through the development of sensitive and bio-

specific imaging nanoparticles. The quantum dot (QD) provides the potential to fulfil these requirements for both in-vivo and in-vitro cancer imaging.

Semiconductor QD's are nanoparticles which have exhibit an extensive interest in bionanomedicine and bionanotechnology through their unique optical and electronic properties, especially two. Firstly, the QD has a very small tendency to photobleach. Secondly, its size distinguishes its own fluoresced wavelength. This makes QD's ideal for fluorescent probing applications to detect specific cancer biomarkers in-vivo and in-vitro cancer therapies from the cell to the whole body.

The most recent development in QD technology consists of QD's, encapsulated in amphiphilic polymers that are linked to tumour-targeting ligands and drug delivery vesicles for targeting, imaging and treating of tumour cells. More research has focused on exploring the massive multiplexing capabilities of the QD's for the simultaneous detection of multiple cancer biomarkers in cancer-based assays. Advancement in QD technology has shown great promise in cancer therapeutics, especially when forming composites with CNTs and SPNP's.

1.4. FOCUS ON MAGNETIC CELL ISOLATION SYSTEMS

For a long time, magnetism has been a fascinating driving force for isolation systems that separate non-magnetic components with magnetic components in a mixture. This has already been widely used when it comes to removing non-ferromagnetic impurities to enrich low grade iron ore.

However, it was not until the 1970's when the idea of using similar magnetic separation for cell isolation came to place. Since then, research has been conducted to develop new magnetic nanoparticles that would be useful for this purpose. Magnetic separation has its many advantages. It allows the targeted cells to directly be separated from the solution that it is currently in, whether it may be blood, bone marrow, water, food, soil etc. It is simple, fast, and static magnetic field does not interfere with the movement of ions in aqueous solutions. This makes it the more suitable technology compared to its non magnetic competitors, which require costly and extensive instrumentation. The gentle procedure of magnetic separation allows the quick handling of active cells in an unfriendly environment, thus simplifying the procedure and ending up with pure, unaltered living cells at larger quantities. As this separation process produces a higher sample throughput at a cheaper price, companies took this research to their advantages and produced commercial technologies for magnetic cell separation.

Magnetic cell isolation technologies: *Dynabeads® Technology* [40] sold by Invitrogen, *PlusCellect™ Technology* [41] sold by R&D Systems, *MACS® Technology* [42] by Miltenyi Biotec, and *EasySep® Technology* [43] by Stemcell Technologies, are a few of many technologies using magnetic beads or nanoparticles, with attached antibodies, for cell separation for downstream assays. A lot of these companies, especially Miltenyi Biotec, are focusing on exploiting these technologies for in-vivo cancer cell separation. The main question that is being asked is if this magnetic separation technology's applications can extend from cancer cell assays to cancer therapeutics.

1.5. PROJECT AIMS/SPECIFICATIONS

A lot of research has been conducted in using the combination of nanoparticles and electrodes technology for bio-sensing purposes. However, there has not been a lot of research in integrating this biosensing unit with a microfluidic chip, to perform a cell separation and isolation process. The nanoparticle hybrids would attach onto the specified cancer cells, attract them onto the set of advanced electrodes through AC dielectrophoresis, isolating the cancerous cells from the normal ones. If this setup was encased into a microfluidic chip, controlling both the in-and outtake of volumes and pressures of the two solutions would be more effective and efficient. These solutions would consist of an aqueous dispersion of nanoparticle hybrids and a blood solution coming from an area, in the body, of highly populated cancerous cells or the tumour itself.

As this operation is occurring in a microfluidic chip outside the body, it would then be classified as an in-vitro therapy and would surpass the main ethical barriers of using nanoparticles in in-vivo therapy. Once the cancerous cells are magnetically attracted, the normal cells can easily get flushed back into the body through fluidics. Thereafter, the caught cancer cells are destroyed through hyperthermia from the MWNTs and thereafter dispose them into a waste solution.

The main aims/specifications for the project are:

Component 1: Micro-and Nanoelectrode Technology

1. Design 5 different micro and nanoelectrode masks
2. Fabricate the microelectrode masks through photolithography
3. Fabricate the nanoelectrode masks through e-beam lithography
4. Evaporate permealloy metal

5. Perform microscopy's to analyze surface smoothness and obtain close-up images
6. Test that there is no conductivity between both electrodes

Component 2: MWNT – SPQD – Antibody Nanoparticle Hybrid

1. Retrieve or fabricate SPQD's from a 3rd party supplier
2. Retrieve MWNTs from a 3rd party supplier
3. Retrieve Antibodies for specified cancer
4. Attach Antibodies onto SPQD's
5. Attach SPQD-Antibody bio-composite onto MWNT
6. Excite SPQD's through UV light
7. Perform Photoluminescence analysis of Antibody-SPQD-MWNT
8. Perform microscopy's to analyze and obtain close-up images
9. Test Antibody-SPQD-MWNT attachment onto cancerous cell
10. Perform microscopy's to analyze and obtain close-up images
11. Perform Photoluminescence analysis of Cancer Cell-Antibody-SPQD-MWNT

Component 3: Microfluidic Operation Chip

1. Design chamber must be included for 1cm by 1cm sample for component 1
2. Design entrance and exit inlets for cleansing normal (non-cancerous) cells
3. Design entrance and exit inlets for cleansing nanoparticle hybrid and cancer cell debris
4. Design inlets for cancer cell solution into chamber
5. Design inlets for nanoparticle hybrid aqueous solution into chamber
6. Calculate pressures, volumes and thickness
7. Design valves to block all inlets
8. Test that all inlets and valves are functional
9. Test that no residue is left before reuse

2. PROJECT PLAN OF ACTION

2.1. BEng PROJECT

The BEng project was completed in 2009 and aided in the completion of a Bachelor of Engineering in Electronic Engineering (BEng) from the Department of Electronics, The University of York. Further research was required and advised to understand the projects maximum potential. A degree in Master of Science in Electronic Engineering (by research) would be awarded after handing in a thesis. For further information on the overview, results, conclusion and future work analysis on the BEng project, please see APPENDIX 12.1.

2.2. CHANGE OF DIRECTION FROM BIO-SENSING TO ISOLATION OF CANCER CELLS

A couple meetings with Dr. Peter O'Toole, Head of Imaging and Cytometry Laboratory in the Biology Department at The University of York, and his colleagues were organized. They suggested that the direction of the project should change from bio-sensing to cell isolation. The main reason was that a lot of research, on improvement of cancer-based biosensors, has been conducted and the market for introducing a new biosensor would be too competitive.

However, through Dr. O'Toole's expertise and connections in the biomedical field, he suggested that the technology could be a new type of magnetic cell isolation technology and can easily be introduced in this very popular growing market.

The top four commercial magnetic cell isolation technologies: Dynabeads® Technology sold by Invitrogen, PlusCellect™ Technology sold by R&D Systems, MACS® Technology by Miltenyi Biotec, and EasySep® Technology by Stemcell Technologies, show the value of this technology in a booming market for technologies,

that use magnetic beads or nanoparticles, with attached antibodies, in cell separation for downstream assays. However, there are no commercial products available which use nanotubes, for this purpose, and not enough research has been conducted to conclude that magnetic particles, attached to nanotubes, would be a better alternative. It is realized that changing the direction of the project from bio-sensing to cell isolation would be very advantageous and have a better chance of entering the market if this technology has is better than that its competitors.

However, to extend the applications for the technology, it would be better to utilize some of the nanotubes explosive properties for in-vitro cancer therapeutics. Integrating advanced electrodes technology and hybrid nanoparticles into a microfluidic operation chip, for cancer cell detection, separation and destruction in an in-vitro environment.

2.3. CHANGING PROJECT FROM MSc to PhD to MSc

After finishing the design plans for the project it was concluded, by my supervisors from electronics and out contacts at Biology, that the aims and specifications of the project could not be aimed after a year and this project would be suitable for a PhD. A transfer to the PhD course was made with the notion that funding maybe available.

This was the only main concern as I needed funding for the project and for covering maintenance costs for the remaining two years. As the project has huge commercial potential, electronics and biology, were working together to come up with funding for the next two years. Money was donated by the electronics department for the second year and however biology was only able to donate money if I achieved half of my goals and specifications by the end of first year, which was not possible. Therefore a transfer was made back to the MSc programme where a thesis was written to earn a degree in MSc Electronic Engineering (by research).

2.4. LITERATURE REVIEW

To fully design the microfluidic cancer cell detection, separation and destruction system using electrodes and magnetic MWNT hybrid technology, a good grasp of literature needs to be conducted to develop the knowledge to design, fabricate and test the technology. Both journals and books can be obtained from the Internet or from The University of York library for the research of the following topics: CNTs, QD's, SPNP's, SPQD's, CNT Aqueous Solutions, CNT Fragmentation, Hyperthermia of CNTs, Hazards of CNTs, Interdigitated Electrodes Technology, Cell Isolation Systems,

Microfluidic Systems, Biosensor Basics, Nanowire-based Biosensors, Magnetic-based Biosensors, Immunosensors, Hybrid Nanoparticle Technology, AC Dielectrophoresis, Functionalization Techniques of CNTs and NP's, Functionalization Techniques of NP's and Antibodies/Biomarkers.

2.5. PROJECT METHODOLOGY

Once the necessary literature for the project has been researched, the system needs to be designed, fabricated and tested, to successfully fulfil the project aims and specifications. The Department of Electronics at The University of York will provide the facilities and most of the materials that is needed for the fabrication of the microfluidic cell separation system.

2.5.1. DESIGN

2.5.1.1. COMPONENT 1: MICRO-AND NANOELECTRODE TECHNOLOGY

During the design process of component 1 several design features need to be decided. The number and thickness of layers as well as materials for each layer needs to be classified. A decision needs to be made on whether to use silicon, glass or quartz for substrate material. Insulating techniques for the electrodes and substrate needs to be decided to completely cut off current between the substrate and electrodes, which was a major issue in the BEng project listed in the *BEng Project Results* section in APPENDIX 12.1. Design five new sets of interdigitated electrodes which will strongly magnetically attract component 2 into forming bridges between the electrodes. Make sure that the gaps between electrodes are smaller then normal lengths of commercial CNTs, which are 10-50 μm in length. Discuss the designs with necessary research staff and thereafter, draw up final design parameters and details of the component, ready for fabrication.

2.5.1.2. COMPONENT 2: MWNT-SPQD-ANTIBODY NANOPARTICLE HYBRID

During the design process of component 2 several design features need to be decided. Locate the cheapest CNT supplier, decide on the type of CNT (MWNT, SWNT, and DWNT) and the length of the CNT, making sure that the length is significantly larger than the electrode gaps to allow electrical conductivity.

Decide on the materials, the size, shape and design of the SPQD. Begin thinking whether or not to fabricate own SPQD's or buy from a 3rd party supplier. Decide on specified Antibody biomarker for cancer cell attachment and the functionalization attachment techniques between SPQD and Antibody. Review functionalization

attachment techniques between CNT and SPQD-Antibody bio-composite. Discuss design with necessary research staff, representatives from Biology and Chemistry Departments. Draw up final design parameters and details of the component, ready for fabrication

2.5.1.3. COMPONENT 3: MICROFLUIDIC OPERATION CHIP

During the design process of component 3 several design features need to be decided. Decide on size and number of inlets for the operation chip, the specific valves that are needed to block inlets and whether or not these valves are automatic or manual. Decide on the thickness of the microfluidic chip and flow techniques. Conclude on fabrication and characterization techniques for microfluidic chip development, materials, and pricing with Dr. Xu and Dr. Will. Review final design with necessary research staff, representatives from Biology and Chemistry Departments. Draw up final design parameters and details of the component, ready for fabrication.

2.5.2. PREPARATION AND FABRICATION

2.5.2.1. COMPONENT 1: MICRO-AND NANOELECTRODE TECHNOLOGY

Several tasks needed to be completed before the preparation and fabrication of component 1. Fabrication techniques, to print 5 advanced electrode designs onto substrate, had to be decided and finalized along with characterization techniques for analysis. Equipment and materials was reviewed with necessary research staff. Training sessions were given by clean room technicians for necessary characterization and fabrication techniques. Equipment was booked, materials were obtained to fabricate component 1.

2.5.2.2. COMPONENT 2: MWNT-SPQD-ANTIBODY NANOPARTICLE HYBRID

Several tasks had to be completed before the preparation and fabrication of component 2. Fabrication and characterization techniques for SPQD, SPQD and Antibody attachment, and SPQD-Antibody bioconjugate attachment onto CNT would have to be finalized. Equipment and materials with necessary research staff would need to be discussed. Relevant training sessions with clean room technicians for necessary techniques had to be organized. Equipment had to be booked and materials would have to be obtained in order to fabricate component 2.

2.5.2.3. MICROFLUIDIC OPERATION CHIP

Several tasks had to be completed before the preparation and fabrication of component 3. Fabrication and characterization techniques for the microfluidic operation chip would have to be finalized. Necessary equipment and materials with necessary research staff would need to be reviewed and finalized. Training sessions with necessary technicians would need to be organized. Equipment had to be booked and materials would have to be obtained in order to fabricate component 3.

2.5.3. TESTING

Testing strategies and equipment had to be discussed, at a later date, with necessary research staff, representatives from Biology and Chemistry Department. Once discussed and finalized, training sessions will need to go through training sessions with technicians on necessary testing techniques. Individual testing methods had to be researched and set up for each component as well as full isolation process

2.6. MANAGEMENT

In order to manage a very ambitious project with restricted time and monetary limits, several constant meetings were organized and several tools were initialized. A simple log was maintained for the tasks that were completed at a weekly basis

Constant meetings with Dr. Yongbing Xu, Mr. Iain Will, Mr. Malcolm Law, and Mr. Jonathon Cremer, were setup throughout the project period, to maintain the progress of the project and reach the necessary deadlines.

2.6.1. MEETINGS WITH ELECTRONIC DEPARTMENT

2.6.1.1. DR. YONGBING XU

Meetings with Dr. Yongbing Xu included management and supervision of the project, discussion of issues and possible solutions, reviewing research techniques and decision making, discussion of purchasing materials and possible unavailable equipment, consultation on available machinery for fabrication and characterization as well as experts for training, deciding on future plans of the project, consultation on research publications, and consultation on patent application.

2.6.1.2. DR. IAIN WILL

Meetings with Dr. Iain Will included discussion on minimizing project aims into achievable final goals in restricted monetary and time limits, discussion on details of project design, operation, applications, testing strategies, and equipment. Guidance was

provided throughout fabrication, testing, purchasing and providing the materials and equipment. Consultation was given on research publications and on patent application.

2.6.1.3. MR. MALCOLM LAW & MR. JONATHON CREMER

Meetings with clean room technicians included training and supervision of necessary equipment, and guidance and supervision on fabrication and characterization techniques.

2.6.1.4. PHYSICAL LAYER RESEARCH: SPINTRONICS GROUP

Meetings with the Spintronics research group included consultancy and guidance with lithography and microscopy methods, size and shape parameters for component 1 and 2, usage of 3D CAD software, and discussion of research knowledge linked to component 1 and 2.

2.6.2. MEETINGS WITH BIOLOGY DEPARTMENT

2.6.2.1. DR. PETER O'TOOLE

Meetings with Peter O'Toole include consultation on commercially available cell isolations techniques, current research on improved cell isolations techniques, improving the design of our cell isolation technique, cancer-based biomarkers and functionalization methods to nanoparticles, advantages and disadvantages of using CNT and SPQD nanoparticles for cancer based isolation techniques, commercial opportunities for project, patent application and provided connections to biomedical companies on assessing the value of the project for further funding opportunities.

2.6.3. MEETINGS WITH JEOL NANOCENTRE

2.6.3.1 MR. IAIN WRIGHT

Meetings with Mr. Iain Wright at the Jeol Nanocentre included training for the following techniques: E-Beam Lithography, Scanning Electron Microscopy, Atomic Force Microscopy, Field Emission Scanning Electron Microscope, Focused Ion Beam and consultation on improvement of the above mentioned techniques.

2.6.4. PURCHASING OF MATERIALS AND EQUIPMENT

2.6.4.1. MULTI-WALLED NANOTUBES

The multi-walled nanotubes were purchased from Thomas Swan & Co Ltd, a UK supplier of CNTs situated in Durham, on May 2009. They sold MWNTs Wetcake in Water for £50 per 1 gram of CNTs with a 5 gram purchasing limit. Dr. Yongbing Xu felt that £250 was a reasonable price and that the leftover CNTs can be used for further research within the group, specifically for the same project during the next academic

year. Due to time constraints and them being the cheapest UK suppliers, immediate orders were made and received in a few days time.

2.6.4.2. SUPERPARAMAGNETIC QUANTUM DOTS

These particles are unfortunately commercially unavailable. A lot of research has already been conducted regarding the particles fabrication and characterization methods. The most successful fabrication method is very advanced, and neither Physics nor Electronics departments have the facilities to fabricate these particles on their own. And due to time constraints, it would be hard to get the Chemistry department involved. However Dr. Xu has an academic friend in China who specializes in nanoparticle hybrid technology and could possible be fabricating someone. No news has been heard regarding obtaining or purchasing these particles from this source. However, if the project was to be researched for another 2 years at a PhD level, then the time would be there to fabricate these particles ourselves.

2.6.4.3. QUANTUM DOTS & MAGNETIC NANOPARTICLES

In case it was hard to either obtain or purchase SPQD's from a 3rd party supplier, the backup plan would be to purchase individual quantum dot and superparamagnetic particles and conjugate those into a hybrid together and attach the cancer biomarker onto them straight afterwards. Even though this procedure is less complex compared to fabricating the SPQD's, more time and money is required to individually conjugate three particles together to for a hybrid.

The quantum dot and magnetic nanoparticles can be purchased from Invitrogen.com. The *Dynabeads® for Human Cell Isolation* [44] product can be used for the magnetic nanoparticle component, however will cost around *800 USD for 5 ml of the product*. The *Qdot® Nanocrystals* [45] product can be used for the quantum dot component, however will cost *510 USD for 200 µl of the product.* However, due to time constraints to convince purchasing these products for over 1000 USD will be problematic.

2.6.4.4. INCUBATION SYSTEM

After there being several complaints and issues about using nanoparticles in the clean room, researchers were halted in using nanoparticles. The clean room went through a review process regarding whether or not the nanoparticles will be filtered through the current microfilters. After a several months review, the microfilters have been replaced with nanofilters. During the review, it was discussed with Dr. Yongbing Xu that an

application be sent to the university funds for £10,000 grant for an incubation centre. This incubation centre will either be located in the clean room or another facility and will host experiments that will include nanoparticles. The incubation centre will have a constant nanoparticle filtration that will filter out these nanoparticles.

2.6.4.5. OPTICAL MICROSCOPE

The project procedure requires the excitation of the quantum dot material and thereafter the photo detection and photoluminescence analysis of the material. It was suggested that an optical microscope be researched that could perform all these processes in one device. The XDY-1 Inverted Fluorescence Microscope [46] by GX Optical seemed to provide those requirements, costing around £10,000 pounds. But, after several meetings with the Biology department, who showed interest in the project, we were given permission to use their Scanning Electron Microscope (JASM-6200 Scanning Electron Microscope ClairScope™ [47]) after suitable training.

2.6.4.6. PHOTOLITHOGRAPHY MASKS

The five advanced microelectrode designs and nanoelectrode contact pads were printed from a third party supplier, micro lithography services [48]. They provide laser plotting at 40,640 dpi achieving down to 10 micron lines and features onto high resolution film. The charge for an A4 size printed film was £73 (including postage and packaging). Two A4 size sheets were purchased resulting on a told expenditure of £146.

3. LITERATURE REVIEW

3.1. CARBON NANOTUBES

3.1.1 INTRODUCTION

From individuals to multi-national corporations, CNTs has become a massive research topic that possibly may have a huge impact in both electrode, for transmitting electrical signals, and sensors, for detecting concentration levels of chemicals and biological molecules, technologies. The ultimate possibilities of functionalizing CNTs to change intrinsic properties are the reason for why they are heavily researched for sensor technology.

For example, when using CNTs on electrodes for electrochemical analysis of an analyte, proper linking strategies with the biological molecules, such as enzymes, proteins, DNA/PNA/RNA, antibodies, receptors, dendrimers and aptamers, need to be made [4]. It is critical that the functionalization and immobilization methods of the desired biological materials, on the CNTs, are appropriate. The functional groups, on the CNTs, will create defects and alter the intrinsic electrical properties of the CNT.

3.1.2 GENERAL DEFINITION OF CNT

CNTs are described with the characteristics listed below:

- Graphene sheet(s) rolled up into a nanoscale tube
- Are allotropes of carbon (Member of the Fullerene structural family)
- Diameter range : 1.4 nm to 60 nm
- Length range : microns to above one centimetre
- Nanostructure can have a length-to-diameter ratio greater than 10,000,000 and as high as 40,000,000

- Exhibit extraordinary strength, distinctive electrical properties, efficient conductors of heat
- A buckyball structure is usually capped, at least, in one end of the cylindrical CNTs.
- Chemical bonding consist of entirely sp2 bond, similar to graphite
- Bonding structure is stronger than the sp3 bonds of diamond, which exhibits its unique strength
- CNTs naturally are held together with Van der Waals forces
- Helicity of the shell classifies CNTs into metallic or semiconducting types.

3.1.3 TYPES OF CNTS

3.1.3.1 SINGLE-WALLED NANOTUBE (SWNT)

SWNTs are described with the characteristics listed below:

- Single Graphene sheet rolled together
- Diameter range: Up to 1 nanometre
- Length Range: Thousands of times longer than diameter
- Structure: One-atom-thick graphene, layer of graphite, wrapped around a flawless cylinder.
- SWNT are the best structure to miniaturize electronics to a electrochemical scale.

3.1.3.2 MULTI-WALLED NANOTUBE (MWNT)

MWNTs are described with the characteristics listed below:

- Multiple graphene sheets rolled together
- Structure (Basic): Multiple layers of graphene rolled together to create a cylindrical shape as shown in Fig. 1.
- Structure (Russian Doll Model): Multiple layers of graphene are arranged in concentric cylinders.
- Structure (Parchment Model): Single sheet of graphene is rolled in around itself.
- Resistance to chemical improves when using multiple sheets of graphene instead of SWNT. NOTE: Very useful for CNT functionalization, when chemical reactions take place at the surface to add or alter the CNTs properties.

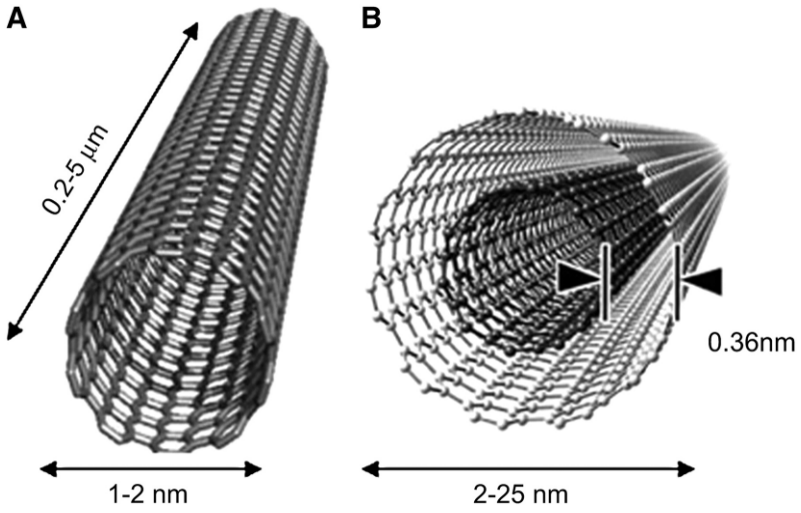

Fig. 1. *Schematic differentiating size between SWNT(left) and MWNT (right)* [49]

3.1.3.3 FULLERITE

Fullerite's are described with the characteristics listed below:

- Solid-state versions of fullerenes
- Highly incompressible CNTs
- Polymerized Single-Walled Nanotubes (P-SWNT) are in the fullerite class and share the same hardness characteristic as diamond.
- When P-SWNTs intertwine, it is hard to cut this fullerite because it does not have the same crystal lattice as a diamond that makes it easier to cut neatly.

3.1.4 PROPERTIES OF CNTS

3.1.4.1 KINETIC

MWNTs show an impressive telescopic property, when you have multiple concentric CNTs placed perfectly into one another. The inner CNT may slide out of its outer CNT, without any friction, creating perfect atomic linear or rotational behaviour.

3.1.4.2 THERMAL

It is a general consensus that all types of CNTs possess ballistic conduction, excellent thermal conductivity. CNTs however could transmit up to 6000 $W \bullet m^{-1} \bullet K^{-1}$ at room temperature. Compared to everyday metals, such as copper which only transmits 385 $W \bullet m^{-1} \bullet K^{-1}$, this is a huge improvement. 2800 ^{o}C is the maximum temperature to keep a CNT stable in a vacuum environment.

CNTs can absorb near infrared (NIR) light to generate heat. For example SWNTs can go up to temperatures over 700 ^{o}C after 2 minutes of continuous irradiation, leading to boiling the solution that they are in.

3.1.4.3 STRENGTH

CNTs are the strongest and most robust materials on earth, when it comes to tensile strength and elastic modulus. The sp^2 bonds, which are formed covalently between the carbon atoms, are the main reason for the CNTs' excessive strength. At the moment, MWNT have been tested to have a tensile strength of 63 gigapascals. This means that a CNT cable with a cross-sectional area of $1mm^2$, can tolerate a weight of 6300 kg.

When applying excessive tensile weight onto the CNT, it will begin to go through permanent deformation. The plastic deformation usually begins at 5% however can continue to go upwards to further test the maximum strain of the CNT till the point of fracture.

3.1.4.4 ELECTRICAL

The unique electronic structure and symmetry of the graphene, allows us to flexibly alter its electrical properties. Usually CNTs are moderate semiconductors, however alterations on their electronic graphene structure allows us to increase its conductivity. Theoretically, CNTs electrical current density is 1000 times greater than other conventional metals, such as copper and silver.

3.1.4.5 EFFECT OF DEFECTS OF CNTS

The defects of CNTs are listed below:

1. Stone Wales Defect: A pentagon and heptagon pair is created under the rearrangement of the bonds. This defect, even though small, will reduce the tensile strength immensely because of how the CNT structure is microscopic. And if there is a single defect on the chain, then it will affect the tensile strength of the entire structure.
2. The electrical properties of the CNT are affected by defects. Usually there will be reduced conductivity in the defective region.
3. The thermal properties of CNT are deeply affected by defects. Defects lead to the scattering of phonons which leads to the reduction of a clear free path, reducing conductivity.

3.1.5 SYNTHESIS

3.1.5.1 ARC DISCHARGE

Arc discharge is when several gasses execute electrical conductions, which is categorized by low potential drop and high current density. Humphry Davy in 1808 discovered the electric arc, when he linked a piece of carbon to both sides of a electric battery, touched both pieces of carbon with each other, and started drawing them

slightly apart. This resulted with ionized air or plasma, in steam-form, with a temperature of 6000 ^{o}C. After further research, the voltage drop of an average arc is 100V with a current drain of 10 A. As the arc has negative resistance, the current increases making the voltage drop decrease. The high temperature gas, begins to rise, however still remains in contact with the electrodes, feeding the current and thereby creating an arc-like shape with upward-moving curve.

Once CNTs were experimented with in 1991, to produce fullerness with a current of 100 amps, arc discharge was present with the carbon particles from graphite electrodes. When CNTs were made in 1992, arc discharge synthesis was used again, and the carbon located in the negative electrode successfully sublimates due to the high temperatures caused by the discharge. Since then it is the popular synthesis technique for CNTs.

3.1.5.2 LASER ABLATION

Laser Ablation is the process of when a pulsed laser vaporizes a source of graphite. This process needs to occur in a high temperature controlled reactor, where a static gas is being fed into the chamber at the same time. As the vaporized carbon condenses, CNTs will be developed in the cooler areas of the chamber.

This process was invented by Richard Smalley at Rice University, when he was experimenting with different metals to see whether or not he could produce different metal molecules, with the use of a laser. When he found out about the CNT discovery, he continued his experiments with graphite to create MWNTs.

This method of synthesis is primarily used to create SWNTs with a controllable diameter. However it is more expensive than the other two syntheses': Arc Discharge and Chemical Vapour Deposition.

3.1.5.3 CHEMICAL VAPOUR DEPOSITION

For the synthesis process, a substrate, with a layer of metal catalyst particles, is prepared. Usually the metal catalyst is nickel, cobalt, iron, or a combination. The sizes of the metallic NP's also determine the diameter of the final grown CNT. To control it, you either pattern the deposition on the metal or by plasma etching of the metal layer.

The substrate is now heated to approximately 700 ^{o}C. To start-up the growth of the CNTs, two gases are injected into a reactor: a process gas (e.g. Ammonia, nitrogen, hydrogen, etc.) and gas with carbon (e.g. acetylene, ethylene, ethanol, methane, etc.)

The CNTs begin growing on the thin layer of metal catalyst. The carbon is detached from the gas particle, attached to the thin metal layer, to form a CNT.

CVD is the more popular choice for commercial production of CNT. It is cheaper and possesses several other advantages compared to the previous two syntheses. Unlike the previous two methods, CVD method grows the CNTs already on the substrate, and does not need to collect the CNTs, like you do in the other techniques. Another advantage is that areas of growth are easily controllable with careful deposition of the catalyst. Plus, CVD is the only synthesis that has made it possible to create vertically aligned CNTs.

3.2. QUANTUM DOTS

3.2.1. INTRODUCTION

QD's are nanocrystal that have a diameter, which ranges from 10 nm as shown in Fig. 2, and are made of semiconductors. The most common would be cadmium selenide capped by zinc sulphide (CdSe/ZnS). Quantum dots are made of 10-50 atoms and they hold electron-hole pairs to a discrete quantified energy level.

When irradiated with ultraviolet light, they fluoresce in different neon colours depending on their size. This determines the energy levels of the QD's. Large particles emit red light whilst the smaller particles emit light in the blue range.

When first developed 20 years ago, their biomedical applications and potential were unknown. For decades, research have made QD's into useful probes for high resolution molecular imaging of biological cells and components as well as tracking the movement and activities of a cell inside a body.

QD's can be attached to proteins, receptors, antibodies and enzymes to molecules. These bio-composites can be followed once the molecule reacts with a cell inside the body. Regarding cancer, they can be linked to antibodies for the detection of cancer markers. The can be used to mark tumour cells to track metastasis to specific organs and tissues [1].

Due to QD's unique spectroscopic properties, they possess several advantages [1, 33] over organic fluorophores. These are:

- Narrow emission peaks will facilitate spectral multiplexed analysis.
- Broad excitation spectrum will allow the excitation of multiple emission-coloured QD's with a single excitation wavelength.
- Their exquisite photostability will enable longer observation times.

- High emission quantum yield will improve the signal to noise ratio in most measurements

Even though QD's do possess many advantages there are several disadvantages [1, 33] in their design that needsto be improved. These are:

- To improve methods synthesizing QD's with high stability in aqueous solutions or biological fluids
- Improve capping of QD's to avoid aggregation
- Develop and optimize the conditions to understand stable and active QD bioconjugates.

The greatest disadvantage of QD's is its basis is of semiconductor material which is a poisonous heavy metal. This is a huge obstacle in clinical applications especially for treatment purposes. Therefore to perfect QD's researchers are actively trying to develop different ways to coat them to block them from causing toxicity.

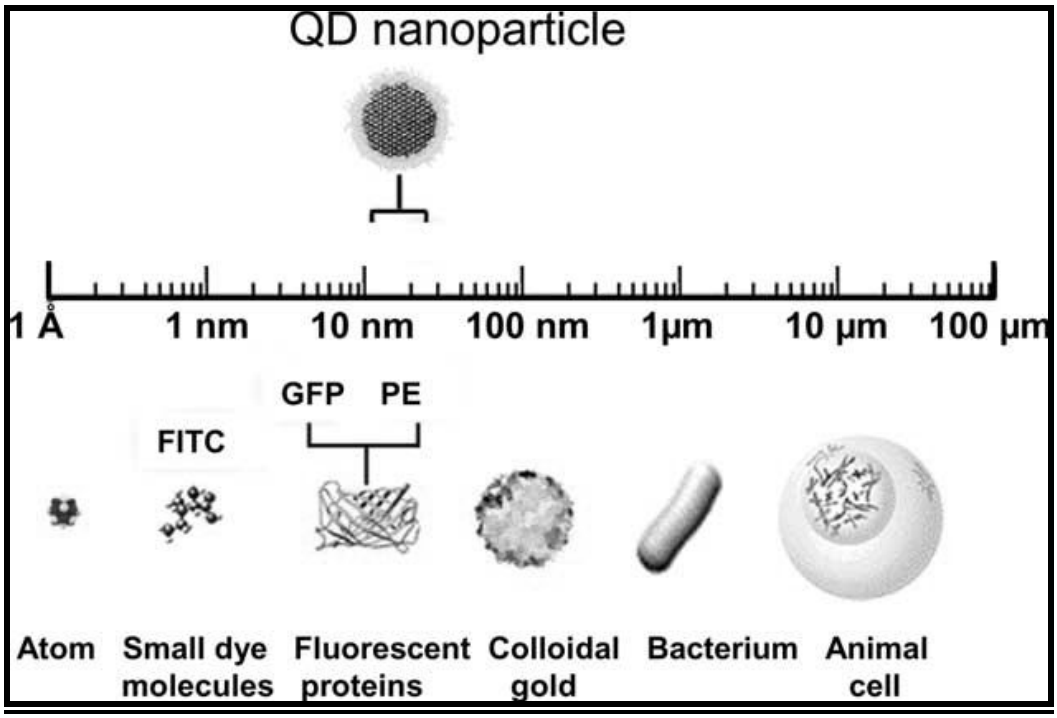

Fig. 2. *The size of a quantum dot (QD) compared to other particles* [58]

3.2.2. QUANTUM DOT DETECTION SCHEMES

3.2.2.1 CELLULAR IMAGING

The use of cellular imaging for QD detection has attracted great interest and has now reached the stage of commercialization. Various extensive researches have generated and studied the use of bio-functionalized QD's that have different sizes to label cells. This allows discrete visualization of cells under continuous lighting to achieve multicolour imaging of cells.

Research has used QD's for in vivo biological imaging. *Niesz et al* [17] have shown that cancer can be targeted and viewed by using CdSe@ZnS core—shell QD's which give red emission. Once attached to tumour targeting antibodies, the fluorescent emission wavelengths could then be detectable even if blood and tissue slightly absorbed the transmission of wavelengths. Through their studies, they found out that QD's should emit at 700—900nm in the NIR.

3.2.2.2. CELLULAR TRACKING

Once attached to cells or molecules, QD's are excellent particles for cell tracking to study cell division, metastasis, or the movement of particle groups. For example in Fig. 3, we can see the QD Detection of Luciferase on nude mice through bioluminescence imaging of QD-labelled cells, which are acquired with a wavelength filter (575—650 nm).

Due to their advantages of high stability and multicolour emission, QD's can be used to attach and act as unique coloured markers for cancer cells. This can then be used for cell purification or isolation of cells techniques, which will allow you to detect concentrations of cells through their colours. In cancer research, they are used to track metastasis and used to detect concentrations of cancer cells in specific areas in the body.

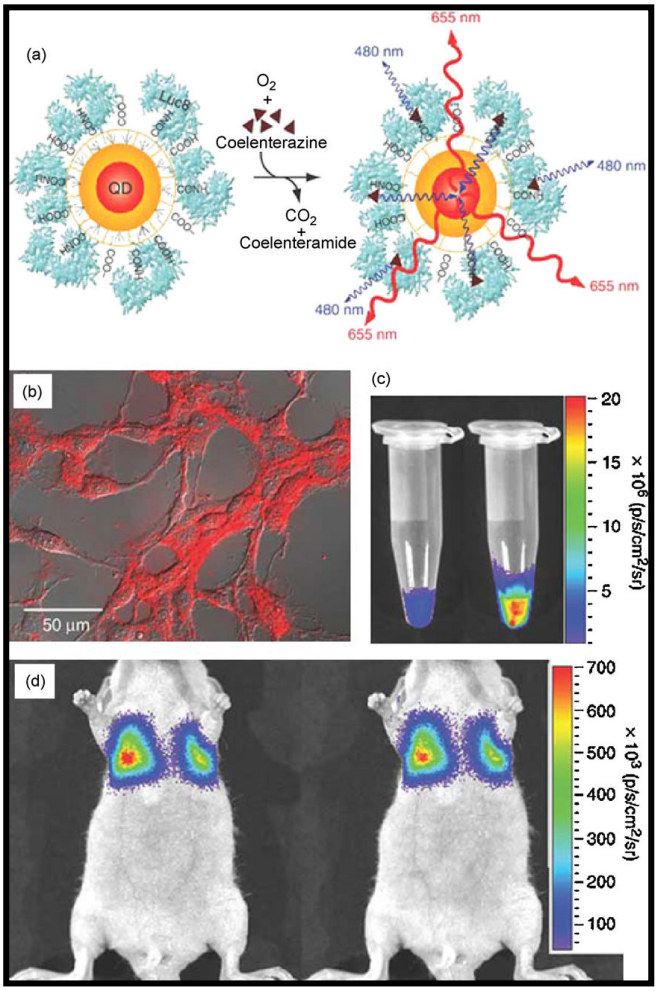

Fig. 3.
Diagram of QD Detection of Luciferase on nude mice

(a)QD is attached to luciferase (Luc8), which is be detected.

(b)Fluorescence imaging of QD conjugates

(c)Bioluminescence images of QD-labelled cells acquired with a wavelength filter (575—650 nm) (left) and without a filter (right)

(d)Bioluminescence images of QD-labelled cells inside nude mice, for area detection. [3]

3.2.2.3. MAGNETIC RESONANCE IMAGING

MRI is a technique used for medical applications to produce detailed images of the human body for diagnostics. Through normal medical practice, MRI is a non-invasive procedure which uses non-ionizing radiation in the radio frequency range through strong magnetic fields, to distinguish diseased from normal tissue.

Current research and development (R&D) of molecular and cellular imaging have used magnetic nanoparticle-QD hybrids to visualize the disease-specific biomarkers at the molecular and cellular levels. Successful experiment generated detection systems such as cellular MRI (CMRI), which can track the movement of specifically labelled cells through the hybrids, within organs and tissues.

3.3. SUPERPARAMAGNETIC PARTICLES

Superparamagnetic NP's consist of iron oxide particles or magnetite (Fe_3O_4) particles that are less than 10 nm in diameter. Being present for many years, they have been used as contrasting agents for MRI. Their qualities have been used in magnetic drug

targeting, where they use of magnetic fields to localize magnetic NP's to targeted sites, such as tumour cells and sources.

These NP's need to be functionalized to be part of the biocomposites. Iron oxide NP's can be made hydrophobic by being coated with liposomes, making magnetoliposomes.

Magnetic NP's can also be remotely activated using electromagnetic fields, and have shown great promise in thermally treating cancers.

When under the influence of an alternating field, these NP's experience Brownian relaxation, in which heat is generated by the rotation of particles in the field. However to reach high critical temperatures, concentrations of 0.01% to 0.1% iron oxide are need for thermal ablation, which are hard to achieve.

3.4. SUPERPARAMAGNETIC QUANTUM DOTS

There are several techniques which allow the multifunctionality of NP's. These include intracellular manipulation, encapsulation, covalent conjunction or non covalent absorption of various molecules. Multifunctionality between NP's allows a new and improved method of recognizing and locating the desired biological cell for further action. We can see in Fig. 4, the different multifunctionality methods and systems which can be created through combining specific particles together to form hybrids. In case of cancer, these methods would start from locating the cancer cell or the tumour, deliver the anticancer drug to kill the cancer cell and then monitor the reaction through imaging technology.

Once understanding the strengths of each particle and then successfully generating multifunctionality, these systems could help treat and possible cure many occurring diseases. The research lies on the strengths of each individual particle and what forms of multifunctional techniques could provide a strong synergy between them. The diagram below gives an example of a possible multifunctionality scheme.

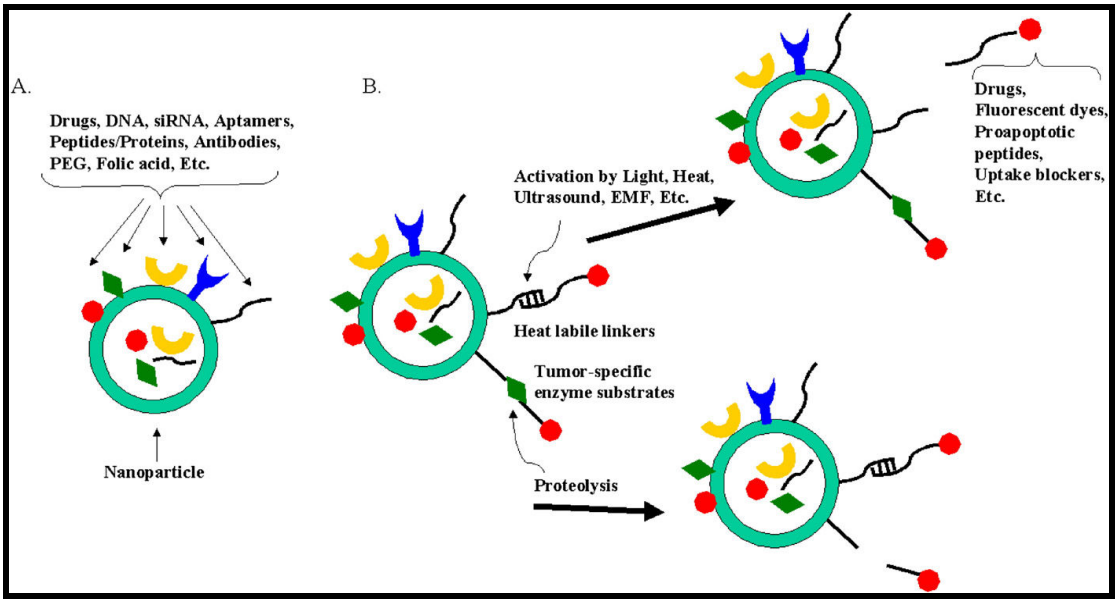

Fig. 4. *Multifunctionality schemes. A, Simple scheme. B, Complex scheme.* [15]

On of the most popular hybrid nanotechnologies is synthesized fluorescent magnetic Fe_3O_4—CdSe. The combination of QD's and magnetic NP's proves to be highly advantageous, as superparamagnetism and fluorescence, two attractive traits, allows the intracellular movements to be controlled through magnetism and can be monitored using a fluorescent microscope. First, these hybrid particles have attached themselves onto the specified cells, through simple surface modification. Thereafter, a small magnetic is turned on attracting these hybrid particles and their attached cells towards the field generated. This application is very useful for biomedical issues, as it allows the investigation of understanding the manipulation of proteins of the desired intracellular location and allows us to understand the basic cellular processes which we would then be able to manipulate. This can be seen in Fig. 5.

Recent research in the field of hybridizing QD material to superparamagnetic nanoparticle has mainly focused on increasing the quantum yields of synthetic QD's, mainly because nanoparticles are already so widely used. So far, various technologies have been developed which synthesize magnetic material to QD material however have achieved very low quantum yield.

Klimov et al [9] was successful in fabricating magnetic-optical nanocrystals by growing the luminescent CdSe shell on the metallic Co nanoparticles. But, the quantum yields of these new hybrids were very low (only 2–3%).

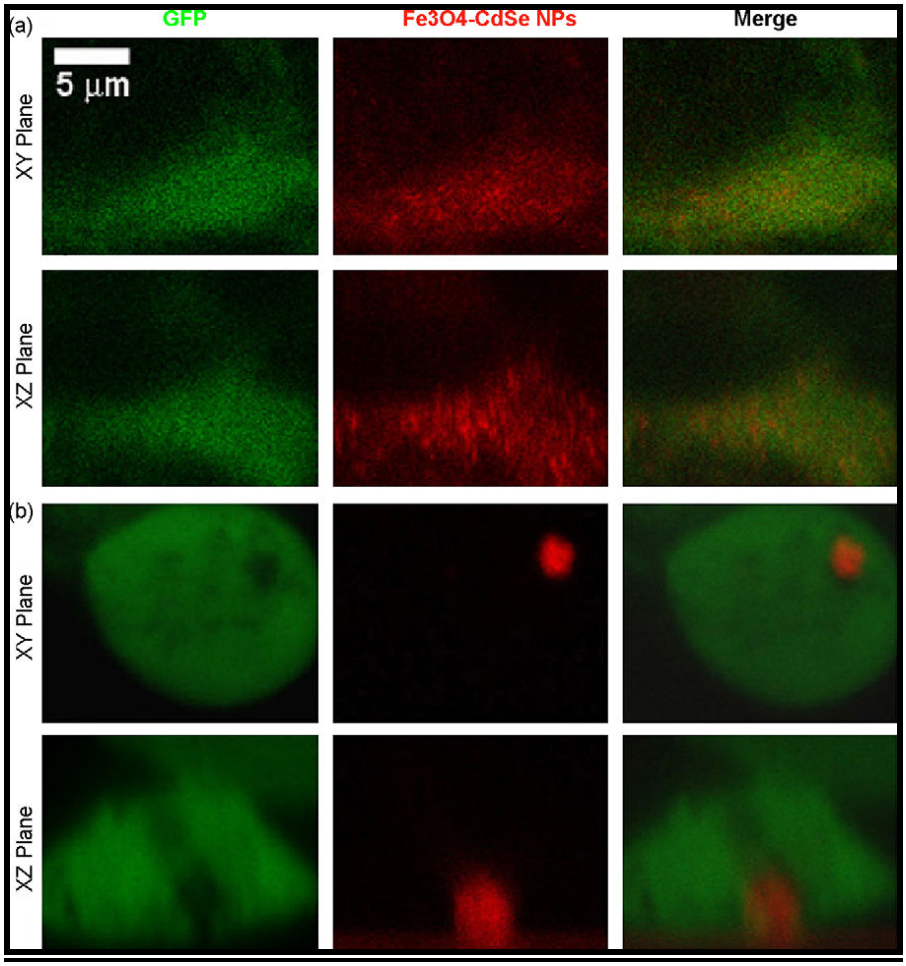

Fig. 5. *As specific cells are incubated with the Fe_3O_4—CdSe@GSH nanoparticles for 8 hours, these confocal images were taken of the cell (a) without a magnetic field and (b) under a magnetic field.* [3]

Du et al [9] have recently fabricated and characterized the properties of Fe_3O_4/CdSe/ZnS magnetic fluorescent nanoparticle hybrids. They were fully characterized by Transmission Electron Microscopy (TEM), shown in Fig. 6, X-ray Photoelectron Spectroscopy (XPS) and X-Ray Diffraction (XRD), whilst their magnetic and optical properties were measured by Superconducting QUantum Interference Device (SQUID), PhotoLuminescence (PL), and UV–vis absorption.

Results showed that the fabricated Fe_3O_4/CdSe/ZnS nanocomposites were superparamagnetic, about 8 nm in size and achieve an impressively increased the quantum yield of the nanocomposites from 2–3% in Fe_3O_4/CdSe to 10–15% in Fe_3O_4/CdSe/ZnS. The increase of quantum yield is due to the excitation of the surface ZnS.

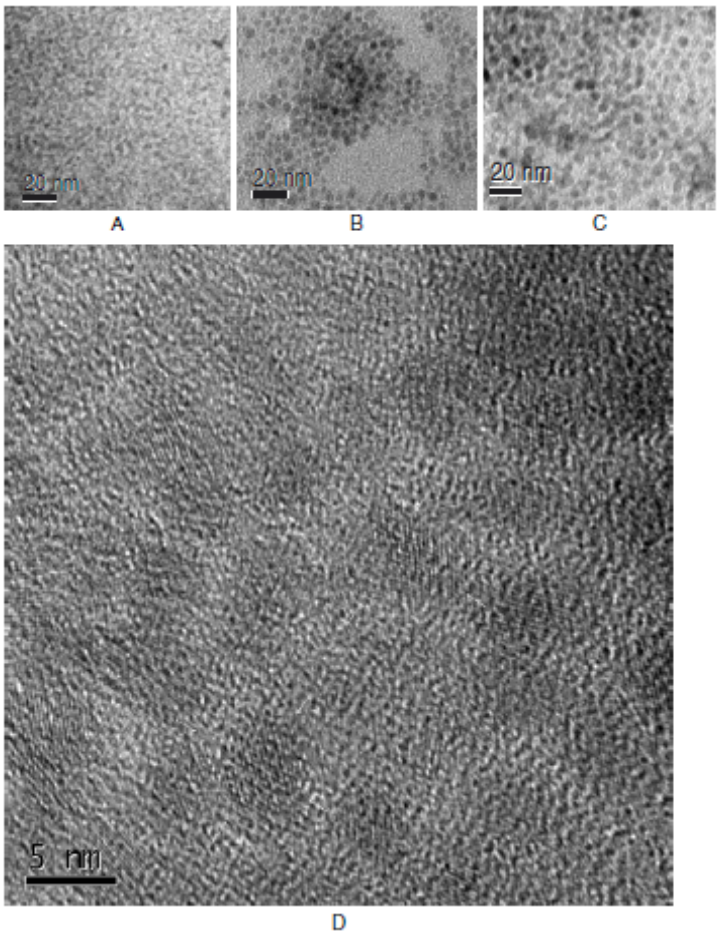

Fig. 6.
TEM image of samples:

(A) Fe_3O_4 NP Hybrid's,

(B) Fe_3O_4 /CdSe NP Hybrid's,

(C) Fe_3O_4 /CdSe/ZnS NP Hybrid's,

(D) HRTEM of Fe_3O_4/CdSe/ZnS NP Hybrid's. [9]

Wang et al [11] focused on creating a high quantum yield hybridized particle however also tested their final fabricated nanoparticle hybrids through antibody conjugation with breast cancer cells. They synthesized water-soluble nanoparticle hybrids consisting of a magnetic polymer core (ç-Fe_2O_3) with luminescent QD shell (CdSe/ZnS). The QD's were attached to the surface of the magnetic beads, via Thiol chemistry, as shown in Fig. 7. These nanoparticle hybrids were characterized using TEM and EDAX analysis. The particles averaged 20 nm in diameter with about 15% size variation, were fully water miscible, and showed smooth morphology. They also exhibited high emission quantum yield and were easily separated from solution using a permanent magnet. Breast cancer specific biomarkers, cycline E, were attached to the nanoparticle hybrids after they were functionalized with carboxylic groups through EDC coupling. The anti cycline E labeled particles were used successfully to separate and detect breast cancer cells in serum.

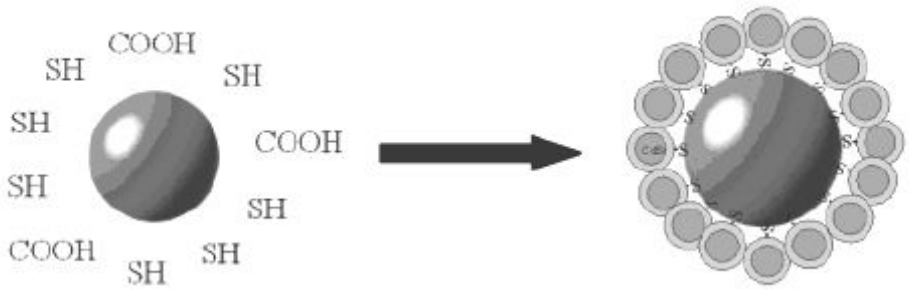

Fig. 7. *Thiol and carboxyl modified ç- Fe_2O_3 beads are reacted with CdSe/ZnS QD's to form the luminescent/magnetic nanocomposite particles* [11]

3.5. CNT AQUEOUS SOLUTIONS

CNTs have shown great interest due to their unique superior properties. However, their applications are very limited due to insufficient availability and difficulty in reaching perfect aqueous dispersions. Recently, MWNTs have reached an all time high regarding large-scale catalytic production. However, these MWNTs are tangled up together into nanocluster entities, as shown in Figs. 8 and 9, which make it seemingly harder to make perfect aqueous dispersions.

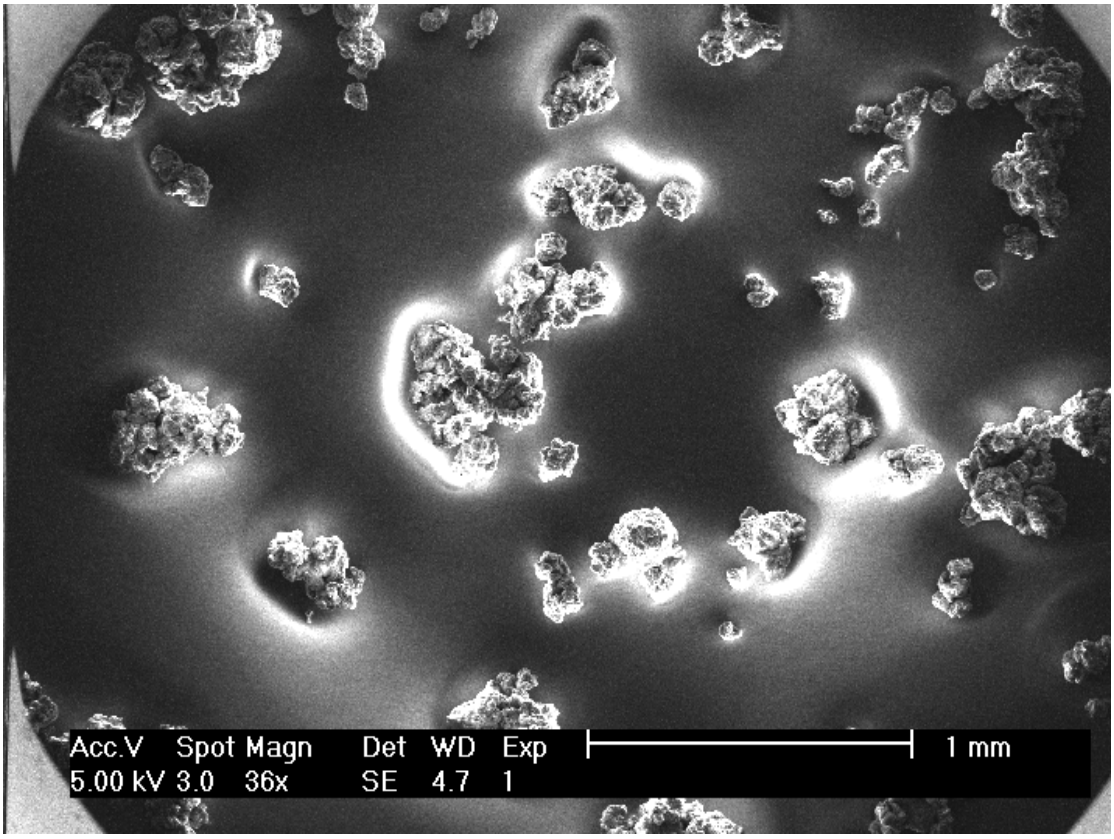

Fig. 8. *MWNT entangled Nanoclusters at a Macroscopic Level*

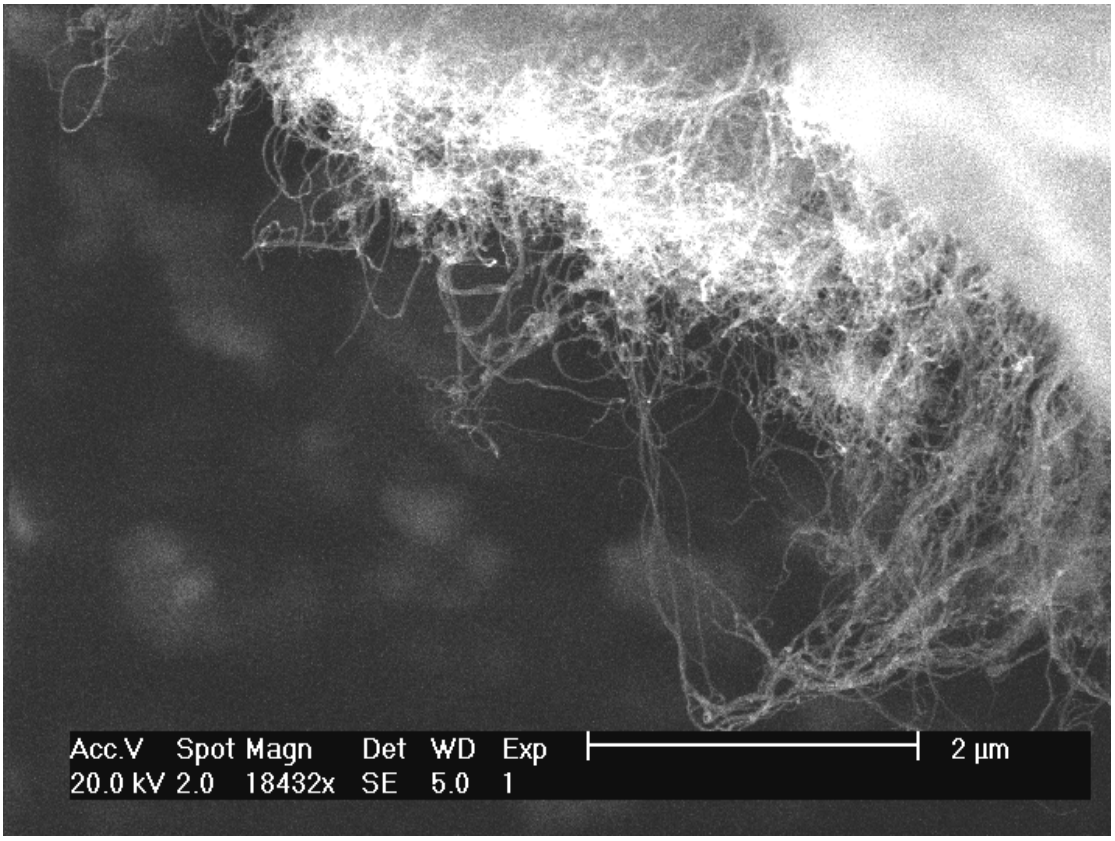

Fig. 9. *MWNT entangled Nanoclusters at a Nanoscopic Level*

For the moment, the only effective way to produce a decent aqueous suspension of MWNTs, is to apply a chemical pre-treatment by refluxing the MWNT in acids such as sulphuric acid, nitric acid, or these combined. Thereafter they are suspended in water. Even though this pre-treatment process can highly increase the dispersion property, several major characteristics of the MWNT would be negatively affected. The length, the conjugated microstructure will be heavily destroyed and altered due to the vigorous acid attack as well as remain acidic due to the residual presence of the acids used. This would limit them to their application specially bioconjugation.

Li et al [12] have developed an effective method of easily creating MWNT aqueous dispersions. The method includes a pre-treatment process with H_2O_2 followed by dispersing with ammonium polyacrylic acid. Structure morphology and surface chemistry were characterized by TEM and FTIS techniques where H_2O_2 pre-treated MWNTs were compared to MWNTs treated in a mix of concentrated HNO_3 and H_2SO_4 acids.

Results prove that the MWNTs which were pre-treated with H_2O_2 had few defects than the other MWNTs. The H_2O_2 pre-treated MWNTs also proved to have decent dispersions stability with a neutral pH and stayed very fluidic without being coagulated.

FT-IR results shows that H_2O_2 pre-treated MWNTs become more hydrophilic because they acquire more –OH groups during oxidation. Even though it's the same or better for the acid pre-treated MWNTs, more surface defects were found with the TEM where their microstructures were heavily distorted. Fig. 10 shows the MWNT time settling differences between pristine MWNTs, H_2O_2 pre-treated MWNTs and acid pre-treated MWNTs.

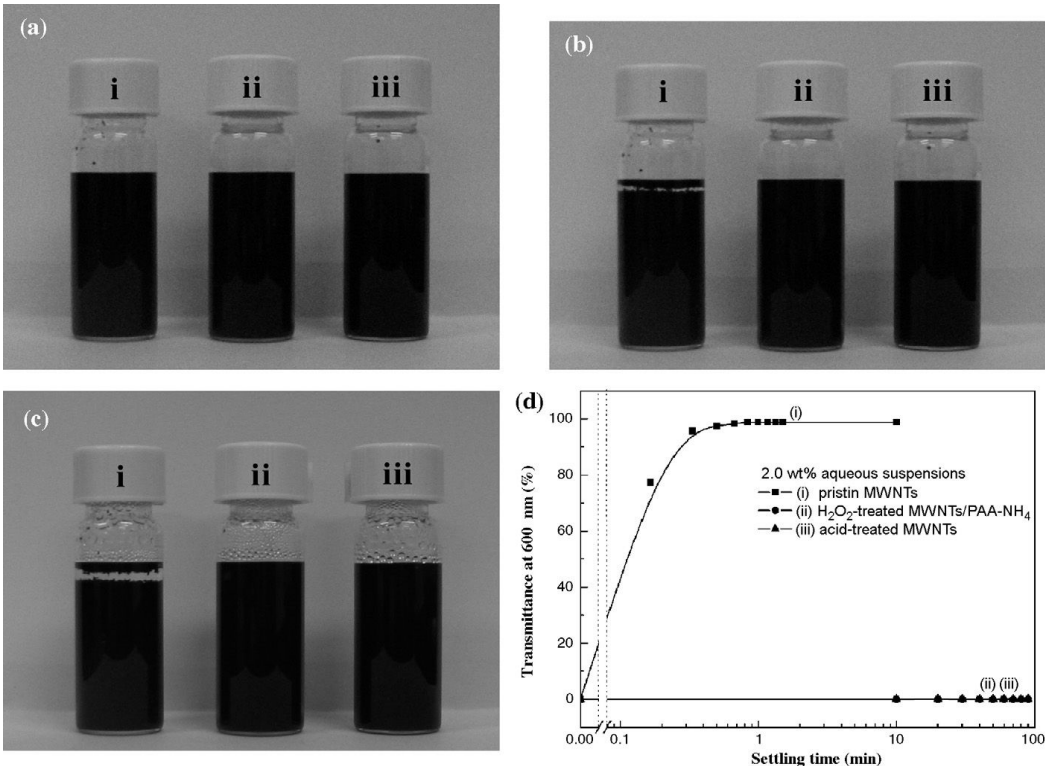

Fig. 10. *Pictures showing settling results aqueous suspensions of: (i) pristine MWNTs, (ii) H2O2-treated MWNTs (iii) acids-treated MWNTs, observed during time periods of: (a) 0 min, (b) 1 min and (c) 3 weeks. (d) shows the transmittance of suspensions.* [12]

3.6. CNT FRAGMENTATION

When CNTs are being mass produced a lot of effort is spent on their modification. Once produced, the nanotubes are purified where oxidative treatment is applied to show the available microstructural vacancies when amorphous carbon is removed. These imperfections are left for functional groups, such as COOH, OH or C=0, to chemically conjugate and occupy the microstructural vacancies. In order to increase the number of active sites (open tips), one needs to cut the tubes into smaller tubes thereby increasing the number of active sites. This can be achieved both by chemical and physical methods.

Niesz et al [17] prepared MWNTs that were chemically and mechanically cut and functionalized for further conjugation and further concluded the planned procedure to be a success.

Breaking MWNTs will be done chemically or mechanically, and is a vital process for several applications that require MWNTs to be cut. For example, the product of chemically cutting MWNTs is used as polymer fillers or for reinforcing materials. As they have reactive functional groups at both the tips and on the outermost shell, they can easily make chemical bonds with the polymers. Mechanically breaking MWNTs, results in a product that decreases in length and diameter. This product can be used as an absorbent for a variety of process.

However in regards to this current project the main reason for breaking the tubes is mainly so that we can achieve a specified length more than obtaining more reactive groups

3.7. HYPERTHERMIA OF CNTS

Ji et al [18] have written a review over CNTs affects towards cancer in thermal therapy. The focus is mainly on its explosive property when irradiated by a NIR light for a short millisecond before it explodes. Using CNTs for thermal therapy is considered to be a harmless, non-invasive and a very effective underrated technique.

Kang et al [19] investigated on the structural changes of SWNTs when ignited with a Q-switched pulse laser. It was believed that the oxidation of metal catalyst accounts for the ignition, segmentation and associated photoacoustic effect.

Gannon et al [18] researched the exposure of CNTs towards radiofrequency (RF) field and how it would lead to significant heat release by SWNTs. Both in-vitro and in-vivo tests have shown and proven the thermal obliteration of cancer cells when either attached or in the prescence of MWNTs.

Also, carbon nanotubes have the property to absorb NIR radiation (700–1100 nm) and then convert it into heat opening up a whole new strategy regarding thermal therapeutics for cancer. *Biris et al* [18] showed that infrared photothermal radiometry, combined with in time-resolved infrared imaging techniques, was very useful in determining the temperature variations of an individual or a group of nanotubes either on or close to cancerous cells.

Researchers believe that nanotubes should already be used in treating small tumours or metastases using thermal therapy.

Moon et al [18] used SWNTs and NIR irradiation on mice having tumour cells, located on their backs. After being injected with SWNTs, the mice received NIR irradiation treatment for 3 mins with a power density of 76 W/cm^2 [18]. Successfully, after twenty days, results showed the complete destruction of the tumours after 20 days of post-treatment. And it was seen that the SWNT debris excreted completely from the mice after 2 months without any repercussions.

Very similar to *Moon et al's* [18] work, a long-term surviving kidney tumour mouse acquired a MWNT based thermal therapy treatment, however using lower laser powers of (3 W/cm^3) and a shorter treatment time of only 30 seconds. In order to improve the selectivity of the treatment, the MWNTs were coated with cell binding strands such as peptides or antibodies. Results showed that there were more detected tumour cells in in-vitro therapy than in in-vivo therapy. Therefore further research is being conducted to explain why this is the case.

3.8. MICROFLUIDICS SYSTEMS

Microfluidic technologies have sky-rocketed since the development of the first LOAC based system in 2000. Since then the field has exponentially grown introducing the birth of a few companies that dedicate themselves to fabricating customer designed LOAC's. Microfluidic technologies are so popular because they work for highly predictable and homogenous samples at are common in the drug discovery, genomic analysis, cell isolation, proteomics or as simple as micro based mixers. Since 2000, microfluidics technologies has evolved in such a way that they have become more advanced and include design parameters and calculations for fluid flow and dynamics, micro construction lithography techniques, flow injection analysis, electrokinetic techniques, etc.

Weigl et al [22] reviews these necessary design parameters as well as fabrication and characterization techniques which are needed to produce a basic well designed microfluidic chip for a chosen application. Microfluidics provides many advantages such as sample handling, reagent mixing, separation, and detection.

Zhang et al [23] reviews the advances of microvalves, micropumps, and micromixers within PCR microfluidic chips over the past ten years at a very large detail. All three components: microvalves, micropumps, micromixers, have evolved simultaneously with micro- or nanotechnology. The advancement in these chips helps us realize the importance of microfluidic chip technology that allows us to use fluidics for any application.

Fiorini et al [55] reviews the recent developments in microfluidics, especially on disposable plastics, and focuses on descriptive fabrication methods for both the unit and the systems involved in it. Thereafter *Fiorini et al* [55] leads to a strong debate on the advantages of this technology for biotechnological applications.

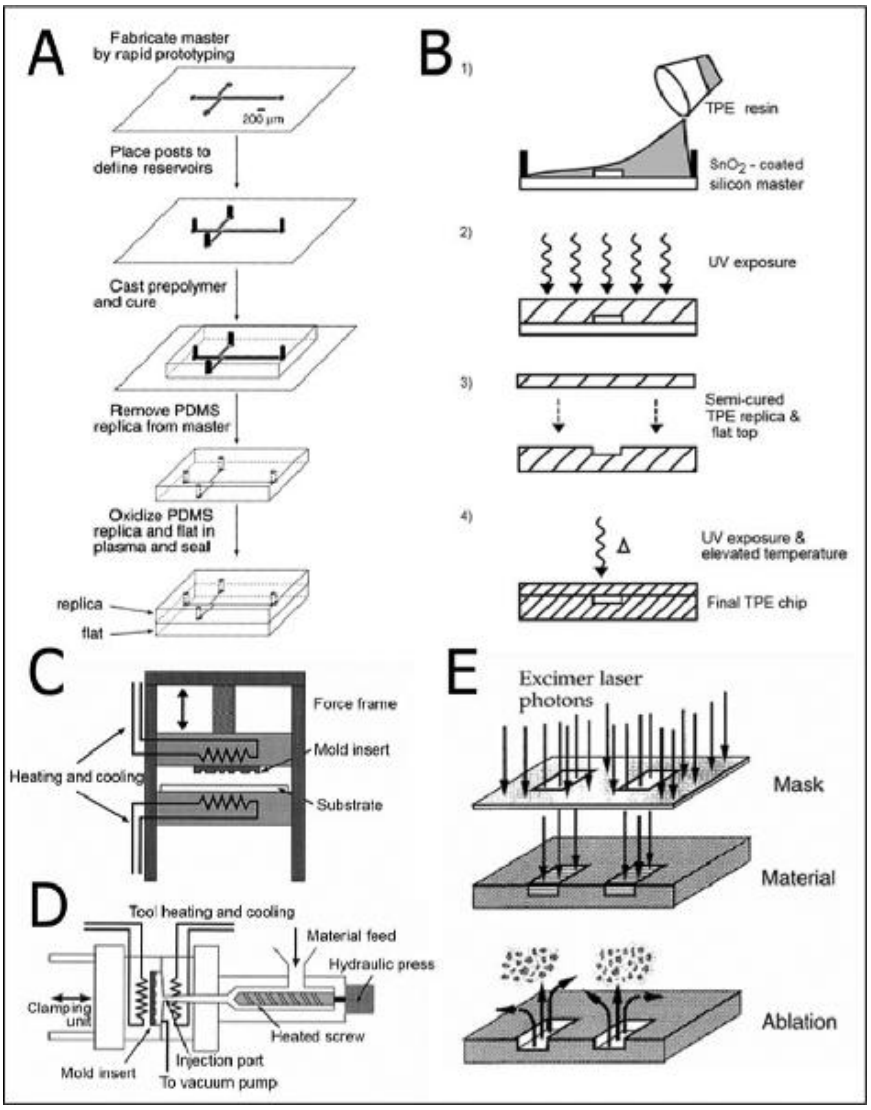

Fig. 11. *Disposable Polymer Microfluidics Fabrication Method. Fabrication of (A) polydimethylsiloxane (PDMS) and (B) thermoset polyester (TPE) devices by replica molding, and fabrication of plastic devices using (C) embossing, (D) injection molding, and (E) laser ablation.* [55]

3.9. MAGNETIC-BASED BIOSENSING

Magnetic biosensors use magnetic labels to detect biological molecules/targets and process the information into an electrical signal. For the past few years, magnetic detection schemes have been a huge research area for biosensor technology. The key factors in a successful magnetic biosensor are high sensitivity, good accuracy and short detection time.

However there are many areas that have not yet be researched heavily. The use of NP's as magnetic labels for bio-sensing technology is slowly expanding coming up with several positive predictive results, however the integration of CNT with these magnetic NP's has been explored to its maximum potential.

Another area that has not been heavily researched is the effects of different types of magnetic labels. From structure to materials to textures to configurations, every aspect of a magnetic label is being altered and researched, in order to determine the most efficient magnetic label. Research has shown that it is possible to alter the physical properties of NP's in order to experiment on their use as magnetic labels. Knowing the factual evidence, it is possible that NP's will be the next key step to increase the sensitivity of current commercial magnetic labels.

3.9.1 BASIC DETECTION SCHEMES

The simplest detection scheme involves when target biological molecules are stopped on the magnetic labels and are passed over an array of specific magnetically labelled probe molecules. Once a current is inputted into the sensor with the probe molecules, the targeted molecules are then attracted to the match probe molecules. The target molecules that suit the magnetic label are then attached whilst the rest are realized. Once the probe confirms a biological change in the sensor, an electrical signal is sent to provide a more measurable reading.

3.9.2 MAGNETIC LABELS

Paramagnetic materials as non-remanent spheres, are mainly used as magnetic labels. There are however a few transition metals such as NiFe or CoFe are hypothesised to have higher magnetization levels. Micro-spheres, micro-beads and nanoparticles are also referred to as magnetic labels. When it comes to choosing the properties of a magnetic label, the following traits are very necessary to decided upon in order to bind the required targeted molecules:

- Size
- Shape
- Magnetic and Chemical Composition
- Surface Properties
- Stability of Chemical Functionalization

3.9.3 DETECTING MAGNETIC LABELS

In order for a magnetic label to be detected by a sensor, a magnetic field is applied using an electromagnetic. Once applied, the magnetic field magnetizes the labels and creates an overall moment in the sensor. The technical term for the magnetic field generating around the label is called a fringe field. The sensor's detection system waits for a change in the magnitude of the fringe field, and hence gives out a detection signal. The biological signal, obtained, is dependent on the following:

- Parameters and properties of the magnetic labels
- Sensor sensitivity
- System setup
- Distance between magnetic label and the sensing of the target molecules

If a weak signal is obtained, after the target molecule successfully bounds to the magnetic labels, then an amplification system can be used to amplify the signal. The sensitivity can be explained in the following; it is the smallest number of biological interactions, between the target molecules and the magnetic labels that can be detected. That is why biosensors using nanometer-particles are more sensitive than those that use micrometer particles.

3.9.4 MAGNETIC MICROSPHERES VS. MAGNETIC NANOPARTICLES

Microspheres, from 1 to 3 micrometers diameter, are the more focused particles in magnetic label research than magnetic NP's. Microspheres usually have a lower percentage of magnetic composition compared to NP's. However, microspheres have a stronger fringe field that NP's, due to it have a higher magnetic moment per label due to volume. This allows the detection signal to be a lot stronger, and therefore increases the chances of attracting the targeted molecule. The only downside to microspheres is their size, and that's when nanoparticles come in.

NP's provide a few solutions to the problems which microspheres have. As NP's are a lot smaller than microspheres, this increases the percentage of targeted molecules binding onto a magnetically labelled probe. However, current technology only provides NP's of various sizes and shapes, which of course hinders the possibility of predicting any achievements. Another issue with NP's is that when exposed to high levels of magnetization, they may then cause rapid clustering, which is when single particles begin to combine with each other to form groups. And when the target

molecules meet with the magnetic labels, the targeted molecules will be bounded to the groups of NP's, sending out exaggerated signals that will be of no use to us.

3.10. IMMUNOSENSING

Immunosensors are systems combining specific antigen-antibody recognition methods with several analysis schemes. They have been used widely in several industries such as the food, environmental and clinical control industry. Like electrochemical sensors, immunosensors are at high demand because they are easy, robust, economical to mass produce, and achieve excellent analysis with small samples. However, with the research boost in nanotechnology, investment is going into building highly sensitive and selective immunosensors, due to their excellent biocompatibility, electron transfer, absorption capacity, large specific surface area, and flexible attachment to NP's.

Significant research has been done on label-free electrochemical immunosensors, using Au NP's as building blocks. These have been successfully demonstrated to when it comes to the detection of a change in the physical properties of an antigen-antibody attachment. Fig. 12 below exhibits electrochemical detection of the antigen through the immunosensing of the antibody.

First of all, the antigens are located and attached using the Au NP's-antibodies hybrids. Then, once attachment to the antigens had occurred, voltammetric measurements can be stripped. Note: Each protein attachment possesses distinct voltammetric properties, which differs in level and size from the rest.

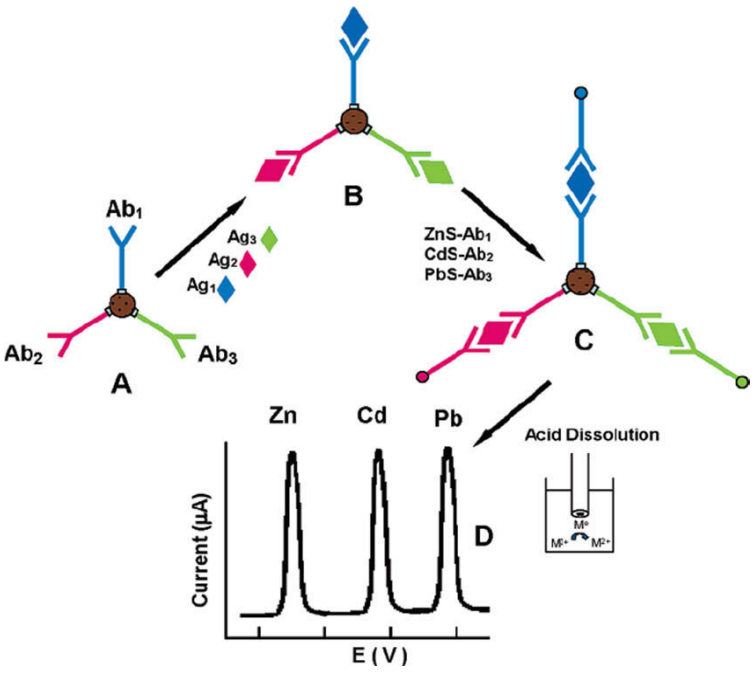

Fig. 12. *Multi-protein electrochemical detection based on different nanoparticle (NP) tracers. (A) Immobilization of antibodies onto magnetic beads; (B) antibodies-magnetic beads hybrids locate and bind with antigens; (C) NP-labelled secondary antibodies captured; (D) Electrochemical detection methods employed to measure NP concentration.* [56]

3.11. AC DIELECTROPHORESIS

Purification methods, wet or dry, are still being researched for the purification of CNTs from impurities such as carbon nanoparticles and amorphous carbon. *Wei et al* [27] for example, focused on the developing a microfluidic device to separate different conducting parts of MWNTs.

Dielectrophoresis is the neutral movement of polarizable particles in a non-uniform electric field. AC Dielectrophoresis utilizes the CNTs high conductance and high polarizability to enable them to be aligned from dispersion between two electrodes, generating an electric field from a sufficient RF voltage. This can be seen in Fig. 13 from *Liu et al* [26], where the nanotubes are horizontally aligned between the electrodes.

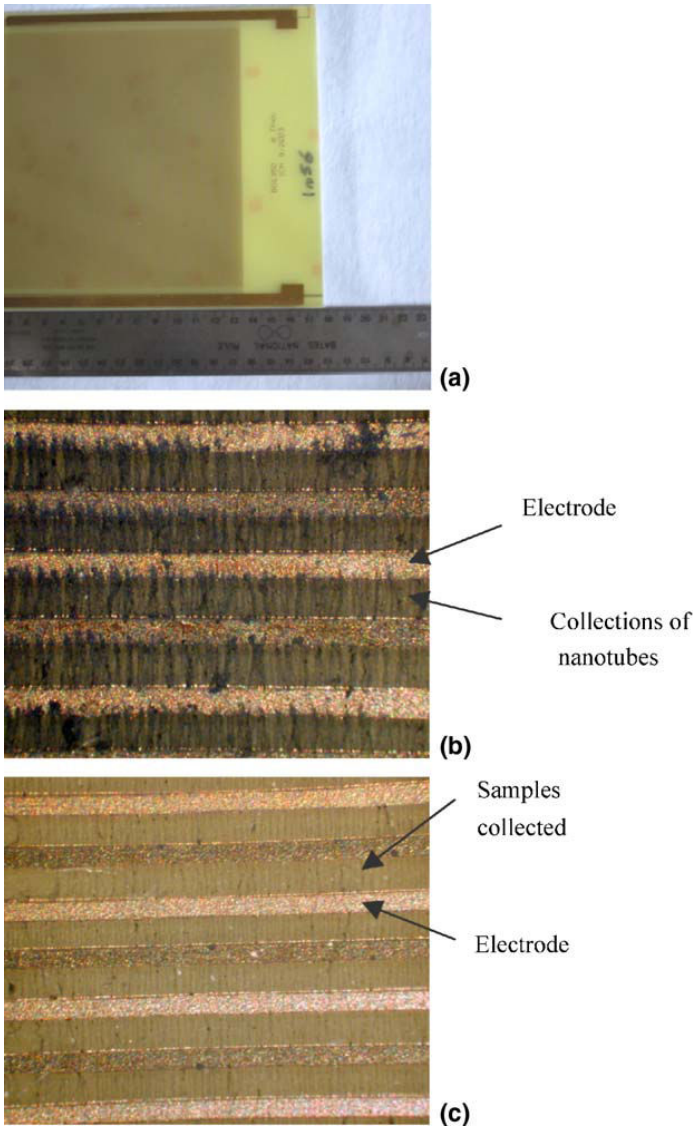

Fig. 13.
Photos of the large array before and after collection of CNTs.

(a) An overall view of the array with IDEs. Dimensions of IDEs are indicated by a ruler: 13.5 cm · 11.5 cm. (b,c) Views, which are magnified by an optical microscope, of CNTs collected on and between electrodes. The electrodes (141 lm wide and 193 lm apart) have a grainy appearance whilst CNTs appear as black threads between them. (b) A heavily deposited area (c) A lightly deposited area. [26]

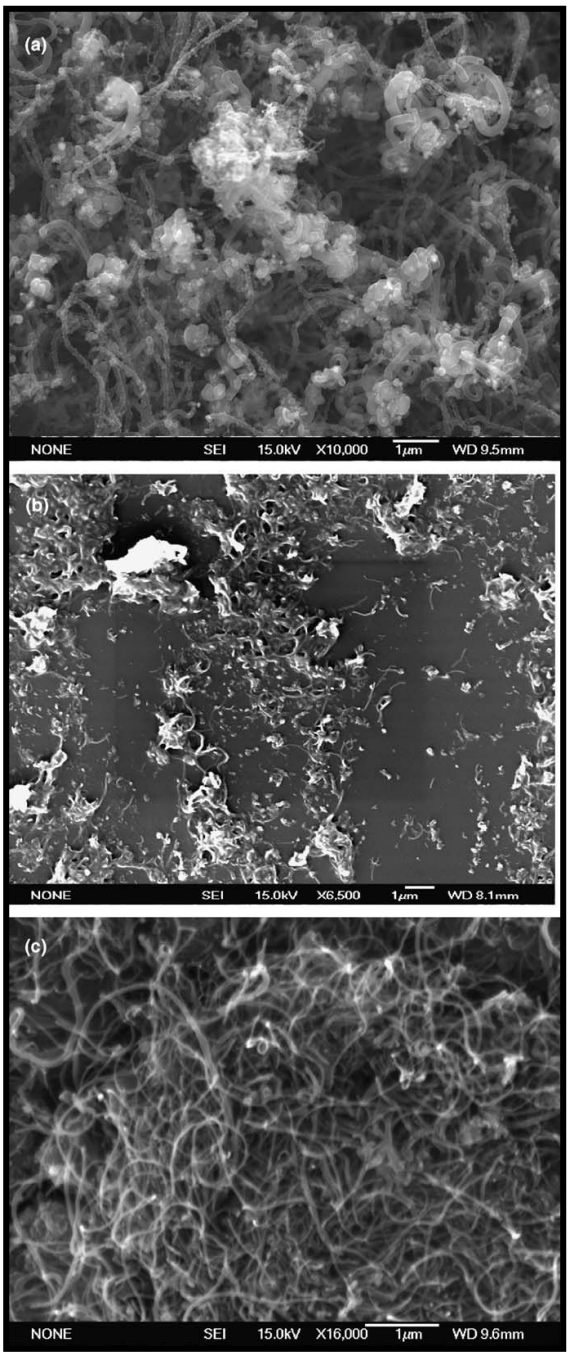

Fig. 14.
SEM images of samples of:

(a) Before being treated;

(b) Remaining in the suspension after being treated;

(c) Collected on the array. All the scale bars in the images are 1 m. [26]

Liu et al [26] shows SEM images in figure Fig. 14, of the state of nanotubes before and after going the process of being fully suspended in an aqueous solution. CNTs in dispersion are more likely to act on dielectrophoretic force than their impurities, such as carbon nanoparticles or amorphous carbon. This is due to nanotubes have a high conductance which signifies higher polarizability. CNTs are collected on the electrodes by dielectrophoretic force while impurities are flushed into the waste.

Unlike *Liu et al*, *Banerjee et al* [25] wanted to use AC Dielectrophoresis to specifically position nanotubes for device fabrication and not just for filtration. SWNTs have attracted much attention with their unique properties and applications. The can be integrated into electronic devices where they can be an active element bridging architectures together. However in order to specifically place a nanotube at one specific area requires precise positioning using AC Dielectrophoresis, which *Banerjee et al* have achieved. Nanotubes have been either fabricated or assembled onto device architectures through either chemical modification, direct growth on substrate, CVD, or

even mechanically stamping. All these techniques however are difficult and inefficient and hence why AC Dielectrophoresis is the technique which surpasses them all for this application. We can see in Fig. 15 how the nanotubes are attracted and aligned between the electrodes due to their high conductance and polarizability.

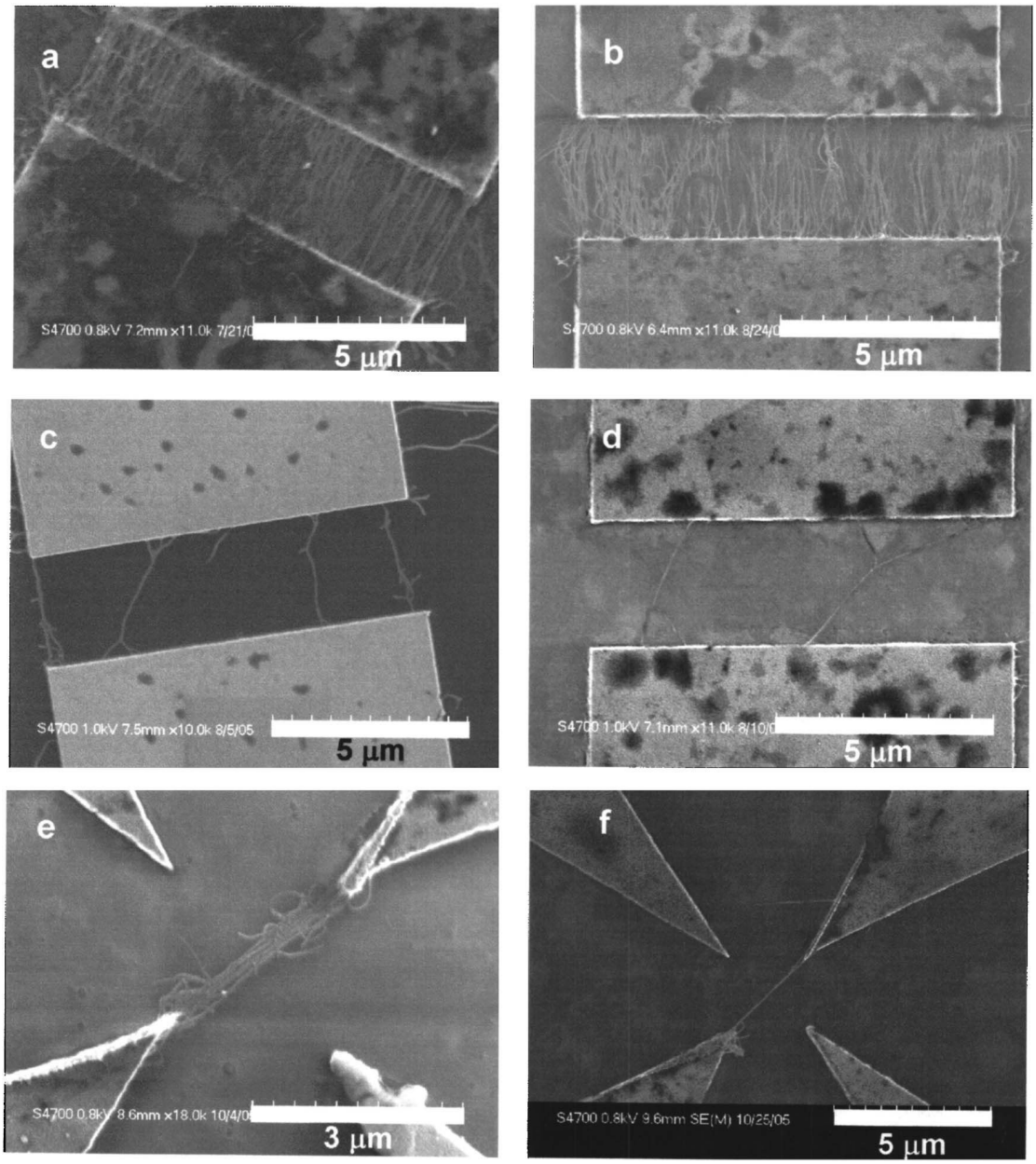

Fig. 15. *SEM images of using AC Dielectrophoresis for precise positioning of nanotubes for device architecture* [25]

Banerjee et al successfully obtained control over the alignment of nanotubes using AC Dielectrophoresis and patterned microelectrodes. They also have fabricated crossed nanotube architectures once having only on nanotube between to opposing electrodes.

3.12. FUNCTIONALIZATION TECHNIQUES FOR CNTS AND QD's

If using CNTs for biosensing, they need to be purified to remove any amorphous carbon, substrate material such as Al_2O_3, and metal catalysts such as Fe, Co, and Ni. Purifying the CNTs can be done using high temperature annealing, plasma treatment or chemical methods so that good crystal structures are obtained.

Surface modification and functionalization of the CNTs can now be performed to immobilize the specified biological molecules. Functional groups such as carboxylic, hydroxyl, ketone, alcohol, ester, amine, thiol, and fluorine can be created by wet and dry chemical modification procedures.

Functionalization is the process of creating defects or oxides on the ends and sidewalls of the CNTs, which unfortunately will lower the electrical conductivity. Even though CNT surfaces are non-reactive, the ends of the CNTs are more reactive to strong acids such as HNO_3, H_2SO_4, $KMnO_4$, $K_2Cr_2O_7$, OsO_4, CCl_4, $O_2(g)$, CF_4, and SF_6 due to the dangling bonds from the Stone-Wales defects.

Pan et al [35] focuses on the fabrication of QD's onto the outer surface of MWNTs forming QD-MWNTs. Conjugation between the QD's and MWNTs is through the interaction of amine groups on the MWNTs with the mercaptoacetic acid modified QD's. Also, QD-MWNT nanoparticle hybrid show excellent solubility in an aqueous solution, which is important for the project. Fig. 16 shows the conjugation process to form QD-MWNTs.

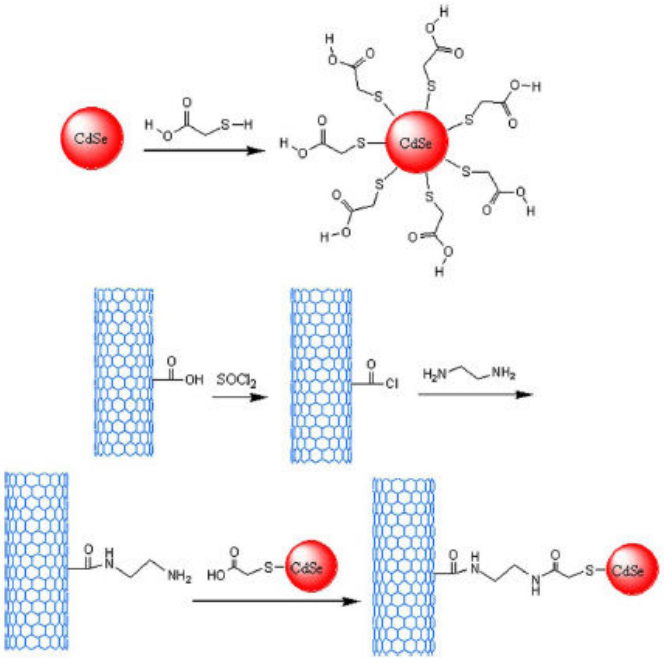

Fig. 16. *Design schematic for covalent attachment of QD to MWNT* [35]

3.13. FUNCTIONALIZATION TECHNIQUES FOR QD'S AND ANTIBODIES/BIOMARKERS

Both *Xing et al* [31] and *Smith et al* [30] provide a concise review over semiconductor QD's, tiny light-emitting nanocrystals. Compared to their alternatives, organic dyes and fluorescent proteins, QD's provide a better function with tuneable emission spectra, improved brightness, superior photostability and simultaneous excitation of multiple colours. The reviews focus heavily on bioconjugation techniques, imaging applications, live cell dynamics, fixed cell labelling, in situ tissue profiling, fluorescence detection, and in vivo animal imaging. The reviews help you decide on the necessary steps one must take to decide upon what specific biomarker needs to be used for what specific imaging application. Specifically what the best attachment methods will be between QD and cancer-specified antibodies. Fig. 17 below helps us choose out bioaffinity setup.

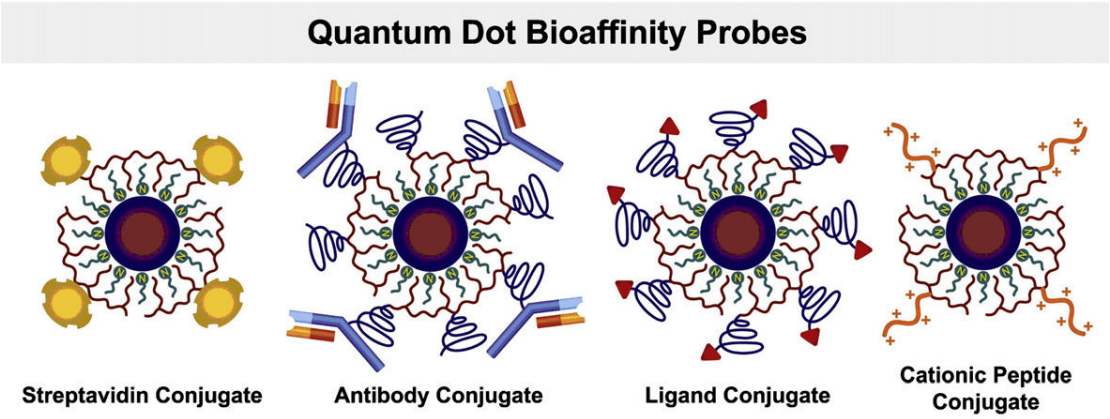

Fig. 17. *Quantum Dot Bioaffinty Probes for attachment to specific cell* [30]

4. DESIGN

Full design schematics of all three components need to be fully designed. This includes size specifications, materials, thickness of evaporated materials, and fabrication and microscopy techniques needed. All schematics are drawn on CorelDraw, 2D vector design software, and Google SketchUp 7, 3D modelling design software.

4.1. COMPONENT 1: MICRO-AND NANOELECTRODE TECHNOLOGY

Five versions of component 1 will be made based on their different electrode designs. Full schematic designs will be exposed with the e-beam lithography for nanoelectrode technology, and photo lithography for microelectrode technology.

The rectangular electrode designs were inspired by *Patil et al* [6] and *Aravamudhan et al* [7] whom used interdigitated electrodes for electrochemical detection and sensing of cytokeratin-7 and blood. Both designs proved to be highly sensitive for their applications mainly due to the interdigitated electrodes design.

Unlike *Patil et al* [6] and *Aravamudhan et al* [7], precious positioning of nanotubes is an important design product, allowing us to control the positioning of the component 2. Design 1 will replicate the basic rectangular interdigitated electrodes design as shown by *Patil et al* [6] and *Aravamudhan et al* [7], however to improve the precise positioning of component 2 the interdigitated electrodes will have attached triangular tips allowing the electromagnetic force to be focused at the smallest point of the tip. Design 2 has micro and nanotips at the end of each micro and nanoelectrode. Design 3 is very similar to design 2, however the lengths of the tips are fairly longer, hypothesizing a larger improvement on the precise positioning of component 2, as component 2 gets more attracted to a finer tip. Design 4 will have a collection of these

triangular tips surrounding the edges of the electrodes. The main reason for this design is analyze component 2 distribution on a triangular tip, surrounded by tips. Design 5 allows us to test orientation of component 2 when attracted to component 1 and see whether or not component 2 will be place horizontally or vertically in the interdigitated by interdigitated electrode design.

For fabrication of micro-electrode technology, the schematic is exposed by UV light with the mask aligner onto a Si substrate, with a 1 micron layer of SiO_2 after doing the spin-off of positive photoresist. For fabrication of nanoelectrode technology, the schematic is exposed by the electron beam with the SEM machine onto another substrate, with identical specifications, but after doing the spin-off of PMMA resist.

The following materials will be evaporated after successful lithography processes:

Layer 1(Bottom layer): Chromium (Cr), 5 nm thick
Layer 2: Permealloy (Ni80Fe20), 40 nm thick
Layer 3: Gold (Au), Capping layer 5 nm thick

The advanced electrodes are obtained by lift-off, soaking the substrate in acetone for adequate time.

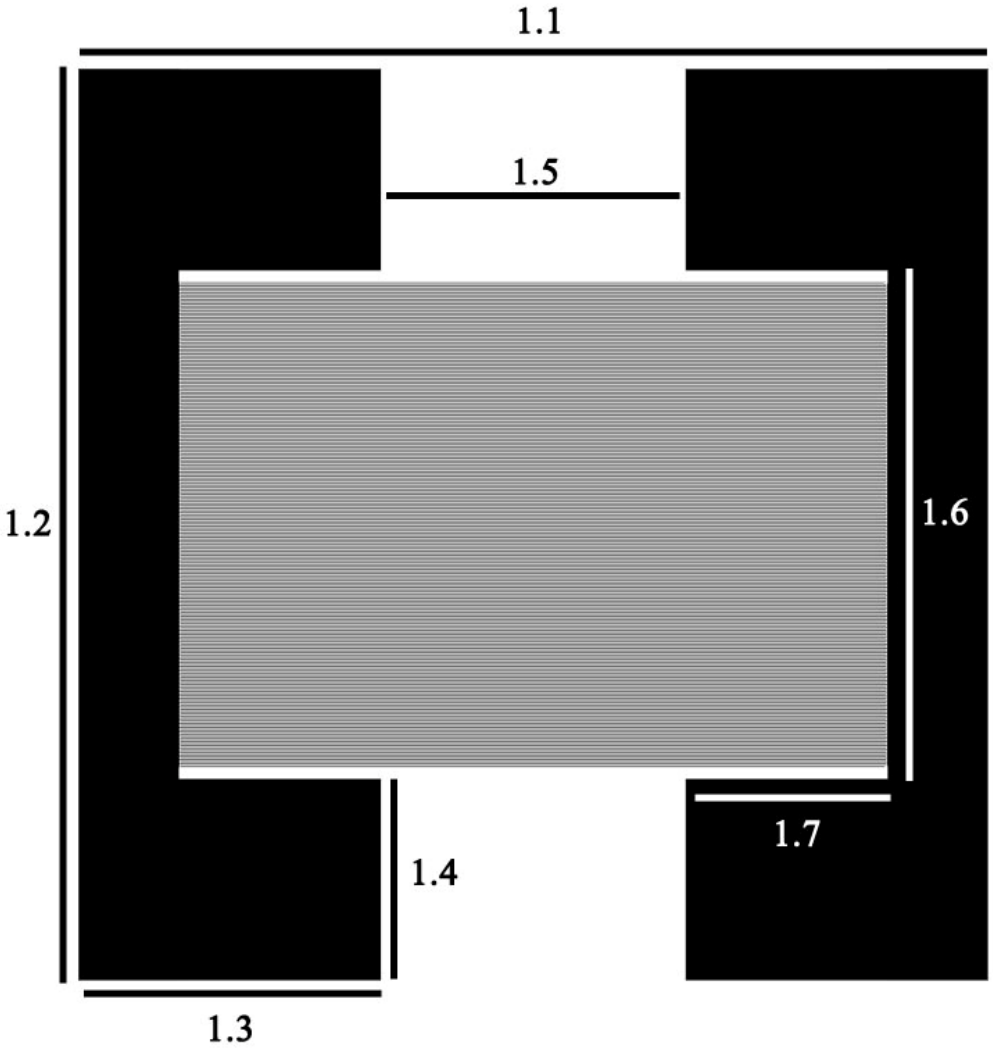

Fig. 18. Design *schematics showing measurements (values in Table 1) for main size of component and main electrical contact pad electrodes*

The following table show the size specifications of both micro-and nanoelectrode technologies. These included the main size of the component and the size of the large opposing electrodes.

Nanoelectrode Technology		**Microelectrode Technology**	
1.1	400 µm	1.1	9 mm
1.2	400 µm	1.2	9 mm
1.3	125 µm	1.3	3 mm
1.4	50 µm	1.4	2 mm
1.5	150 µm	1.5	3 mm
1.6	300 µm	1.6	5 mm
1.7	75 µm	1.7	2 mm

Table 1. *Size measurements for main size of component and main electrical contact pad electrodes shown on Fig. 18*

4.1.1. ADVANCED ELECTRODE DESIGN 1

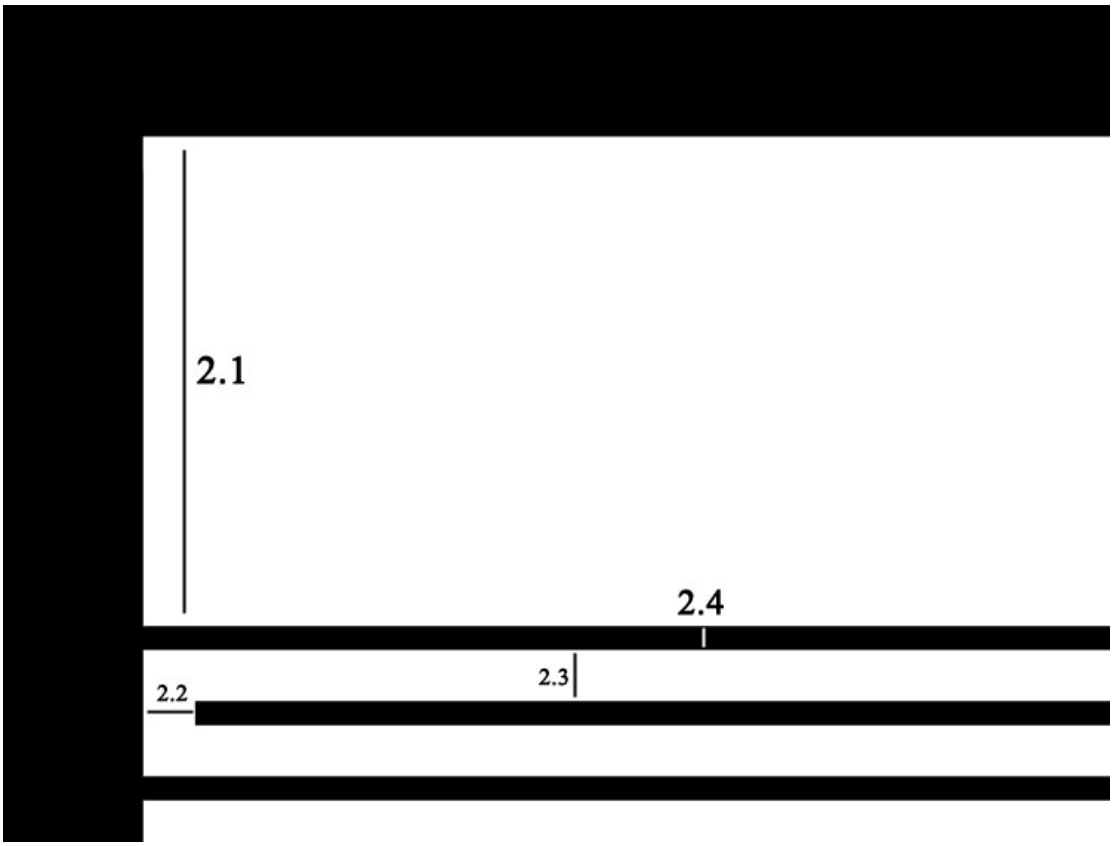

Fig. 19. *Design schematics showing measurements (values in Table 2) for advanced electrodes design 1*

The individual electrodes in Fig. 19 have simple rectangular shape. The following component specifications should be achieved from using Table 2 below:

Nanoelectrode Technology		**Microelectrode Technology**	
2.1	25 µm	2.1	90 µm
2.2	500 nm	2.2	10 µm
2.3	500 nm	2.3	10 µm
2.4	1 µm	2.4	10 µm

Table 2. *Size measurements for advanced electrodes design 1 shown on Fig. 19*

For electrode designs in Fig. 19, a total of 166 electrodes (83 on each side) should be developed with lengths of 299.5 µm, for the nanoelectrode technology. For the micro-electrode technology, a total of 240 electrodes (120 on each side) should be developed with lengths of 6990 µm. Figs. 20 to 23 show a 3D interpretation of the final sample after fabrication.

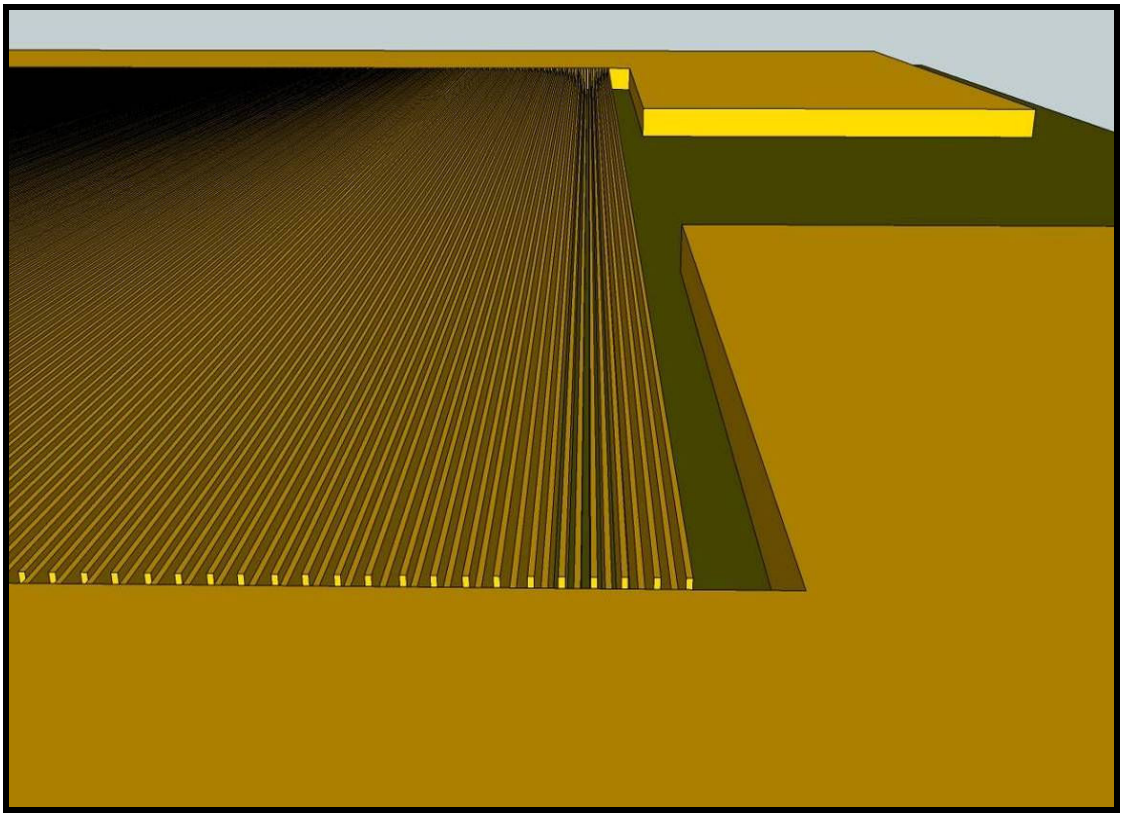

Fig. 20. *3D image interpretation of advanced electrodes design 1 – Angle 1*

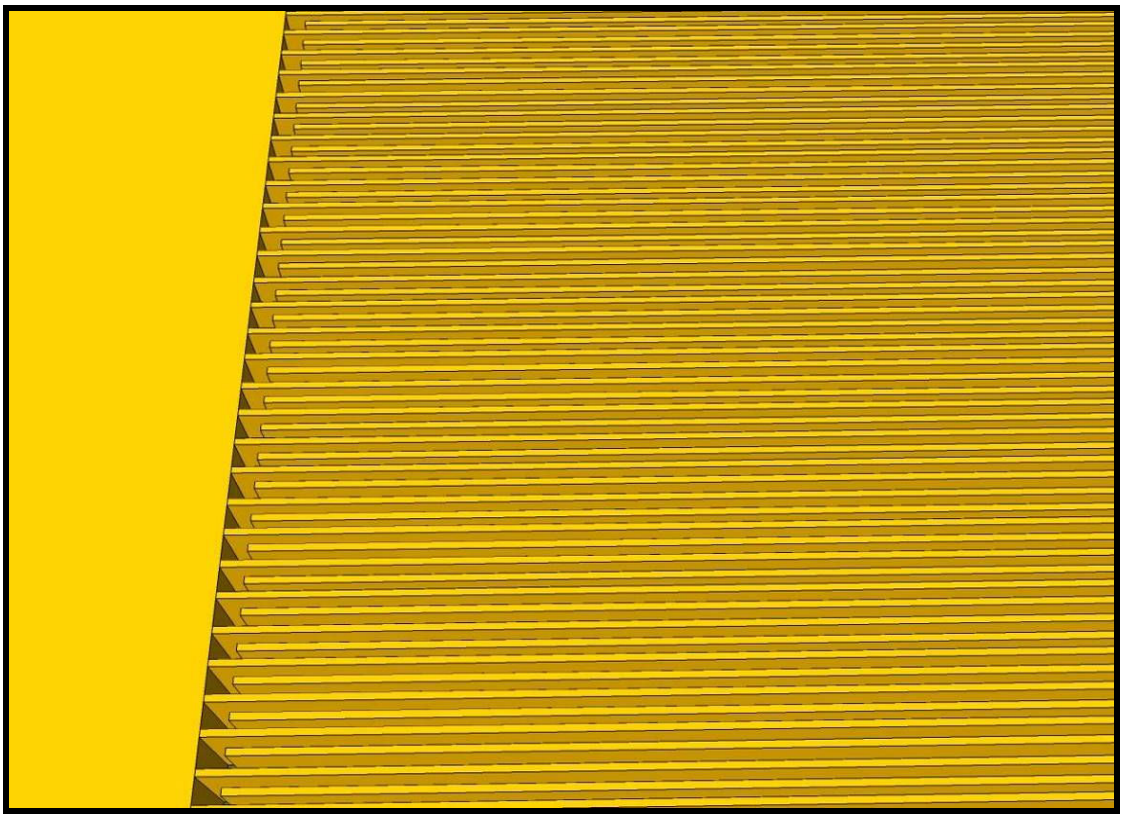

Fig. 21. *3D image interpretation of advanced electrodes design 1 – Angle 2*

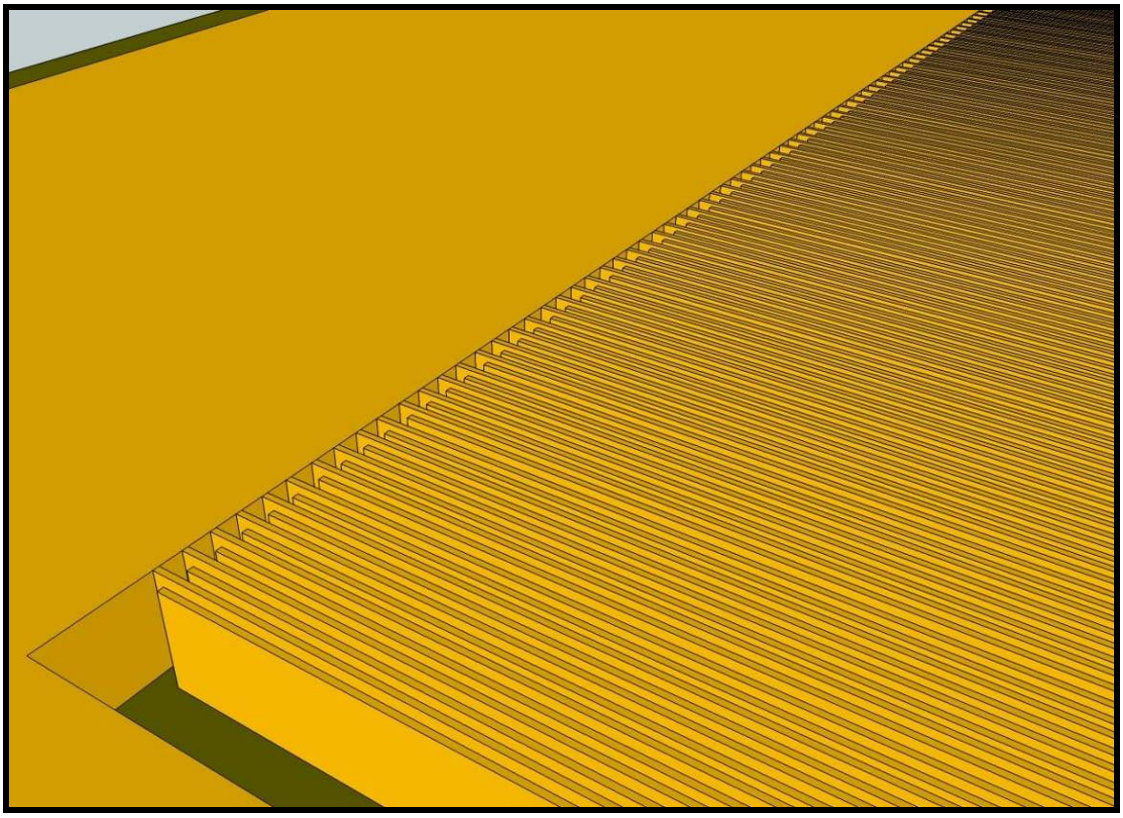

Fig. 22. *3D image interpretation of advanced electrodes design 1 – Angle 3*

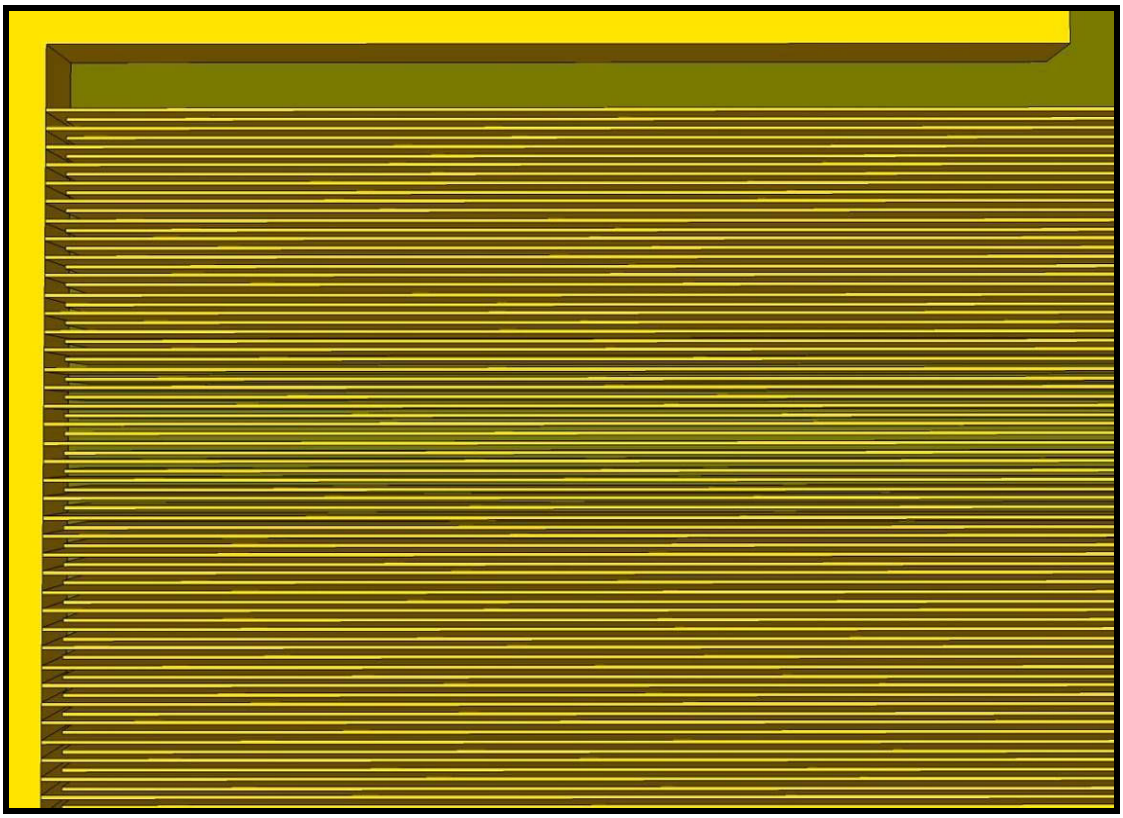

Fig. 23. *3D image interpretation of advanced electrodes design 1 – Angle 4*

4.1.2. ADVANCED ELECTRODE DESIGN 2

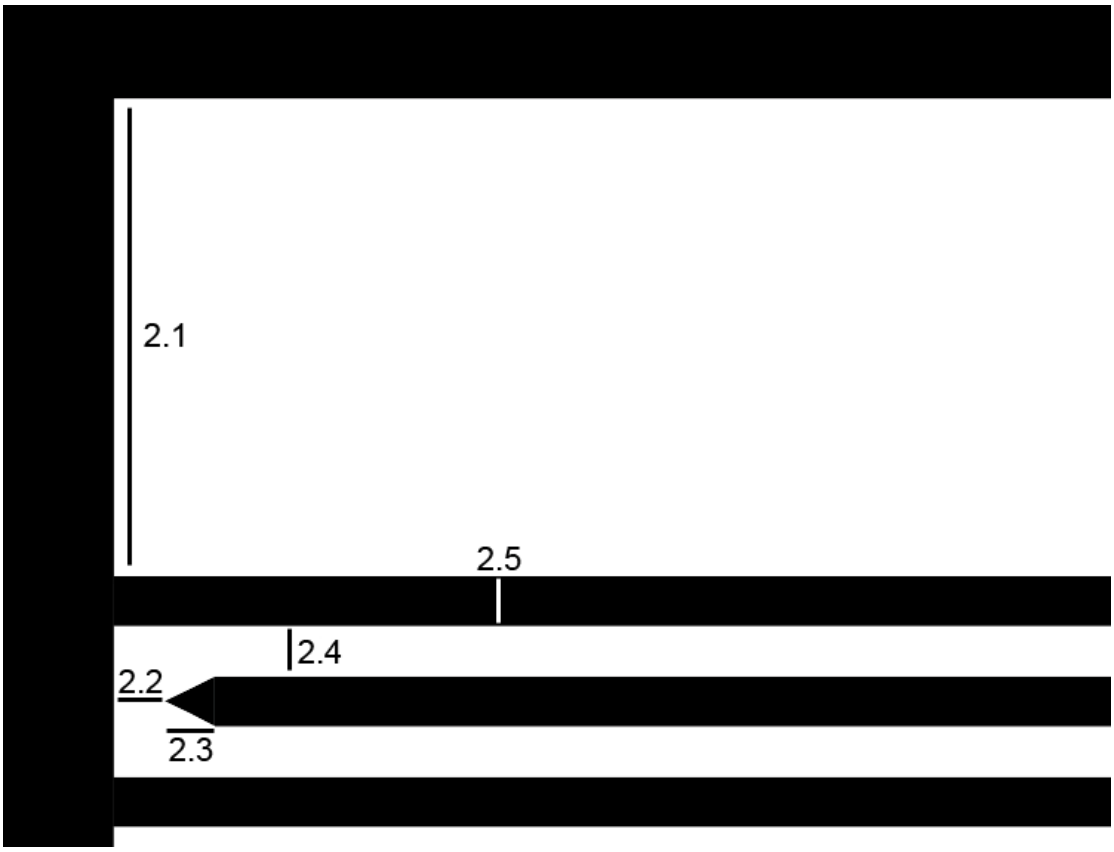

Fig. 24. *Design schematics showing measurements (values in Table 3) for advanced electrodes design 2*

The individual electrodes in Fig. 24 have simple rectangular shape, similar to that of Fig. 19, but have a triangular tip at its end, attracting all the nanotubes towards the tips specifically The following component specifications should be achieved from using table below:

Nanoelectrode Technology		**Microelectrode Technology**	
2.1	25 μm	2.1	90 μm
2.2	500 nm	2.2	10 μm
2.3	500 nm	2.3	10 μm
2.4	500 nm	2.4	10 μm
2.5	1 μm	2.5	10 μm

Table 3. *Size measurements for advanced electrodes design 3 shown on Fig. 24*

For electrode designs in Fig. 24, a total of 166 electrodes (83 on each side) should be developed with lengths of 299.5 μm, for the nanoelectrode technology. For the micro-electrode technology, a total of 240 electrodes (120 on each side) should be developed

with lengths of 6990 µm (6980 µm for rectangular length & 10 µm for triangular tip). Figs. 25 to 28 show a 3D interpretation of the final sample after fabrication.

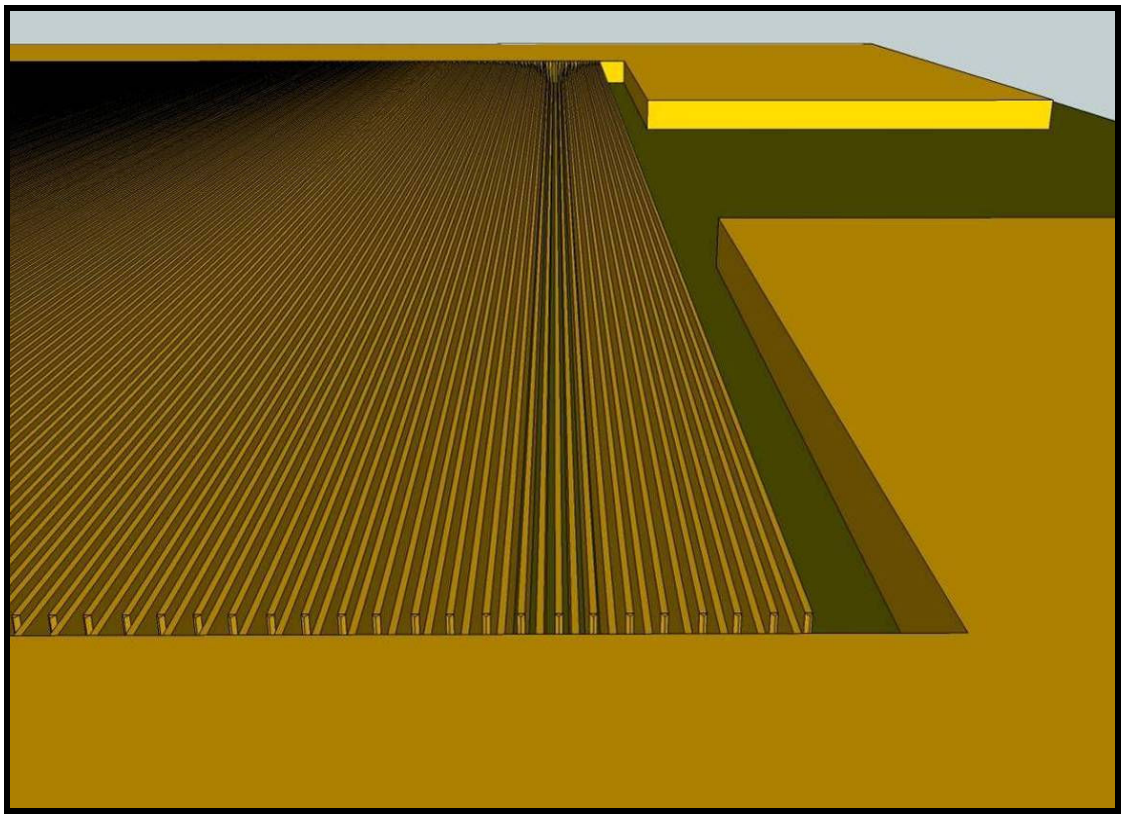

Fig. 25. *3D image interpretation of advanced electrodes design 2 – Angle 1*

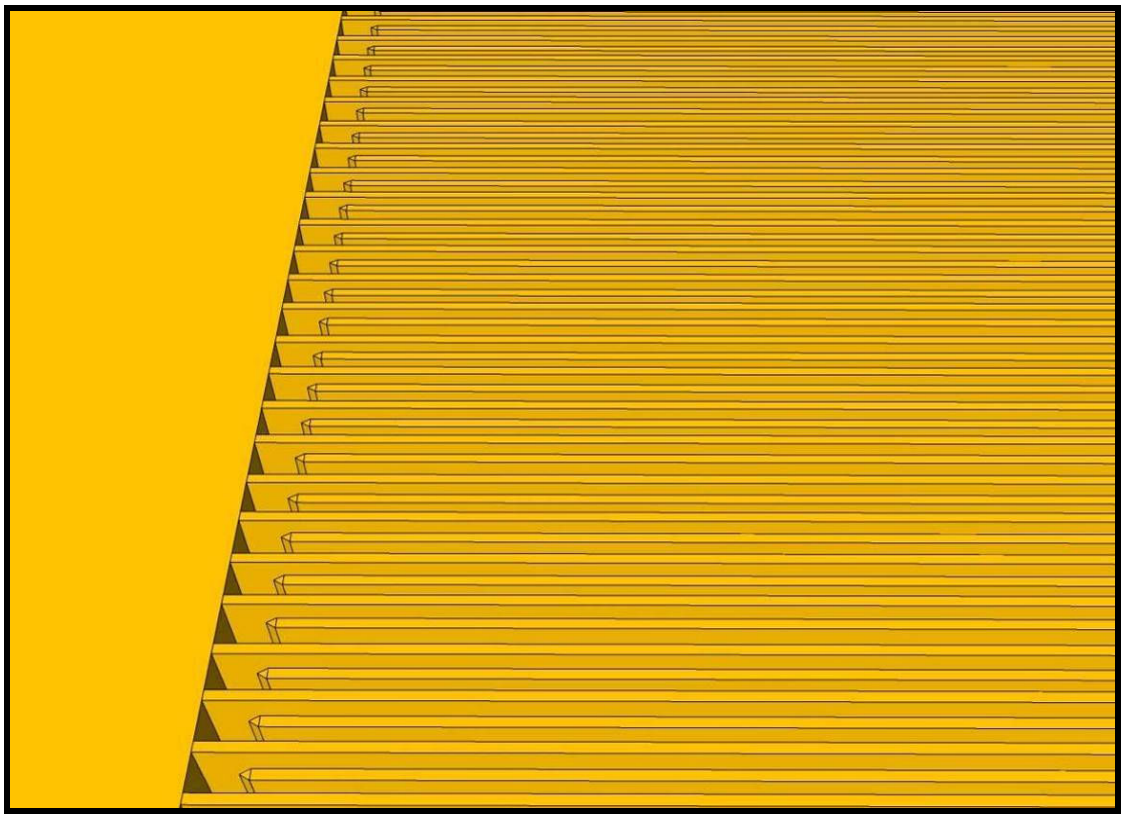

Fig. 26. *3D image interpretation of advanced electrodes design 2 – Angle 2*

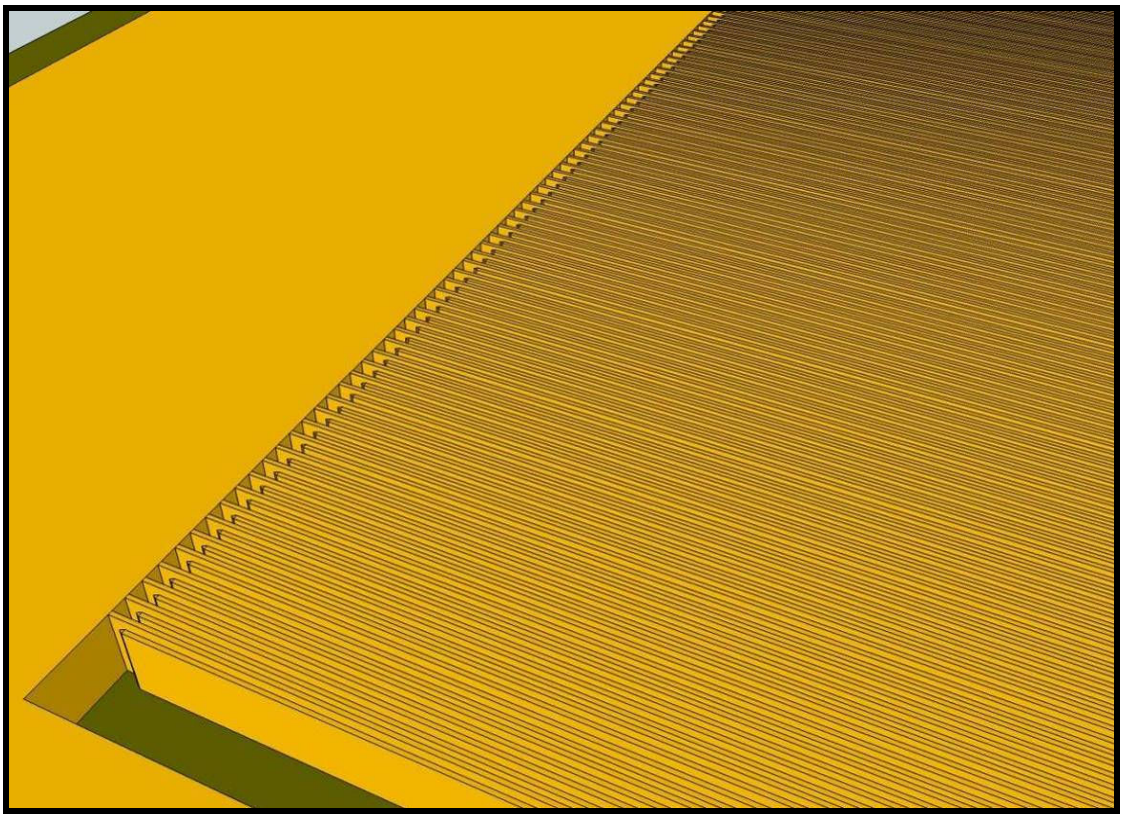

Fig. 27. *3D image interpretation of advanced electrodes design 2 – Angle 3*

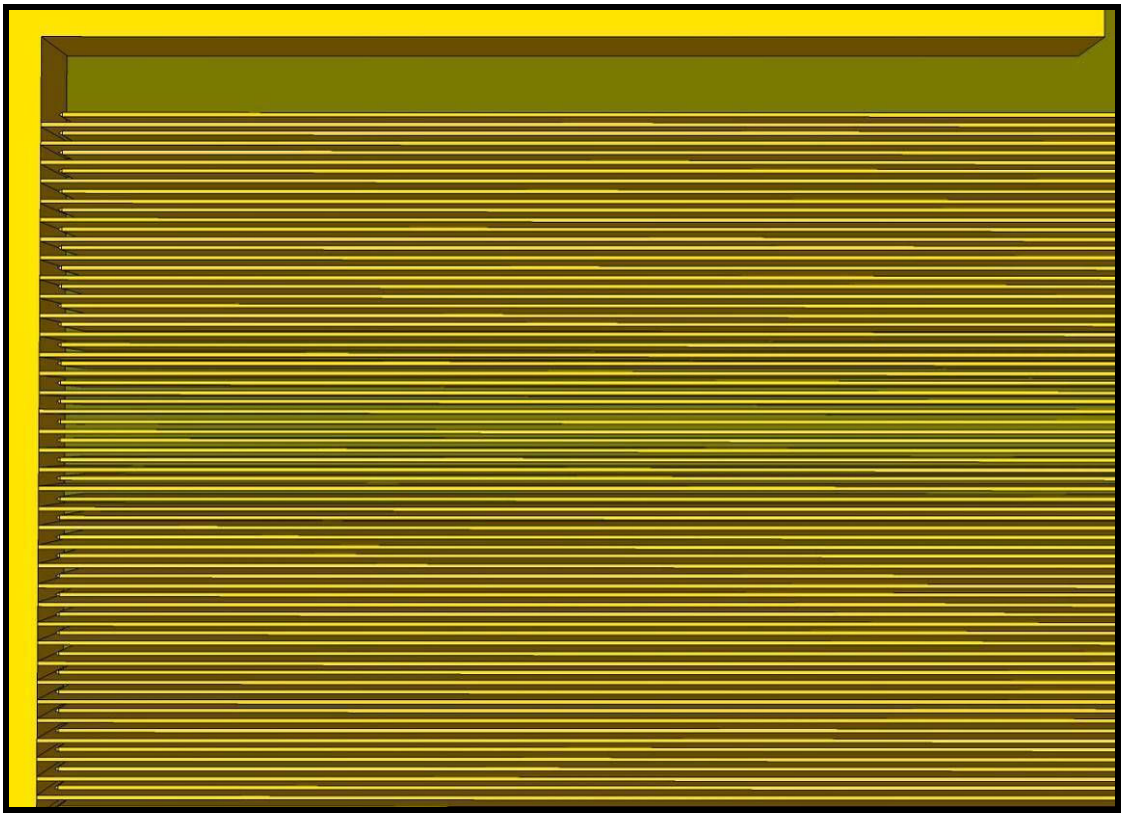

Fig. 28. *3D image interpretation of advanced electrodes design 2 – Angle 4*

4.1.3. ADVANCED ELECTRODE DESIGN 3

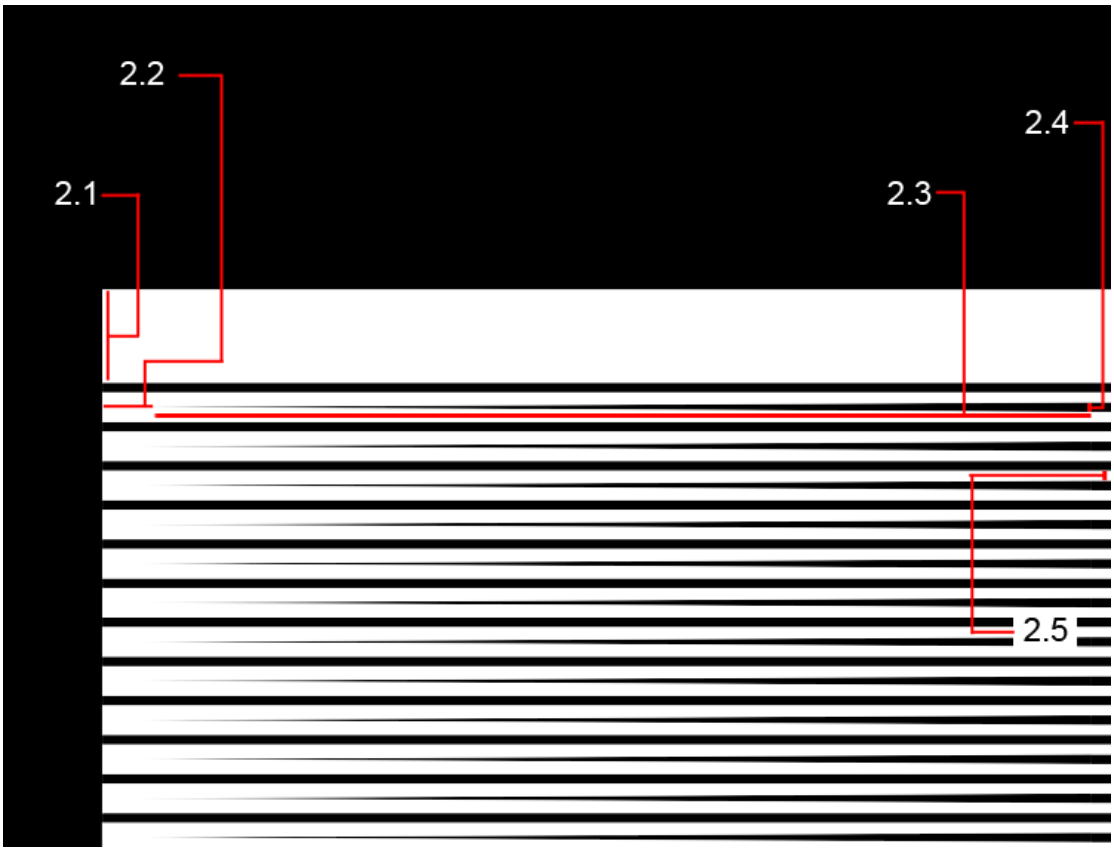

Fig. 29. *Design schematics showing measurements (values in Table 4) for advanced electrodes design 3*

The individual electrodes in Fig. 29 have simple rectangular shape, similar to that of Fig. 24, but have a longer triangular tips at their ends. The following component specifications should be achieved from using table below:

Nanoelectrode Technology		**Microelectrode Technology**	
2.1	25 µm	2.1	90 µm
2.2	500 nm	2.2	10 µm
2.3	50.5 µm	2.3	1000 µm
2.4	1 µm	2.4	10 µm
2.5	500 nm	2.5	10 µm

Table 4. *Size measurements for advanced electrodes design 3 shown on Fig. 29*

For electrode designs in Fig. 29, a total of 166 electrodes (83 on each side) should be developed with lengths of 299.5 µm (179 µm for rectangular length & 50.5 µm for triangular tip), for the nanoelectrode technology. For the micro-electrode technology, a total of 240 electrodes (120 on each side) should be developed with lengths of 6990 µm

(6890 µm for rectangular length & 100 µm for triangular tip). Figs. 30 to 33 show a 3D interpretation of the final sample after fabrication.

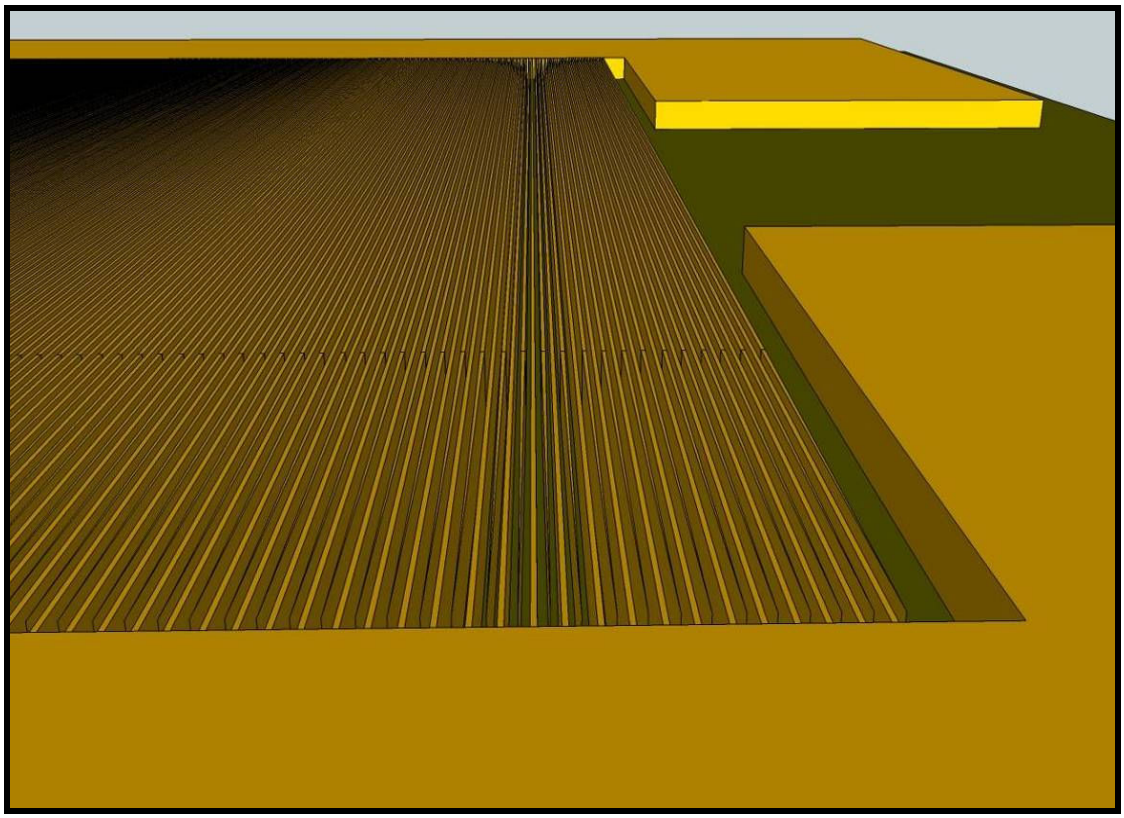

Fig. 30. *3D image interpretation of advanced electrodes design 3 – Angle 1*

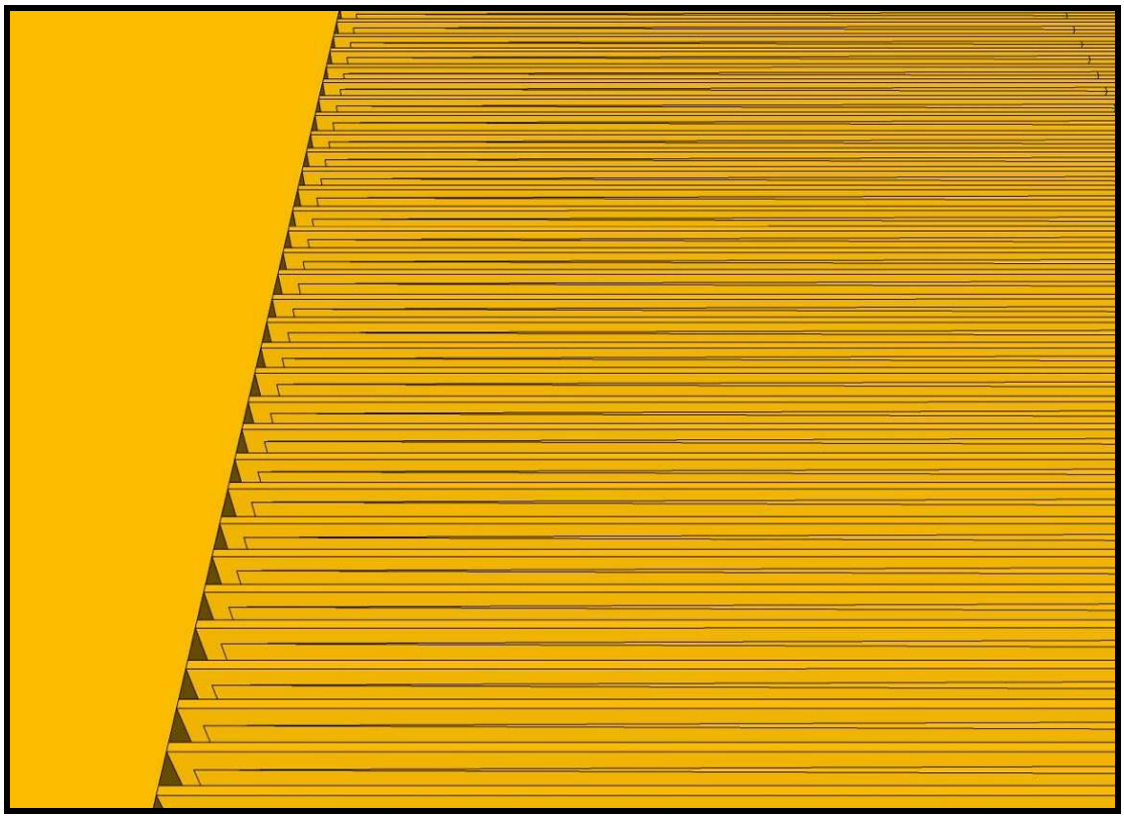

Fig. 31. *3D image interpretation of advanced electrodes design 3 – Angle 2*

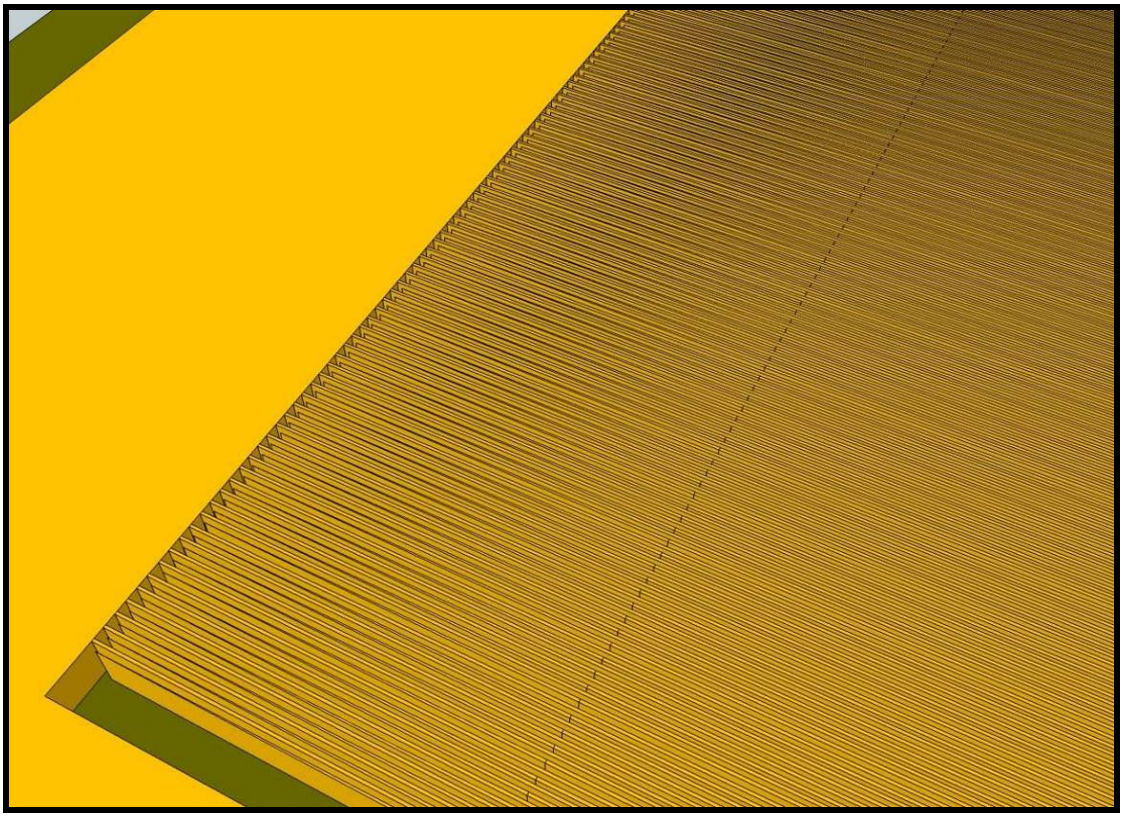

Fig. 32. *3D image interpretation of advanced electrodes design 3 – Angle 3*

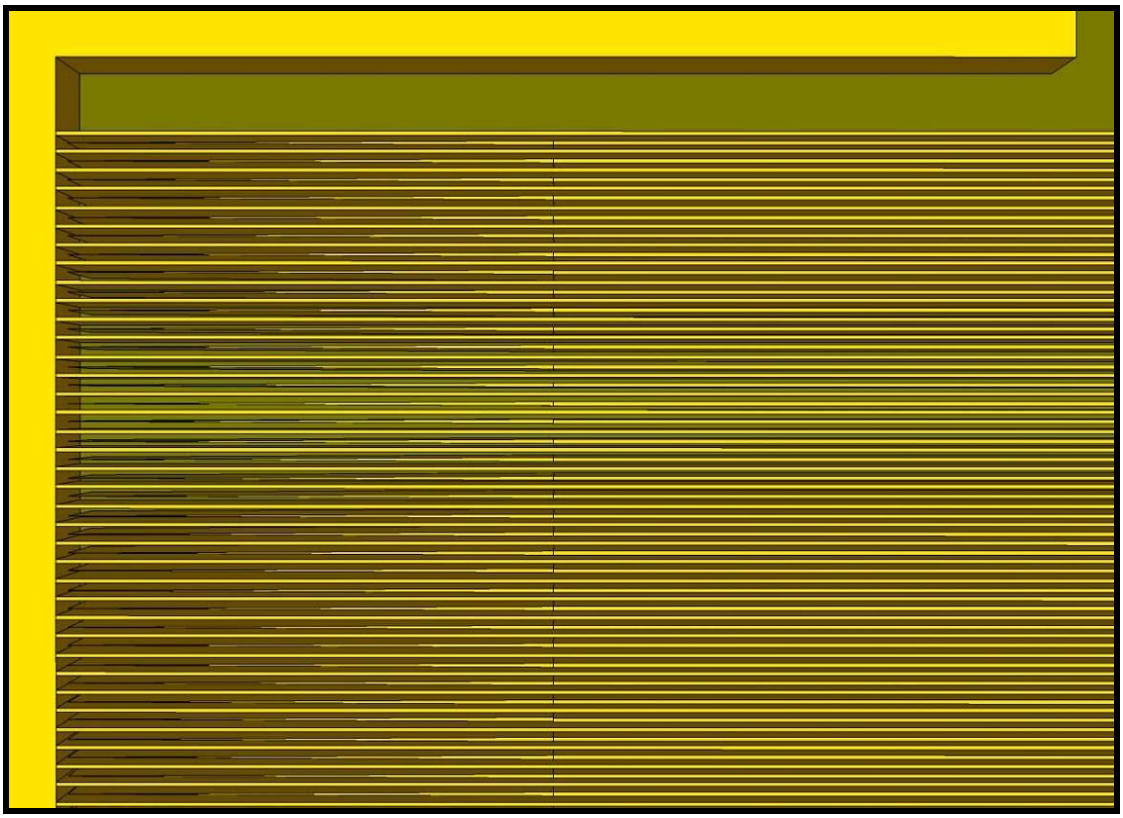

Fig. 33. *3D image interpretation of advanced electrodes design 3 – Angle 4*

4.1.4. ADVANCED ELECTRODE DESIGN 4

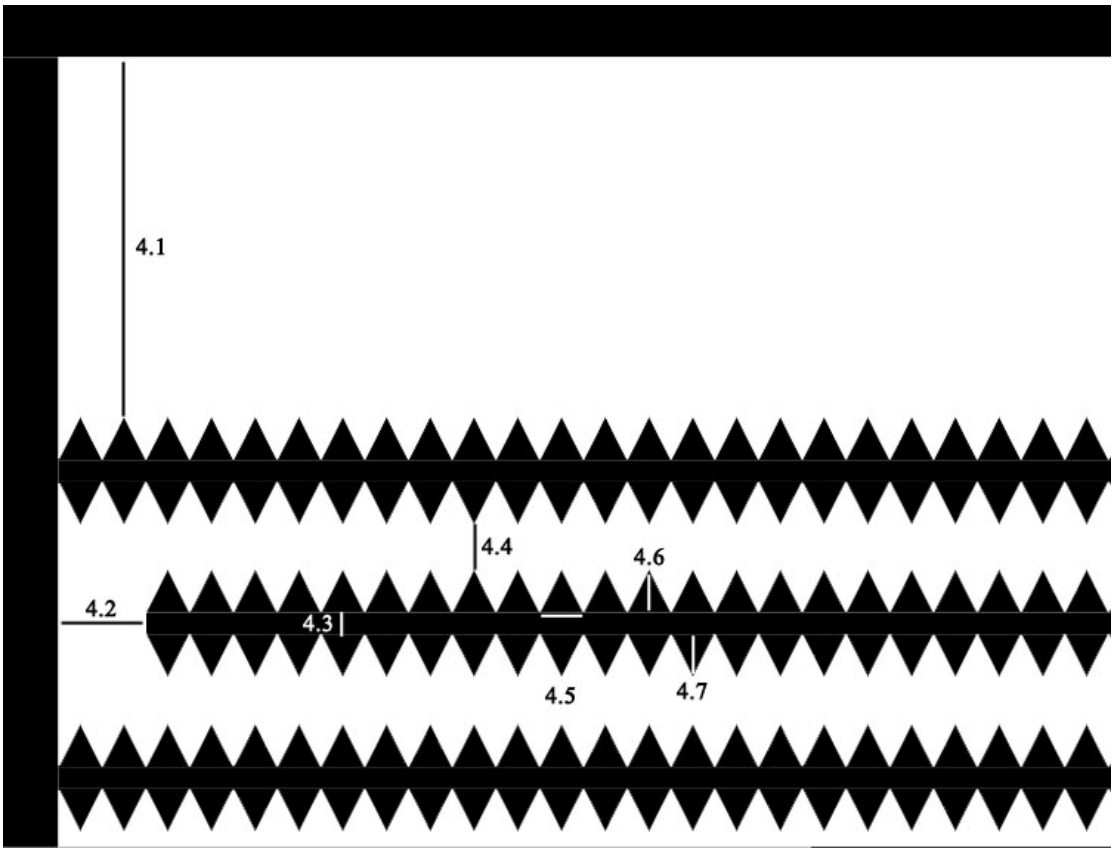

Fig. 34. *Design schematics showing measurements (values in Table 5) for advanced electrodes design 4*

The electrodes in Fig. 34 have simple rectangular shape surround by teeth. The following component specifications should be achieved from using table below:

Nanoelectrode Technology		Microelectrode Technology	
4.1	25 µm	4.1	95 µm
4.2	500 nm	4.2	40 µm
4.3	1 µm	4.3	10 µm
4.4	500 nm	4.4	20 µm
4.5	500 nm	4.5	20 µm
4.6	500 nm	4.6	20 µm
4.7	500 nm	4.7	20 µm

Table 5. *Size measurements for advanced electrodes design 4 shown on Fig. 34*

For electrode designs in Fig. 34, a total of 110 electrodes (55 on each side) should be developed with lengths of 299.5 µm, for the nanoelectrode technology. For the micro-electrode technology, a total of 68 electrodes (34 on each side) should be developed

with lengths of 6990 µm. Figs. 35 to 38 show a 3D interpretation of the final sample after fabrication.

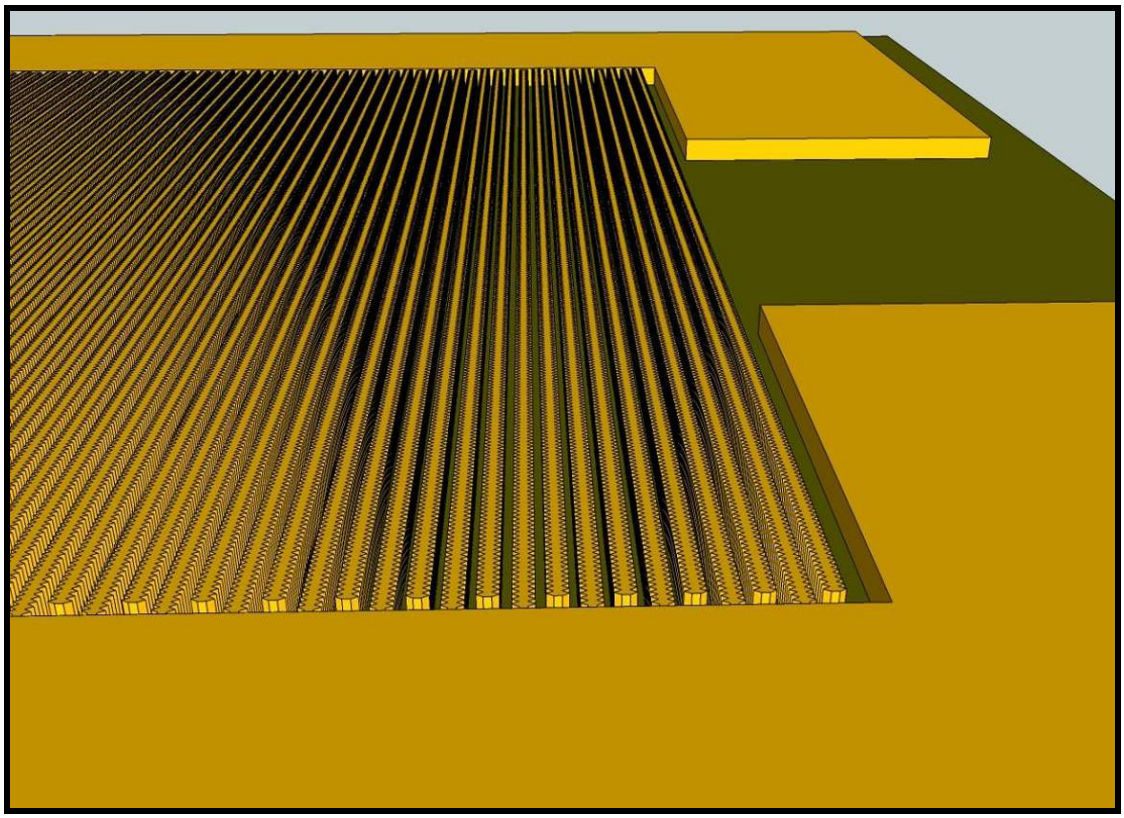

Fig. 35. *3D image interpretation of advanced electrodes design 4 – Angle 1*

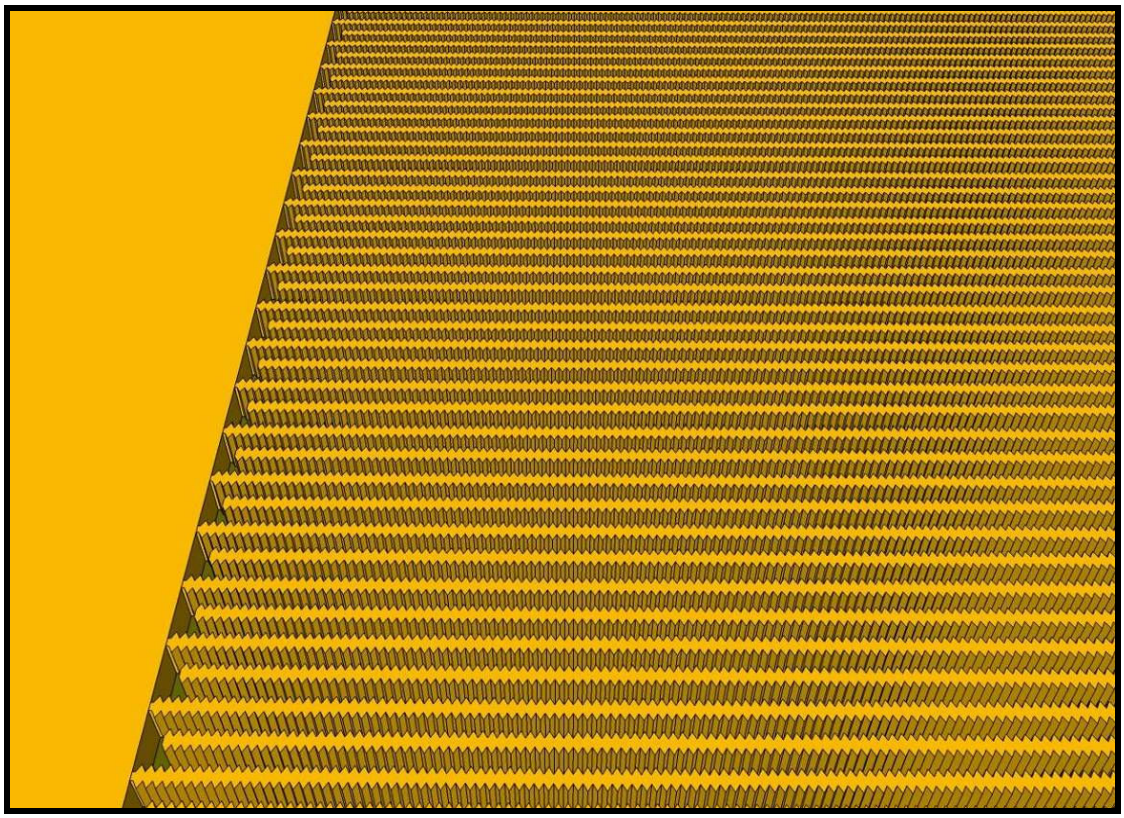

Fig. 36. *3D image interpretation of advanced electrodes design 4 – Angle 2*

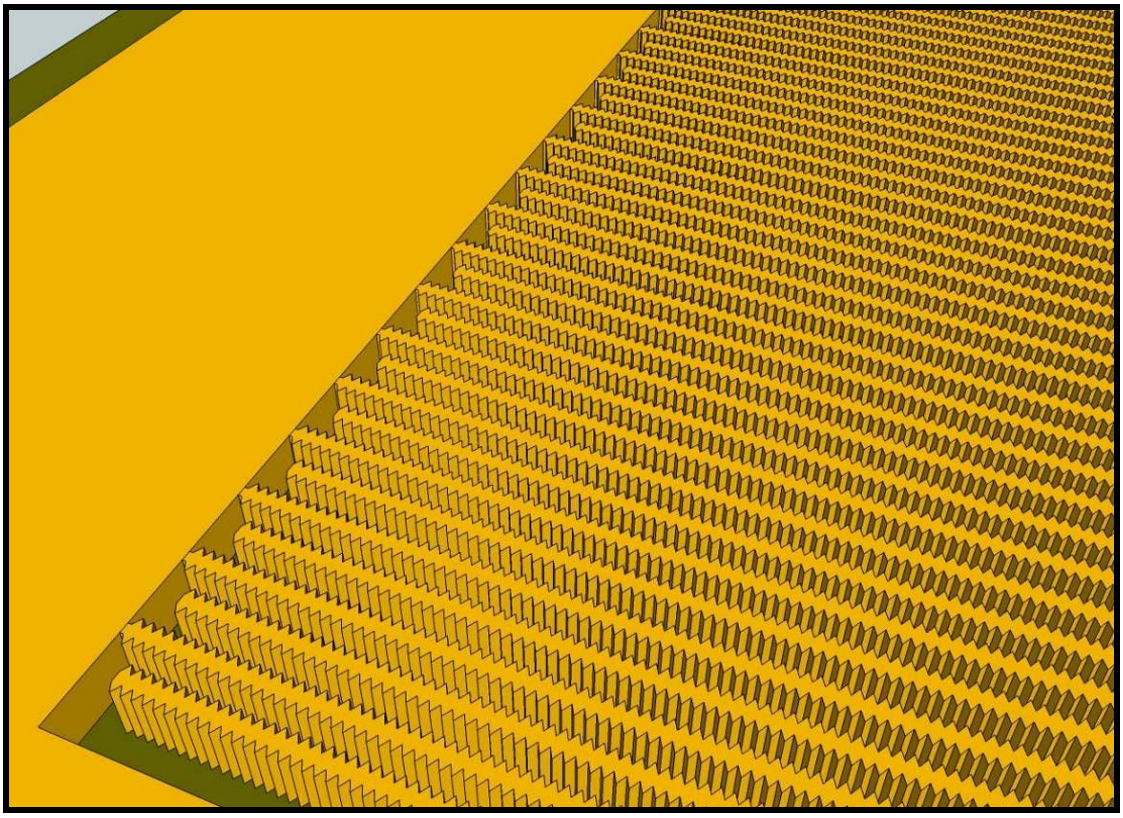

Fig. 37. *3D image interpretation of advanced electrodes design 4 – Angle 3*

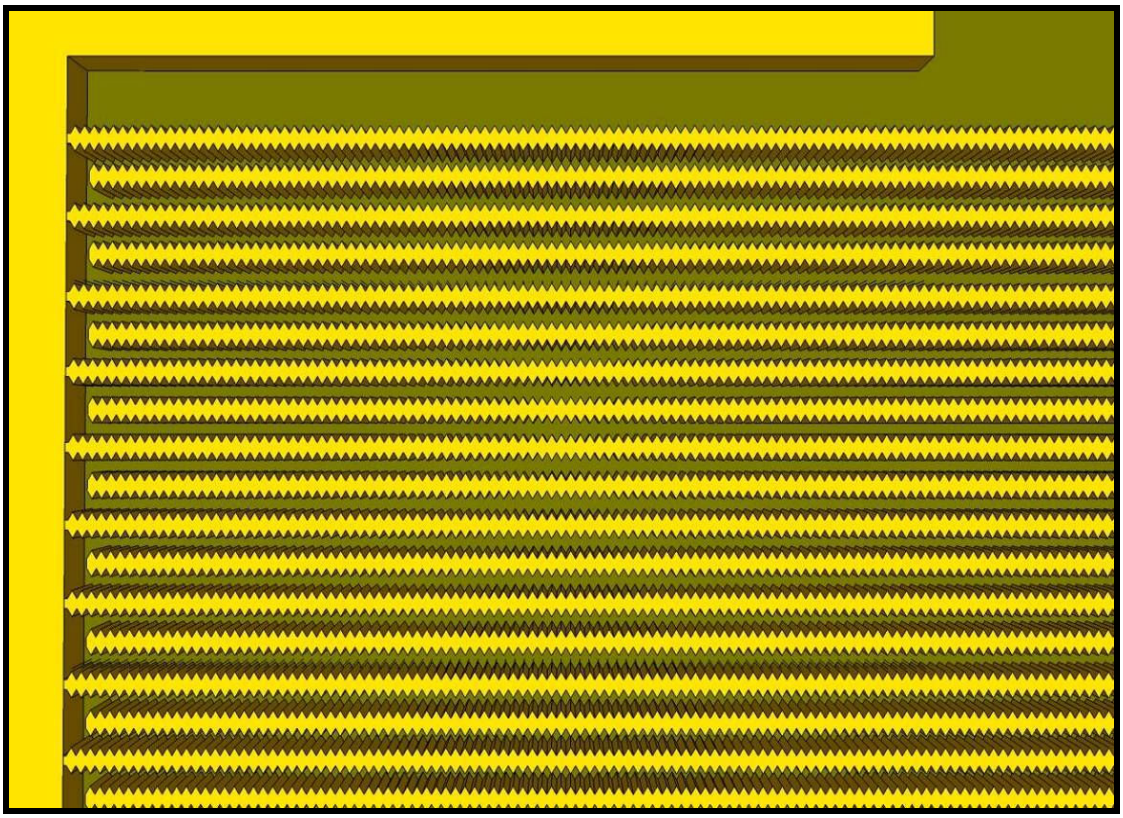

Fig. 38. *3D image interpretation of advanced electrodes design 4 – Angle 4*

4.1.5. ADVANCED ELECTRODE DESIGN 5

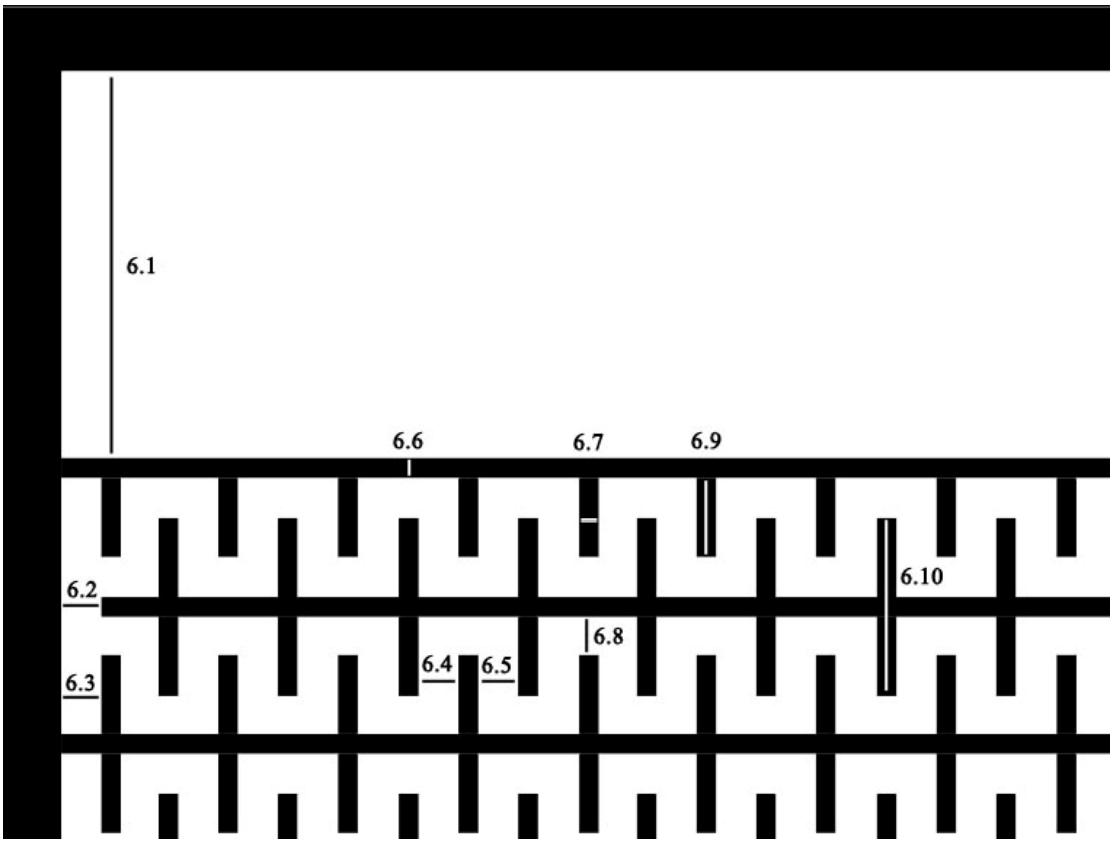

Fig. 39. *Design schematics showing measurements (values in Table 6) for advanced electrodes design 5*

The electrodes in Fig. 39, have simple rectangular shape, with minor interdigitated electrodes facing vertically. The following component specifications should be achieved from using table below:

NanoElectrode Technology		**Micro-Electrode Technology**	
6.1	25 µm	6.1	125 µm
6.2	500 nm	6.2	50 µm
6.3	500 nm	6.3	50 µm
6.4	500 nm	6.4	20 µm
6.5	500 nm	6.5	20 µm
6.6	1 µm	6.6	10 µm
6.7	1 µm	6.7	10 µm
6.8	500 nm	6.8	20 µm
6.9	1.5 µm	6.9	50 µm
6.10	4 µm	6.10	110 µm

Table 6. *Size measurements for advanced electrodes design 5 shown on Fig. 39*

For nanoelectrode designs in Fig. 39, a total of 100 electrodes (50 on each side) should be developed with lengths of 299.5 μm. For the micro-electrode technology, a total of 60 electrodes (30 on each side) should be developed with lengths of 6990 μm. Figs. 40 to 43 show a 3D interpretation of the final sample after fabrication.

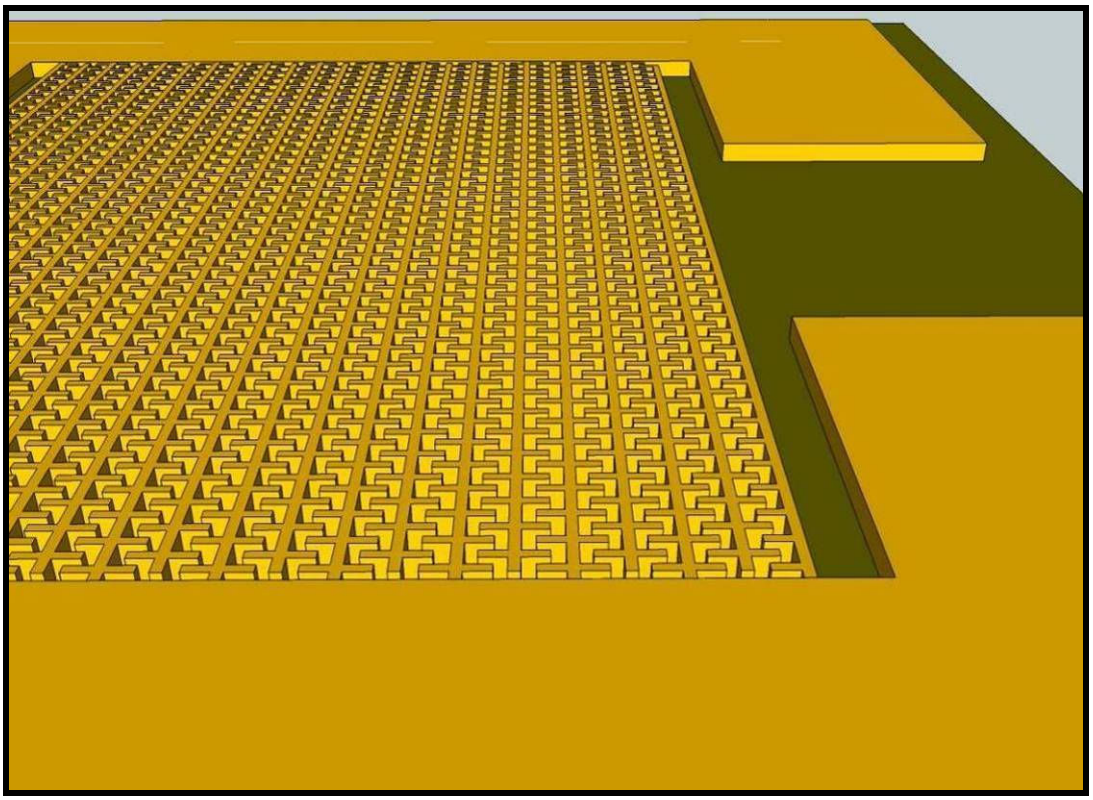

Fig. 40. *3D image interpretation of advanced electrodes design 5 – Angle 1*

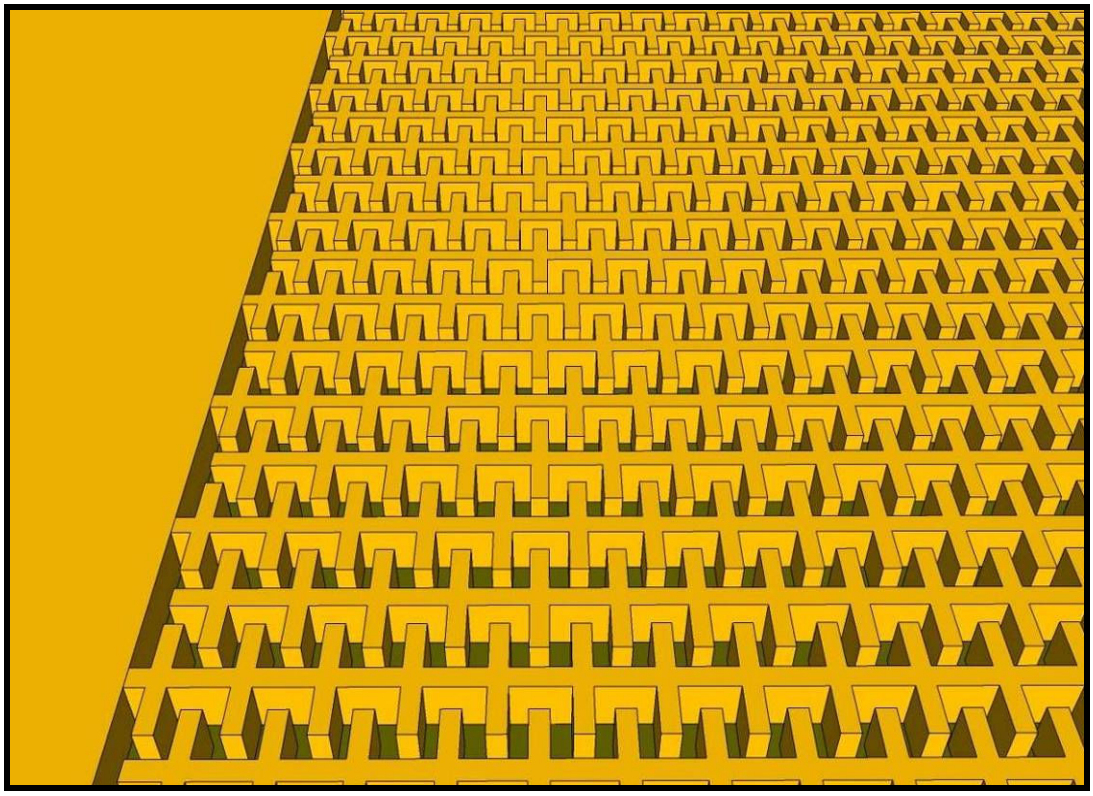

Fig. 41. *3D image interpretation of advanced electrodes design 5 – Angle 2*

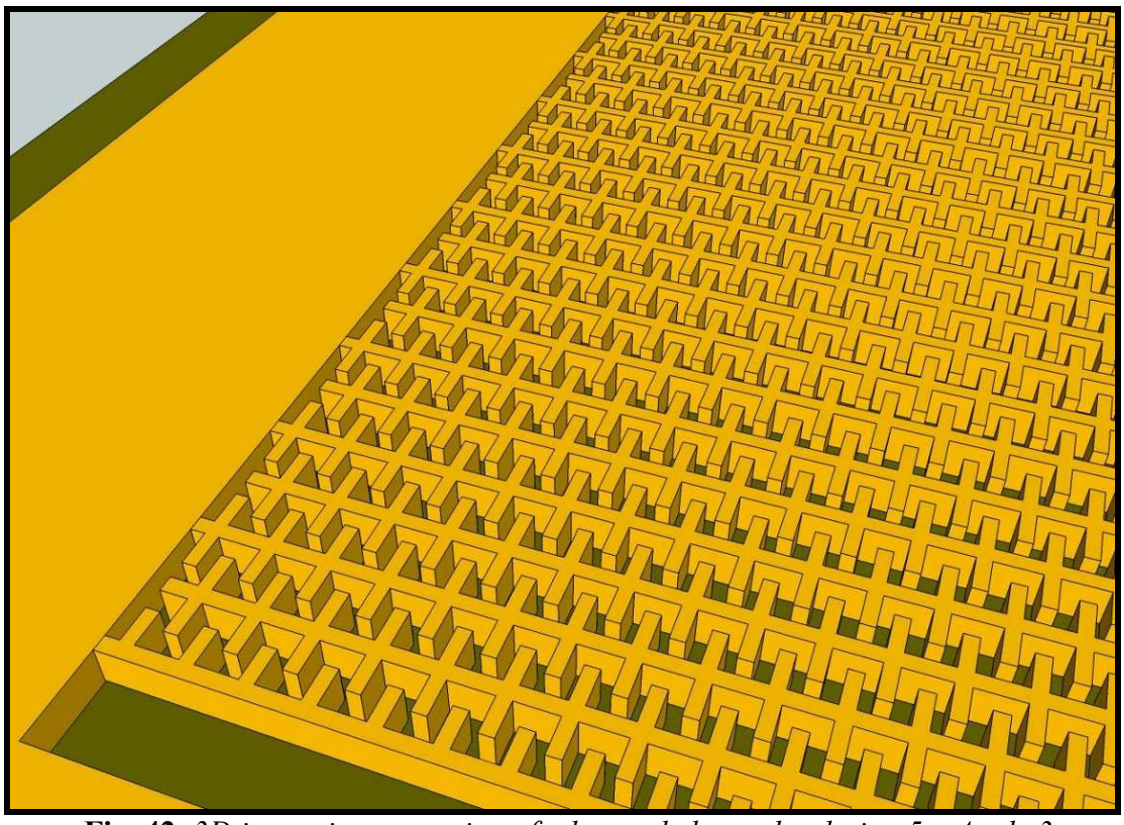

Fig. 42. *3D image interpretation of advanced electrodes design 5 – Angle 3*

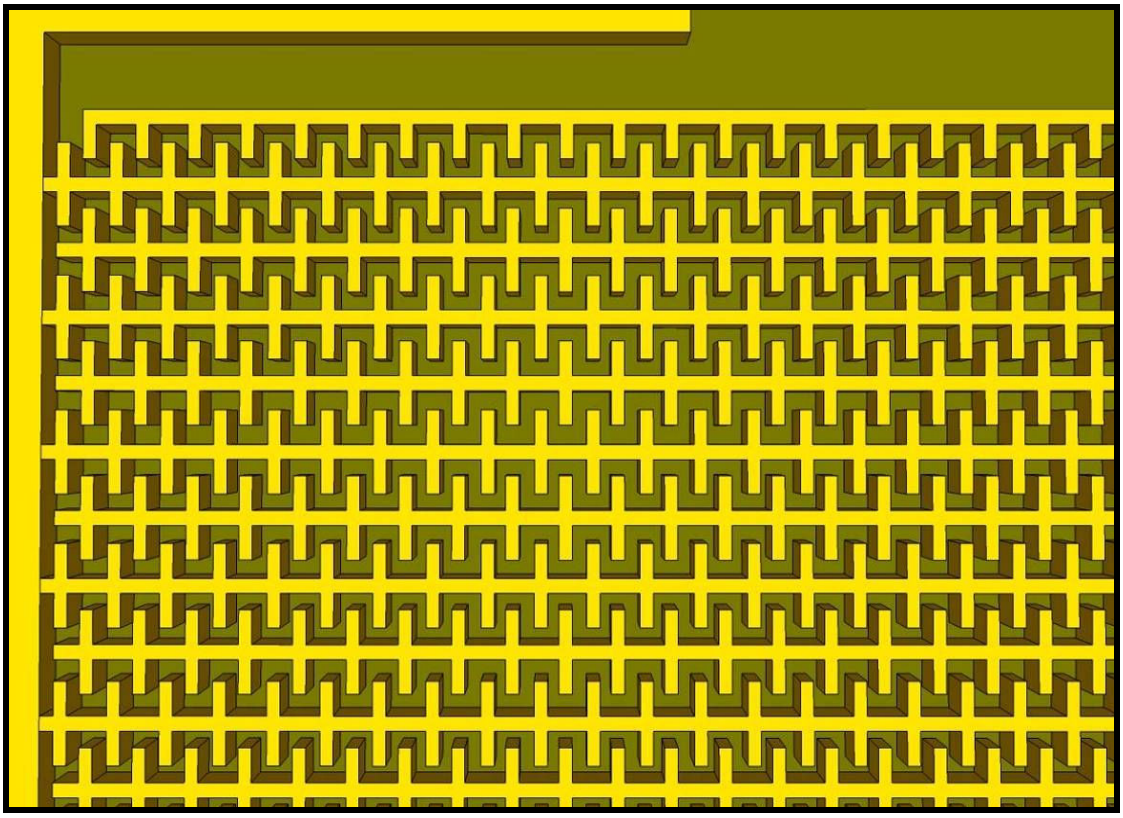

Fig. 43. *3D image interpretation of advanced electrodes design 5 – Angle 4*

4.1.6. NANOELECTRODE MEASUREMENT CONTACT PADS DESIGN

The electrical measurement contact pads layer is the second lithography level for the nanoelectrodes technology. The measurement pads will be exposed by photolithography using an optical lithography mask with the design on Figs. 44 and 45. The devices, generated from e-beam lithography are each individually centered on the contacts.

The following materials will be evaporated after successful lithography processes:
Layer 1(Bottom layer): Aluminium (Al), 100 nm thick
Layer 2: Gold (Au), Capping layer 50 nm thick

The contact pads are obtained by lift-off, soaking the substrate in acetone for adequate time.

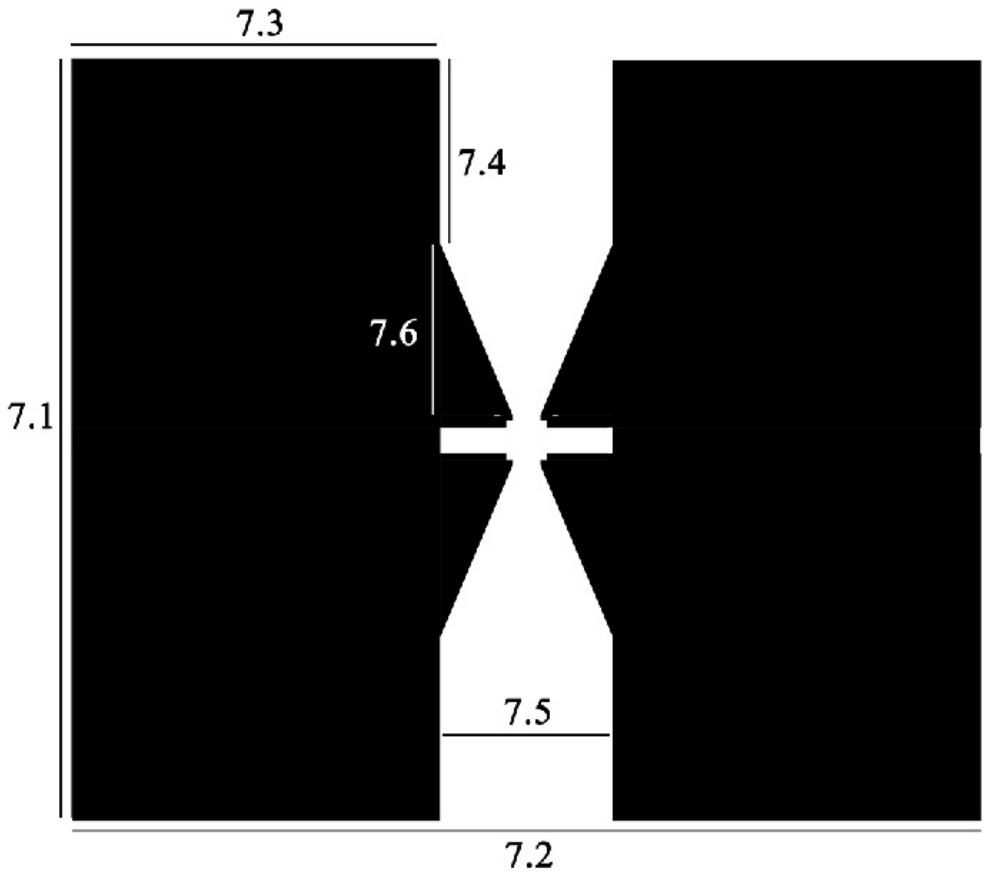

Fig. 44. *Size measurements for the nanoelectrode contact pads shown on table 7*

The following specifications should be achieved for Fig. 44:

Fig. 44	
7.1	6.2 mm
7.2	7.4 mm
7.3	3 mm
7.4	1.5 mm
7.5	1.4 mm
7.6	1.4 mm

Table 7. *Size measurements nanoelectrode measurement contact pads on Fig. 44*

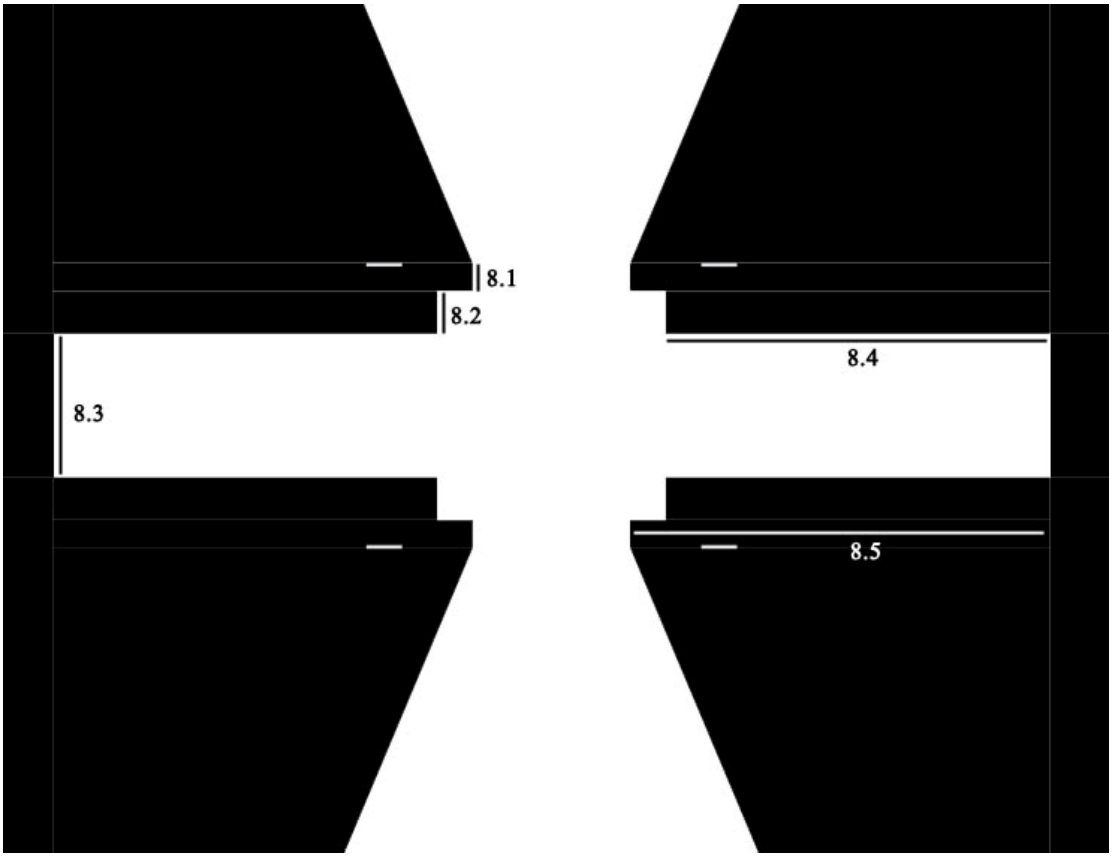

Fig. 45. *Close-up size measurements for the nanoelectrode contact pads shown on table 8*

The following specifications should be achieved for Fig. 45:

Fig. 45	
8.1	0.04 mm
8.2	0.06 mm
8.3	0.2 mm
8.4	0.54 mm
8.5	0.59 mm

Table 8. *Size measurements for close-up nanoelectrode measurement contact pads on Fig. 45*

Figs. 46 to 49 show a 3D interpretation of the final sample after fabrication.

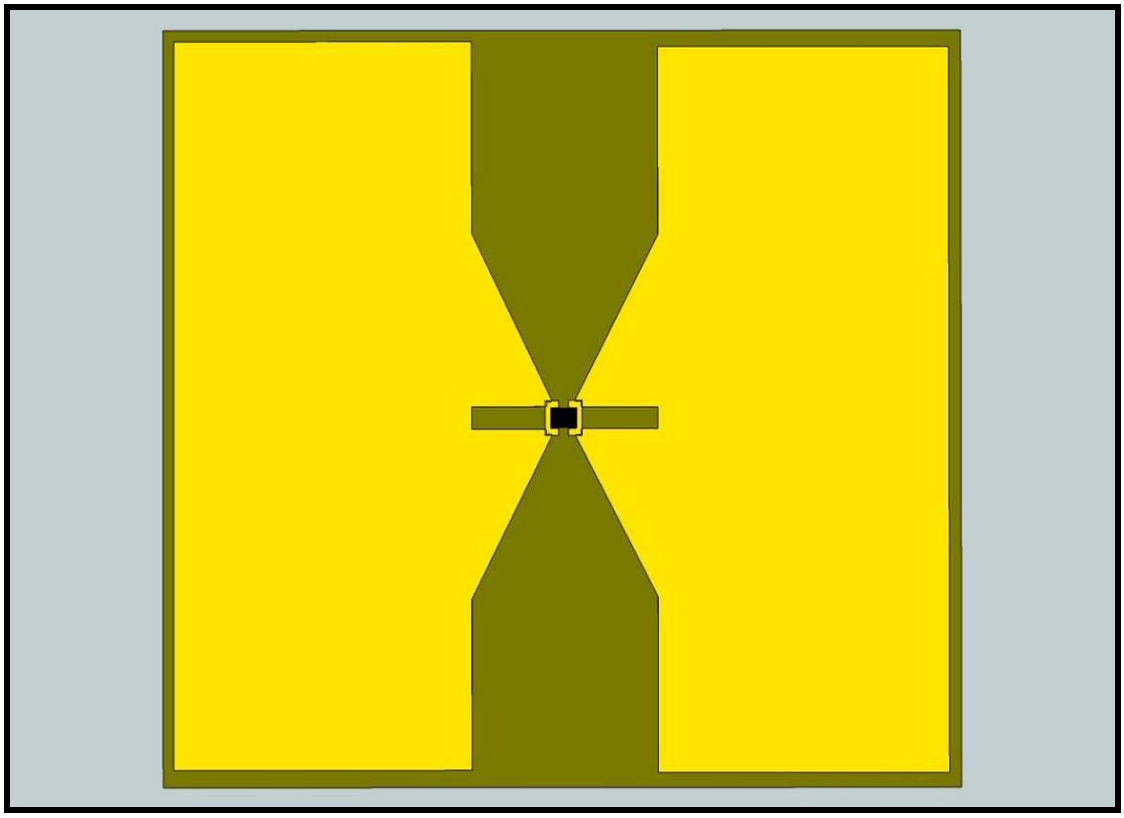

Fig. 46. *3D image interpretation the nanoelectrode contact pads – Angle 1*

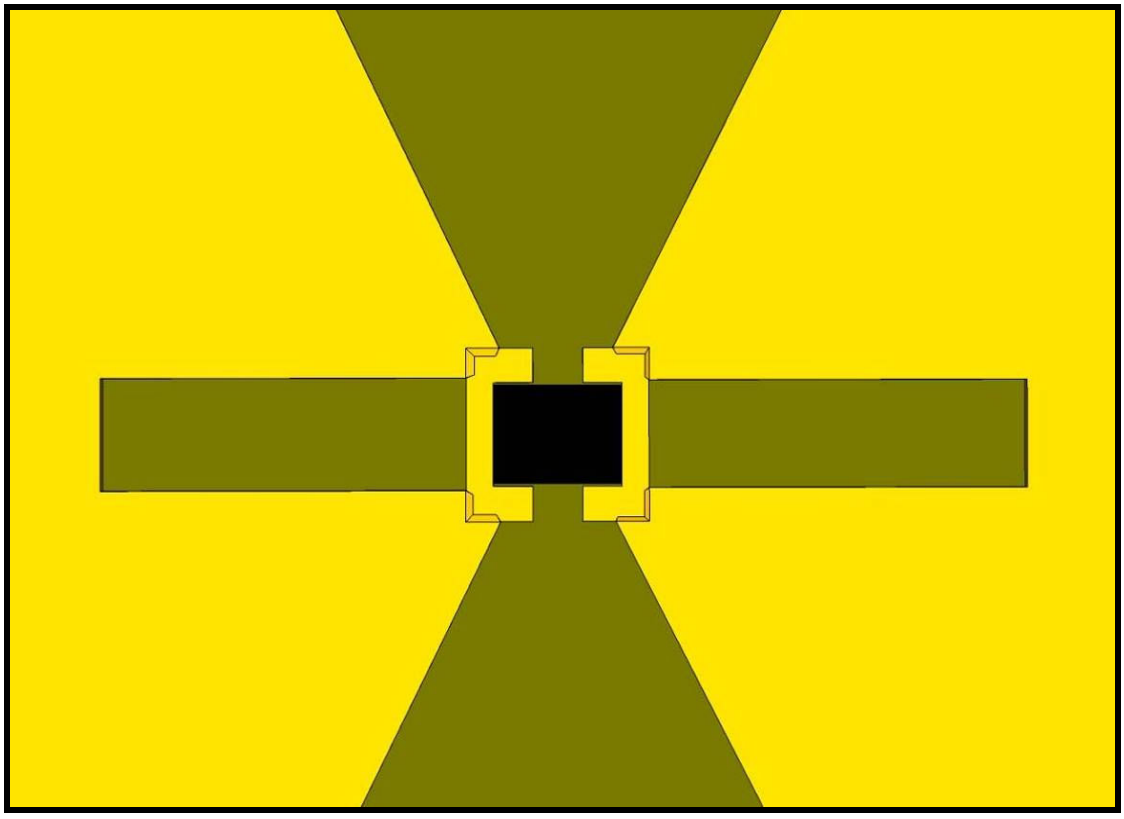

Fig. 47. *3D image interpretation the nanoelectrode contact pads – Angle 2*

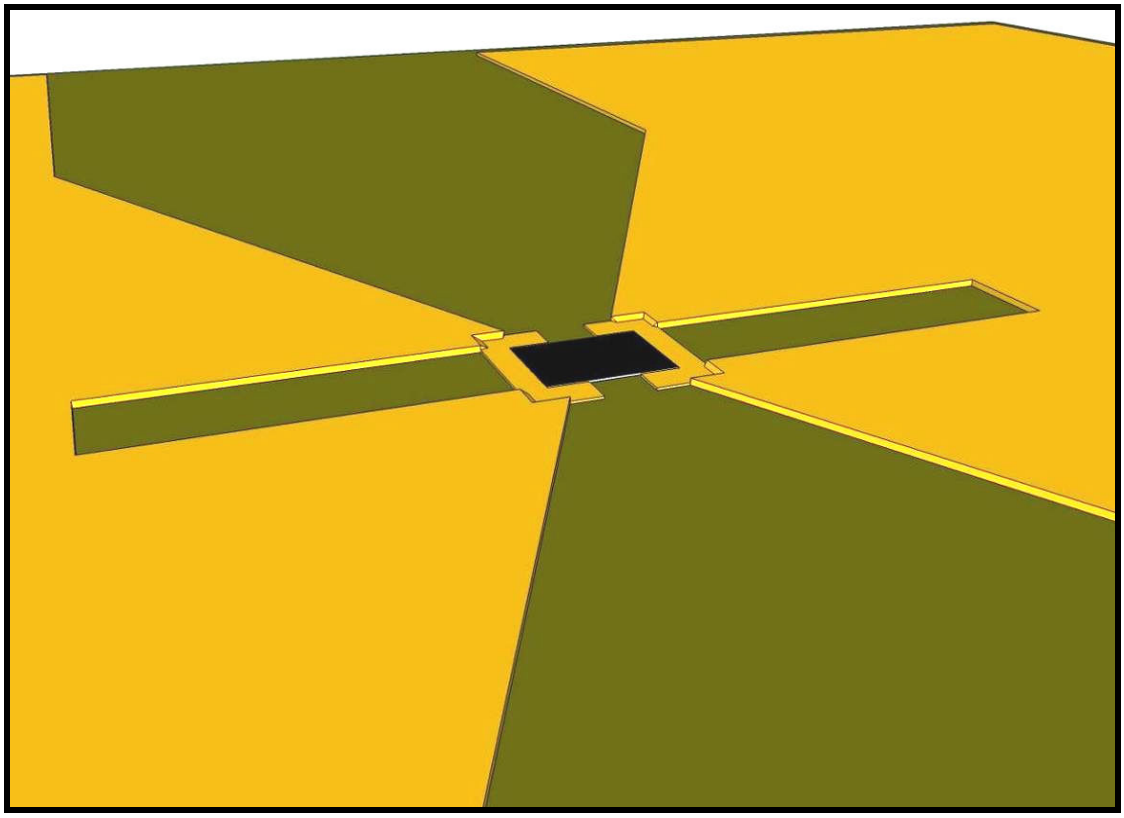

Fig. 48. *3D image interpretation the nanoelectrode contact pads – Angle 3*

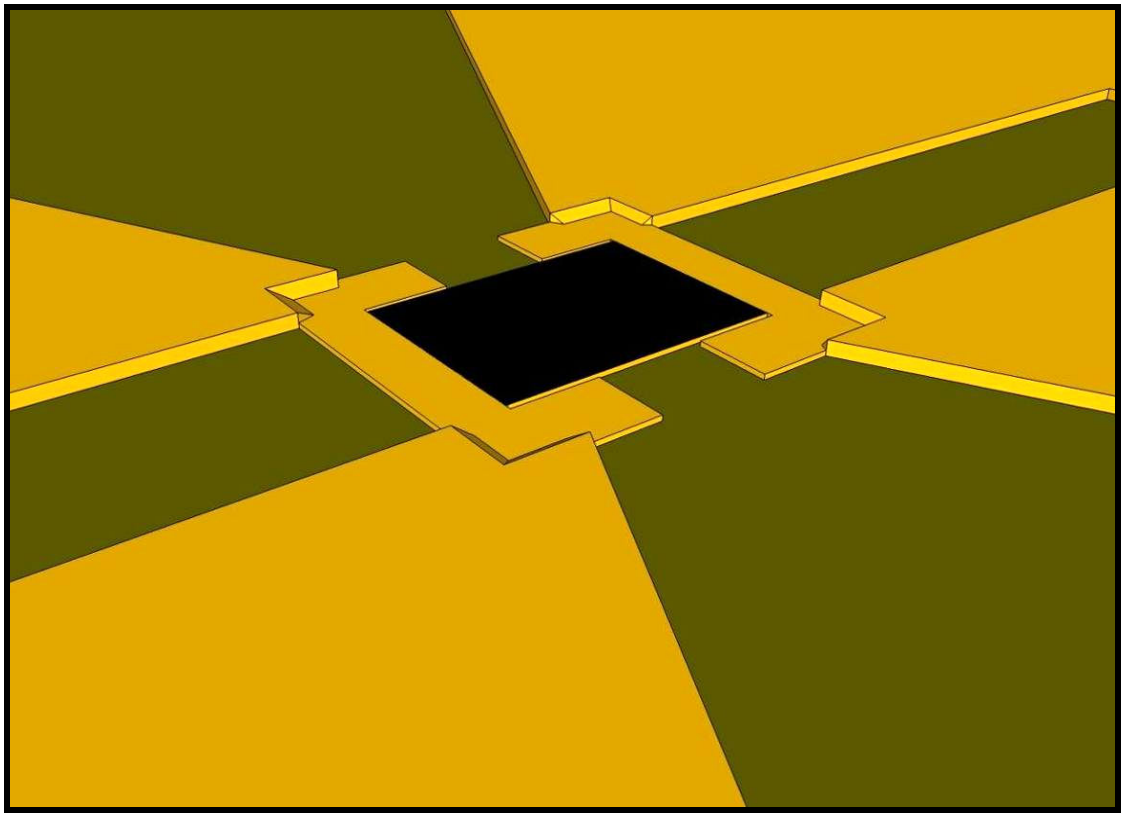

Fig. 49. *3D image interpretation the nanoelectrode contact pads – Angle 4*

4.2. COMPONENT 2: MWNT-SPQD-ANTIBODY NANOPARTICLE HYBRID

The final SPQD/Monoclonal Antibody/MWNT product should be produced with the following characteristics and measurements:

- SPQD: Fe_2O_3 superparamagnetic cores - 10nm diameter (Part 9.3 in Fig. 50)
- SPQD: 1st Outer Layer: Cadmium Selenide (CdSe) Quantum Dot – 4nm addition in diameter to Fe_2O_3 core (Part 9.4 in Fig. 50)
- SPQD: 2nd Outer Layer: Zinc Sulphide (ZnS) – 4 nm addition in diameter to CdSe/Fe_2O_3 (Part 9.5 in Fig. 50)
- SPQD: Total size of particle: 18 nm
- Monoclonal Antibody attached onto SPQD through Avidin or Strepavidin (Part 9.6 in Fig. 50)
- Monoclonal Antibody/SPQD bioconjugate attached onto MWNT, with dimensions of 500 nm to 1 μm (Part 9.1 in Fig. 50) by 5 nm (Part 9.2 in Fig. 50), through covalent conjugation of COOH groups.

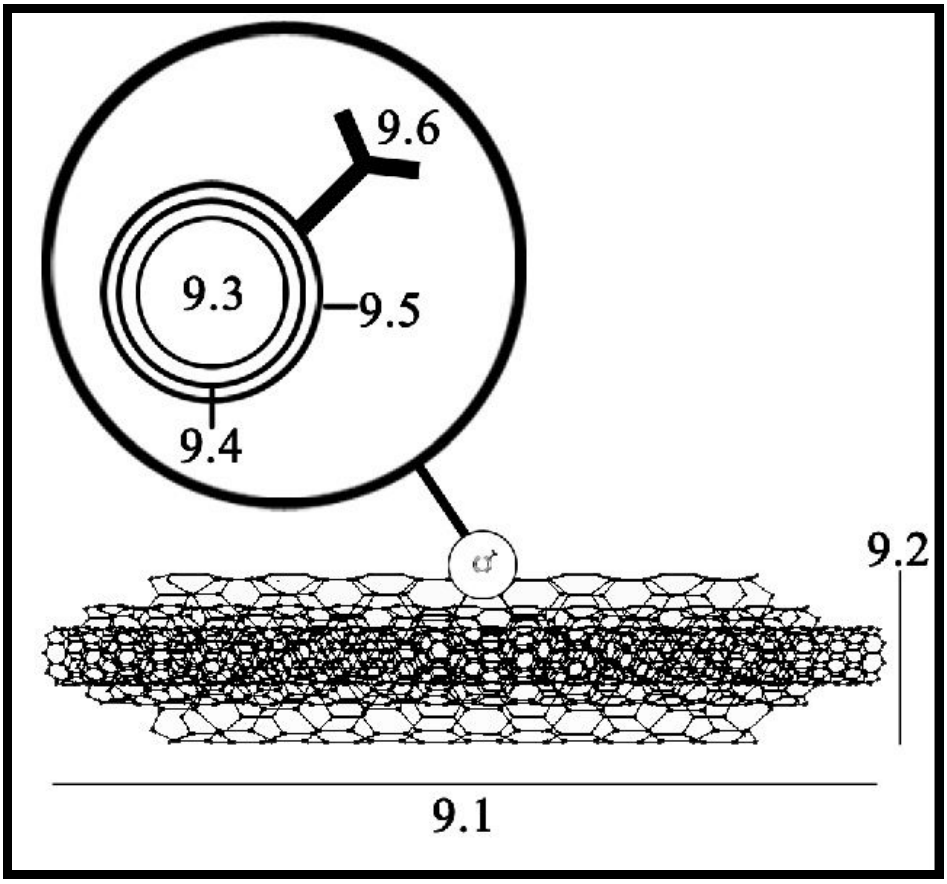

Fig. 50. *Design schematics showing measurements (values in Section 4.2) for MWNT-SPQD-Antibody Nanoparticle Hybrid*

Once constructed, the nanoparticle hybrids will be prepared in a perfectly dispersed aqueous solution. This will be used for the cancer cell isolation system and will be excited with UV light right before the process, to excite the SPQD component of each nanoparticle hybrid. This will be used for fluorescence imaging and tracking of the nanoparticles throughout the process. Throughout Figs. 51 to 56, we can see how the SPQD-Antibody bioconjugate is placed on top of the MWNT. The yellow outer layer represents the ZnS, the green inner layer represents CdSe and the grey core represents Fe_2O_3 particle. Attached onto the SPQD is the purple coloured antibody.

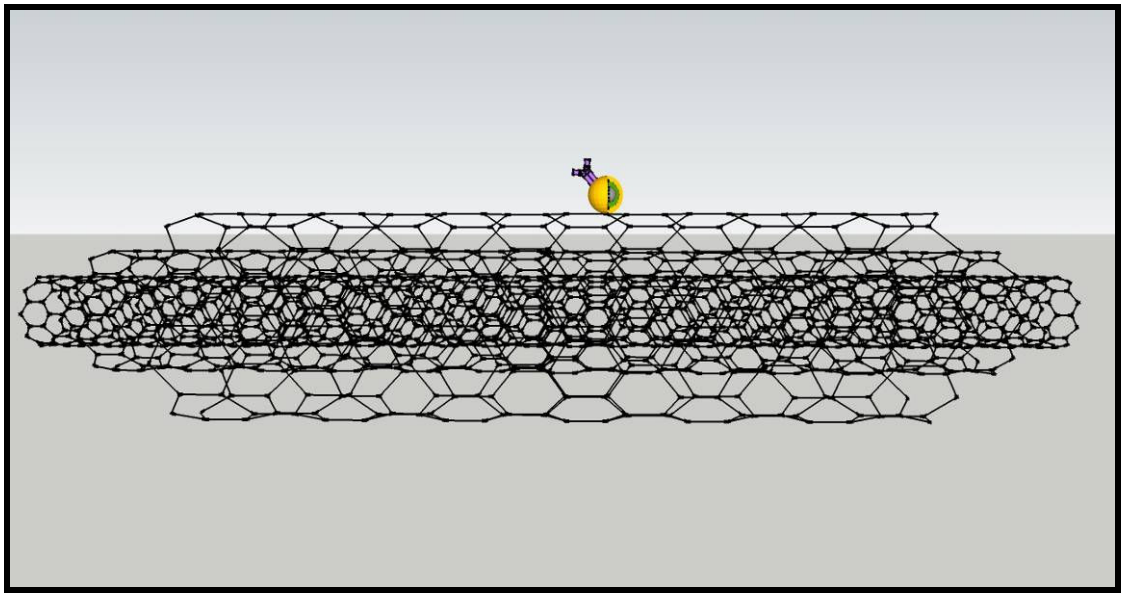

Fig. 51. *3D image interpretation of MWNT-SPQD-Antibody NP Hybrid – Angle 1*

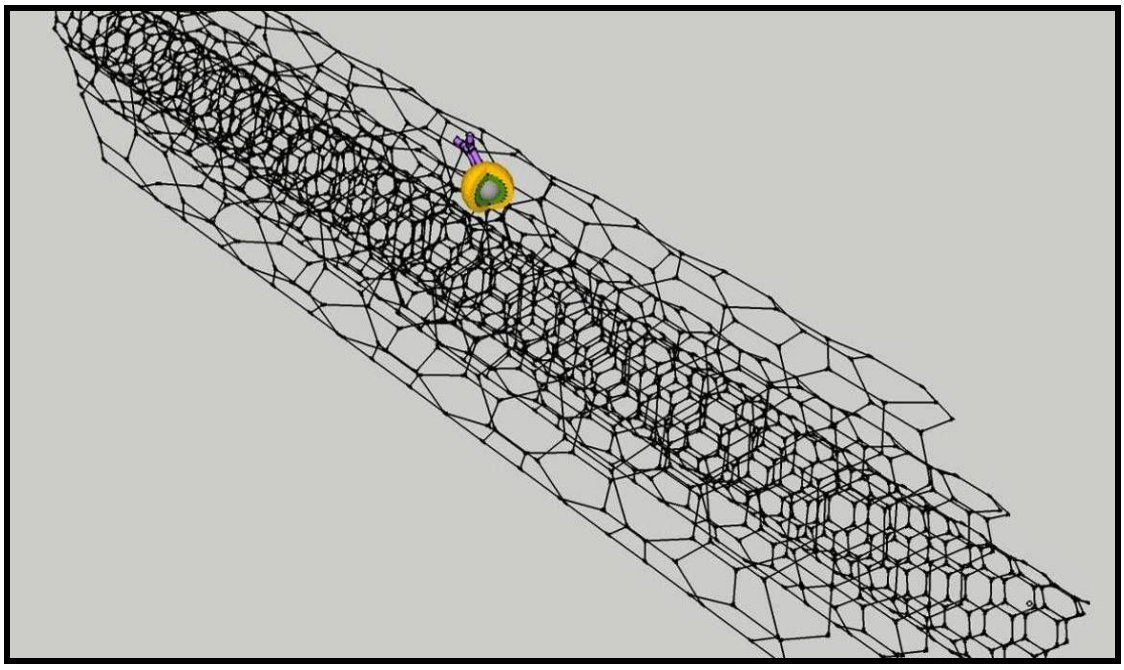

Fig. 52. *3D image interpretation of MWNT-SPQD-Antibody NP Hybrid – Angle 2*

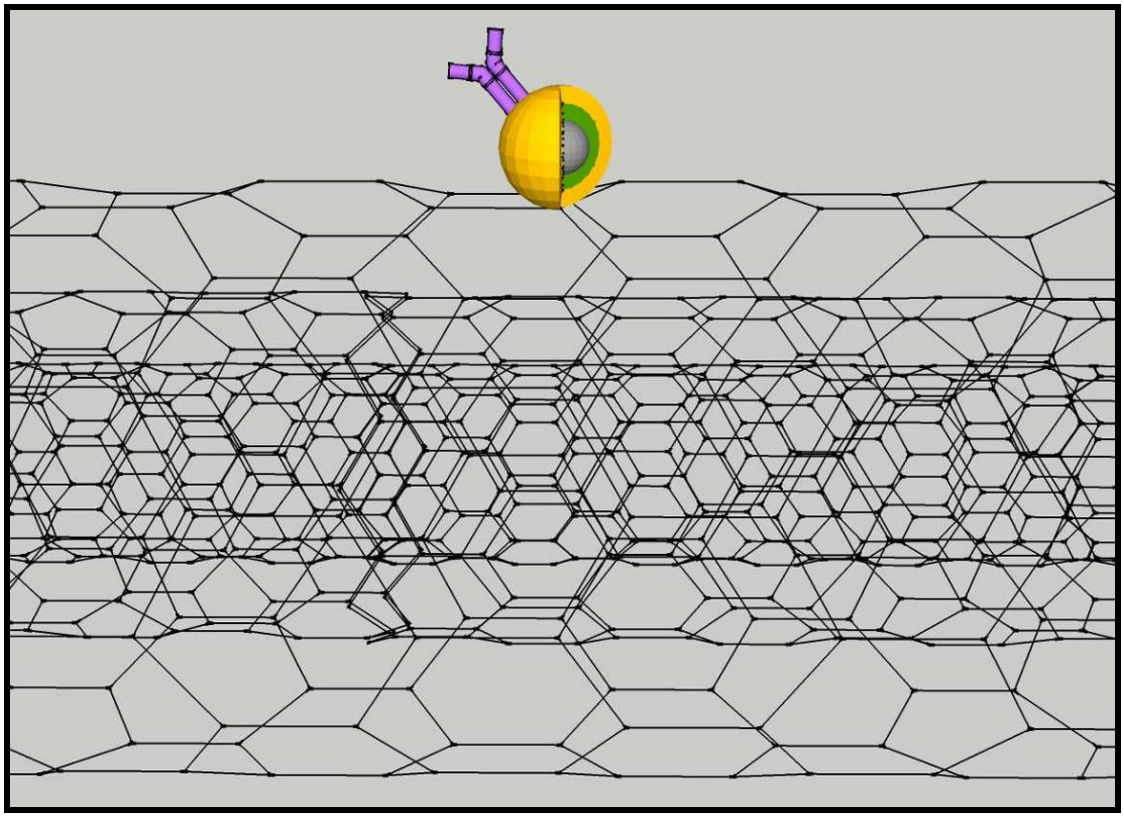

Fig. 53. *3D image interpretation of MWNT-SPQD-Antibody NP Hybrid – Angle 3*

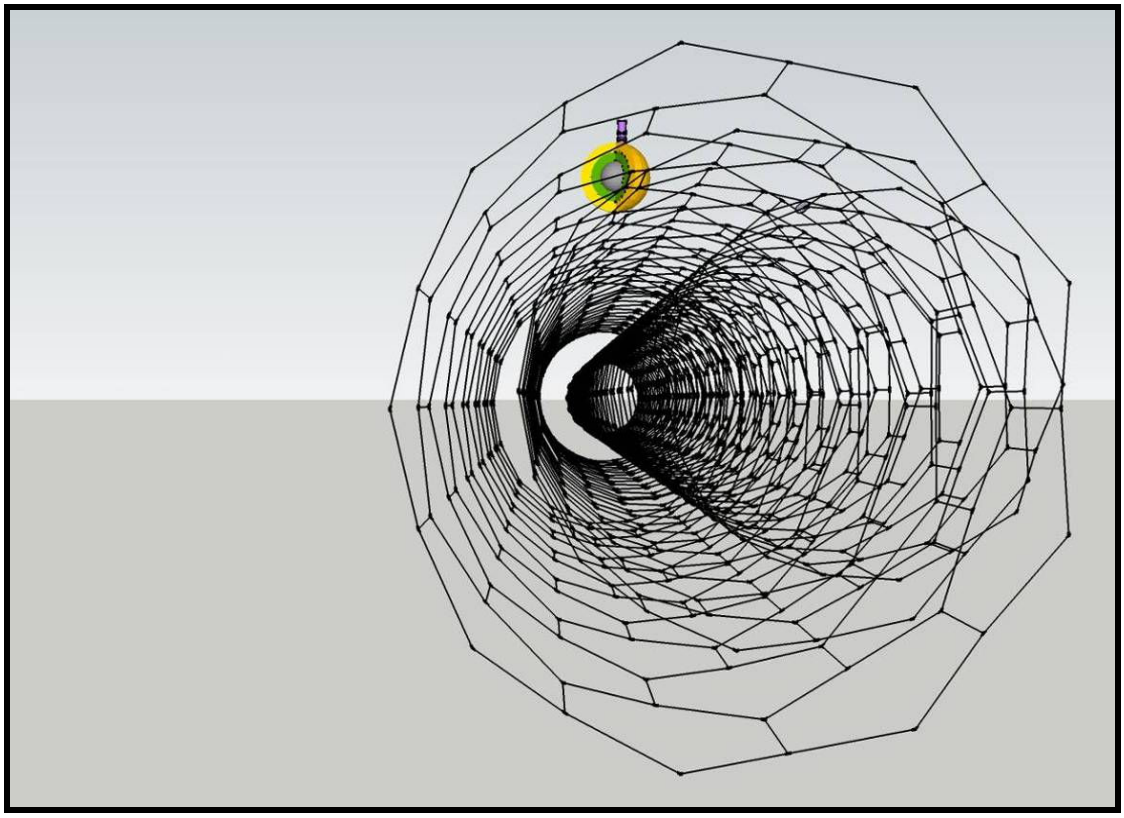

Fig. 54. *3D image interpretation of MWNT-SPQD-Antibody NP Hybrid – Angle 4*

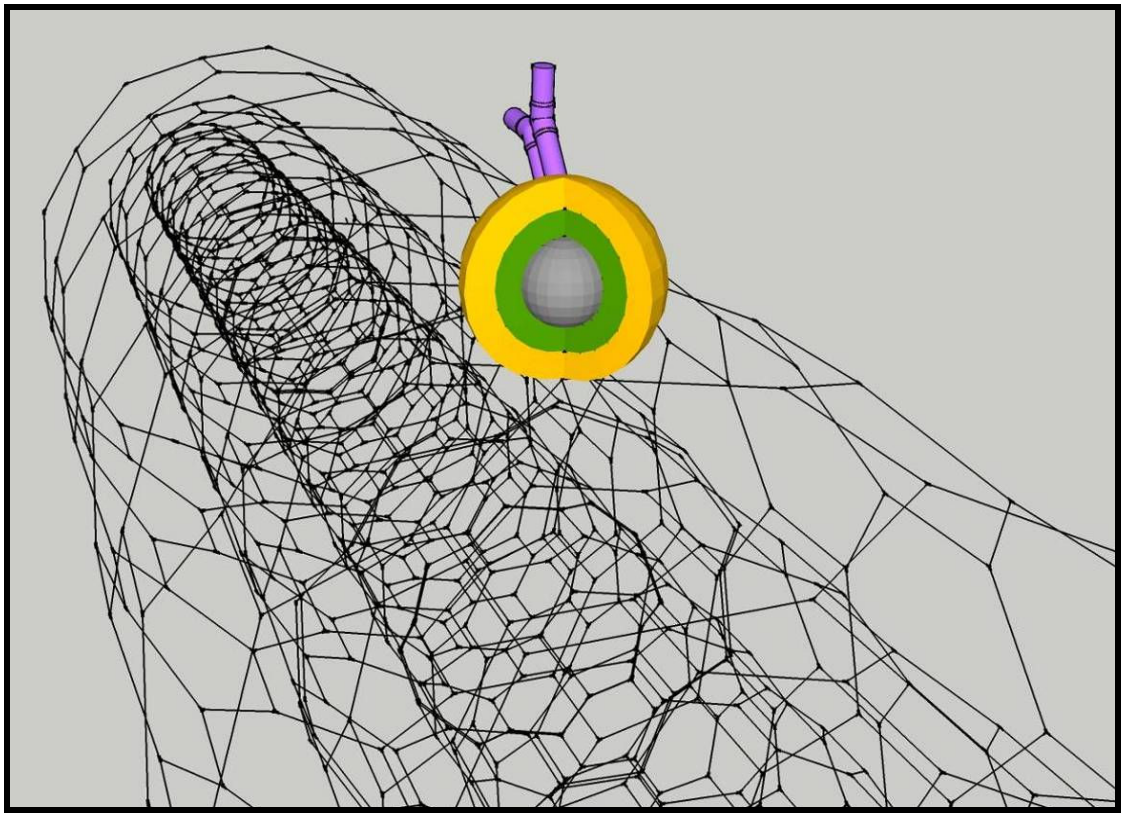

Fig. 55. *3D image interpretation of MWNT-SPQD-Antibody NP Hybrid – Angle 5*

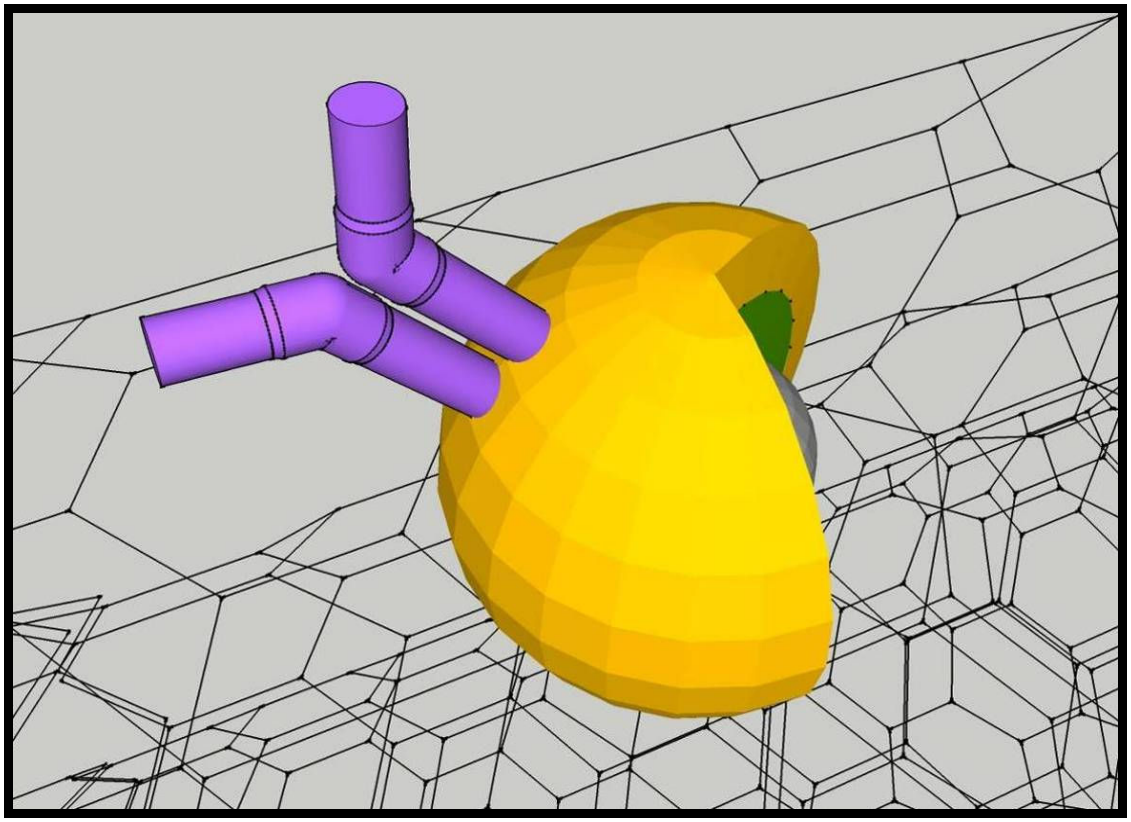

Fig. 56. *3D image interpretation of MWNT-SPQD-Antibody NP Hybrid – Angle 6*

4.3. COMPONENT 3: MICROFLUIDIC OPERATION CHIP
4.3.1. BOTTOM HALF OF COMPONENT 3

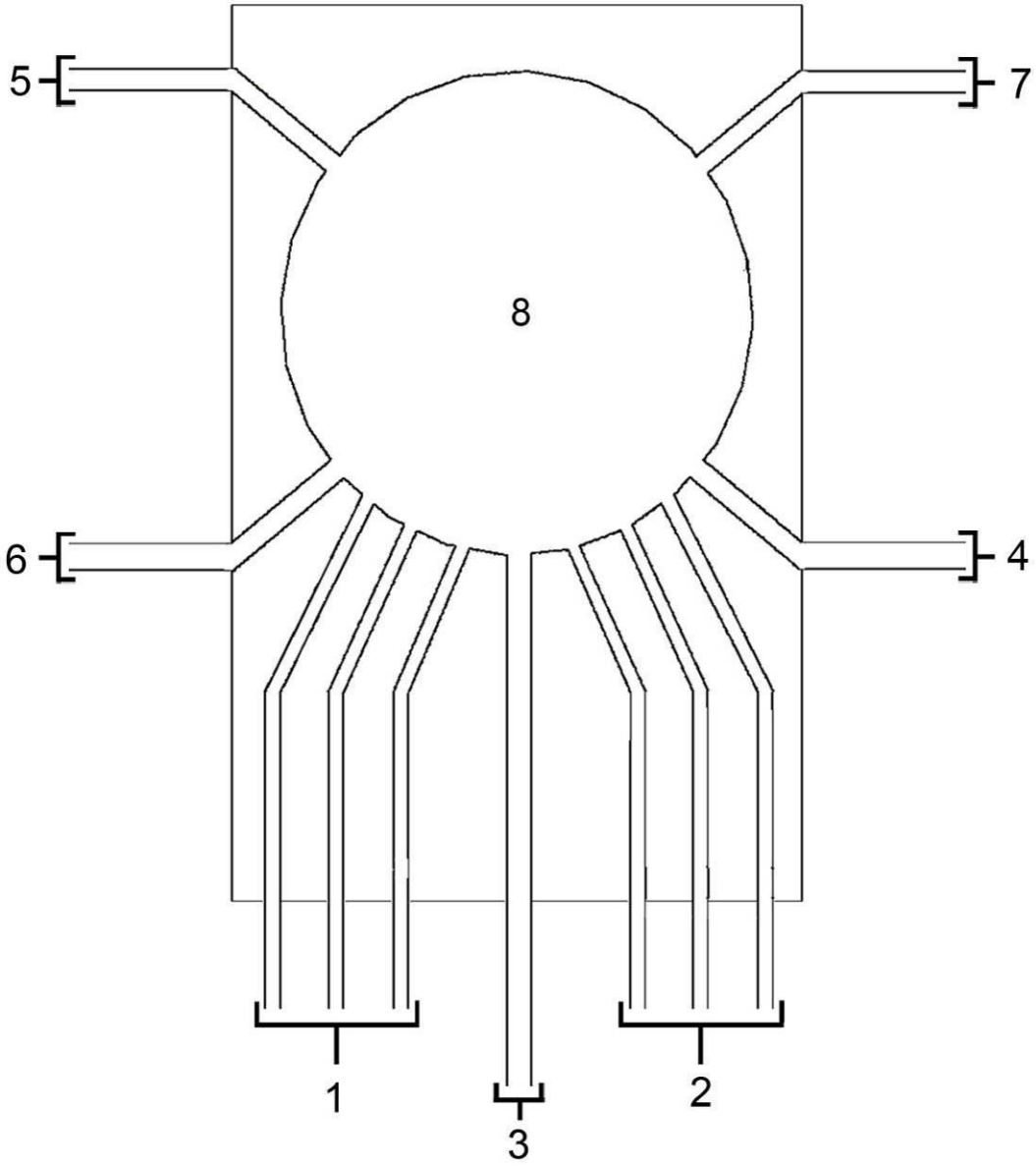

Fig. 57. *Design schematics showing the main parts in the bottom half of component 3*

The bottom half of component 3 consists of 8 major parts. Part 1 is a collection of 3 inlets, which the cancer cell sample goes through. This allows us to control the flow of the sample through fixed volume and pressure. Part 2 is a collection of 3 inlets, which the nanoparticle hybrid (component 2) aqueous solution goes through. This allows us to control the flow of the nanoparticle solution through a fixed volume and pressure. Part 3 is an inlet for water supply which will be used in stage 8 of the cancer cell isolation operation. Part 4 is the clean entrance inlet which lets in gas and will push out the non-cancerous cells through Part 5, the clean exit inlet, back into the body. Part 6, the waste entrance inlet, lets in gas to push out the destroyed cancerous cells through Part 7, the

waste exit inlet. Part 8 is the operation chamber, where the full cancer cell separation process occurs. It holds component 1, which is used to attract the cancerous cells. The full thickness of the bottom half of component 3 will be 0.2 cm. The next design schematic shows the size specifications of the bottom half of component 3.

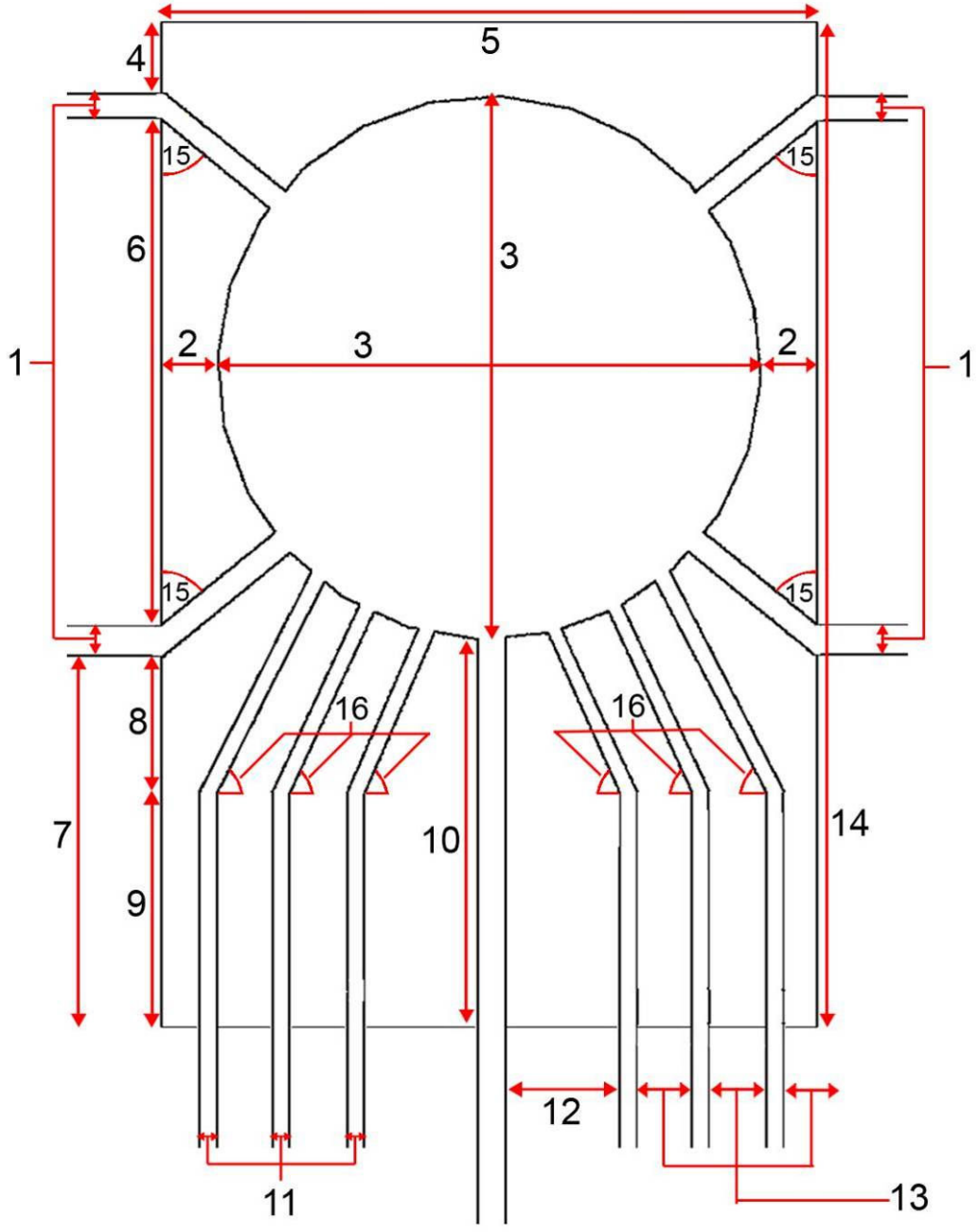

Fig. 58. *Design schematics showing the size measurements (values in Table 9) for the bottom half of component 3*

The following table below shows the size and angle specifications for Fig. 58:

Fig. 58	
1	0.25 cm
2	0.5 cm
3	2 cm
4	0.25 cm
5	3 cm
6	1.5 cm
7	1.75 cm
8	0.5 cm
9	1.25 cm
10	1.75 cm
11	0.1 cm
12	0.455 cm
13	0.2 cm
14	4 cm
15	55°
16	55°

Table 9. *Size measurements for the bottom half of component 3 (Microfluidic Operation Chip) on Fig. 58*

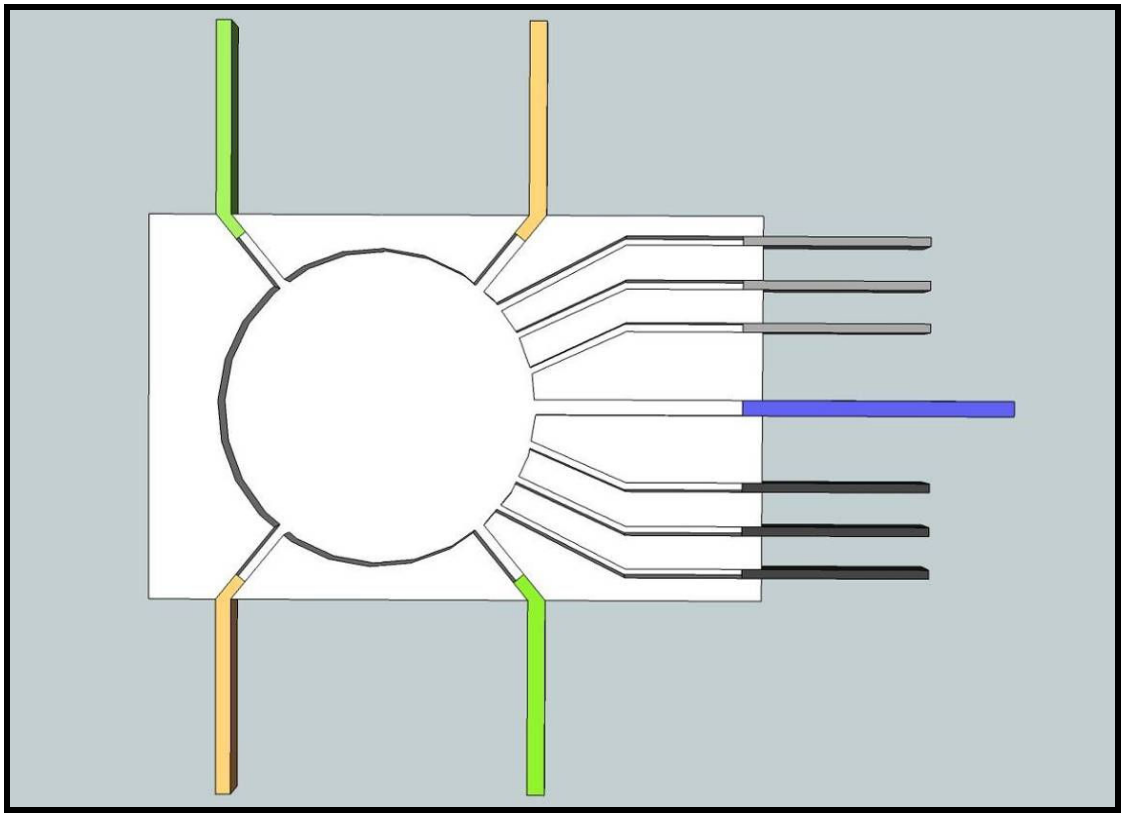

Fig. 59. *3D image interpretation of the bottom half part in component 3 – Angle 1*

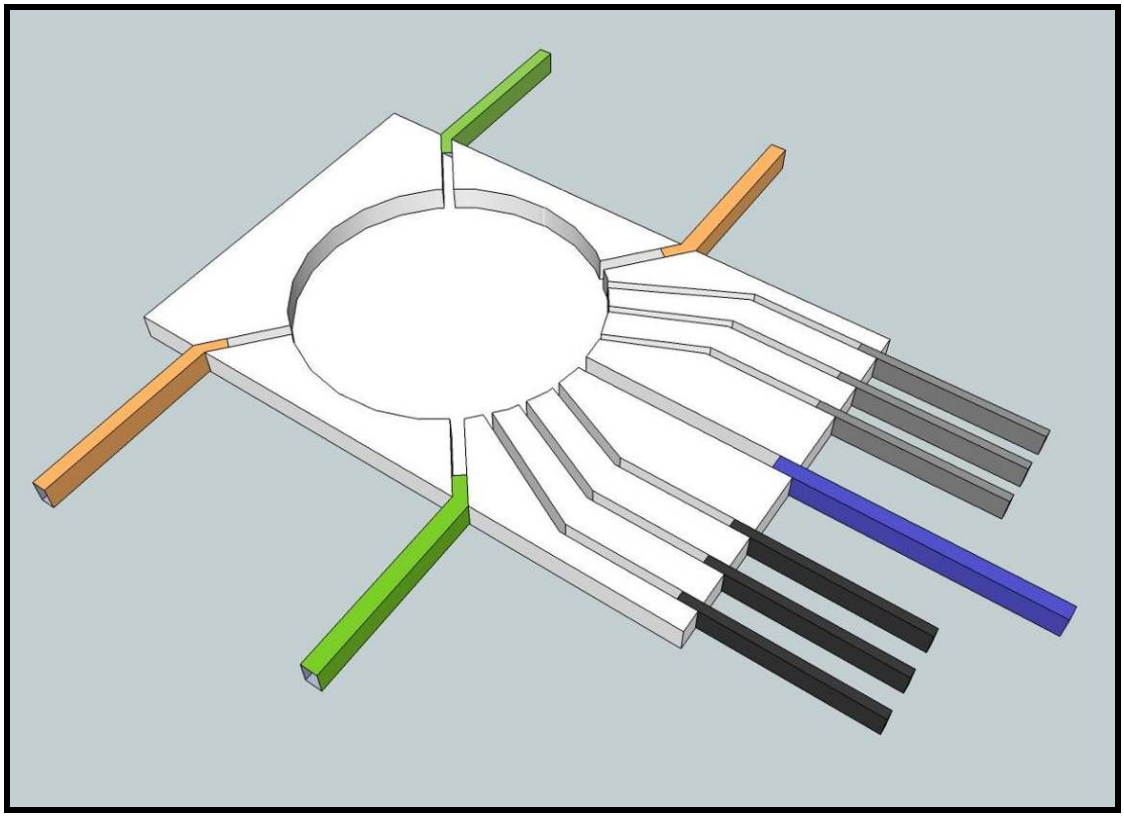

Fig. 60. *3D image interpretation of the bottom half part in component 3 – Angle 2*

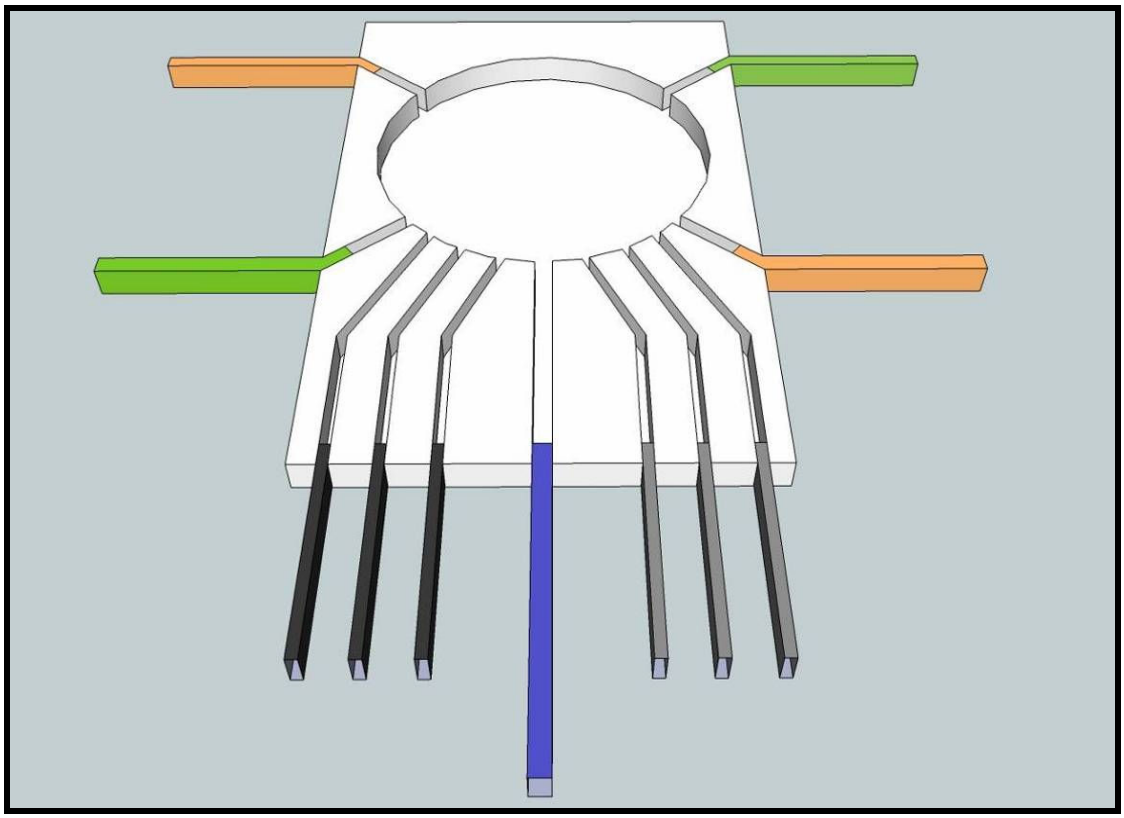

Fig. 61. *3D image interpretation of the bottom half part in component 3 – Angle 3*

4.3.2. TOP HALF OF COMPONENT 3

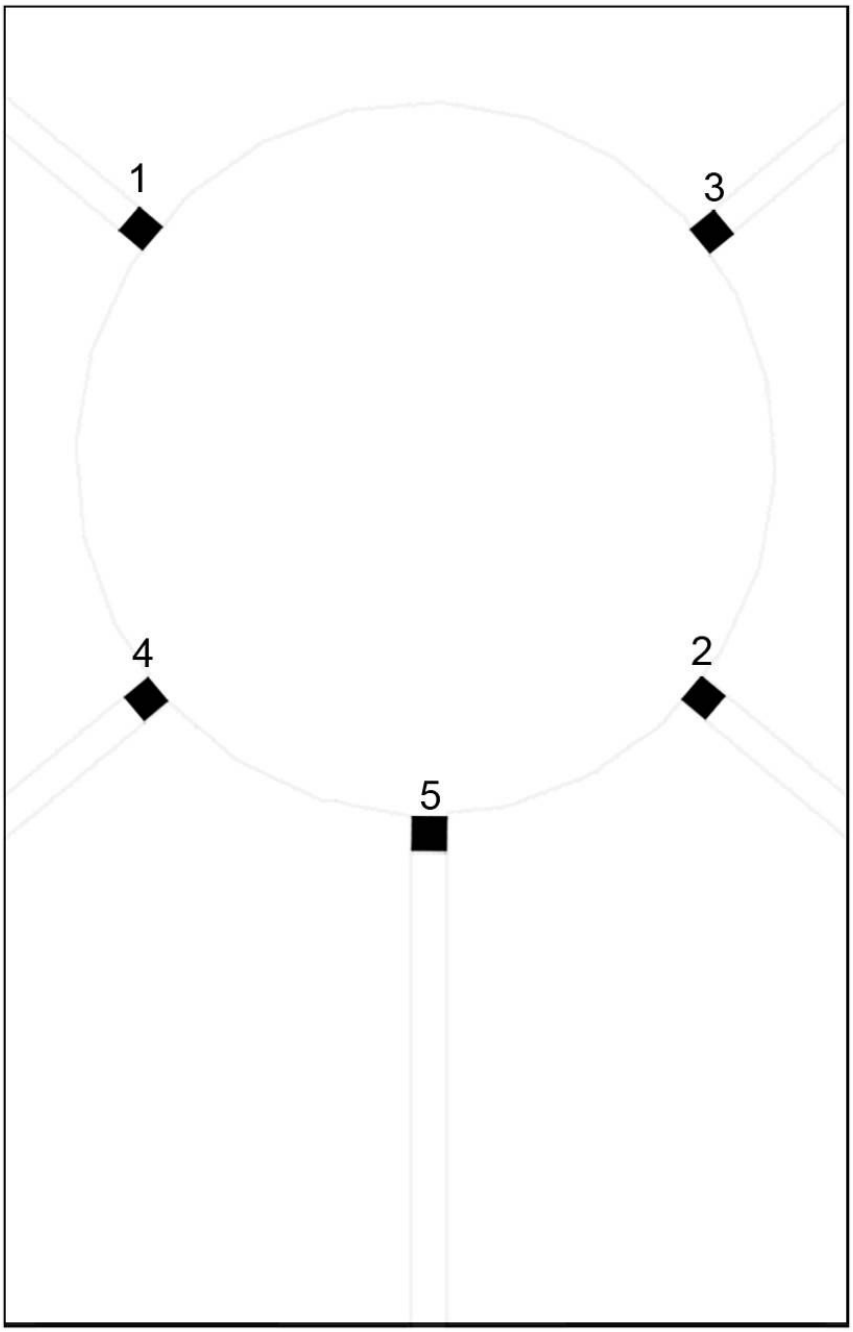

Fig. 62. *Design schematics showing the main parts in the top half of component 3*

The top half of component 3 consists of 5 major parts. All of these parts are ONLY valves which are used to close off the major inlets in the bottom half of component 3. Part 1, is the hole and the valve used to block off the clean exit inlet (Part 5 in Fig. 57). Part 2, is the hole and the valve used to block off the clean entrance inlet (Part 4 in Fig. 57). Part 3, is the hole and the valve used to block off the waste exit inlet (Part 7 in Fig. 57). Part 4, is the hole and the valve used to block off the waste entrance inlet (Part 6 in Fig. 57). Part 5, is the hole and the valve used to block off the water supply inlet (Part 5

in Fig. 57). The full thickness of the top half of component 3 will be 0.2 cm, and the valves should have a height of 0.8 cm. For the first prototype of the technology these valves would manually be pushed in. Later on after further research on automated valve systems, these valves would operate in a controlled automatic setup which would not require any human force and manual effort.

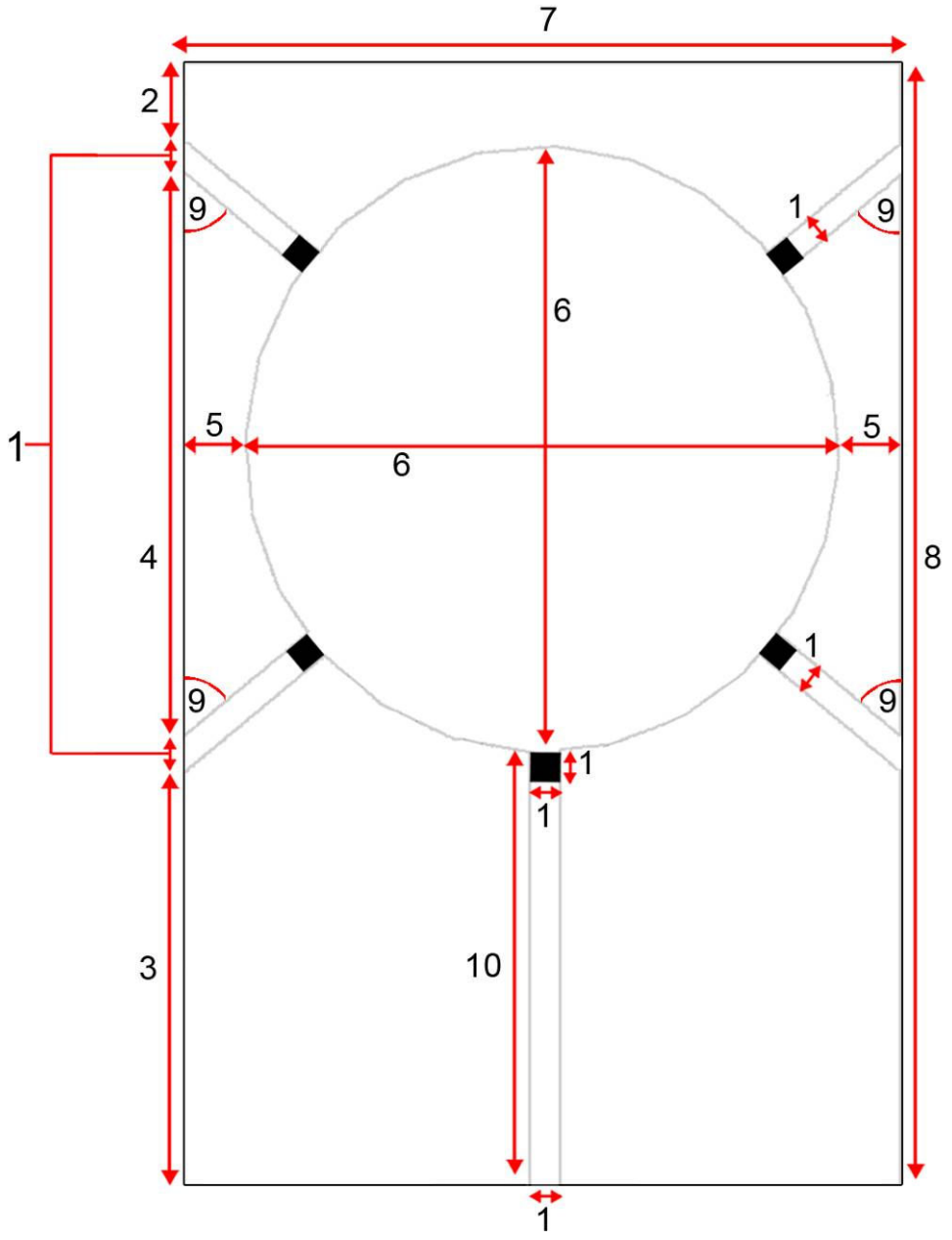

Fig. 63. *Design schematics showing the size measurements (values in Table 10) for the top half of component 3*

The following table below shows the size and angle specifications for Fig. 63:

Fig. 63	
1	0.25 cm
2	0.25 cm
3	1.75 cm
4	1.5 cm
5	0.5 cm
6	2 cm
7	3 cm
8	4 cm
9	55°
10	1.75 cm

Table 10. *Size measurements for the top half of component 3 (Microfluidic Operation Chip) on Fig. 63*

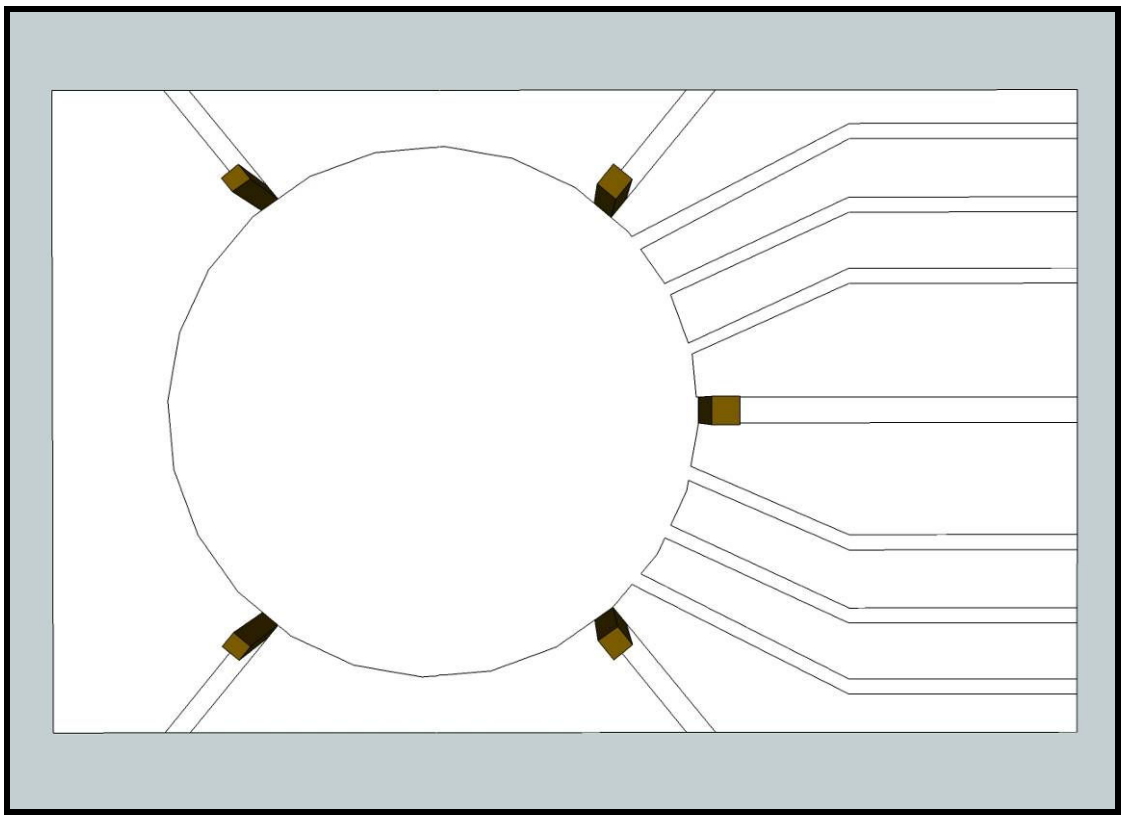

Fig. 64. *3D image interpretation of the top half part in component 3 – Angle 1*

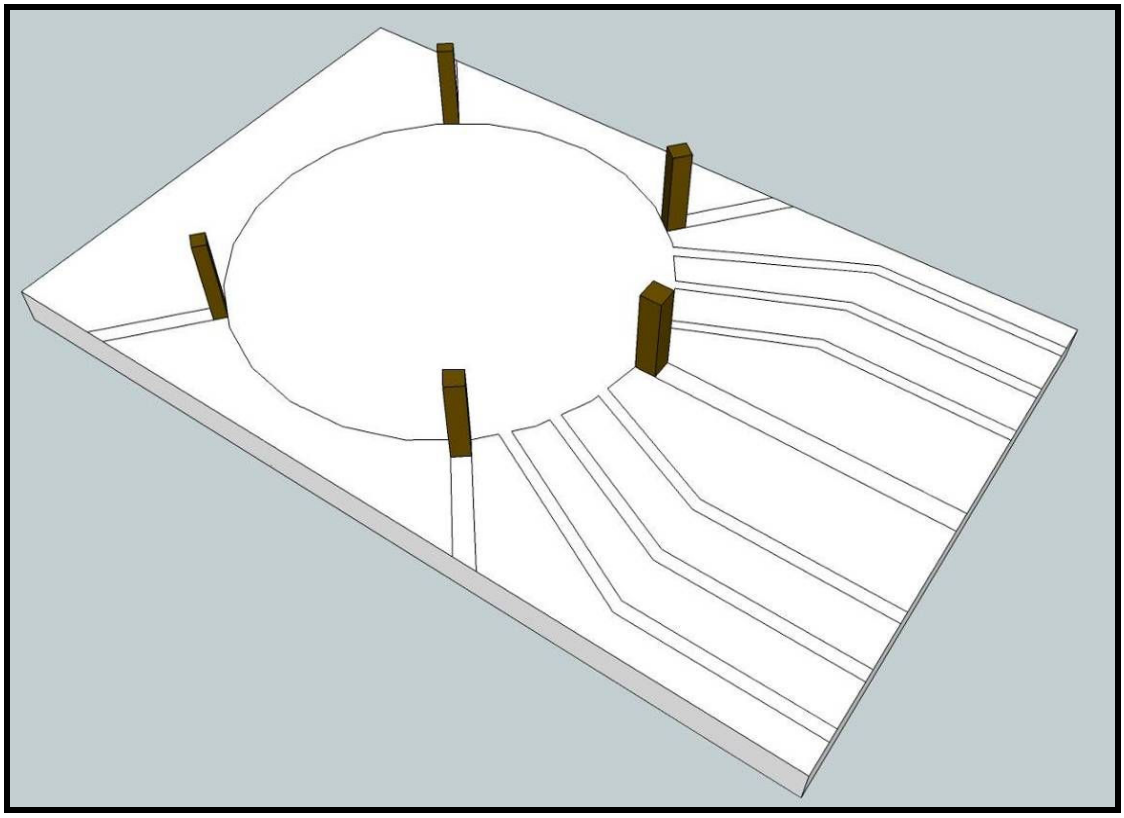

Fig. 65. *3D image interpretation of the top half part in component 3 (Microfluidic Operation Chip)– Angle 2*

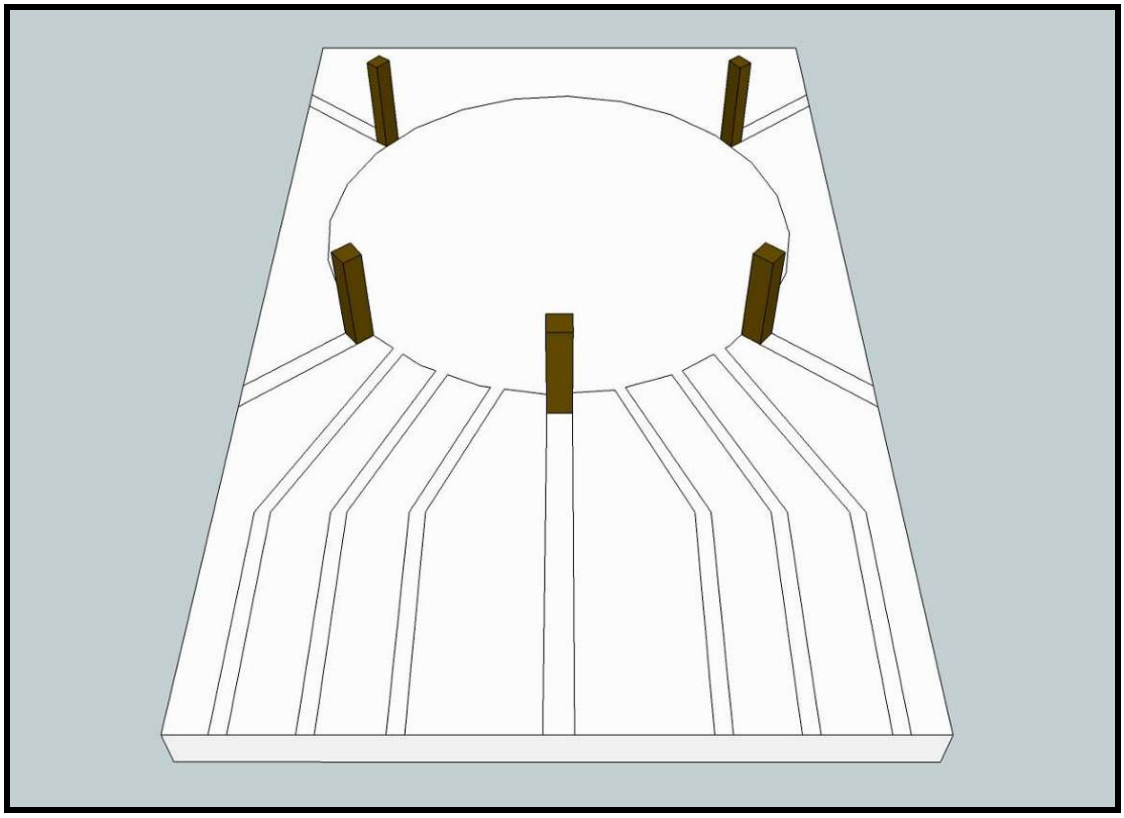

Fig. 66. *3D image interpretation of the top half part in component 3 (Microfluidic Operation Chip)– Angle 3*

4.4. FULL COMPONENT INTEGRATION

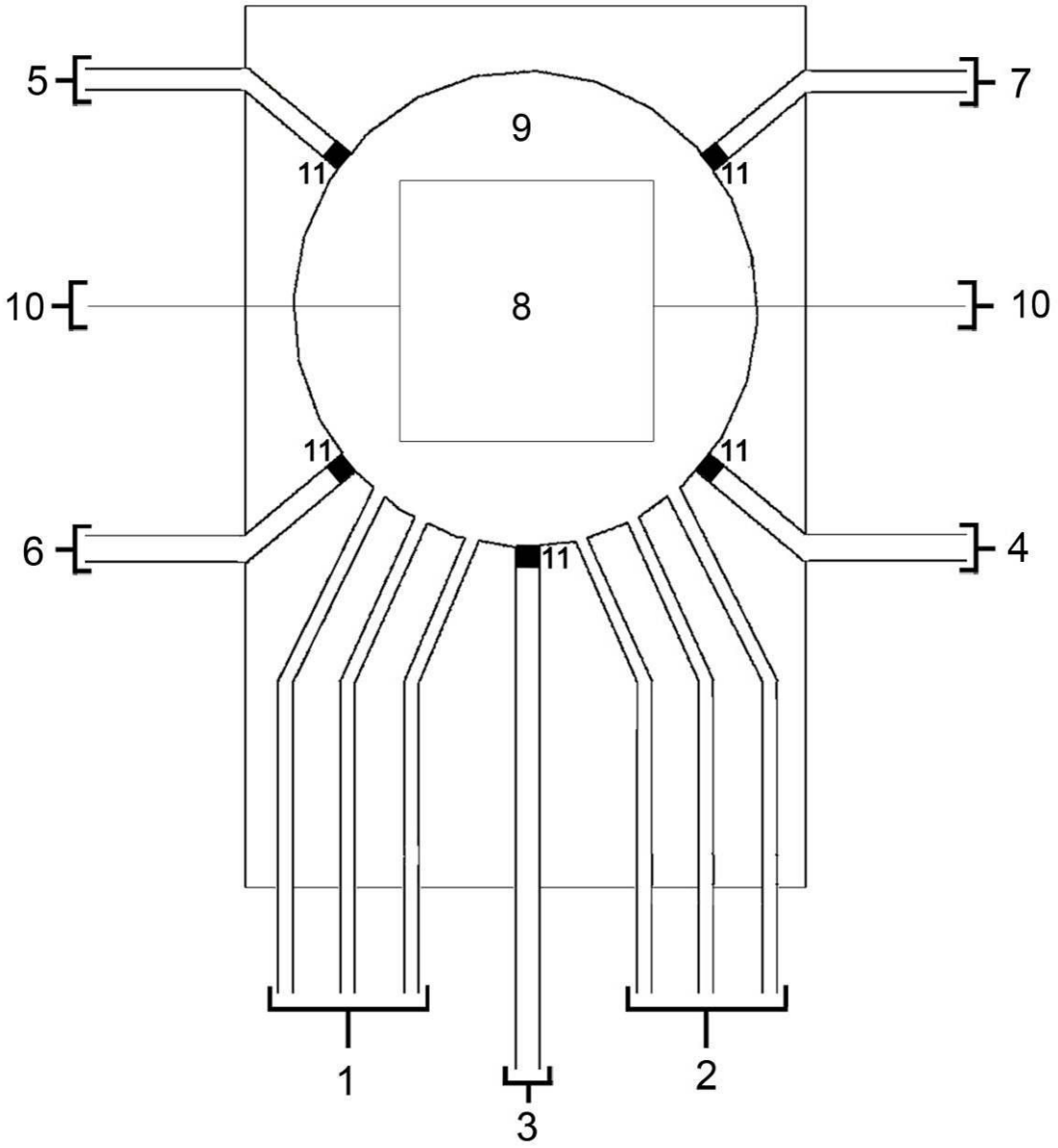

Fig. 67. *Design schematics showing the main parts of the full microfluidic cancer cell operation chip*

The full product is the integration of component 1 and component 3. Component 1 (Part 8) is placed into the main operation chamber (Part 9), which is part of the bottom half of component 3.Electrical wires (Part 10) are soldered onto the main electrodes of component 1 and punctured through the sides of the bottom half of component 3. The top layer for component 3 is placed into top of the system, where the valves (Part 11) are synchronized with the inlets (Parts 3, 4, 5, 6, and 7) that they are blocking.

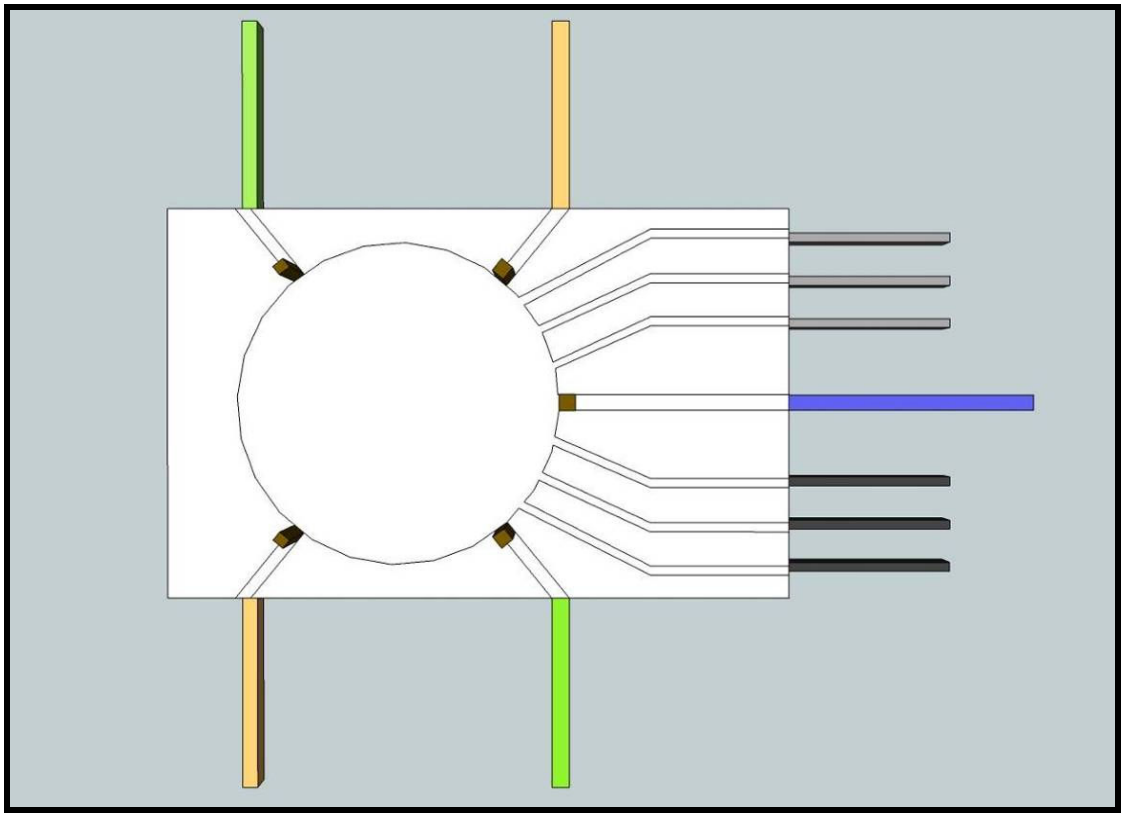

Fig. 68. *3D image interpretation of component 3 – Angle 1*

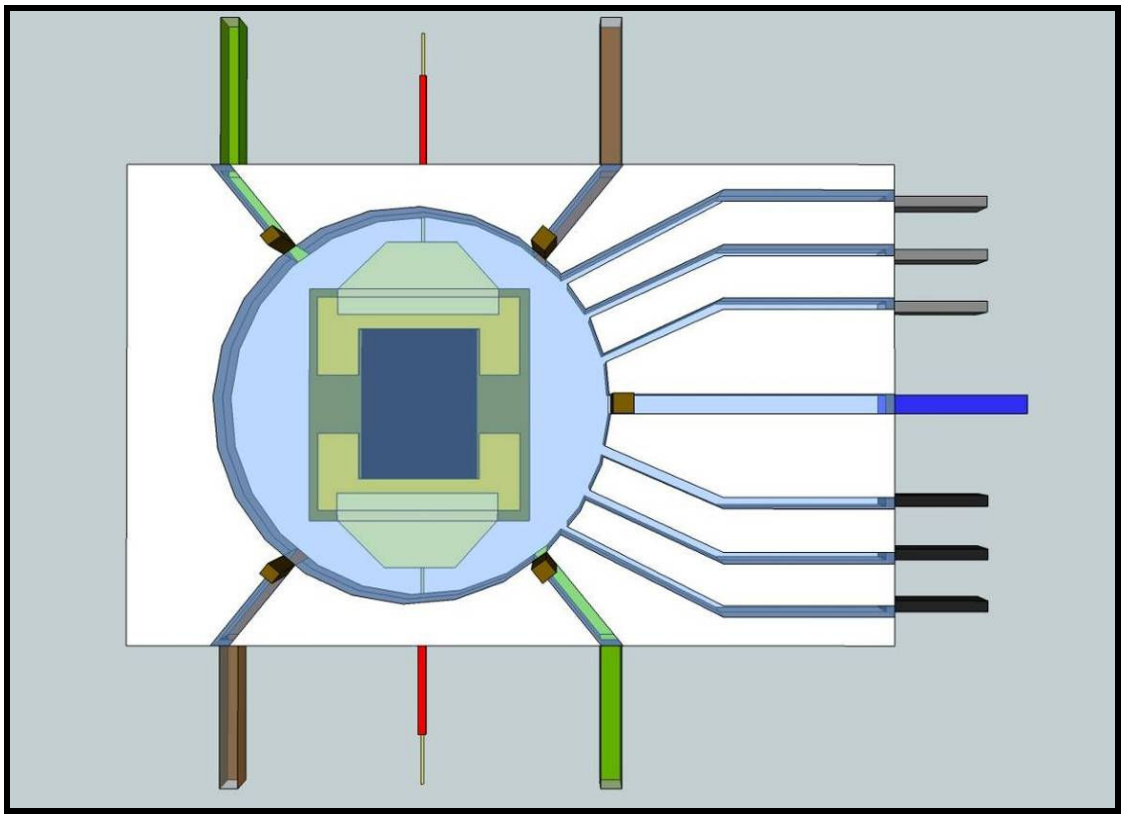

Fig. 69. *See-through 3D image interpretation of component 3 – Angle 1*

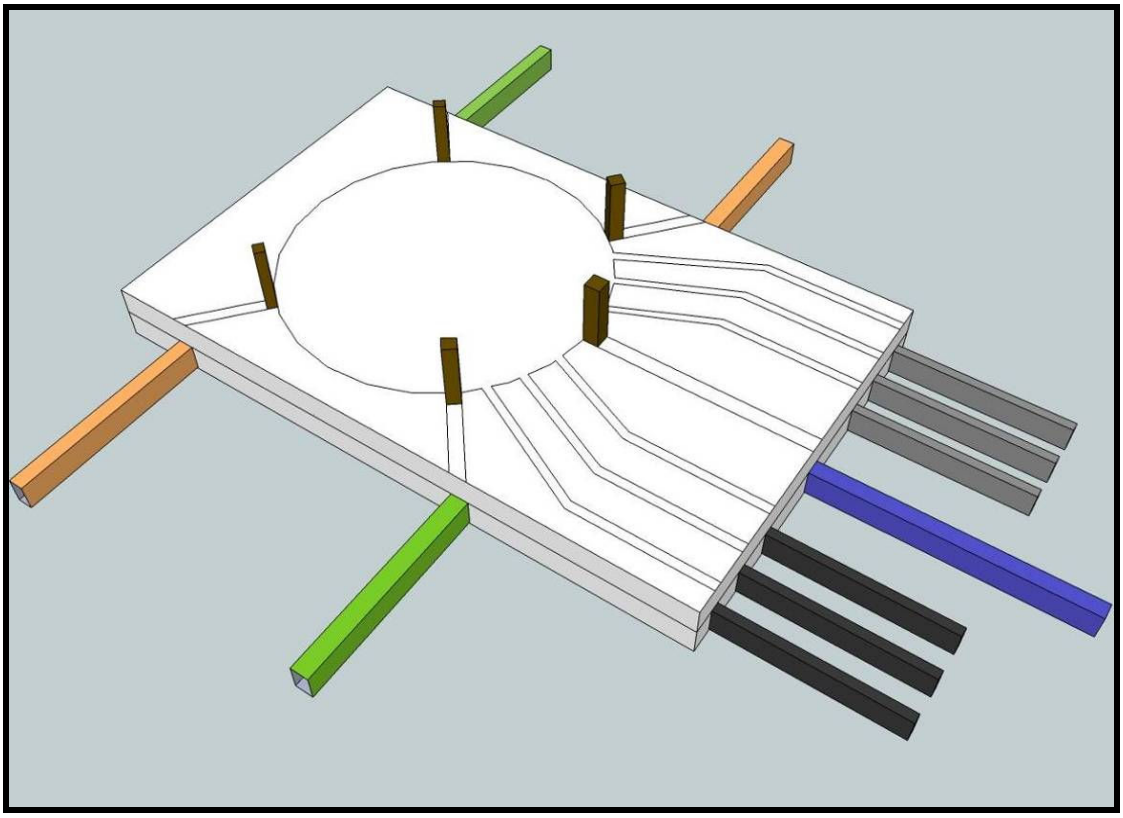

Fig. 70. *3D image interpretation of component 3 – Angle 2*

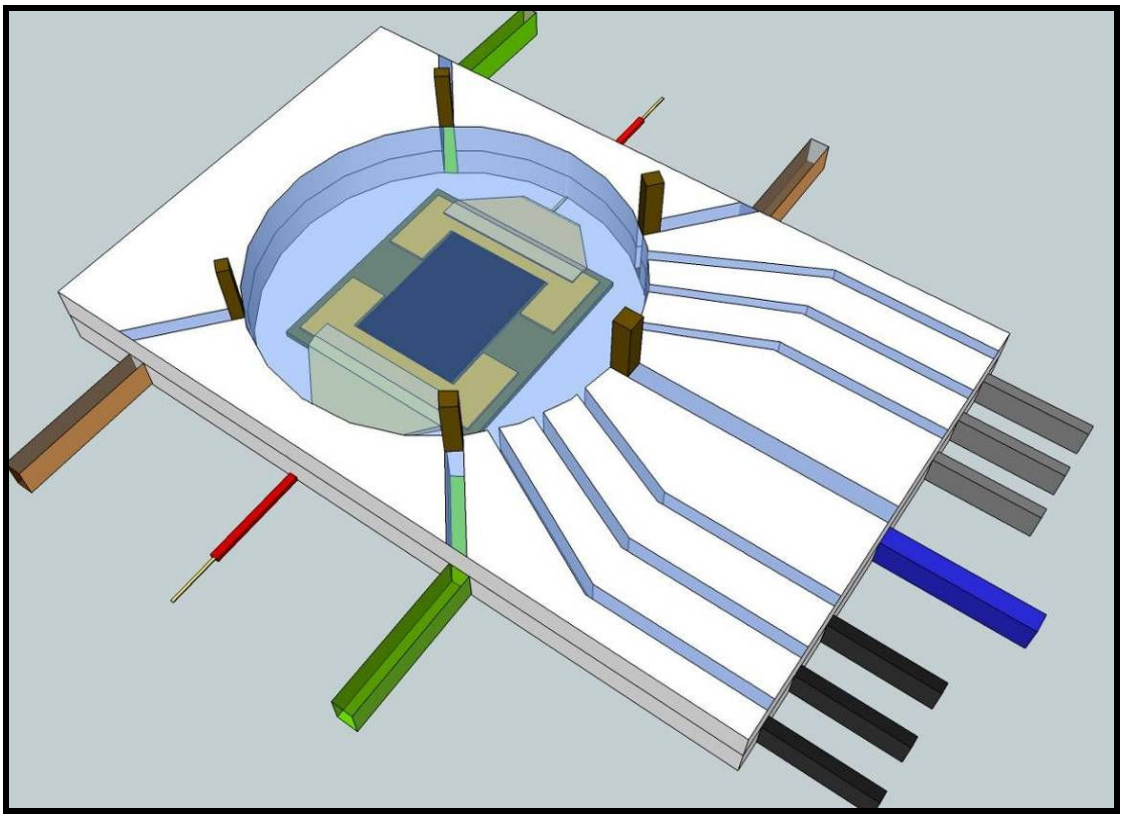

Fig. 71. See-thru *3D image interpretation of component 3 – Angle 2*

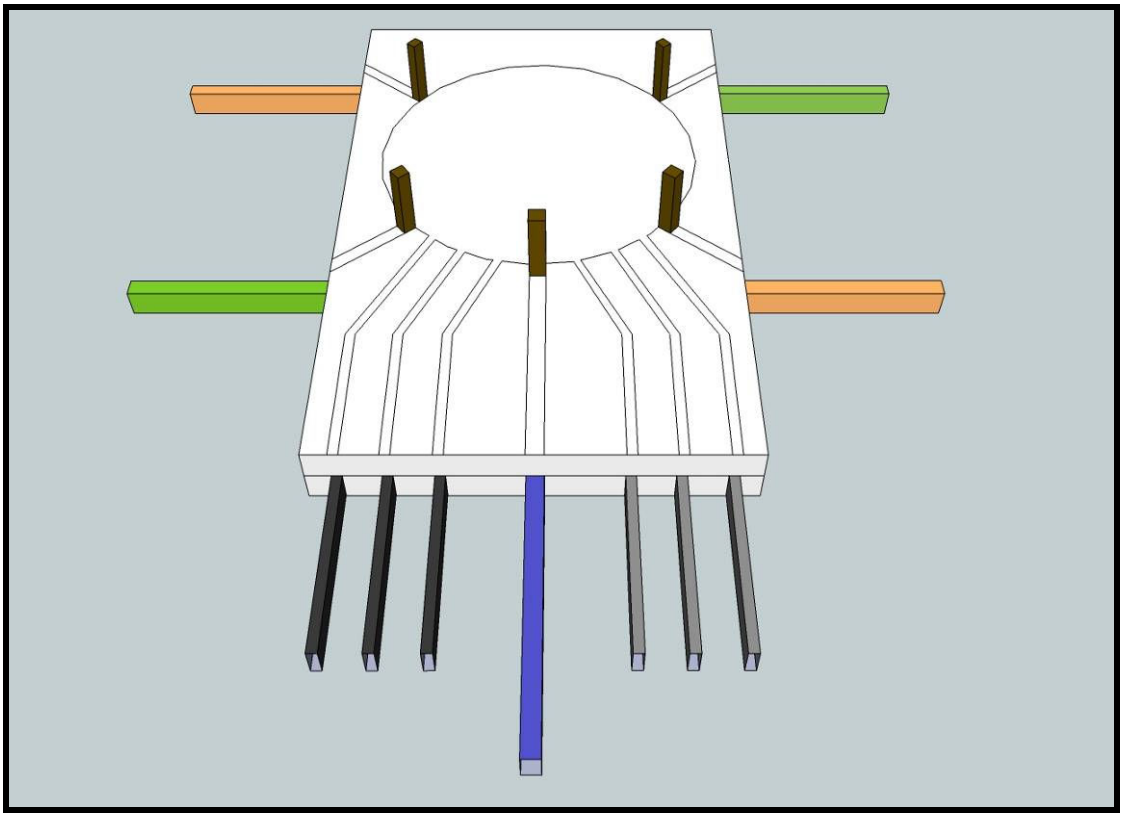

Fig. 72. *3D image interpretation of component 3 – Angle 3*

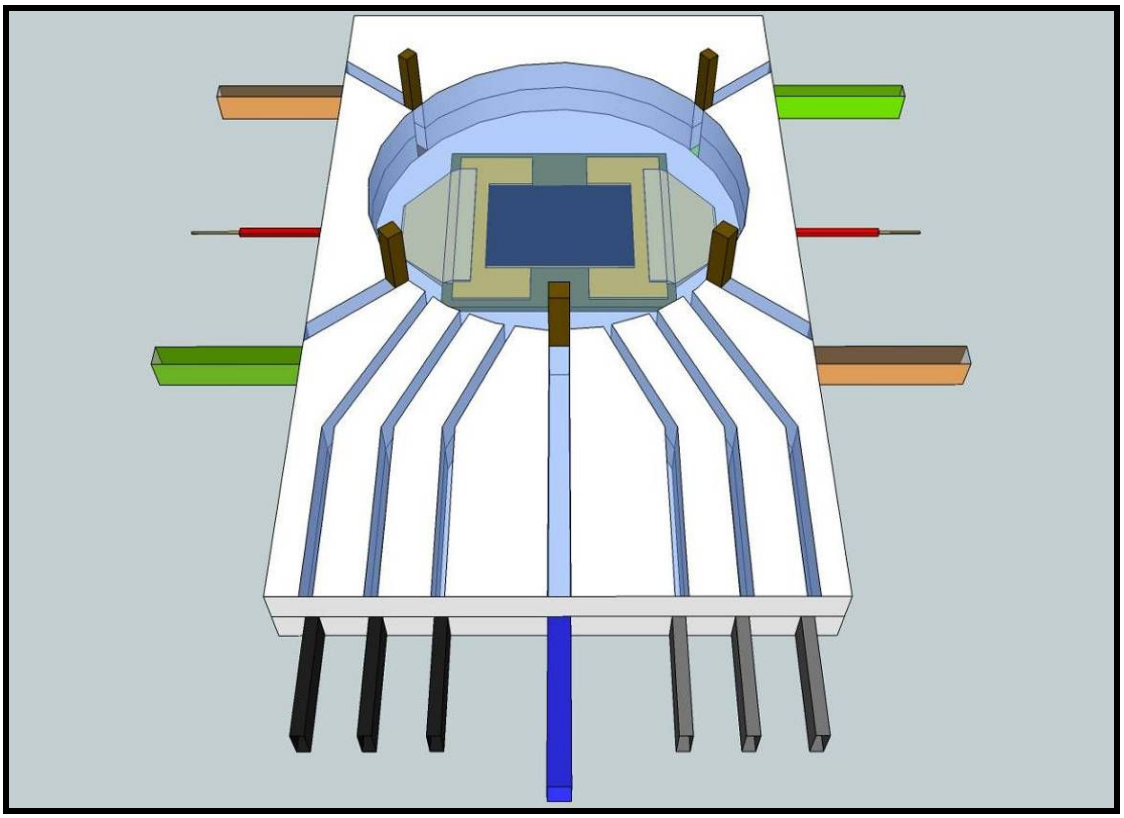

Fig. 73. *See-thru 3D image interpretation of component 3 – Angle 3*

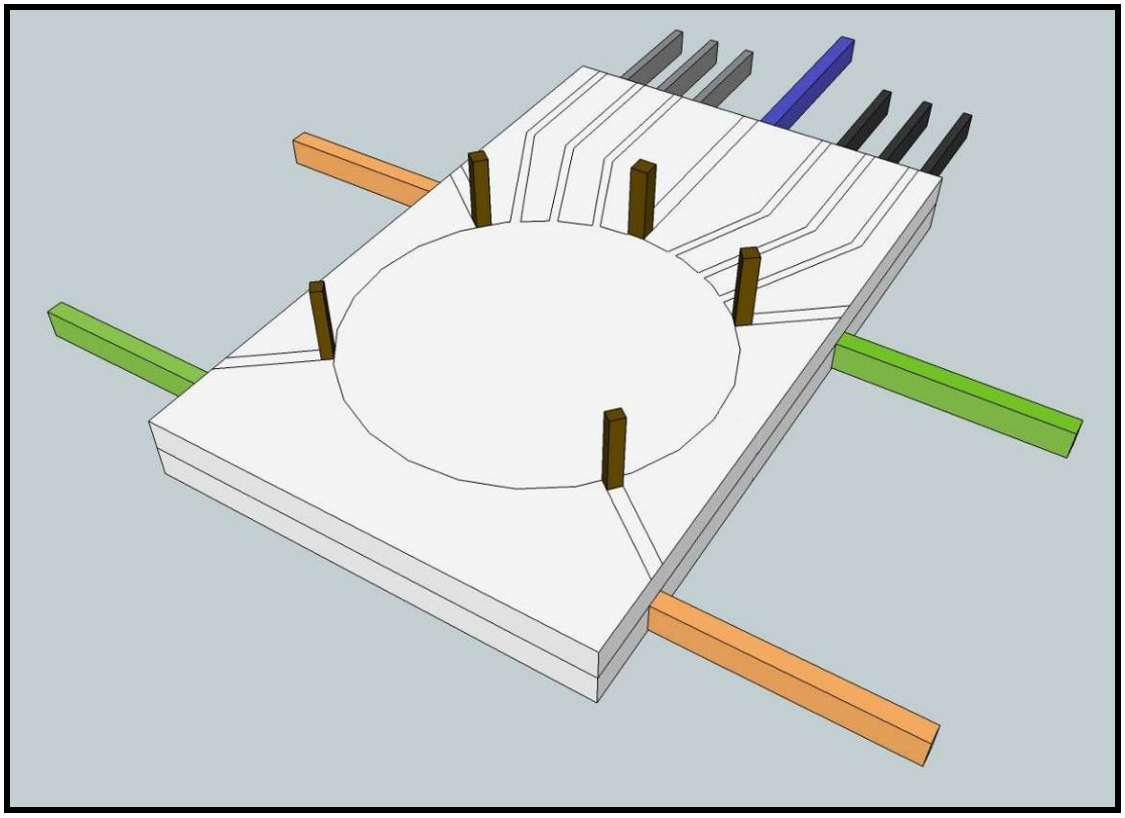

Fig. 74. *3D image interpretation of component 3 – Angle 4*

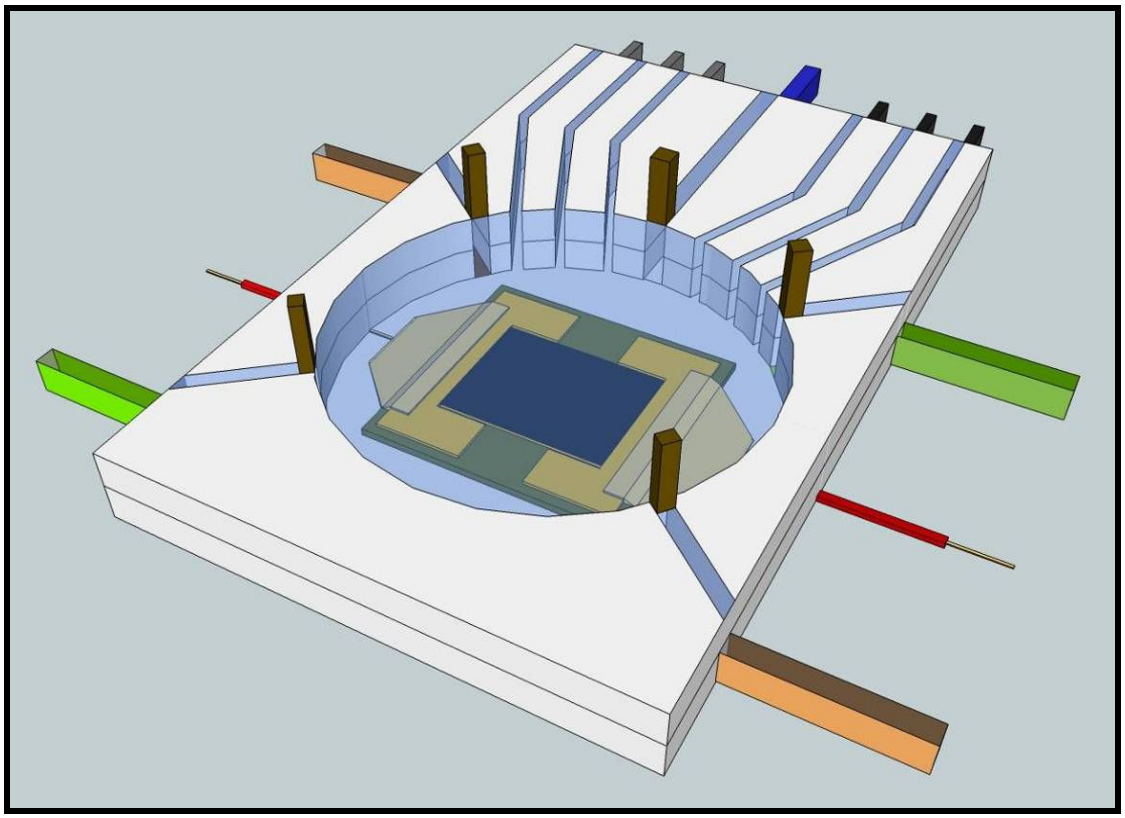

Fig. 75. See-thru *3D image interpretation of component 3 – Angle 4*

4.5. CANCER CELL ISOLATION OPERATION
4.5.1. STAGE 1 – INSERTION OF TEST SOLUTIONS

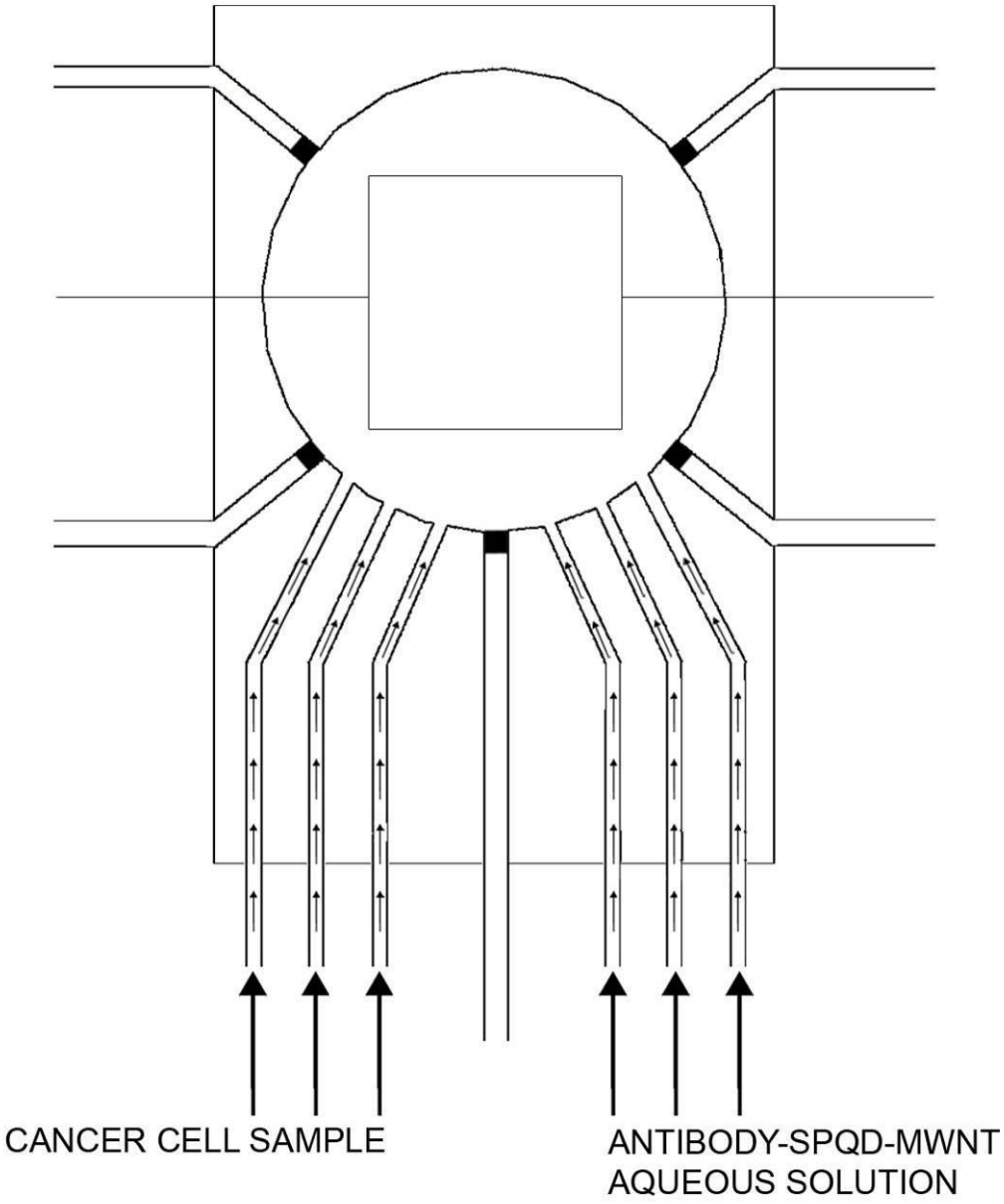

Fig. 76. *Design schematics showing the 1st stage of the cancer cell isolation operation – Insertion of cancer cell and nanoparticle hybrid solutions*

The operation of the cancer cell isolation system begins with the injection of 2 solutions: cancer cell diluted sample and nanoparticle hybrid aqueous solution. Both solutions are injected into their designated inlets (Parts 1 and 2 on Fig. 57) with calculated volumes and pressures. Both these solutions are led into the operation chamber (Part 9 on Fig. 57), which includes component 1, and are mixed together. Once the right calculated volumes of both mixtures have gone in, the injection process stops.

4.5.2. STAGE 2 – BIO-CONJUGATION OF HYBRIDS AND CANCER CELLS

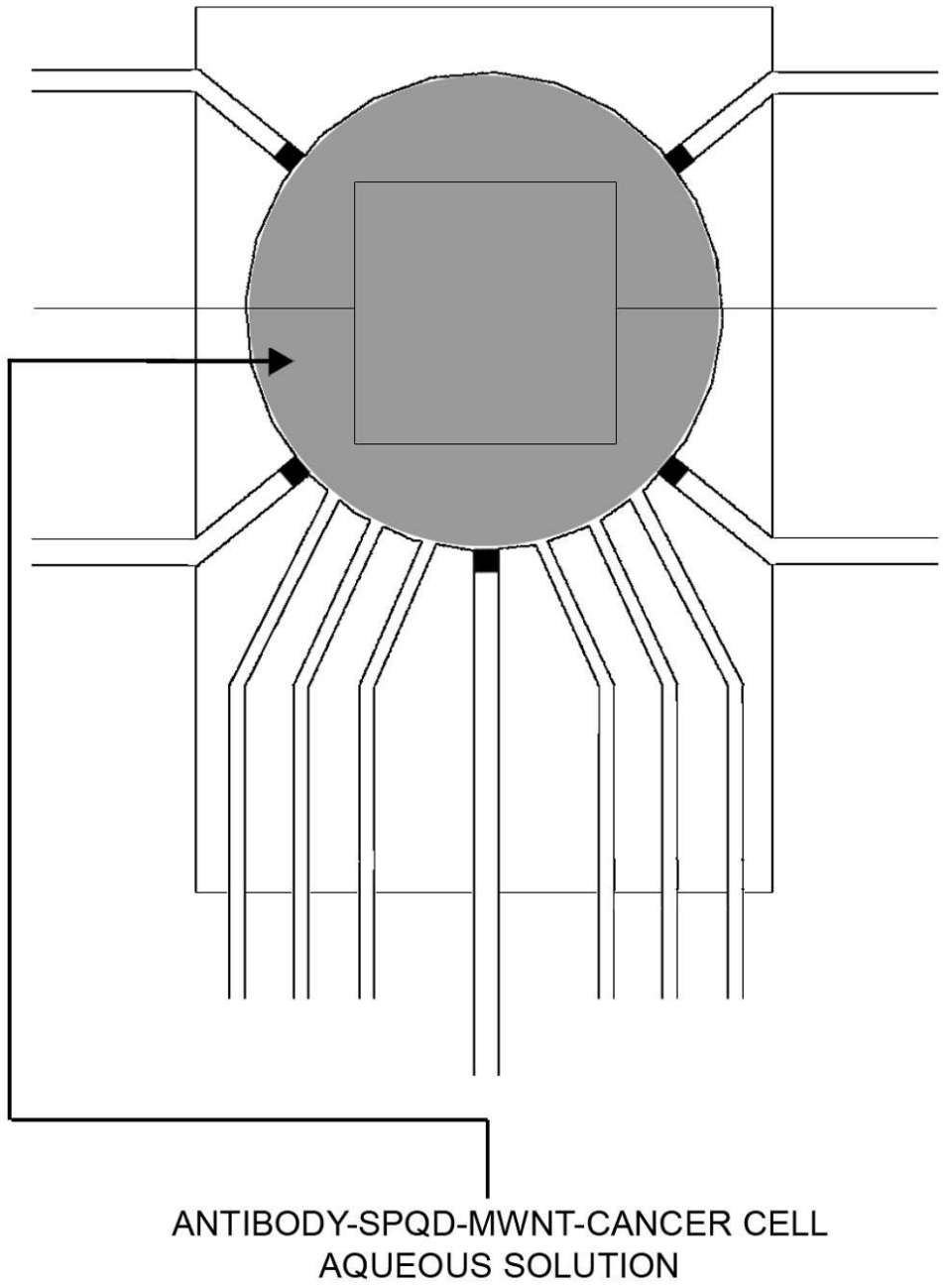

Fig. 77. *Design schematics showing the 2nd stage of the cancer cell isolation operation – Bioconjugation of the nanoparticle hybrids and specified cancer cells*

Once both solutions have been injected into the operation chamber (Part 8 on Fig. 57), the nanoparticle hybrids begin to attach with the cancerous cells forming bio-conjugates through antibody attachment. As all these particles are at a constant motion in the chamber, where no catalytic reaction is required, the nanoparticle hybrids will attach onto the specified cancer cells through the antibody component. After then, the operation is ready to commence to stage 3.

4.5.3. STAGE 3 – VOLTAGE (AC DIELECTROPHORESIS) ON

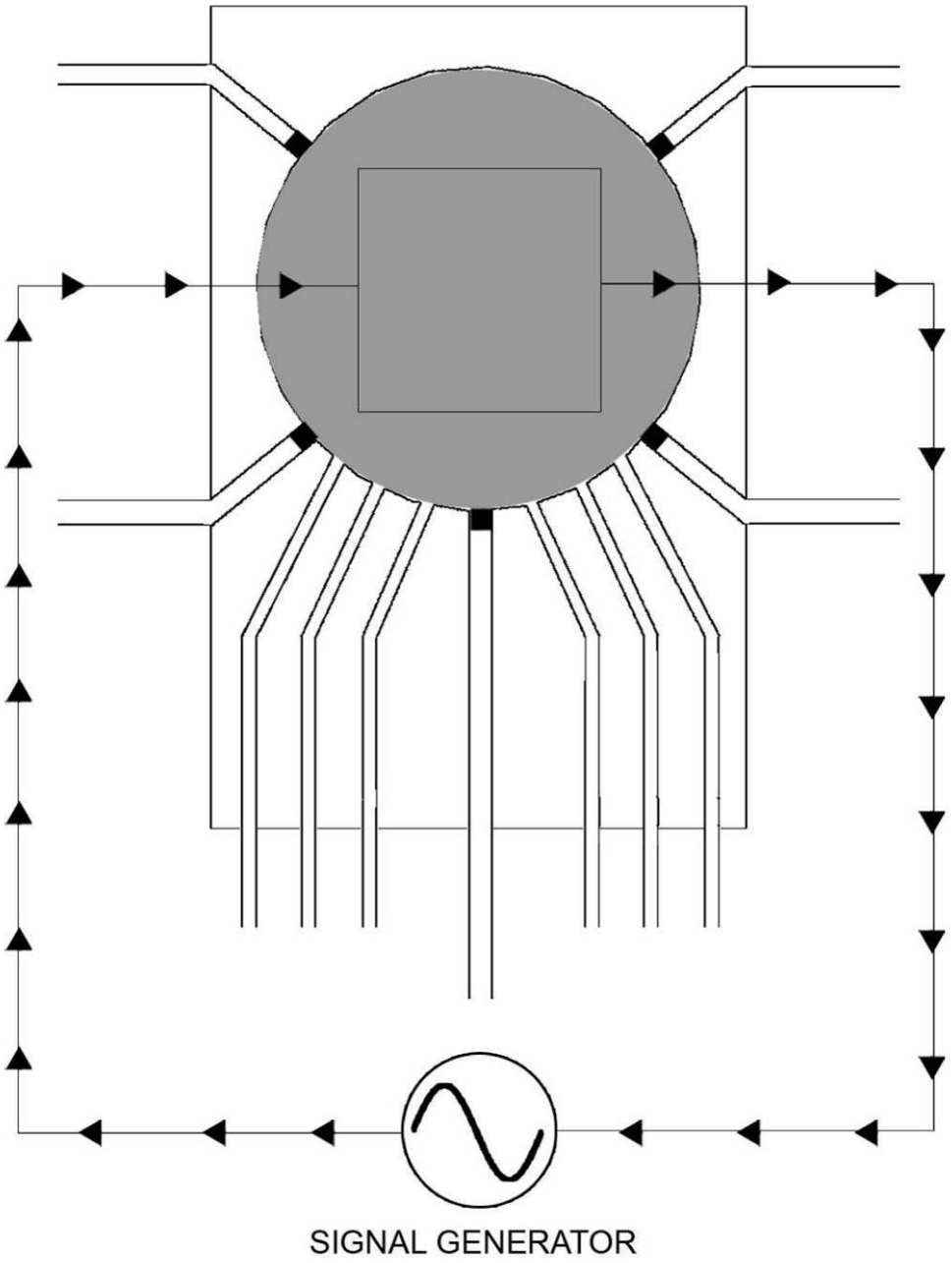

Fig. 78. *Design schematics showing the 3rd stage of the cancer cell isolation operation – Voltage, under AC Dielectrophoresis is turned on*

The device is connected to a voltage supply and signal generator through the electrical wires (Part 10 of Fig. 67) which connected to component 1 (Part 8 of Fig. 67). The current passing through component 1 will be under AC dielectrophoresis with a frequency of 5 MHz and the voltage supply will be running approximately 8V, according to *Banerjee et al* [25]. This will magnetically attract the nanoparticle hybrids, with the cancer cell attached, onto the electrodes and form bridges between them. This allows the current to pass from one set of electrodes to the other. AC dielectrophoresis

will specifically help nudge the nanoparticle hybrids so that they are aligned properly to form bridges. The whole process can be viewed under a real time fluorescence imaging microscope allowing us to optically view the movement of the nanoparticle hybrid-cancer cell bioconjugate.

4.5.4. STAGE 4 – OPENING CLEAN VALVES 1 & 2

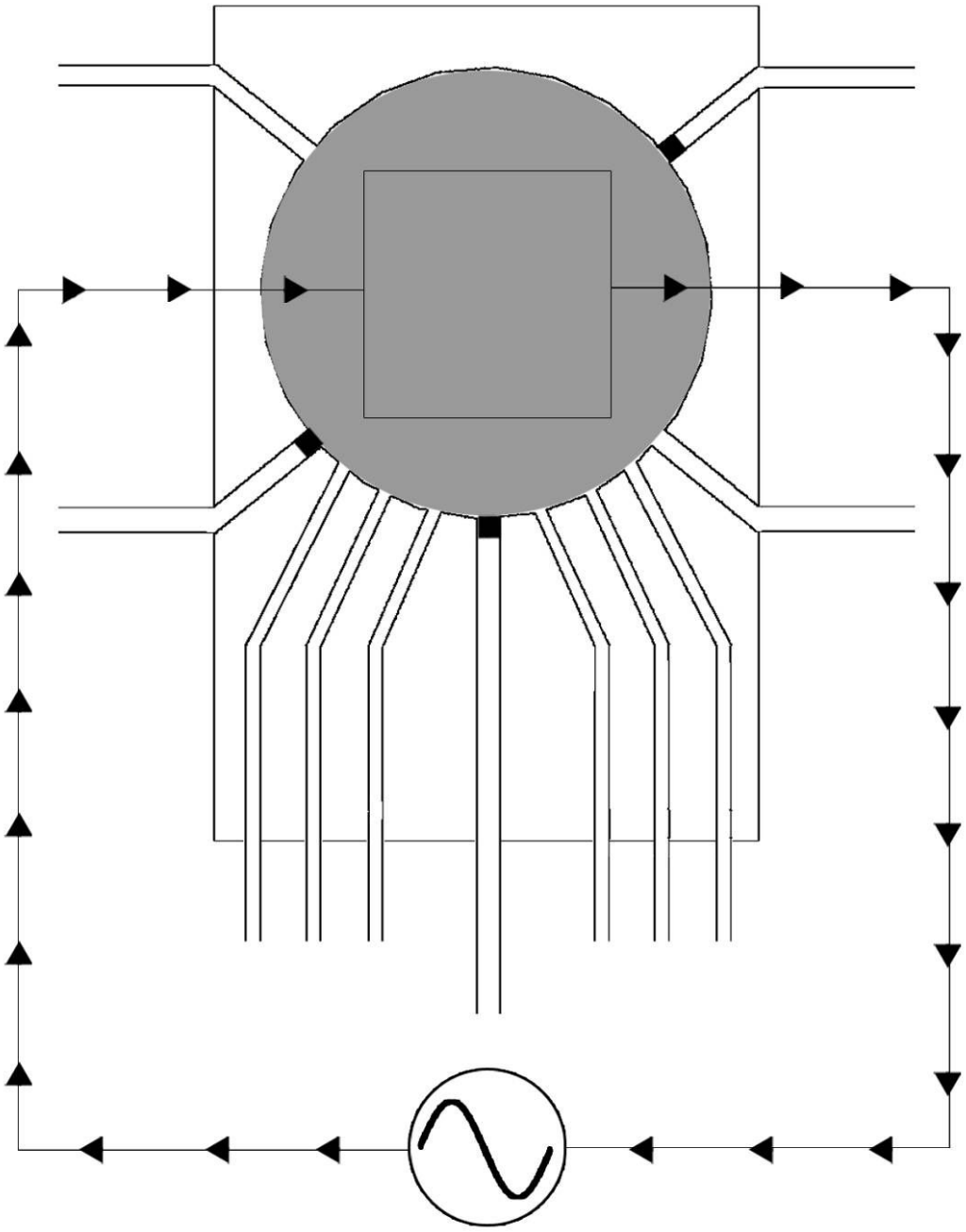

Fig. 79. *Design schematics showing the 4th stage of the cancer cell isolation operation – Opening clean valves 1 & 2*

Whilst the nanoparticle hybrid-cancer cell bioconjugates are magnetically attracted to component 1 (Part 8 in Fig. 67), the clean valves (Parts 1 and 2 in Fig. 62) are opened.

4.5.5. STAGE 5 – CLEANSING OF NORMAL CELLS

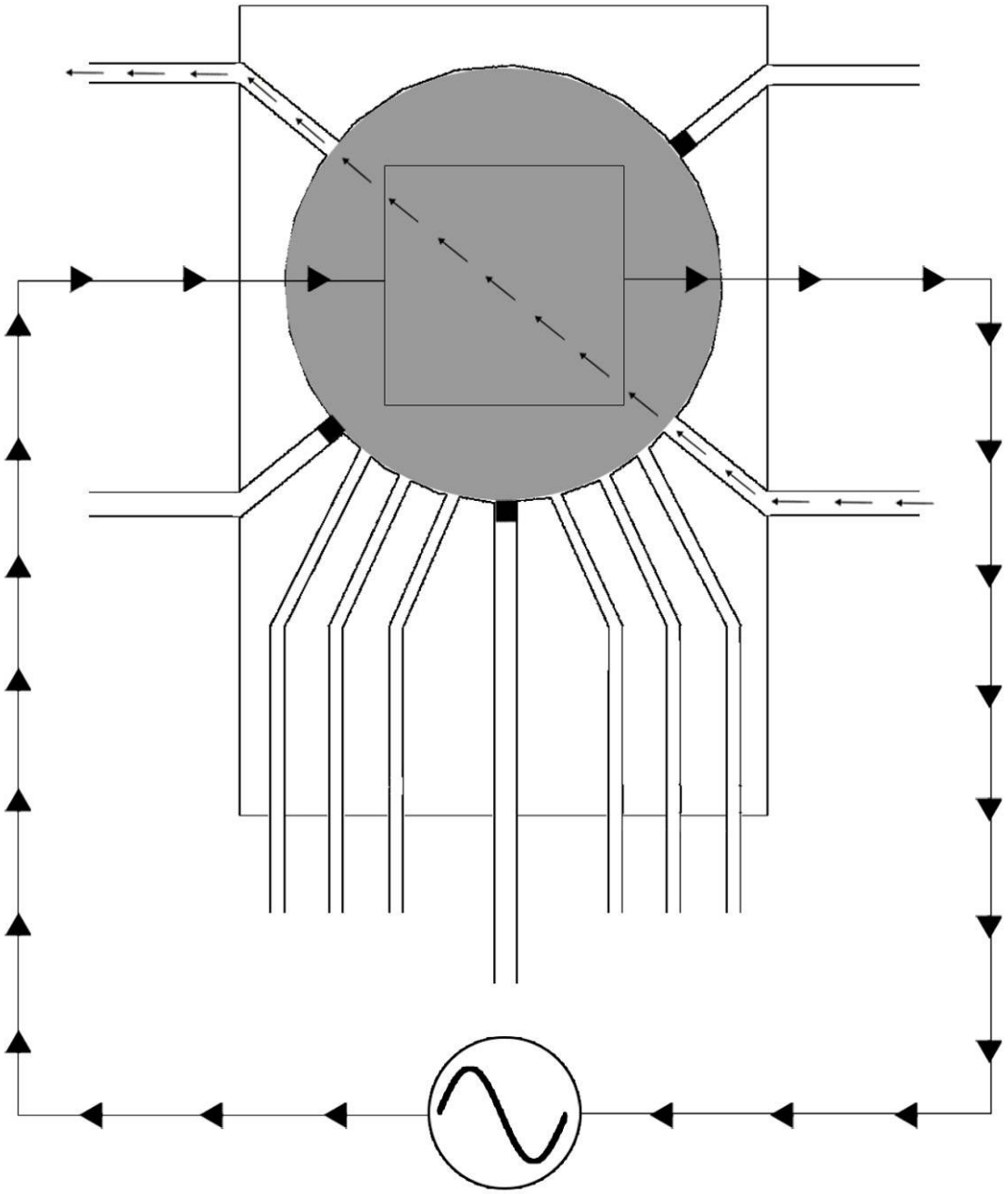

Fig. 80. *Design schematics showing the 5th stage of the cancer cell isolation operation – Cleansing of Normal (Non-Cancerous) Cells*

Once the clean values have opened, low-pressured air is blown into clean entrance inlet (Part 4 in Fig. 67). This gradually pushes out the normal (non-cancerous) cells, in a solution, out from the operation chamber (Part 9 in Fig. 67) and through the clean exit inlet (Part 5 in Fig. 67). All the clean cells would then exit back into the body, whilst the cancerous cells would still be magnetically attracted to component 1.

4.5.6. STAGE 6 – CLOSING CLEAN VALVES 1 & 2

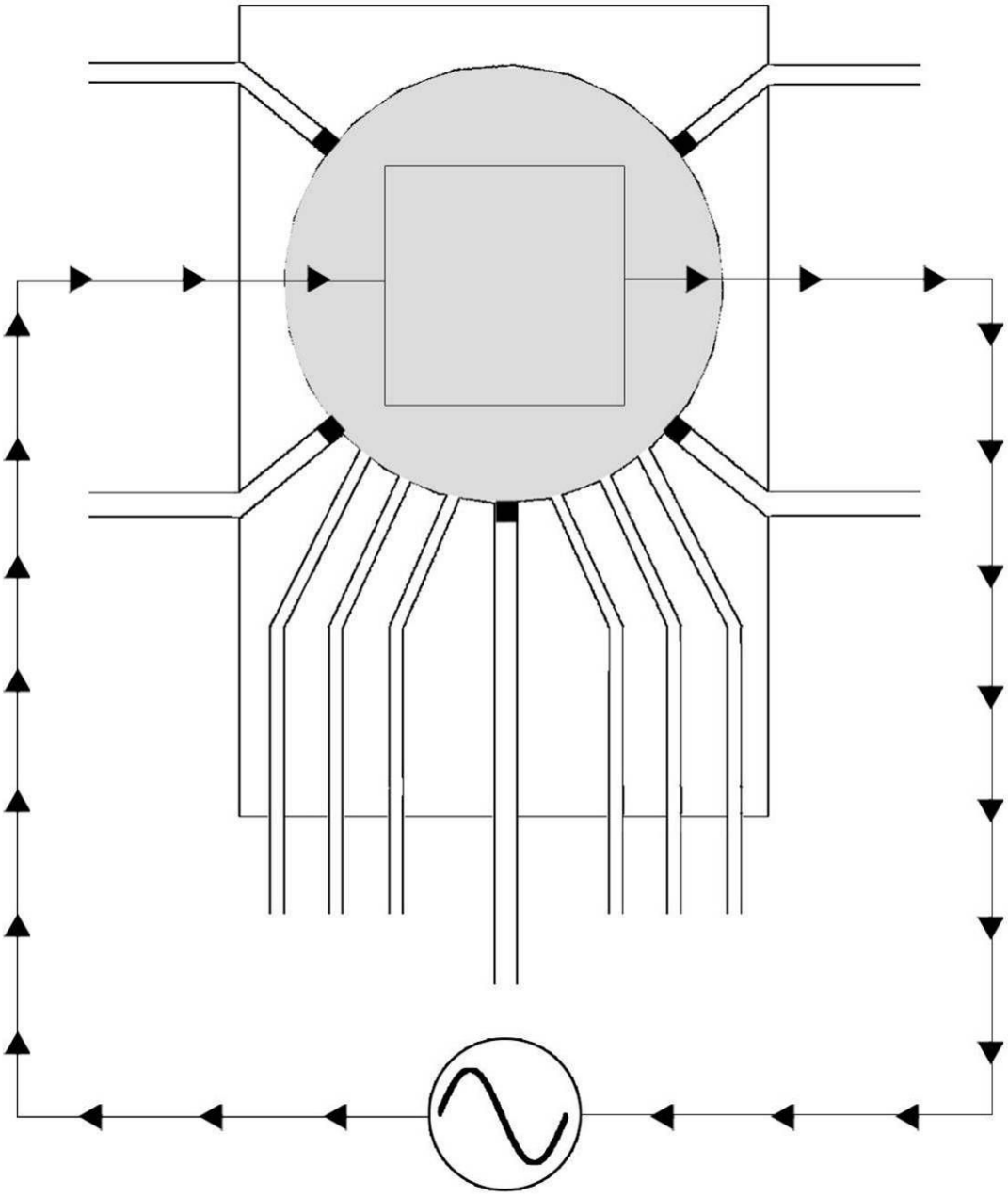

Fig. 81. *Design schematics showing the 6th stage of the cancer cell isolation operation – Closing clean valves 1 & 2*

Once the normal (non-cancerous) cells have been flushed back into the body and the nanoparticle hybrid-cancer cell bioconjugates are still magnetically attracted to component 1 (Part 8 in Fig. 67), the clean inlets (Parts 1 and 2 in Fig. 62) are then closed.

4.5.7. STAGE 7 – OPENING WATER SUPPLY VALVE

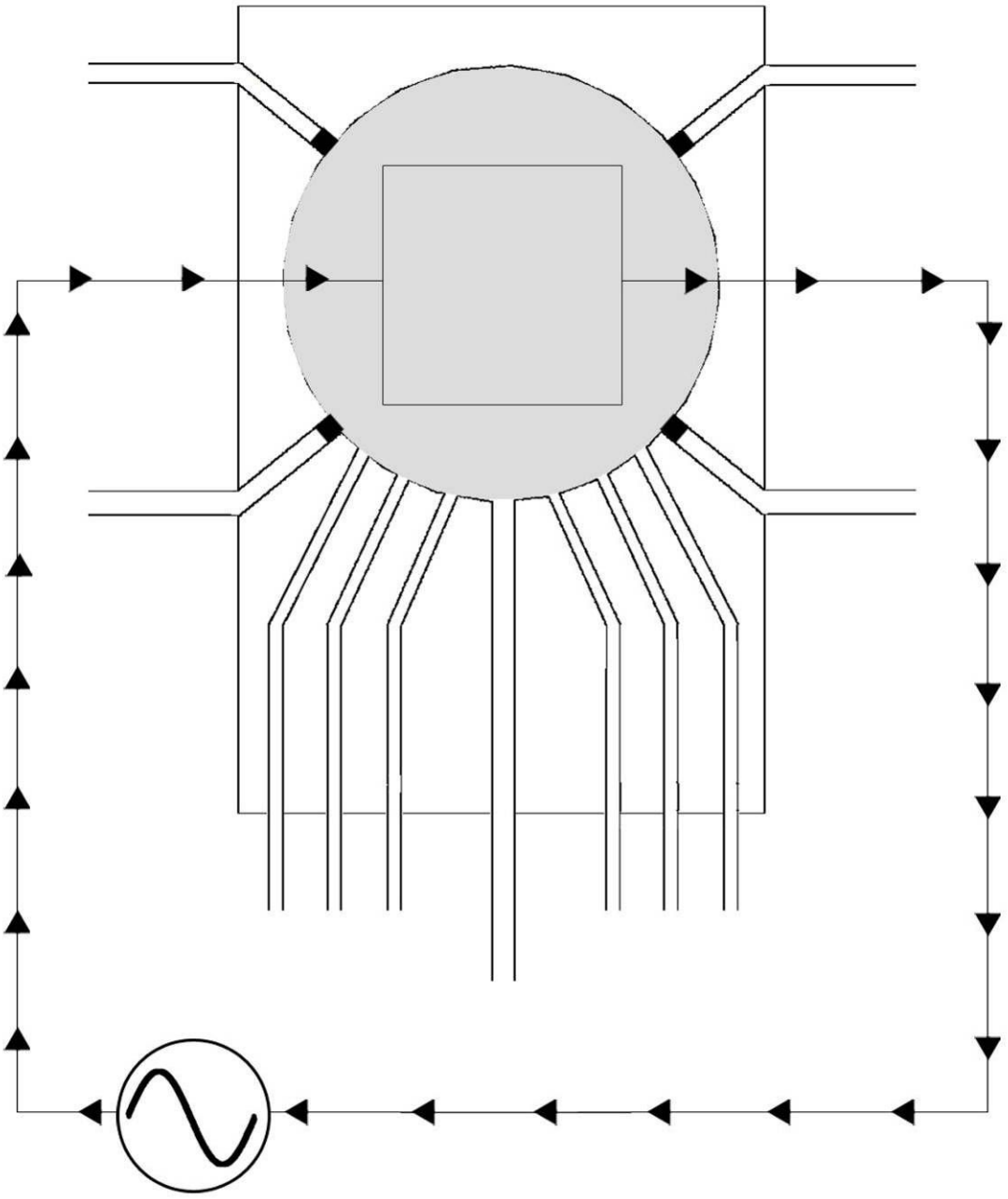

Fig. 82. *Design schematics showing the 7th stage of the cancer cell isolation operation – Valve for water supply inlet is opened*

As the normal (non-cancerous) cells were flushed out along with most of the aqueous liquid, the cancerous cells, attached to the nanoparticle hybrids, were still magnetically attracted to the electrodes. The operation chamber needs to be filled up with water in order for the cancerous cells to flow freely in the next several stages. This is why the valve (Part 5 in Fig. 62) for the water supply inlet (Part 3 in Fig. 67) is opened.

4.5.8. STAGE 8 – INSERTION OF WATER

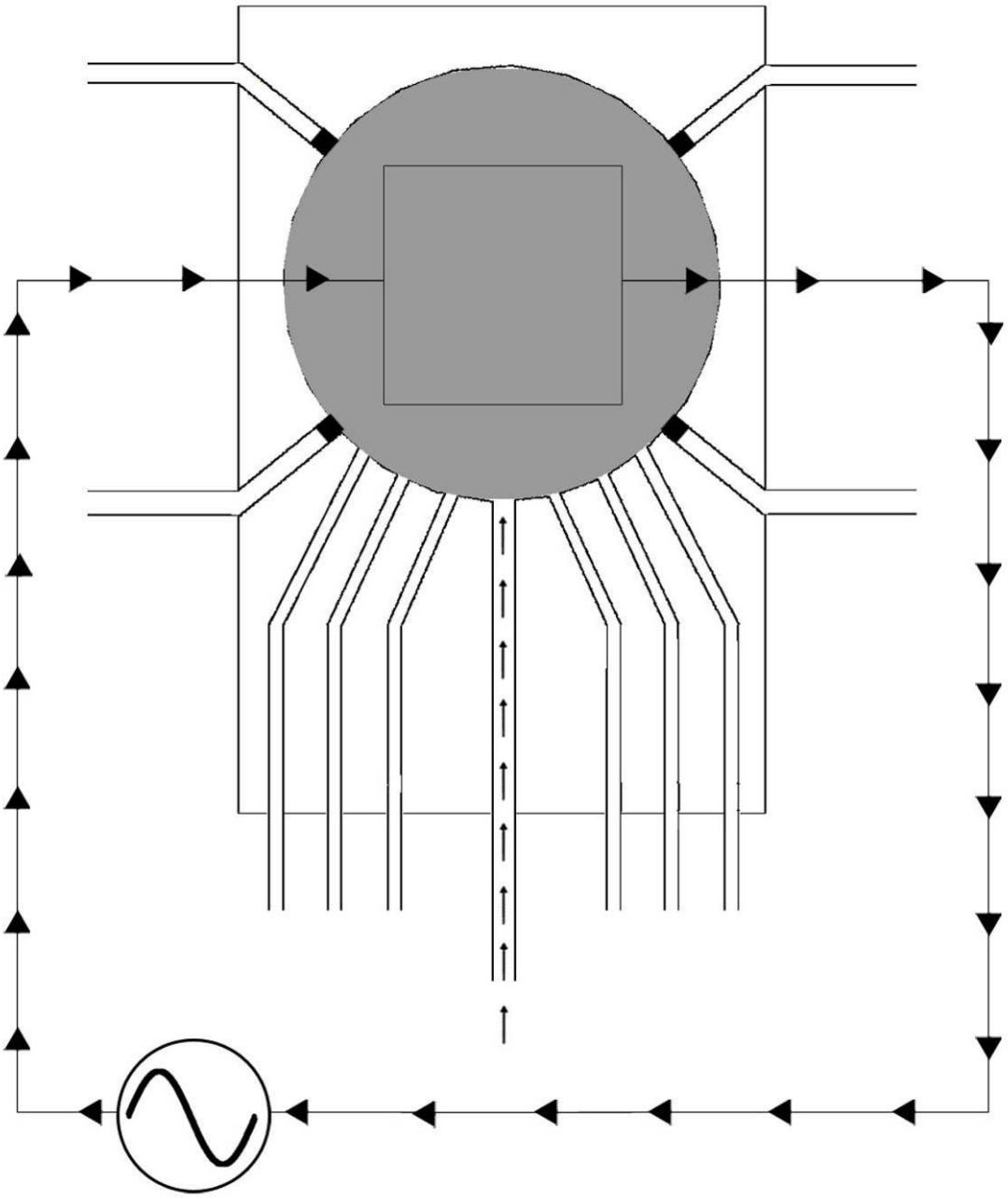

Fig. 83. *Design schematics showing the 8th stage of the cancer cell isolation operation – Insertion of water*

Once the water supply inlet valve (Part 5 of Fig. 62) is opened, a calculated volume of water is inserted into the operation chamber (Part 9 in Fig. 67) at low pressure.

4.5.9. STAGE 9 – CLOSING WATER SUPPLY VALVE

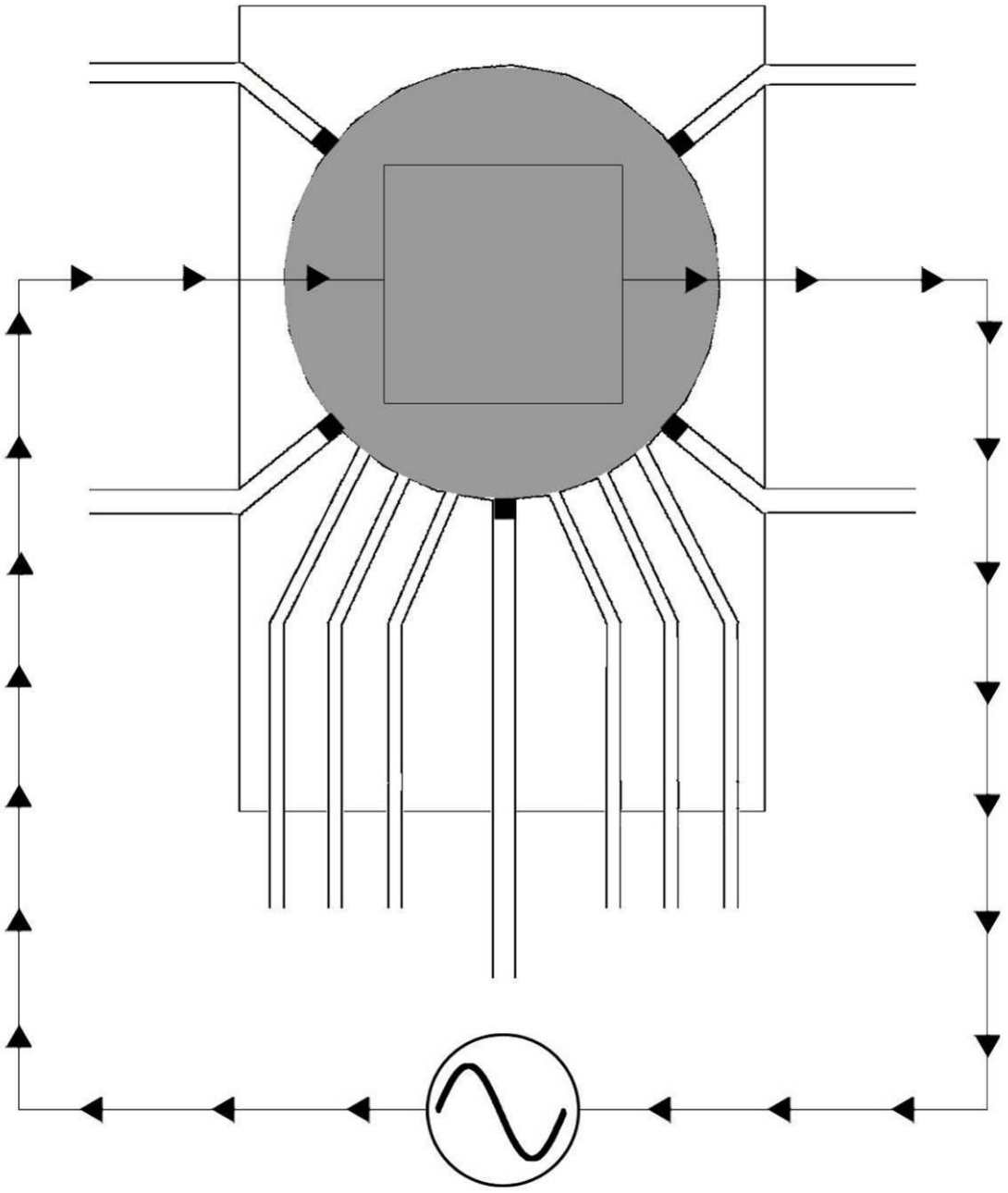

Fig. 84. *Design schematics showing the 9th stage of the cancer cell isolation operation – Valve for water supply inlet is closed*

Once the operation chamber (Part 9 of Fig. 67) is completely filled with water, the water supply inlet valve (Part 5 of Fig. 62) is closed. This then leads to the next stage where the voltage supply will shut off.

4.5.10. STAGE 10 – VOLTAGE (AC DIELECTROPHORESIS) OFF

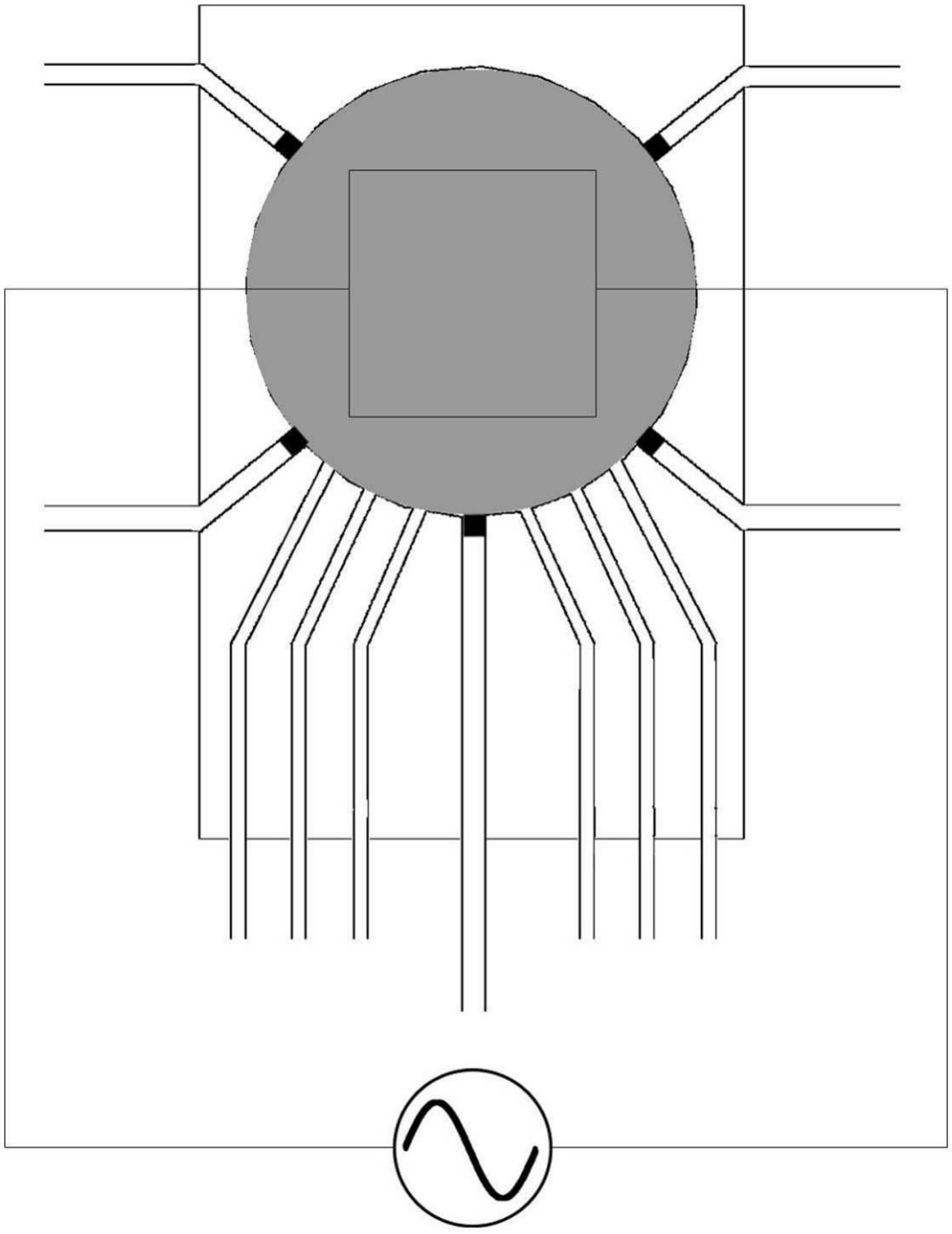

Fig. 85. *Design schematics showing the 10th stage of the cancer cell isolation operation – Voltage, under AC Dielectrophoresis is turned off*

Once the water supply inlet valve (Part 5 of Fig. 62) has been closed, voltage supply is then shut down. This stops the nanoparticle hybrids, with their attached cancer cells, from being magnetically attracted to component 1 (Part 8 of Fig. 67). Now as the operation chamber is filled with a liquid, the nanoparticles, with the attached cancerous

cells, can roam around freely. At this stage we have the chance to destroy cancerous cells.

We can apply a short millisecond pulse of energy from a 1064 nm laser, producing a nanoexplosion through a hyperthermia. As nanotubes absorb very strongly in the near infrared range, while most biological species are transparent in this region (controls studies showed cells without nanotubes are undamaged by the laser). The nanotubes absorb the laser energy, causing severe local heating and non-linear transfer of heat into the surrounding cell, a process that generates a shock wave that reaches upwards of 100 MPa in magnitude, and destroy the cells in a matter of milliseconds. Studies have shown that using this technique, 85% cells with nanotube uptake were destroyed within 20 seconds, while 90% of cells without the nanotubes survived. [20]

The main reason for destroying the cancer cells first before flushing them out is the possibility of several of bioconjugates still remaining in the operation chamber (Part 9 of Fig. 67) The destruction of these cancerous cells will fully verify that they have been destroyed and will be easier to flush out through the waste exit inlet (Part 7 of Fig. 67).

4.5.11. STAGE 11 – OPENING WASTE VALVES 3 & 4

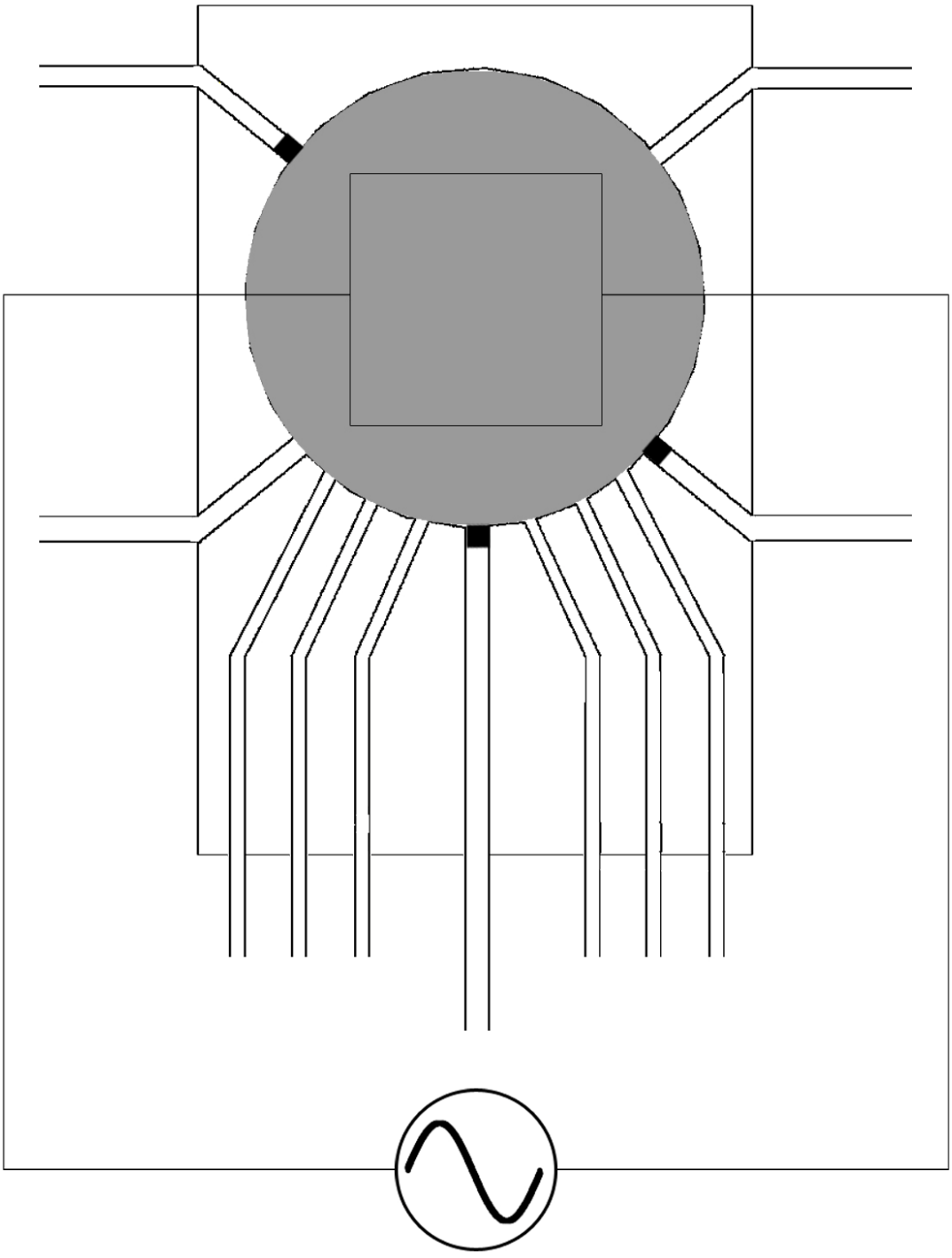

Fig. 86. *Design schematics showing the 11th stage of the cancer cell isolation operation – Opening waste values 3 & 4*

After a short millisecond, the nanotubes have irritated and created nanoexplosions destroying their attached cancerous cells. Debris from both the nanoparticle hybrids and cancerous cells are floating in the aqueous liquid in the operation chamber (Part 9 of

Fig. 67). Now both the waste exit inlet (Part 7 in Fig. 67) and the waste entrance inlet (Part 6 in Fig. 67) are now opened.

4.5.12. STAGE 12 – CLEANSING OF NANOPARTICLE HYBRID AND CANCER CELL DEBRIS

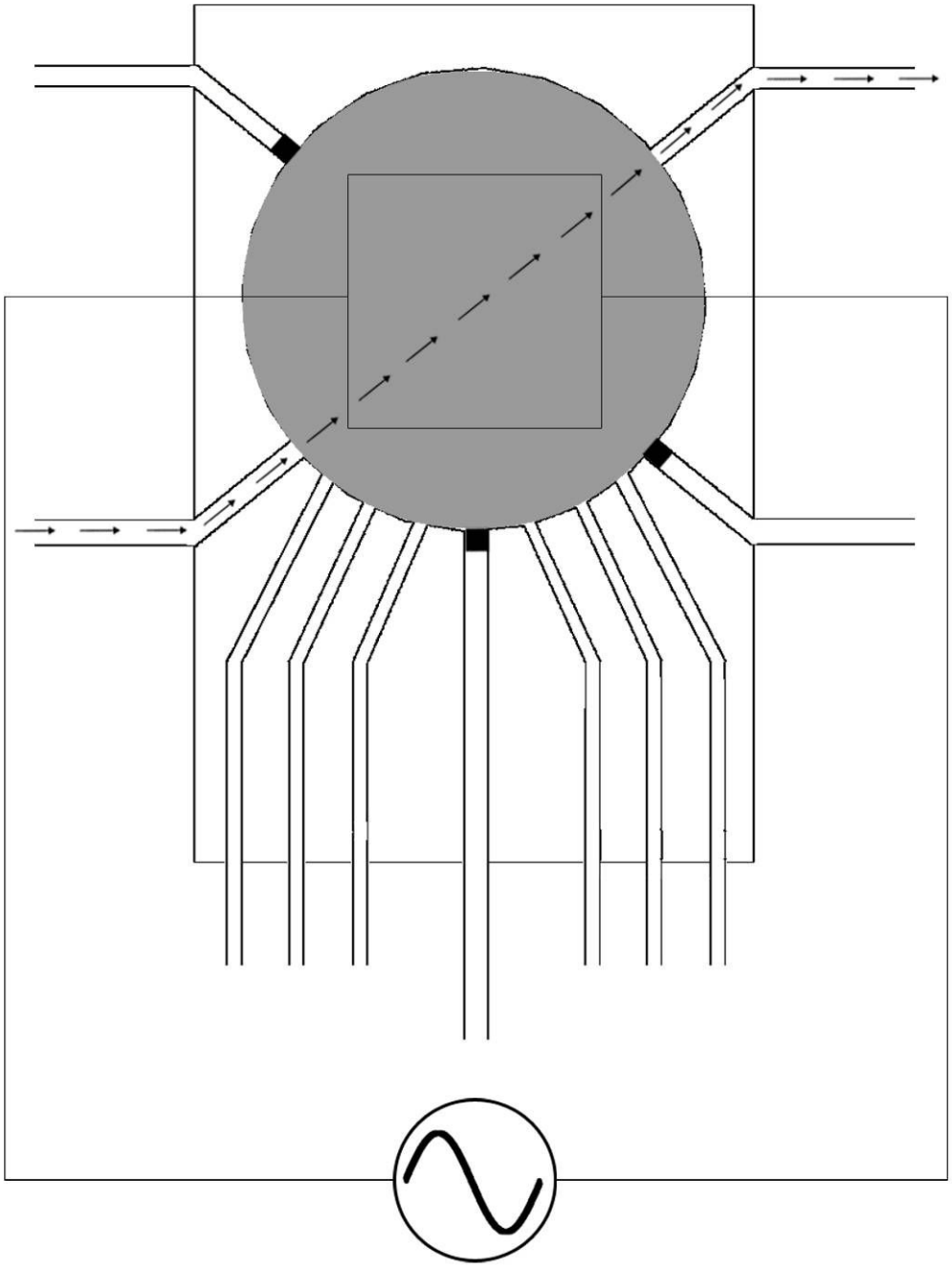

Fig. 87. *Design schematics showing the 12th stage of the cancer cell isolation operation – Cleansing of nanoparticle hybrid and cancer cell debris*

Once the waste values have opened, low-pressured air is blown into waste entrance inlet (Part 6 in Fig. 67). This gradually pushes out the debris, in the solution, out from

the operation chamber (Part 9 in Fig. 67) and through the waste exit inlet (Part 7 in Fig. 67) and into a waste container. The operation chamber is fully cleansed of particles, waiting to be reused.

4.5.13. STAGE 13 – CLOSING WASTE VALVES 3 & 4

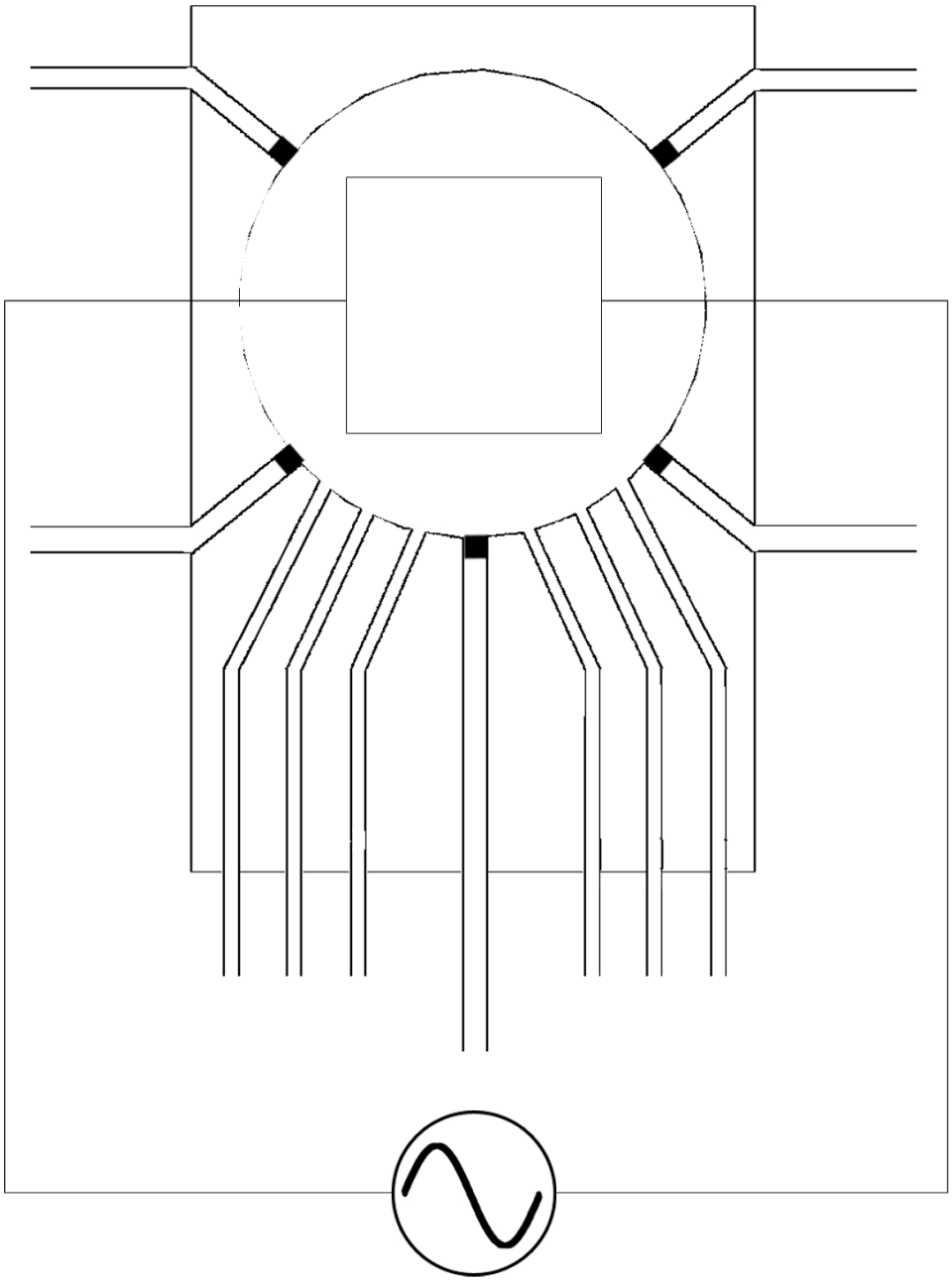

Fig. 88. *Design schematics showing the 13th stage of the cancer cell isolation operation – Closing exit valves 3 & 4*

Once the cancer cell and nanoparticle debris has been flushed out of the operation chamber (Part 9 of Fig. 67) through the waste exit inlet (Part 7 of Fig. 67), both inlets are then closed leaving the system at its initial state for further reuse.

5. RESEARCH TECHNIQUES

For the past two years, research skills were developed to improve my level of knowledge in both fabrication and microscopy techniques. The following techniques have been introduced and developed in The Department of Electronics and The York Jeol Nanocentre, both at The University of York. Professional training, regarding preparation, machine operation, and health and safety procedures, was provided beforehand.

These are the list of research techniques gained throughout the past 2 years:

1. **Optical/Photolithography**
2. Electron Beam Lithography
3. **Atomic Force Microscopy**
4. **Scanning Electron Microscopy**
5. Field Emission Scanning Electron Microscopy
6. Molecular Beam Epitaxy
7. Focused Ion Beam
8. Wire Bonding

Please note that the techniques highlighted are the ones that will be explained in more detail, as these have been used for the past year for fabrication and characterization. The other techniques will not be as they will be used in later stages of the project and will be mentioned throughout the report regarding future fabrication, characterization, testing and analysis of the project.

5.1. OPTICAL/PHOTO-LITHOGRAPHY

5.1.1. INTRODUCTION

Photolithography is the procedure of writing geometric circuit designs, from a photomask, onto the surface of a wafer, usually silicon. The basic steps involved for photolithography are wafer cleaning, barrier layer formation, photoresist application, soft baking, mask alignment, exposure and development, and finally hard-baking.

5.1.2. WAFER PREPARATION

The wafers are chemically cleaned to remove any excess particles on the surfaces. This may include any traces of organic, ionic, and metallic impurities. After the cleaning process, a barrier layer of silicon dioxide is deposited onto the surface of the silicon wafer. Depending upon the thickness of the layer this can either be achieved naturally or then through a high temperature baking process. After the formation of the SiO_2 layer, photoresist is applied to the surface of the wafer to produce a thin uniform layer of photoresist, also know as “Spin Coating”, which then undergoes high-speed centrifugal whirling of silicon wafers.

5.1.3. POSITIVE AND NEGATIVE PHOTORESIST

There are two types of photoresist: positive and negative. The positive photoresist is exposed with UV light wherever the original material is to be removed. The chemical structure of the resist changes, when exposed to UV light, to a point where it becomes more soluble in the developer. The developer solution washes away the exposed resist leaving windows of the bare underlying material. The mask, therefore, contains an exact copy of the pattern which is to remain on the wafer.

Negative resists work the complete opposite. The negative resist becomes polymerized, when exposed to UV light, becoming difficult to dissolve. This means the negative resists stays on the surface wherever it is exposed to UV light, letting the developer solution remove the unexposed areas. The photomasks used for negative photoresists contain the inverse of the pattern that needs to be transferred.

The Fig. 89 shows the pattern differences generated from the use of positive and negative resist.

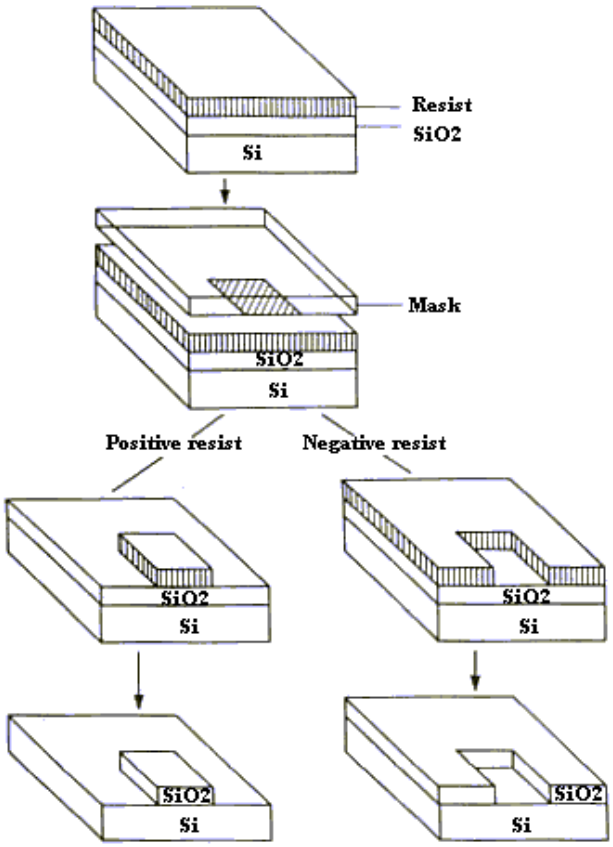

Fig. 89. *Diagram showing pattern differences generated from the use of positive and negative resist in photolithography* [50]

Even through negative resists were popular earlier in IC processing, positive photoresist became more popular because it provides better process controllability to generate designs with smaller attributes. And because of that advantage, it is the main photoresist for IC manufacturing processes.

5.1.4. SOFT BAKING

The critical step is used to remove all the solvents from the photoresist coating and plays a vital role in photolithography. The photoresist coating becomes photosensitive only after being soft-baked and that is why it is vital that it is baked for the correct time. Oversoft-baking will degrade the photosensitivity of the resist that could lead to reducing the developer solubility. Undersoft-baking will prevent light from reaching the sensitive areas of the photoresist, cause incomplete exposure if considerable solvent remains in the coating.

5.1.5. MASK ALIGNMENT AND EXPOSURE

This process includes a photomask, a square glass plate with a patterned emulsion of metal film on one side, aligned with a wafer. This alignment process allows the pattern to be transferred onto the wafer surface. Once the photomask is accurately aligned with the wafers surface, the photoresist will be exposed by the UV light generating a pattern, identical to that on the photomask. There are three primary exposure methods: contact, proximity, and projection. They are shown in the Fig. 90 below:

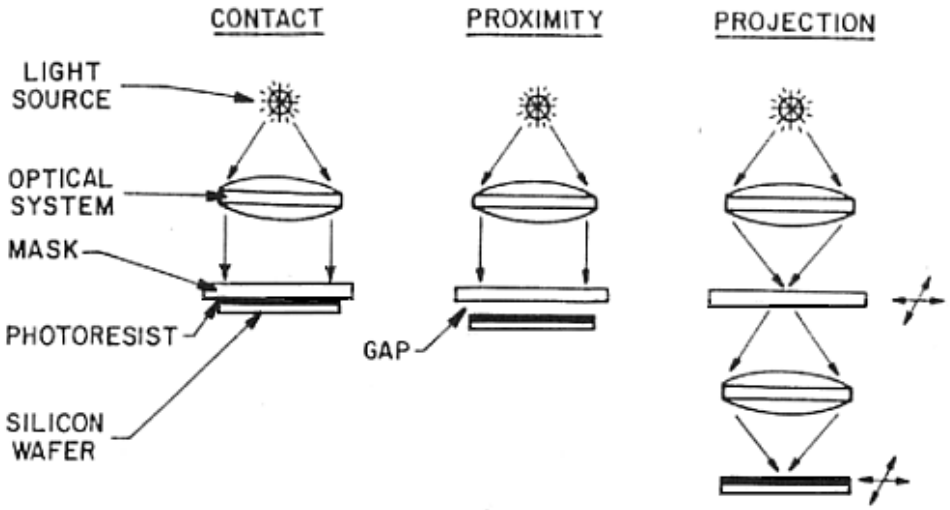

Fig. 90. *Diagram showing three primary exposure methods: contact, proximity, and projection in photolithography* [50]

The mask alignment system at The University of York for optical lithography follows the contact exposure method. In this printing method, the photoresist coated silicon wafer is brought into physical contact with the glass photomask. As the wafer is held in a vacuum chuck, the whole assembly then rises until the wafer and the photomask are in contact. After a few changes in settings, the photoresist is exposed with UV light. Very high resolution is achievable in contact printing as the wafer is in direct contact with the photomask. Design features down to 1 micron can be achieved with positive photoresist. The only disadvantage with contact printing is that debris can be trapped between the resist and the photomask. This can damage the mask and cause defects in the design that can affect the performance. This is why sample preparation is vital in particle free environment.

5.1.6. DEVELOPMENT

The development stage is one of the last steps of photolithography. The Fig. 91a shows response curves for negative and positive resist after exposure and development.

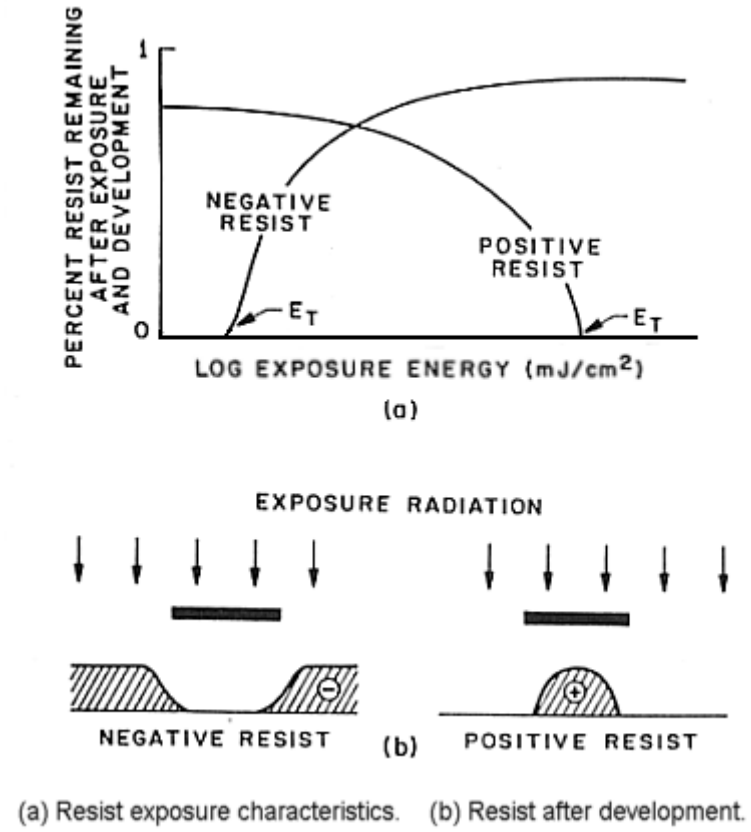

Fig. 91. *Diagram showing response curves for negative and positive resist after exposure and development in photolithography* [50]

The Fig. 91b shows the effect of exposure energies to the development of designs on photoresist. As we can see, the negative resist remains completely soluble in the developer solution under low-exposure energies. As the exposure increases over the threshold energy E_t more of the unwanted resist does not dissolve with the developer and remain on the wafer. The solubility of positive photoresist in its developer is finite, even at zero-exposure energy. So for optical lithography using positive photoresist, the main focus will lie on strengthening the photoresist polymers and not worrying about any remaining photoresist under development.

5.1.1.6. HARD-BAKING

This is the final step in photolithography. It is vital that this baking process hardens the photoresist to improve adhesion of the photoresist to the wafer surface.

5.2. ATOMIC FORCE MICROSCOPY

5.2.1. INTRODUCTION

Atomic force microscopy is a characterization technique that analyzes samples at a microscopic level. We are able to look at surface characteristics ranging from 100 μm to 1 μm with very accurate resolution imaging. The operation of AFM consists of allowing an extremely fine tip, usually 2 microns long and less than 100Å in diameter, which either comes in contact or in very close proximity to the characterized sample.

This tip is located at the end of a cantilever which is 100 to 200 μm long, and is scanned underneath the tip. When in operation, different forces attract and repel the tip producing deflections which imaging software records and processes to a topological representation of the deflections.

5.2.2. HOOKES LAW MEASUREMENT

The cantilever probes, located at the end of the cantilevers, acts like a spring under operation. The amount of force between the probe and the sample is dependent on the spring constant (firmness) of the cantilever and the distance between the probe and the sample surface.

This force can be described using Hooke's Law: $F = - k \times x$

F = Force

k = spring constant

x = cantilever deflection

5.2.3. PROBE MATERIALS

Si_3N_4 and Si are the two popular materials for cantilever probes. However, depending upon the sample, different cantilever materials and lengths are used to achieve certain spring constants and resonant frequencies. Even sometimes probes may be coated with other material for additional Scanning Probe Microscopy (SPM) applications, i.e. Magnetic Force Microscopy (MFM) and Chemical Force Microscopy (CFM).

5.2.4. INSTRUMENTATION

The instrumentation required for AFM is quite similar to Scanning Tunneling Microscopy (STM). The movement of the probe across a sample surface is controlled equally to when one is using the feedback loop and piezoelectronic scanners. However, the main difference in the instrumentation is how the probe to sample surface forces is

observed. When a probe deflects, the data is then measured by a "beam bounce" method. A semiconductor diode laser bounces light back off the cantilever towards a positioned sensitive photodiode detector. The bending of the cantilever during the tip is measured by the detector which is then used to create a topographical image of the sample surface.

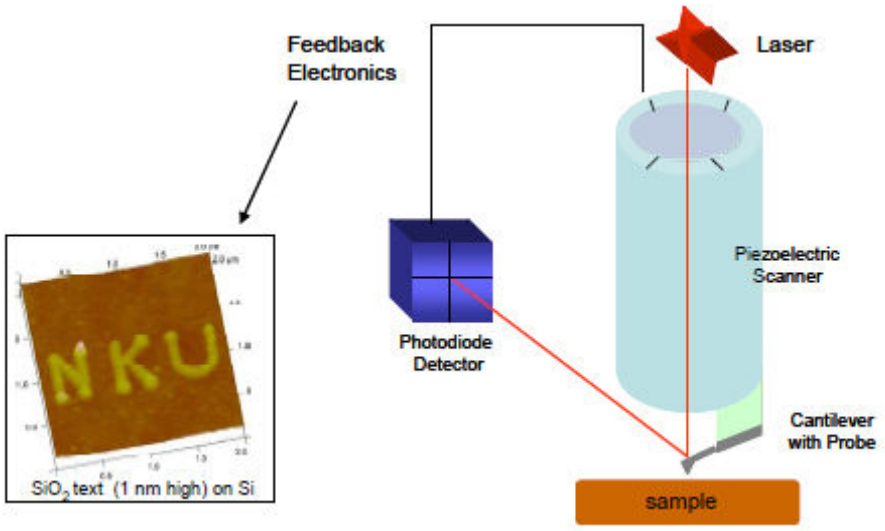

Fig. 92. *Schematic of AFM Instrumentation showing "beam bounce" detection scheme for imaging* [51]

5.2.5. TYPES OF FORCES MEASURED

The van der Waals force is the most common interatomic force in AFM. The relationship between force and distance can be seen in Fig. 93.

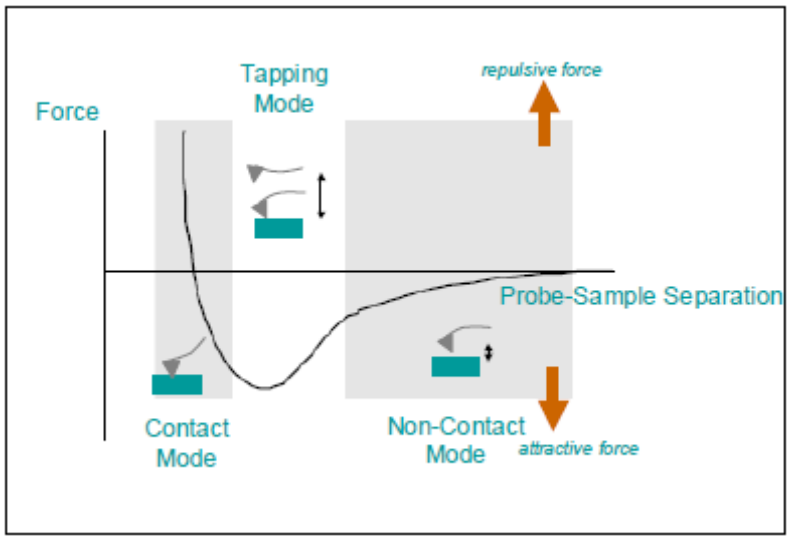

Fig. 93. *Force as a function of Probe-Sample Separation in AFM* [51]

In the contact mode region, the distance between the cantilever and the sample surface are less than a few angstroms (10^{-10} m) making the interatomic force between them repulsive. In the non-contact region, the distance between the cantilever and sample surface is on the order of tens to hundreds of angstroms making the interatomic force between them attractive.

Different scanning modes are used to operate in different regions of the curve shown in Fig. 93. Non–contact in the attractive region, contact mode in the repulsive and tapping mode oscillates between the two.

5.2.6. MODES OF OPERATION

There are three main imaging modes in AFM:

<u>Contact Mode AFM</u> - 0.5 nm probe-surface separation – Repulsive vdW

The cantilever bends with the spring constant of the cantilever is less than the surface. As the force on the tip is repulsive, the force between the probe and the sample remains repulsive by maintaining a constant cantilever deflection. This then provides a topographical image.

Advantages: quick scanning, ideal for rough samples, used a lot in friction analysis

Disadvantages: soft samples could be damaged with large samples, however introduction of liquids could solve this.

<u>Intermittent Tapping Mode</u> - 0.5-2 nm probe-surface separation

Cantilever is oscillating at resonant frequency. The cantilever probe taps onto the sample surface during scanning, obtaining an image which is very similar to that in contact mode. Make sure that there is a constant oscillation with no variance in amplitude allowing a constant force for cantilever tip and surface sample interation.

Advantages: good for biological and soft samples that usually get damaged in contact mode AFM.

Disadvantages: slower scan speeds and harder to create an image in liquid unlike in contact mode AFM.

<u>Non-contact Mode AFM</u> - 0.1-10 nm probe-surface separation – Attractive vdW

Even though there is no contact between the sample surface and cantilever probe, the tip oscillates above the fluid layer absorbed on the surface during scanning. The feedback look is used to monitor variances and maintain amplitude due to the attractive van der Waals forces.

Advantages: very small force is applied on surface, extension in life-span

Disadvantages: reduced resolution images, contaminated layer on surface can affect amplitudes in oscillations, process needs to be done in a ultra high vacuum.

5.2.7. FORCE CURVES

These are the measurement of force felt by the cantilever probe top when brought close to or in contact with a surface sample. The force curve analysis shown in Fig. 94 shows how a probe is repeatedly in contact with a surface and thereafter retracted. We can use force curve analysis to determine mechanical and chemical properties such as adhesion, robustness, elasticity and etc.

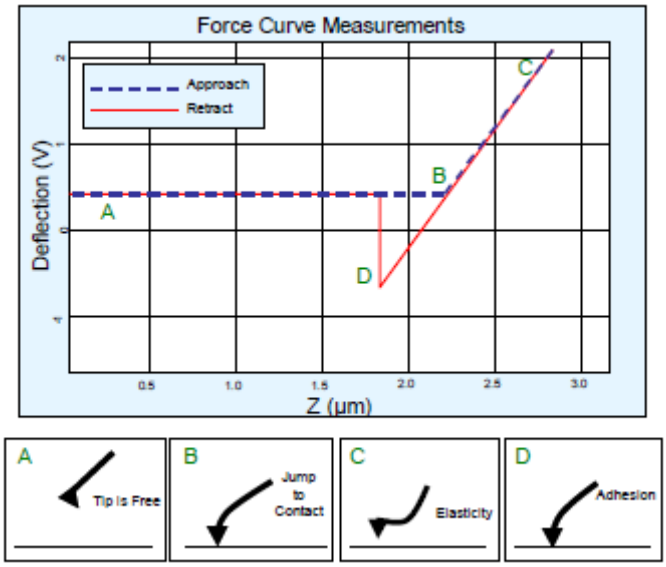

Fig. 94. *Generic force curve analysis for AFM* [51]

5.2.8. LIMITATIONS AND COMPARISONS

AFM has the advantage to characterize a variety of metal, plastic and biological samples. However, it is very hard in achieving images with atomic resolutions, which is mainly due to the cantilever probe not ideally sharp to a point where high atomic resolution images are achievable. Also the AFM image does not truly represent the sample topography as it generates an image based on probe-sample surface interactions.

So usually images have a main issue called tip convolution which widens the characterized sample due to an increase in radius of curvature of the probe. Fig. 95 shows the difference between high and low aspect top and how it affects the probe-sample surface interactions.

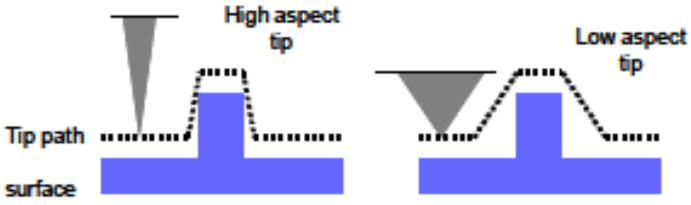

Fig. 95. *Comparison of tip convolution between high and low aspect tips* [51]

AFM versus SEM:
Compared with Scanning Electron Microscopy, AFM provides a better topographical result regarding height definition and surface smoothness.

AFM versus TEM:
Compared with Transmission Electron Microscopy, AFM provide 3D imaging with cheaper sample preparation procedures and provide more 2D imaging information than a TEM.

AFM versus Optical Microscope:
Compared with Optical Microscope, AFM provide height and surface smoothness measurement differentiating materials through their reflectivity.

5.3. SCANNING ELECTRON MICROSCOPY

5.3.1. INTRODUCTION

The big bang of SEM's began once scientists had used optical microscopes to their maximum limit. Being one of the most popular forms of microscopes around the world, their dependence towards light had become their main hurdle to evolve. Optical microscopes main flaw is how light tends to diffract around the edges of optical lenses. It is due to this diffraction which limits the microscope to obtain high resolution images.

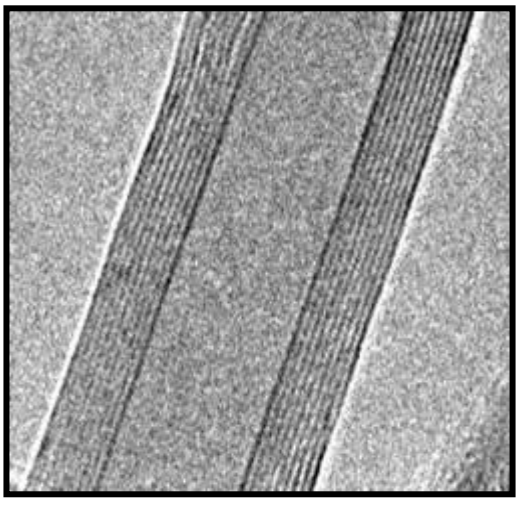

Fig. 96. *TEM image of MWNT* [52]

Realizing this flaw, scientists develop the Transmission Electron Microscope (TEM). This microscope beamed electrons directly through a sample and then obtains a projected high resolution image onto a fluorescent screen. Fig. 96 shows a TEM image of a multiwall nanotube, where electrons have beamed directed through the particle revealing its many layers. Since the development of TEM, the SEM was born by Professor C.W. Oatley at The University of Cambridge. Realizing its potential, Oatley exhibited the SEM's magnification potential of producing 3D images, which was the TEM's main drawback. Key components will be explained in the next section and can be seen in Fig. 98, a generic diagram of an SEM.

5.3.2. KEY COMPONENTS

Electron Gun

This component produces a steady stream of electron which is necessary to obtain a decent image and operate the SEM. There are two types of electron guns: Thermionic and Field Emission. Thermionic guns, being the most common, get their image by applying thermal energy to a tungsten filament to coax electrons from the gun to the sample. Field emission guns pull electrons away from the atoms, on the sample, using a strong electrical field. The electron gun fires a beam of electrons either from the top or from the bottom. However, these electrons do not naturally bombard the sample. They go through the next component.

Lenses

The SEM uses a series of non-conventional lenses to obtain high resolution images. These lenses are made of magnets that bend the path of electrons, projected from the electron gun. The lenses focus and control the electron beam precisely directing the electrons to the area they need to go.

Sample chamber

The sample chamber is the SEM component where you put your sample in for examination. In order to produce clear images the sample must but be kept very still. Usually the sample holder will have an adhesive base which holds the sample down very sturdily and completely isolated from any vibrations. The sample holder can also be placed at different angles, allowing you to observe the sample from many viewpoints.

Detectors

The detectors on the SEM are the component which collects the electron beams interaction with the sample and produces the high resolution images. For example, Everhart-Thornley detectors collect secondary electrons, which are electrons removed from the outer surface of the sample. These detectors produce some of the most high resolution images up to date. Fig. 97 shows the detector collecting secondary electrons and multiplying it towards a high resolution image. There are other detectors such as X-ray and backscattered electron detectors, which can provide experimental data, such as composition of a substance, as well as a high resolution image.

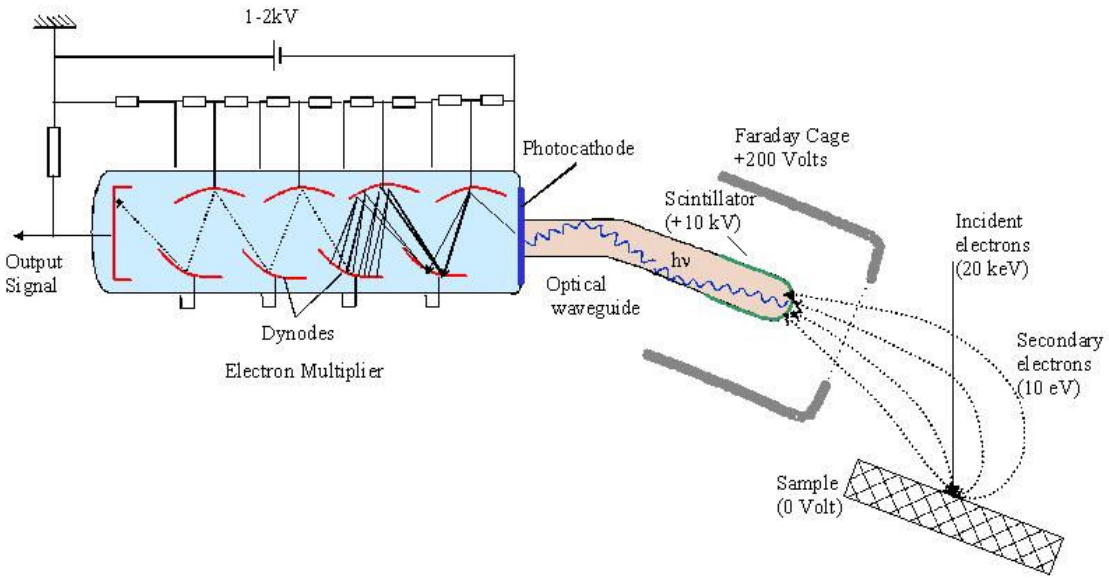

Fig. 97. *A secondary electron scintillator-photomultiplier detector following the design of Everhart and Thornley* [53]

Vacuum Chamber

The entire microscope is required to be under vacuum. Without the vacuum, the electron beam particles would collide with air particles causing constant interference which will affect the detail and resolution of the image.

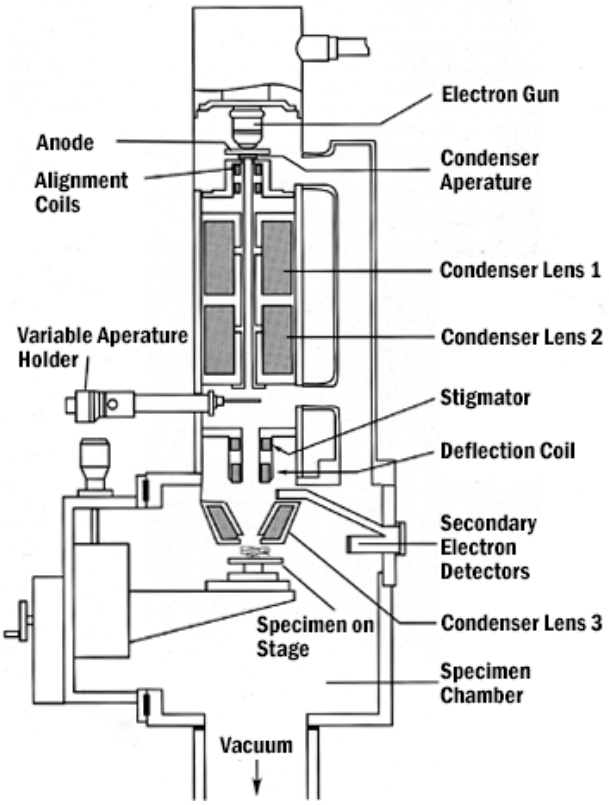

Fig. 98. *Generic Diagram of the main components of SEM* [54]

5.3.3. GENERAL OPERATION

The main function of the SEM is to trace an image over the specimen, creating a identical 3-D replica on the monitor with shades. The electron beam interacts with the surface of the specimen, when tracing over the object, and removes any secondary electrons from the surface of the sample. The secondary electron detector then attracts those secondary electrons, and formulates details such as brightness and contrast levels. Other sensors attract the backscattered electrons, which are reflected off the samples surface. The SEM has scanning or deflecting coils, as shown in Fig. 98, which uses oscillating voltage to control and manipulate the movement of the electron beam.

6. EXPERIMENTAL HYPOTHESIS

After conducting discrete literature review followed with hypothetical ideal designs and goals, these are hypothesises that I have concluded for the duration of the project for all three components and operation itself.

6.1. COMPONENT 1: MICRO-AND NANOELECTRODE TECHNOLOGY

We are expecting the full fabrication of ten samples of component 1's. As five electrodes are designed, two samples have been perfectly fabricated with the microelectrode parameters on one and nanoelectrode parameters on the other.

Each sample will have the following characteristics after fabrication:

- An evenly smooth 1 μm layer of SiO_2
- Perfectly evaporated layer of 5 nm thick Chromium (Cr) –
  Identical to the design
- Perfectly evaporated layer of 40 nm thick Permealloy ($Ni_{80}Fe_{20}$) –
  Identical to the design
- Perfectly evaporated layer of 5 nm thick Gold (Au)–
  Identical to the design
- All the electrodes are smooth and are not rigid
- All the electrodes are fabricated perfectly to their desired design requirements
- No debris
- No bridges between the electrodes (No Short Circuits)
- A current does not pass from one set of electrodes to the other until a bridge (component 2) makes that link to pass.

6.2. COMPONENT 2: MWNT-SPQD-ANTIBODY NANOPARTICLE HYBRID

We are expecting an aqueous solution with the perfect dispersion of component 2 particles. The nanoparticle hybrids are fabricated to match their desired design requirements, and then undergo a process of being perfectly distributed in an aqueous solution.

Each particle will have will have the following characteristics after fabrication:

- Each MWNT, after undergoing a breaking process, will be of lengths 500nm to 1 μm for the nanoelectrode sample for component 1 and 20 μm to 30 μm for the microelectrode sample for component 1.
- There will only be one SPQD-Antibody bioconjugate attached to each nanotube
- Each SPQD's will fluoresce a neon green colour once excited with UV light.
- Each antibody on component 2 will ONLY attach onto cancerous cells.
- Each nanoparticle hybrid will be attracted onto Component 1 via the electrostatic force generated, when a current under AC dielectrophoresis is applied. They will form bridges allowing the current to pass from one set of electrodes to the other.
- The nanotubes will create nanoexplosions once irradiated with a laser, wavelength of 1064nm, following with the destruction of the attached cancer cell.

6.3. COMPONENT 3: MICROFLUIDIC OPERATION CHIP

We are expecting a perfect construction of the microfluidic operation chip which is perfectly fabricated with the required design parameters.

Each chip will have will have the following characteristics after fabrication:

- The cancer cell solution will perfectly flow into the operation chamber (Part 8 of Fig. 57) from cancer sample inlets (Part 1 of Fig. 57)
- The nanoparticle hybrid aqueous dispersion will perfectly flow into the operation chamber (Part 8 of Fig. 57) from nanoparticle hybrid aqueous dispersion inlets (Part 2 of Fig. 57)
- Water will perfectly flow into the operation chamber (Part 8 of Fig. 57) from water supply inlets (Part 3 of Fig. 57)

- The normal (non-cancerous cells) will perfectly flow from the operation chamber (Part 8 of Fig. 57) out through clean exit inlet (Part 5 of Fig. 57) when low pressured air is being blown from clean entrance inlet (Part 4 of Fig. 57)
- The cancerous cells and nanoparticle hybrid debris will perfectly flow from the operation chamber (Part 8 of Fig. 57) out through waste exit inlet (Part 7 of Fig. 57) when low pressured air is being blown from waste entrance inlet (Part 6 of Fig. 57)
- Clean exit valve (Part 1 of Fig. 62) will successfully block clean exit inlet (Part 5 of Fig. 57)
- Clean entrance valve (Part 2 of Fig. 62) will successfully block clean entrance inlet (Part 4 of Fig. 57)
- Waste entrance valve (Part 4 of Fig. 62) will successfully block waste entrance inlet (Part 6 of Fig. 57)
- Waste exit valve (Part 3 of Fig. 62) will successfully block waste entrance inlet (Part 7 of Fig. 57)

6.4. CANCER CELL ISOLATION OPERATION

We are expecting a perfect integration of all three components together to perform the microfluidic cancer cell operation system as shown in section 4.4. We hypothesize that the operation is identical to that what was explained in section 4.5.

1. Insertion of test solutions
2. Bioconjugation of nanoparticle hybrids and cancer cells
3. Voltage (AC Dielectrophoresis) on
4. Opening clean entrance and exit valves
5. Cleansing of normal cells back into body
6. Closing clean entrance and exit valves
7. Opening water supply valve
8. Insertion of water
9. Closing water supply valve
10. Voltage (AC Dielectrophoresis) off
11. Opening waste entrance and exit valves
12. Cleansing of nanoparticle hybrid and cancer cell debris
13. Closing waste entrance and exit valves

7. FABRICATION

7.1. COMPONENT 1: ADVANCED ELECTRODE TECHNOLOGY

7.1.1. MICRO ELECTRODE TECHNOLOGY

The procedure below explains the step by step photolithography process needed to optically pattern the 5 mask designs, from section 4.1.1. to 4.1.5, onto silicon substrates. The entire procedure was conducted at The University of York, Department of Electronics, Clean Room. The silicon substrates, before photolithography, went through silicon oxide growth procedure, where 1 um layer was grown onto the substrate. The photolithography procedure explains the materials and equipment needed, the procedures for general preparation of substrates, photoresist coating, application of Chlorobenzene, mask alignment, UV exposure, sample development and evaporation of 20 nm Permealloy and a 5 nm Gold capping layer. The final sample product should follow the hypothetical specifications for component 1 in section 6.1.

7.1.1.1. MATERIALS & EQUIPMENT

Here is a list of materials needed for the fabrication of component 1:

1. RBS (Cleaning Agent)
2. Deionised(DI) water
3. Sulphuric Acid (H_2SO_4)
4. Hydrogen Peroxidise (H_2O_2)
5. Chlorobenzene (C_6H_5Cl)
6. Silicon(Si) Wafers
7. Gold Wire (Au)
8. Permealloy (20% Fe and 80% Ni)
9. Titanium Wire
10. Positive Photo-resist

11. Liquid Nitrogen

Here is a list of equipment needed for the fabrication of component 1:

1. Plastic Cases
2. Flats (Cleaving Si Wafer)
3. 250 ml Plastic Beaker (Hydrofluoric Acid use)
4. 250 ml Glass Beaker
5. 25 ml Plastic Measuring Cylinder (Hydrofluoric Acid use)
6. Petri Dishes
7. Nitrogen Blow Dryer
8. Hotplate Set
9. Spinner Machine
10. Evaporator
11. Microscope with attached Camera
12. Mask Aligner (Photolithography)
13. Ultrasonic Machine
14. 5 Micro-electrode photomasks
15. Soldering Iron
16. Waste Container
17. Pressure Meters (Evaporation)
18. Nano-thickness Meter (Evaporation)

7.1.1.2. PROCEDURE

GENERAL PREPARATION OF SILICON SUBSTRATE

1. Scribe the silicon wafer and cleave parallel or at right angles to the flats, so that you end up with 1.5 cm by 1 cm substrates.
2. Prepare RBS/water solution in a petri dish, by mixing DI water and a few drops of RBS.
3. Turn on the hotplate oven and set it at 150 ^{o}C.
4. Add the silicon pieces in the RBS/water solution and clean them with a cotton bud. (NOTE: This will remove the silicon particles)
5. Add the RBS/water solution and the silicon samples, from the petri dish, into a 50 ml glass beaker, and fill it with more deionised (DI) water.
6. Put the glass beaker into the water filled metal dish, in the ultra sonic machine, till it sinks to the bottom.

7. Turn the timing dial to 5 minutes and switch on the machine. Wait for 5 minutes. (NOTE: This will remove the silicon particles)
8. Take the beaker out and over wash with deionised (DI) water.
9. Wear protective gloves and mask.
10. Obtain Sulphuric Acid (H_2SO_4) and Hydrogen Peroxide (H_2O_2)
11. Make up a mixture of 1:1 H_2SO_4:H_2O_2. Pour approx 25 ml H_2O_2 into a 250 ml glass beaker then add approx 25 ml H_2SO_4.
12. Place the silicon in a petri dish and then add the sulphuric-peroxide mixture. (NOTE: This will remove organics from the surface.)
13. Setup the countdown timer for a cleaning time of 10 minutes, and leave the silicon in the sulphuric-peroxide mixture. (NOTE: Reaction will have died after 10 minutes)
14. Over wash and clean the silicon samples, the petri dish, and the 250 ml glass beaker with deionised (DI) water.
15. Blowdry the silicon samples with nitrogen gun.
16. Bake the silicon samples on a hotplate set at 150C for 1 hour.

THE SAMPLES ARE READY FOR PHOTO-RESIST COATING PROCEDURE

PHOTO-RESIST COATING

1. Turn on the hotplate oven and set it at 115 ^{o}C
2. Turn on the spinner and vacuum pump switches
3. Flip the spinner machine switch to turn on the machine
4. Turn the time dial to 40 sec
5. To test the speed put a silicon sample onto the spinner
6. Tap the footswitch to turn on the spinner
7. Turn the speed dial to 4000 rpm
8. Tap the footswitch to turn off the spinner
9. Using a dropper, apply positive photo-resist onto the silicon sample covering the entire area
10. Put on the protective plastic dish over the silicon sample
11. Tap the footswitch to turn on the spinner
12. Wait for 40 sec, until the spinner stops automatically
13. Bake the photo-resist covered silicon sample onto the hotplate set at 115C for 1 minute.

THE SAMPLES ARE READY FOR CHLOROBENZENE PROCEDURE

CHOLOROBENZENE

1. Obtain petri dish, syringe, Chlorobenzene (NOTE: The Chlorobenzene bottle is leak-proof and chemical can only be obtained through puncturing cloth-covered lid with a syringe)
2. Put the photo-resist covered silicon samples onto the petri dish
3. Assemble the syringe together
4. Open up the lid for the Chlorobenzene and tip it to its side
5. Puncture the cloth-covered lid and fill the syringe completely
6. Apply the first dosage into the petri dish and start the countdown timer for 1 minute
7. Apply a second dosage straight afterwards
8. Slowly twirl the petri dish until the countdown is completed
9. Over wash with deionised (DI) water
10. Blow dry the silicon samples with nitrogen gun.

THE SAMPLES ARE READY FOR PHOTOLITHOGRAPHY PROCEDURE

PHOTOLITHOGRAPHY
SWITCHING ON MASK ALIGNER MACHINE

1. Turn the compressed air supply (green tap), located on the right side of the machine.
2. Switch on the mask aligner vacuum pump, located on the wall switch, above the spinner machine.
3. Flip the switch, located on the bottom left of the machine, on the power to the 200nm lamp.
4. Push the green toggle switch, located on the bottom left of the machine, and check if the meter will read when the lamp has struck.
5. Check the power is switched on to the mask aligner.
6. Press the green button, located on the bottom right of the machine, which will power up the rack, allow the microscope to align itself and illuminate the CRT screen.
7. Select a number from 1-9 on the left-hand keypad. (NOTE: This will activate the monitor screen, which will display further instructions.)
8. Allow 30 minutes for mask aligner's 200nm lamp to warm up.

9. Select manual operation by pressing 7 on the left-hand keypad of the mask aligner.
10. Place mask on the mask holder.
11. Plug the vacuum tube into one of the two fast connectors on the left of the mask holder.
12. Prepare and apply parameter settings.

SETTING UP PARAMETERS

1. Press the parameter mode button on the left-hand keypad. (NOTE: This mode can be configured and reconfigured before step # 3 (exposure), when UV light is exposed onto the silicon substrate.)
2. To move to the parameter for resetting, repeatedly press the parameter key until the parameter you wish to alter is flashing. To exit 'parameter' mode press the start key.

These are the settings that can be changed during the photolithography process:

- **VACUUM CHAMBER:**
  - '0' disables this feature '1' enables this feature.
- **SUBSTRATE VACUUM:**
  - During the vacuum chamber operation '0' will turn off the vacuum to the chuck, '1' will leave the vacuum switched on.
- **PROXIMITY:**
  - '0' enters 'contact' mode '1' establishes 'proximity' mode.
- **SEPARATION TIME:**
  - Can be set between 0 and 15 seconds by entering the desired time on the numbers key pad. This represents the time between separation and validation of the controls.
- **PROXIMITY OR CONTACT:**
  - Proximity will be displayed in 'proximity mode, 'contact' will be displayed in contact mode. The distance between the substrate and mask can be set in proximity mode. The range is between 5 and 97.5 µm in 2.5 µm increments. Values are set using the key pad, values must be less than the separation distance. In contact mode the number of times contact has been established is displayed**.**
- **SEPARATION:**

- This is the distance between mask and substrate during alignment. The range is between 5 and 97.5 μm in 2.5 μm increments. The values are set using the key pad and must be greater than the proximity value if in proximity mode.

- **EXPOSURE TIME:**
  - This is set in minutes, seconds and then tenths of a second, with the maximum time of 30 minutes.
- **FORCE OF CONTACT:**
  - This is the force pressing the sample against the mask. This can be set between 200g and 1000g in increments of 10 grams, although 300g is more of a realistic minimum. Each number entered is automatically multiplied by 10, for example when setting the force entering the number 50 will equal 500g

PHOTOLITHOGRAPHY MANUAL MODE

1. Place the silicon substrate onto the chuck.
2. Press the start button, located on the right-hand side keypad, and "1 loading" will flash, on the CRT screen.
3. Press the start button again and the sample will load. (NOTE: The machine will beep 2 or 3 times before it loads in. However if it only beeps once, then there is a loading failure and one needs to slightly adjust the chuck before it beeps twice or thrice again.)
4. When loading is complete, press the start button again, and "2 alignment" will flash. (NOTE: At this stage, stage 3: exposure or stage 4: unloading can be selected by typing in 3 or 4.
5. Press the start button, to gain access to the alignment mode. (NOTE: Read section "Using a sample in alignment mode" for further instructions)
6. Press the start button to exit alignment mode, and "3 exposure" will flash. (NOTE: You can either press "4", to unload the sample, or press "start", to start up the exposure process. If you continue with exposure, remember to double check your PARAMETERS.)
7. Press the start button to start the process of exposing the silicon to UV light.
8. Once the machine has been detached and ready for use, press the start button again. (NOTE: UV lamp will turn on. Do not look directly into the light.)
9. After exposure, a message will appear on the CRT where you press:
    a. Stop Button: where "Stop key validates alignment cycle."

i. Alignment cycle puts microscope back over the mask and prepares another full operation for the next sample.

b. Start Button: where "Start key validates first exposure cycle."

i. UV lamp is left on top of the mask and the alignment cycle is then skipped.

10. Press the start button once more to choose the unloading stage, "4 unloading".
11. Press the start button once more to activate the unloading stage.
12. Wait for the chuck to come out. (NOTE: Sometimes the chuck gets stuck when coming out of the machine, hence use a small rod to push it out.)
13. Pick up substrate for development stage.

DEVELOPMENT

1. Prepare a clean, dry, empty petri dish.
2. Add the silicon substrates, which have gone through the photolithography procedure, into the petri dish.
3. Prepare the countdown timer, by setting it up to countdown 1 minute.
4. Add in the developer solution (APPENDIX 12.11) and begin timing.
5. After 1 minute, over wash with deionised (DI) water.
6. Use the nitrogen gun and blow dry the samples.
7. Setup a table as shown below and note down observations:

TEST #	SAMPLE #	DESIGN #	CONTACT TIME (sec)	CONTACT FORCE (gm)	DEVELOPER TIME (sec)
Overall Conclusions and Further Experimentation:					

ONCE YOU HAVE A SATSIFIEDPHOTO ON YOUR SUBSTRATE, PROCEED TO THE EVAPORATOR PROCEDURE

EVAPORATION

Close the Valves

1. Switch on rotary pump.
2. Switch on Pirani Gauge.
3. Open backing valve.
4. Turn on water to diffusion pump.
5. Switch on diffusion pump and allow 20 minutes to warm up.
6. Open air admittance valve.

7. Remove bell jar.

To Start if Left Under the Vacuum

1. Check that roughing valve is closed and backing valve open.
2. Switch off penning gauge if operating.
3. Close baffle valve.
4. Open air admittance valve.
5. Remove bell jar.

To Load Chamber

1. Place boat or filament across electrodes, note red and yellow wire are source colours, blue is common.
2. Load boats / filaments with source materials.
3. Support samples on frame face down.

To Pump Down Chamber

1. Replace the bell jar and safety cover.
2. Close air admittance valve.
3. Close backing valve.
4. Open roughing valve.
5. Check backing pressure is not rising, then change over to chamber pirani.
6. If backing pressure is rising rapidly close roughing valve open backing valve, then call for assistance.
7. Fill trap with liquid nitrogen, unless already filled.
8. When pressure on Pirani reads better than 0.2 Torr, close roughing valve, open backing valve and open baffle valve.
9. Switch on Penning gauge

When pressure reaches 4 x 10^{-5} plant is ready for operation

To Evaporate Material

1. Switch on power to variac. (Toggle switch)
2. Select source colour on rotary switch. (Colours marked by wires insulation)
3. Increase variac by 10-volt stages until material starts to evaporate.
4. Open shutter.
5. If using rate meter then close shutter when required thickness is reached.

6. If using predefined weight or all material then wait until all material has evaporated.
7. Immediately on completion zero the variac.
8. Switch source selector to the off position.
9. Switch off the power to the variac.

To Remove Samples

1. Switch off penning gauge.
2. Close baffle valve.
3. Open air admittance valve.
4. Remove the bell jar.
5. Remove samples.
6. For further evaporations return to loading chamber

After Last Evaporation

1. Remove boats / filaments.
2. Replace the bell jar and safety cover.
3. Close air admittance valve.
4. Close backing valve.
5. Open roughing valve.
6. Check backing pressure is not rising, then change over to chamber pirani.
7. If backing pressure is rising rapidly close roughing valve open backing valve, then call for assistance.
8. When pressure on Pirani reads better than 0.2 Torr, close roughing valve, open backing valve and open baffle valve.

8. MICROSCOPY PROCEDURE

8.1. ATOMIC FORCE MICROSCOPY

AFM is used to gain a topographical image of the electrodes and assess the height of the electrodes by analyzing the difference between the substrate and the evaporated material. A difference of 25 nm is expected as 20 nm of Permealloy is evaporated with a 5 nm Gold capping layer on top of it. The topographical data shall also help us assess the surface smoothness of the evaporated material to hopefully assess a uniform flat surface on the electrodes, which shall represent an even distribution of evaporated material on a flat SiO_2 surface.

8.1.1. EQUIPMENT

Here is a list of equipment needed gathering microscopy data for component 1:

1. Tweezers
2. Plastic cases to hold 1cm * 1cm substrate samples
3. Latex gloves
4. Cantilever

   Model: Veeco MESP

   Material: 0.01 – 0.025 Ohm0cm Anitmony (n) doped Si

   Tip Width: 2.5 – 3.5 μm

   Tip Length: 200 – 250 μm

   Tip Width: 23 – 33 μm

   Initial Frequency: 60 – 100 kHz

   Front Side Coating: TOP-10-250nm Co/Cr/BOT-1-10nm Cr

   Back Side Coating: TOP-10-250nm Co/Cr/BOT-1-10nm Cr
5. JEOL JSPM-5200 [58]

(Located at The York JEOL Nanocentre, The University of York) [59]

8.1.2. PROCEDURE

8.1.2.1. SETTING UP

1. Log onto the computer with the following details:
   Login: guest
   Password:
2. Double click onto WinSPM(Scanning) icon
3. Use the following personal details to access software:
   Login: “dm526”
   Password: “dm526”
4. Select AC-AFM
5. Select Clock Speed (Advised Default Setting: 33333666.67, 1ms)
6. Manually take glass jar off (Keep it off as this may affect the viewing angle)
7. Push the OM(Optical Microscope) side button to turn light on and use the microscope
8. Use the UP-DOWN wheel, located at the bottom front of the SPM, to move the XY Translation Stage (sample holder) all the way down
9. Take sample holder off using the small screw-in rod
10. Place sample onto holder and slide it back into the sample holder
11. Remove small rod from holder by screwing it off
12. Take off the conductivity cartridge and put on the cantilever
    NOTE: Tip should be facing downwards – Marks side down.
13. Slide the conductivity cartridge back in
14. Switch on the laser of white box [LD-ON]
15. Put microscope back
16. Use the UP-DOWN wheel to move the sample holder upwards so that it’s very close to the tip but not touching it. Use the reflection from the sample.

8.1.2.2. CALIBRATION

17. Align prism by rotating the 2 screws on the top of the SPM
    NOTE: Laser has to be on the top of the tip and glowing red
18. Switch on the photodetector panel and software and use software to get a high blue level (approximately 5 to 7 V)

19. Use the taped screw, on the front left of the SPM, to move the red spot horizontally in centre
20. Use wheel, on the left side of the SPM, to move the red spot vertically onto the centre
21. Push the OM(Optical Microscope) side button to turn light off
22. Setup the Autotune Levels:

    AC-AFM: Oscillation Amplitude (V) – 0.100

    Time Frequency of Cantilever:

    Resonance Frequency Detection: 50Hz to 350 Hz (this depends on you know what frequency your tip is)

    NOTE: Higher the Q values the better the quality.
23. Click OK
24. Check on the bottom of the computer screen window, in the WinSPM Scanning Software, that it says **WIDE 2 SCANNER (WZS)**
25. Click on the Cantilever Autotune icon
26. Select Normal Approach

8.1.2.3. SCANNING

27. Change ***Scan Size*** parameter to 60.0 μm and ***Clock Speed*** to 667 us
28. Note the following for Control 2 Course Stage:
    1) Needs to be at midpoint (O)
    2) Not and issue if its between (-100 and 100)
    3) Visibly has to be in middle
29. Push the OM(Optical Microscope) side button to turn light on and use the microscope
30. Use the two dials at the front to move the sample around horizontally on the XY plane to locate an area to scan. NOTE: both dials move the sample diagonally
31. Push the OM(Optical Microscope) side button to turn light off
32. Select RETRACT ON the software
33. Click the APPROACH icon

    Wait for the Approaching process

    Retract triangle will be in centre now
34. Select AUTOGRAB checkbox
35. Click the SCAN button
36. Now the SPM will scan the area that you have selected.

37. Reduce ***Loop Gain*** if you getting oscillating peaks on the pulse.
    NOTE: LOOP GAIN is in CONTROL 1
38. Reduce ***Speed*** to get a more detailed scan
39. Once image is scanned and you are satisfied click RETRACT so that its OFF
40. Click on WinSPM Processing software icon
41. Click on Copy Data scanning software icon to copy data to clipboard
42. Click JEOL icon on the processing software to obtain data
43. Process the image for measurements
44. Move wheel all the down to move platform
45. Repeat steps 29 to 44 for all your images

8.1.2.4. SHUTTING DOWN

46. Click big X, small X and OK
47. Laser off (Switch LD-ON) off
48. Take the conductivity cartridge out and take out cantilever
49. Take sample holder off using the small screw-in rod
50. Take sample of sample holder and slide it back into the sample holder
51. Remove small rod from holder by screwing it off
52. Glass jar back on
53. Close PROCESSING SOFTWARE

8.2. SCANNING ELECTRON MICROSCOPY

The SEM is being used to assess the size specifications of the electrodes and match them to their desired design specifications. The other usage of the SEM is to assess the electrode rigidity and check whether or not the edges, of the electrodes, are smooth. It was hoped to achieve size specifications, smooth edges with no electrode rigidity, identical to the design features shown in section 4.1.1. to 4.1.5.

8.2.1. EQUIPMENT

Here is a list of equipment needed gathering microscopy data for component 1:

1. Tweezers
2. Plastic cases to hold 1cm * 1cm substrate samples
3. Latex gloves
4. Metal studs with double side adhesive (sample holders)
5. FEI Sirion S-FEG FESEM
   (Located at The York JEOL Nanocentre, The University of York) [60]

8.2.2. PROCEDURE

1. Log onto both machines (SEM computer and Raith computer). Start program escremot.exe from the SEM computer. Start Microscope controller (SEM computer) and Elphy Quantum software (Raith computer).
2. Check the black box switch that is set to RAITH, switch on shutter controller and connect it to the SEM machine.
3. Select 'Detector' on menu and then the 'CCD'.
4. Vent chamber, use gloves and the SEM tweezers inserting the sample and close chamber door.
5. Pump chamber (hold the door closed with hand for the first few seconds) and wait for 'Vacuum OK' sign's appearing on the SEM Microscope controller software.
6. Press HT button on the SEM bench.
7. Maximize 'Stage' window. Choose a point at the lower right of the sample on the chart and click on it.
8. Select 'Detector' and then the 'SE'.
9. Click the '5kV' button in 'Beam'window first to get an image.
10. Select 'Beam' and then '20kV', click the button shows the value in 'Beam' window. After that a window will appear asking for you to focus.
11. Set the required beam spot-size (3) from the Microscope controller software on the SEM.
12. If image does not appear, click on 'ACB' and fiddle with the contrast/brightness controls. If there is still no image adjust upward the gun tilt till the image turns to white, and then click on 'ACB' again and fiddle with the contrast/brightness controls. Increase the magnification by pressing '+' to get clearer image if necessary. Filter value can also be changed during the focus.
13. Focus by holding down the right mouse button moving left or right.
14. Click on 'OK' in the window appeared after beam was turned on.
15. Select 'Detector' and then the 'CCD'. Select '+10.00' in Z window and click on 'Go to'. Select 'Detector' and then the 'SE'.
16. Focus by holding down the right mouse button moving left or right. Select 'Z<->FWD'.
17. Select 'Detector' and then the 'CCD'. Select '+5.00' in Z window and click on 'Go to'. Select 'Detector' and then the 'SE'.

18. Focus by holding down the right mouse button moving left or right. Select ‘Z<->FWD’.
19. Click the ‘lens modulator’ check button and the image will begin to jiggle. Press the left mouse button moving upward and downward till the image stops jiggling. Repeat the adjustment in direction of left and right, and then finish it by clicking the check button.
20. Press ‘Shift’ and right mouse button at the same time, and move in four directions to adjust the spot shape to a circle.

9. RESULTS

9.1. COMPONENT 1: MICRO-ELECTRODE TECHNOLOGY

9.1.1. PHOTOLITHOGRAPHY RESULTS

NOTE: All 10 silicon samples went in blast furnace for growth of SiO_2 layer (Wet process – 1200 °C – 2hrs – growth of 1 μm layer)

Please refer to APPENDIX 12.12 for further information regarding the choice of time and temperature to achieve 1 μm layer of SiO_2

Please refer to initial lab notes in APPENDIX 12.13. if necessary.

SESSION 1

TEST #	SAMPLE #	DESIGN #	CONTACT TIME (sec)	CONTACT FORCE (gm)	DEVELOPER TIME (sec)
1	S1	D1	4	400	30
2	S2	D1	4	400	30

Table 11. *Photolithography results for session 1*

The initial values for photolithography parameter settings were chosen from the results obtained from the BEng project in 2009. However tests 1 and 2 unfortunately concluded that these parameter settings were not ideal for the new masks. Issues of overdevelopment, debris and signs of defective mask marks concluded sample preparation needs to be improved and both Contact Time and Contact Force need to be increased separately. Another issue at hand was excessive electrodes rigidity. This is when the electrode edges are not smooth and end up with minor random ridges around the electrode edges. Increasing these two parameters separately will help us decided on whether or not either or both parameters need to be increased to improve the quality of the sample.

SESSION 2

TEST #	SAMPLE #	DESIGN #	CONTACT TIME (sec)	CONTACT FORCE (gm)	DEVELOPER TIME (sec)
3	S1	D5	4	800	30
4	S4	D5	4	600	30
5	S3	D5	4	400	30

Table 12. *Photolithography results for session 2*

Test 3 tested and increase in contact force by 400 gm from Test 2. Unfortunately, this still showed signs of underdevelopment, through the visible defective mask design mark, overdevelopment, where there was a short circuit between the opposing electrodes, and electrode rigidness. Small signs of debris showed poor sample preparation again. The general idea would be to keep the distance between the sample and the mask as small as possible to avoid diffraction and get the electrodes to the correct width. However we didn't want the contact force at its maximum because then the electrodes on the mask could be destroyed due to the amount of force applied.

To understand the effect of the contact force, Tests 4 and 5 were conducted by decrementing in 200 gm. The reduction of 800 gm to 600 gm in Test 4 did not improve the results. The same issues were replicated as in Test 3, however Test 4 showed greater signs of poor sample preparation which could possibly have affected the results.

Test 5 continued with the reduction of 200 gm, from 600 gm to 400 gm. The main conclusion was that to achieve good sample results with minimal electrode rigidity, no short circuits, and no cuts, the Contact Force parameter had to be at the highest level, 1000 gm. The test confirmed that reducing the Contact Force any lower will continue to reduce the quality of the electrodes. There were clear signs of excessive electrode rigidness and the widths of the electrodes were larger than the mask and the required specification by 3-4 μm, which was a clear sign of diffraction from increasing the space between the mask and the silicon substrate.

SESSION 3

TEST #	SAMPLE #	DESIGN #	CONTACT TIME (sec)	CONTACT FORCE (gm)	DEVELOPER TIME (sec)
6	S2	D5	4	1000	30

Table 13. *Photolithography results for session 3*

Test 6 tested the sample with the Contact Force being at its maximum parameter value, 1000 gm. Even though there were signs of underdevelopment and signs of debris, it could be seen that 1000 gm definitely improves the electrodes rigidness and maintains the widths of the electrodes with minor variations up to 1 μm. Even though there was

not much of an improvement from 800gram, 1000grams was definitely concluded to be the correct contact force if we want to maximize the masks full potential in obtaining smoother and more defined electrodes. The mask was not affected when applied with this parameter. Hence this shows that we can continuously use this type of mask with the full contact force. But even though we achieved smooth and defined electrodes, there was a huge issue of overdevelopment. That is why in the next series of tests, the Contact Time needs to be altered.

SESSION 4

TEST #	SAMPLE #	DESIGN #	CONTACT TIME (sec)	CONTACT FORCE (gm)	DEVELOPER TIME (sec)
7	S3	D5	5	800	30
8	S4	D5	5	800	25
9	S1	D5	5	800	25
10	S2	D5	5	800	20
11	S3	D5	5	1000	35
12	S4	D5	10	1000	30

Table 14. *Photolithography results for session 4*

Further testing commenced on experimenting the effect of Contact Time and Developer Time on the sample. Test 7 tested the increase of Contact Time by 1 second. This however showed excessive underdevelopment throughout the entire sample.

Test 8 and test 9 tested the effects of the reduction in Developer Time by 5 seconds from Test 7. This led to an increase in underdevelopment, where major areas of the electrodes design continued to not develop and there were clear signs of electrode rigidness in the areas which were developed. There are several reasons to why the electrodes are continuously rigid and why the sample is underdeveloped. Firstly, the Contact Force is not at its maximum. This distance between the mask and the substrate, causes the electrode rigidness to be more revealing than smooth due to diffraction.

Test 10 showed improvement in electrode rigidity, reduction in underdevelopment and satisfactory electrode widths, with variances up to 1 μm. Secondly, the developer time was too short and did not provide enough time for the mask design to properly develop.

Test 11 increased the development time by 5 seconds from the initial 30 seconds, in conjunction with the Contact Force being at 1000 gm. Results gave a decent exposure, however there were still signs of underdevelopment and the size of electrodes had increased by 2-3 μm. Thirdly, the exposure time was to short so increasing the exposure time under UV would significantly improve the smoothness and quality of the

electrodes. This is because more electrons will be used to bombard the mask to make a more detailed electron mask on the sample. So increasing the exposure times significantly was tested afterwards.

Test 12's results showed that increasing the Contact Time improved on the sample. There were no signs of under or over development and the rigidness of the electrodes had decreased.

SESSION 5

TEST #	SAMPLE #	DESIGN #	CONTACT TIME (sec)	CONTACT FORCE (gm)	DEVELOPER TIME (sec)
13	S1	D5	20	1000	30
14	S2	D5	30	1000	30
15	S3	D5	30	1000	25

Table 15. *Photolithography results for session 5*

Previous experimentation showed that increasing the Contact Times, whilst maintaining the Contact Force at a full parameter setting of 1000 gm and the Developer Time at 30 seconds, started to provide successful sample results. Both the under and over development issues in the previous experiments were surpassed, the electrode widths were maintained to the desired specifications with variations of 1 μm, and electrode rigidness began to reduce.

Test 13 tested the increase of contact time by 10 seconds from the Test 12's 10 seconds. Even though there was decent exposure, there was overdevelopment causing short circuits. On the other hand, there was a slight improvement on electrode rigidity.

Test 14 tested the increase in Contact Time by 10 seconds. This so far, proved to be the best exposure, even if there still were short circuits. There was a massive improvement on electrode rigidness and in order to reduce overdevelopment, a reduction in Developer Time was needed.

Test 15 tested the reduction of 5 seconds from Test 14's 30 seconds. This reduced the massive short circuit issue and concluded that for Mask Design 5 the final parameters were Contact Time: 30 seconds, Contact Force: 1000 gm, and Developer Time: 25 seconds.

SESSION 6

TEST #	SAMPLE #	DESIGN #	CONTACT TIME (sec)	CONTACT FORCE (gm)	DEVELOPER TIME (sec)
16	S1	D1	30	1000	25
17	S3	D1	30	1000	20

Table 16. *Photolithography results for session 6*

The same parameters achieved for Mask Design 5 were used as the default settings to achieve the right parameter for Mask Design1. Test 16 showed that these parameters unfortunately did not produce a successful sample. There was excessive overdevelopment, excessive electrode rigidity. A reduction of 5 seconds in Developer Time was tested in Test 17 and unfortunately still showed excessive overdevelopment, electrode rigidity and adhesion. This meant that the sample was not properly cleaned during preparation which may have affected these results. It was then considered to reduce the Developer Time to 10 seconds as a large amount of electrons were not needed for such simple design. This could improve the adhesion issue as there will be fever particles that would repel through electrostatic forces.

SESSION 7

TEST #	SAMPLE #	DESIGN #	CONTACT TIME (sec)	CONTACT FORCE (gm)	DEVELOPER TIME (sec)
18	S4	D1	30	1000	10
19	S6	D1	5	1000	20

Table 17. *Photolithography results for session 7*

A reduction of 10 seconds for the Developer Time was tested in Test 18. This results to excessive overdevelopment, however better than Test 17's, excessive electrodes rigidity, and excessive signs of adhesion which is still surprising as the preparation procedure was well thought out and followed. Also excessive mask marks were shown which concluded that if the Developer Time was reduced once more then the mask marks would get larger reducing the performance of the device drastically. Hence further testing was done by reducing the Contact Time and increasing the developer time in Test 19.

Test 19 unfortunately proved to fail as well. There was excessive overdevelopment compared to test 18, excessive electrode rigidness, signs of adhesion which resulted the patterned photoresist coming off. A very surprising result as sample preparation was conducted in an extreme fashion.

SESSION 8

TEST #	SAMPLE #	DESIGN #	CONTACT TIME (sec)	CONTACT FORCE (gm)	DEVELOPER TIME (sec)
20	S1	D1	15	1000	20
21	S2	D1	15	1000	10
22	S3	D1	20	1000	10
23	S4	D1	10	1000	10

Table 18. *Photolithography results for session 8*

Tests 20-23 throughout showed repetitive patterns of issues: Excessive Overdevelopment, Excessive Electrode Rigidness, Excessive Signs of Adhesion (except for Tests 21 and 23), and general random areas of both under and overdevelopment in the samples. Throughout these tests 16-23, it was hard to find the right balance between all three parameters. Also the signs of adhesion were very surprising, as even after precise sample preparation, there still were signs of adhesion. These results only conclude that the issue was in the mask used to print Mask Design 1. Hence therefore, this mask will not be used for fabrication.

SESSION 9

TEST #	SAMPLE #	DESIGN #	CONTACT TIME (sec)	CONTACT FORCE (gm)	DEVELOPER TIME (sec)
24	S5	D4	30	1000	25
25	S6	D4	40	1000	30
26	S7	D4	40	1000	30
27	S8	D3	30	1000	25
28	S9	D3	40	1000	30

Table 19. *Photolithography results for session 9*

Test 24-26 was used to determine the parameter settings for Mask Design 4. Test 24 used the concluded parameter values from design 5. Successfully, the sample was perfectly exposed with no issues except for the tips being slightly curved. Even the electrode rigidness was largely improved and very close to being smooth. Increasing the Developer Time by 5 seconds will hopefully sharpen the tips.

Test 25 used a developing time of 30 seconds and had a decent exposure, improving the sharpness of the tips, however resulted with one short circuit. This could be a result of poor sample preparation, and therefore the test was repeated again in Test 26 where a successful sample was fabricated and it was concluded that the parameter values to achieve successful sample using Mask Design 4 were, Contact Time: 30 seconds, Contact Force: 1000 g, Developer Time: 25 seconds.

Test 27 and 28 were used to identify the parameter values for Mask Design 3. Test 27 used the initial parameter values concluded for Mask Design 5. There were no signs of under or overdevelopment and adhesion. The sample was very well exposed however not at the remaining 0.05 mm of each set of electrodes. The tips began to breakup gradually mainly due to how the tips start off with a base of 10 μm and slowly decreases in size to a point of nanometre size. Now as the mask aligners limits are around 10 μm we can begin to conclude that it will be difficult to properly pattern Mask Design 3 onto the substrate.

Test 28 consisted of increasing the Contact Time by 10 seconds and Developer Time by 5 seconds to possibly increase the number of electrons at the final 0.05 mm tips to increase detail and improve development. However this did not improve the development of the electrodes and it was concluded that the mask design was too defined for this mask aligner and will be difficult or impossible to develop.

SESSION 10

TEST #	SAMPLE #	DESIGN #	CONTACT TIME (sec)	CONTACT FORCE (gm)	DEVELOPER TIME (sec)
29	S4	D2	30	1000	25
30	S1	D2	30	1000	15
31	S3	D2	30	1000	10
32	S7	D2	30	1000	15

Table 20. *Photolithography results for session 10*

Test 29-32 were used to determine the parameter values needed to successfully pattern Mask Design 2 onto the substrate.

Test 29 initially starts the experimentation by using the final parameter values concluded for Mask Design 5. The sample itself had decent exposure with no issues of adhesion and underdevelopment except for 2 areas which were overdeveloped. Therefore a reduction in 10 seconds in the Developer Time was done for Test 30. This was a successful exposure with no issues except for one minor short circuit. However through experience, this element might not appear if done again. Therefore Test 31 tested the development of the mask onto the substrate by reducing the Developer Time to 10 seconds. This unfortunately caused excessive underdevelopment and it was realized in Test 32, that 15 seconds was the correct developer time for the sample as there was perfect development. Therefore the final parameter values for patterning Mask Design 2 onto a substrate are Contact Time: 30 seconds, Contact Force: 1000 g, and Developer Time: 15 seconds.

SESSION 11

TEST #	SAMPLE #	DESIGN #	CONTACT TIME (sec)	CONTACT FORCE (gm)	DEVELOPER TIME (sec)
33	S1	D5	30	1000	25
34	S2	D5	30	1000	25
35	S4	D5	30	1000	25

Table 21. *Photolithography results for session 11*

Session's 11 and 12 were dedicated in successfully fabricated 6 samples, 2 samples for each of the 3 mask designs (Mask Design's 2, 4, 5). Test 33-35 were dedicated in fabricating samples for Mask Design 5. However, all those three tests ended up getting one short circuit.

SESSION 12

TEST #	SAMPLE #	DESIGN #	CONTACT TIME (sec)	CONTACT FORCE (gm)	DEVELOPER TIME (sec)
36	**S1**	**D5**	**30**	**1000**	**25**
37	S3	D5	30	1000	25
38	S4	D4	30	1000	25
39	**S6**	**D4**	**30**	**1000**	**25**
40	**S7**	**D4**	**30**	**1000**	**20**
41	S9	D2	30	1000	15
42	**S10**	**D2**	**30**	**1000**	**15**
43	**S4**	**D5**	**30**	**1000**	**25**
44	S6	D4	30	1000	20
45	**S9**	**D2**	**30**	**1000**	**15**

Table 22. *Photolithography results for session 12*

Tests 36, 37 and 43 were dedicated in successfully patterning Mask Design 5 onto the substrate. Even though 36 and 37 had a very small short circuit, test 43 produced a perfect sample. Both 43 and 36 were selected for evaporation.

Tests 38, 39, 40, and 44 were dedicated in successfully patterning Mask Design 4 onto the substrate. Even though 38 had a very small short circuit, test 39 and 40 produced a perfect sample. It was seen after test 39 that Developer Time needs to be reduced to 20 from 25. This is why test 40 was more successful than 39 when it comes to electrode rigidness and size specifications. Both 39 and 40 were selected for evaporation.

Tests 41, 42, and 45 were dedicated in successfully patterning Mask Design 2 onto the substrate. As all samples successfully had Mask Design 2 patterned onto them, the electrode widths and prescence of debris was used to distinguish the two samples for evaporation. Samples 42 and 45 were chosen for evaporation.

SESSION 13 – LIFTING OFF

Thin film evaporation consisted of the evaporation of following materials:

Layer 1: Permalloy (Ni80Fe20), 20 nm thick (Bottom)

Layer 2: Gold (Au), Capping layer 5 nm thick (Top)

TEST #	SAMPLE #	DESIGN #	CONTACT TIME (sec)	CONTACT FORCE (gm)	DEVELOPER TIME (sec)
36	**S1**	**D5**	**30**	**1000**	**25**
39	**S6**	**D4**	**30**	**1000**	**25**
40	S7	D4	30	1000	20
32	S10	D2	30	1000	15
43	S4	D5	30	1000	25
45	**S9**	**D2**	**30**	**1000**	**15**

Table 23. *Photolithography results for session 13*

After one hour of lift, there we still some filaments in all of the samples that hadn't lifted off. However after putting each individual sample into a beaker with acetone, they were put into a ultrasonic machine, where they went through approximately 10-15 one second burst sessions. After then, all the filaments were removed and all the samples were successful in the lift off session. Sample 1 was chosen for design 5, sample 6 was chosen for design 4 and sample 9 was chosen for design 2 for final characterization analysis through atomic force microscopy and scanning electron microscopy.

9.1.2. ATOMIC FORCE MICROSCOPY RESULTS

9.1.2.1. SILICON SUBSTRATE SMOOTHNESS ANALYSIS

Before taking the silicon sample through photolithography and evaporation, 1μm layer of SiO_2 was grown on to the silicon samples to increase resistivity and thus reducing the risk of any current going between both sets of electrodes without any bridges.

AFM analysis was conducted to test the variations of SiO_2 surface smoothness between the starting 10 samples. We wanted to see whether or not the variations may be so large, that they may affect the quality of the final electrodes after evaporation. The cantilever frequency was 271.635 kHz and the Q Factor was 432.496; both very high numbers concluding decent cantilever tip. Figs. 99 and 100 equally represent the generic results that were retrieved between the 10 samples for the surface smoothness of the SiO_2 layer on the silicon substrate.

We can see with Fig. 99 how there is a huge peak that starts from approximately 105.5 nm and rises all the way to 825.5 nm (APPENDIX 12.2). This was consistent between a few samples at random areas and proved how the SiO_2 growth process in the furnace is not efficient when it comes to even distribution.

In Fig. 100 we can see another general example of uneven growth of SiO_2, however at a much smaller scale. These concurring 'dips' were present throughout all 10 samples and start from a variation of 30 nm (APPENDIX 12.3) to 100 nm.

Several conclusions can be formulated. The first one would be that the bought silicon wafer, untouched, would not be smooth from the start and hence the SiO_2 growth process would actually be consistent. The other conclusion is the complete opposite. The silicon is very smooth with possible variations of 10 nm, however the SiO_2 growth process with the furnace is not consistent. Further AFM testing should have been conducted with the untouched silicon sample with now SiO_2 layer, however due to time constraints this was not possible and needs to be testing in the future.

The main reason for the growth of a 1 μm thick SiO_2 layer on the substrate is to reduce conductivity between the evaporated electrodes. However, if it turns out that the growth process with the furnace is the cause of these variations then more research needs to be conducted to find more effective techniques for SiO_2 growth. Also it would reduce the electrodes performance if they evaporated and shaped in these uneven areas.

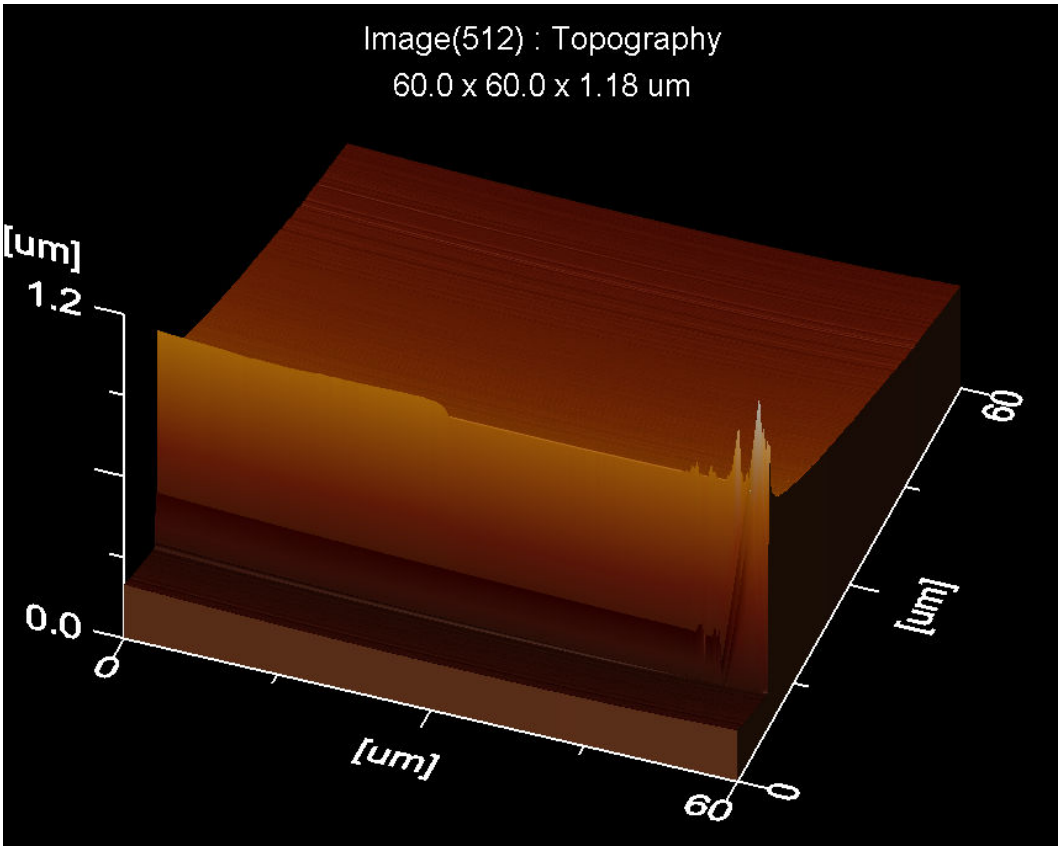

Fig. 99. *3D diagram showing surface smoothness for general silicon substrate with 1 µm layer of SiO_2*

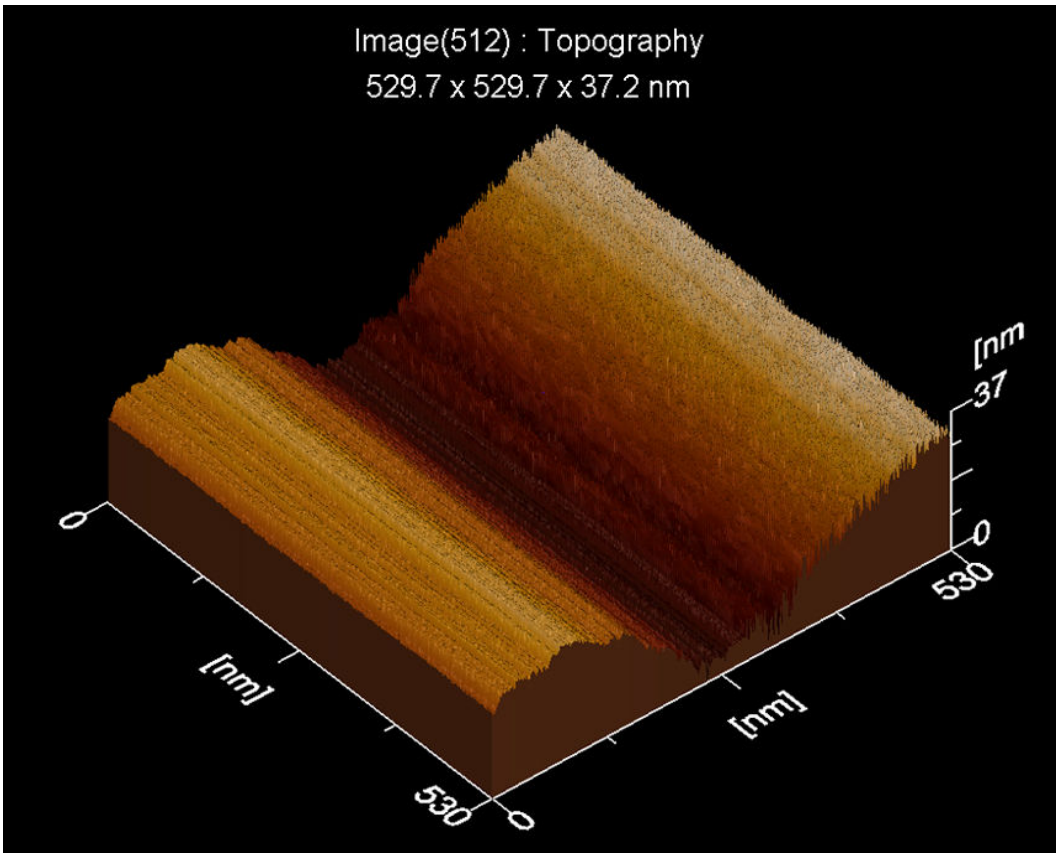

Fig. 100. *3D diagram 2 showing surface smoothness for general silicon substrate with 1um layer of SiO_2*

9.1.2.2. ADVANCED ELECTRODE DESIGN 2

Figs. 101 and 102 are very successful AFM images which show some interesting results regarding the height of the evaporated electrodes (APPENDIX 12.4) as well as the even distribution of the evaporated material on the electrodes (APPENDIX 12.5).

As approximately 20 nm of Permealloy was evaporated followed by 5 nm of Gold, we can say that the difference between the silicon substrate and the evaporated material would be approximately 25 nm. In APPENDIX 12.4 results show that the height variation between the silicon substrate and the evaporated electrodes is approximately 25 nm ± 3 nm. However, there were some anomalies in between the electrodes that peaked several times. This could potentially be debris, leftover filaments from lift-off or these huge variations of the grown SiO_2 layer.

Our main concern was whether or not these SiO_2 variations on substrate would affect the smoothness of the evaporated material on the electrodes. APPENDIX 12.5 confirms height variations from 5 nm to 20 nm.

These results stress on the fact that an uneven distribution of SiO_2 layer would affect the height and smoothness of the electrodes as well when it comes to evaporation.

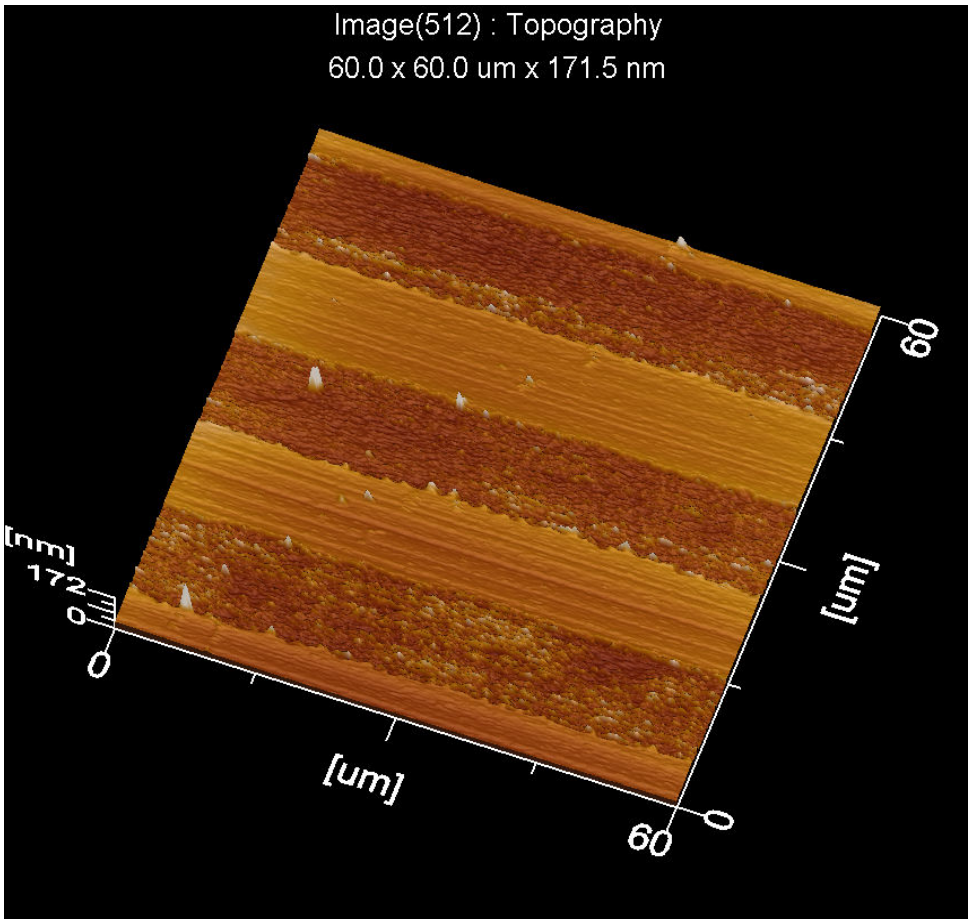

Fig. 101. *3D diagram showing AFM analysis for sample 9 with design 2*

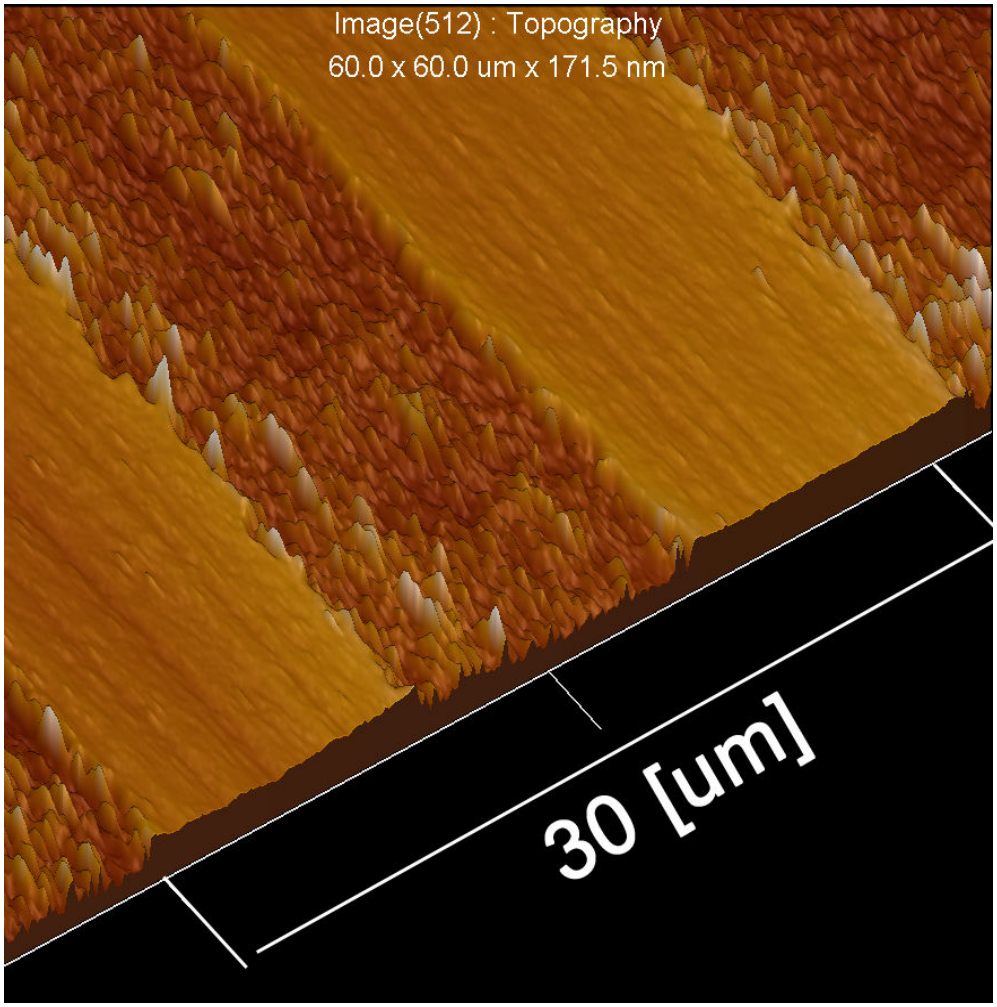

Fig. 102. *3D diagram 2 showing AFM analysis for sample 9 with design 2*

9.1.2.3. ADVANCED ELECTRODE DESIGN 4

As with advanced electrode design 2, Figs. 103 and 104 are very successful AFM images which show some interesting results regarding the height variation and smoothness of the evaporated electrodes (APPENDIX 12.7).

Like design 2, 20nm of Permealloy and 5 nm of Gold were evaporated. APPENDIX 12.6 and 12.7 show us the variations of height and smoothness of the evaporated electrodes being 20 nm ± 3 nm, which of course implies that that some areas only just have 2-5 nm of evaporated material, if the silicon substrate was smooth. This however is not the case and suggest the areas that seem to have only 2-5 nm of evaporated material are those areas where there are approximately 20 nm dips.

Once again these results stress on the fact that an uneven distribution of SiO_2 layer would affect the height and smoothness of the electrodes as well when it comes to evaporation.

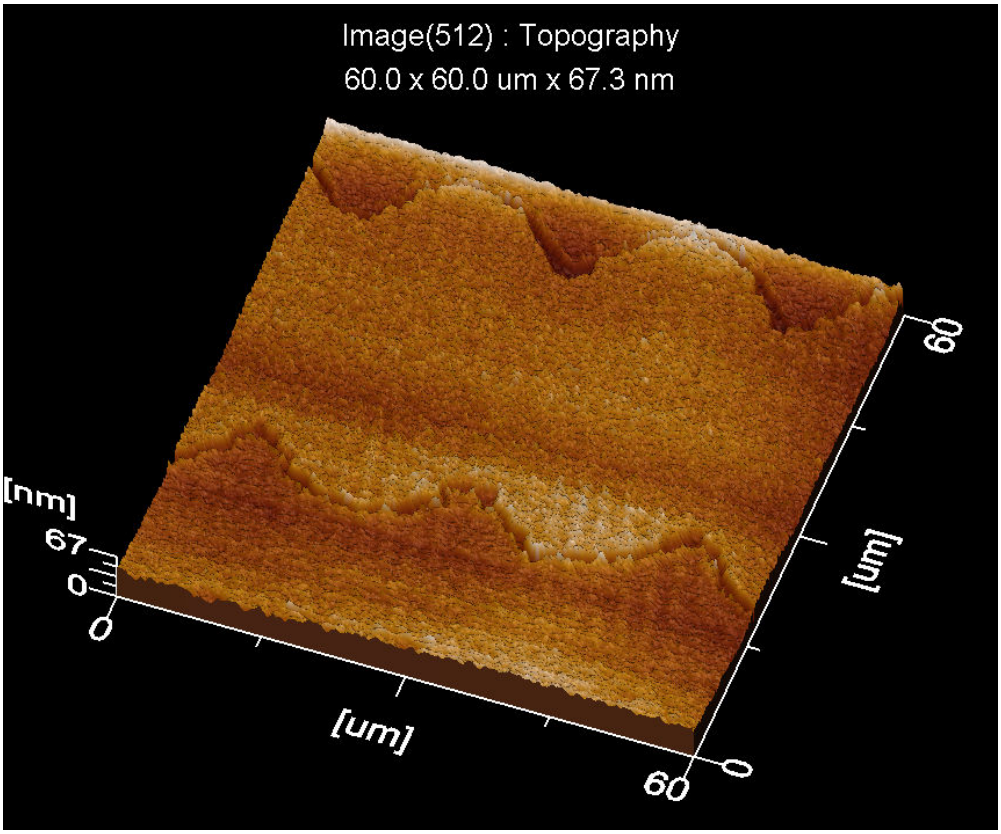

Fig. 103. *3D diagram showing AFM analysis for sample 6 with design 4*

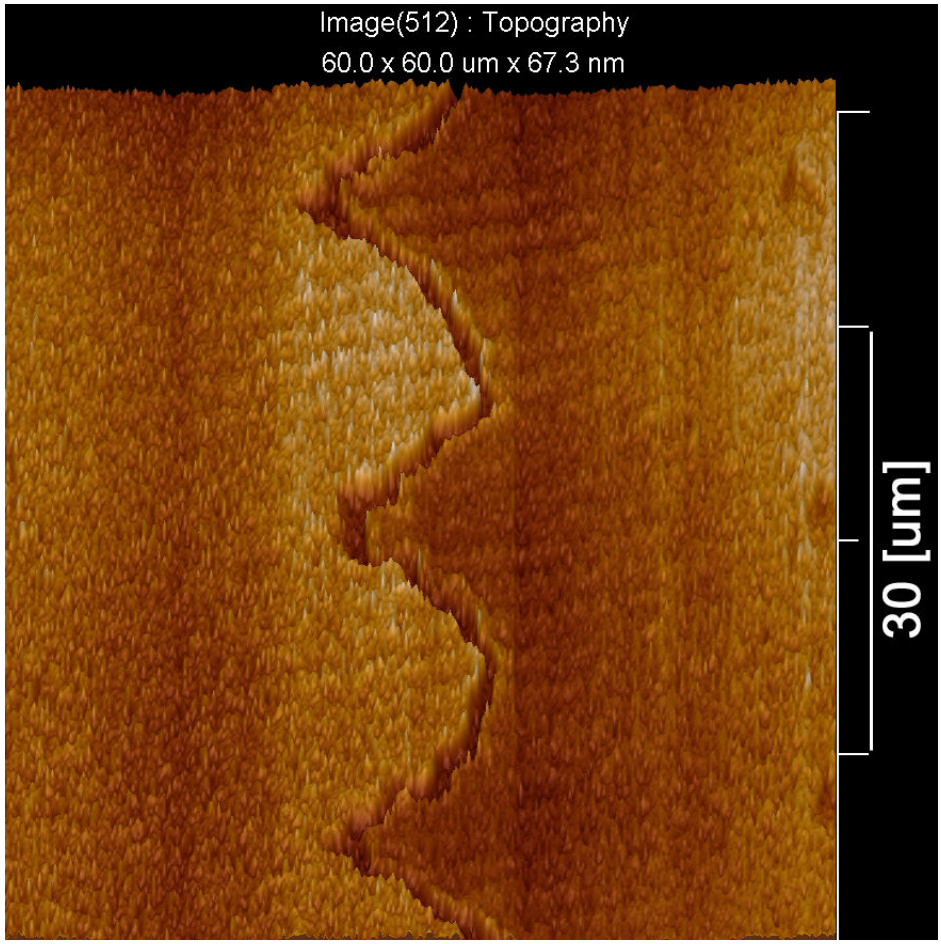

Fig. 104. *3D diagram 2 showing AFM analysis for sample 6 with design 4*

9.1.2.4. ADVANCED ELECTRODE DESIGN 5

As with advanced electrode design 5, Figs. 105 and 106 are very successful AFM images which show some interesting results regarding the height variation and smoothness of the evaporated electrodes (APPENDIX 12.9).

Like design 2 and 4, 20nm of Permealloy and 5 nm of Gold were evaporated. APPENDIX 12.8, 12.9 and 12.10 disprove the variations of height and smoothness of the evaporated electrodes being 20 nm ± 3 nm. This proposes that this sample would have smaller variations in the SiO_2 layer that has not affected the height has drastically as it was for the previous two samples.

APPENDIX 12.8 exhibits the approximate height of 25 nm of evaporated material, even though APPENDIX 12.10 shows more of a ±10nm variation on the surface smoothness compared to the ± 5nm variation in APPENDIX 12.8 and 12.9

Once again these results stress on the fact that an uneven distribution of SiO_2 layer would affect the height and smoothness of the electrodes as well when it comes to evaporation.

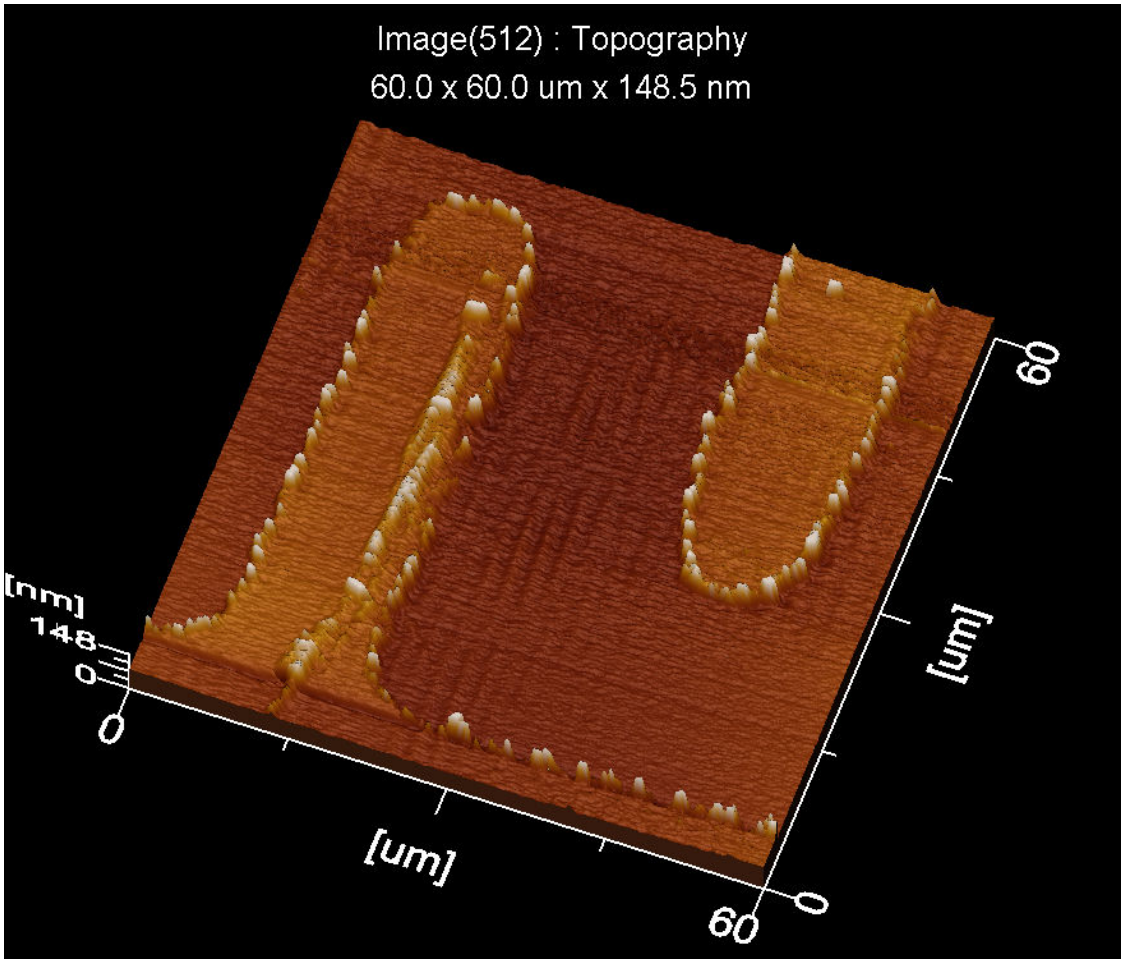

Fig. 105. *3D diagram showing AFM analysis for sample 1 with design 5*

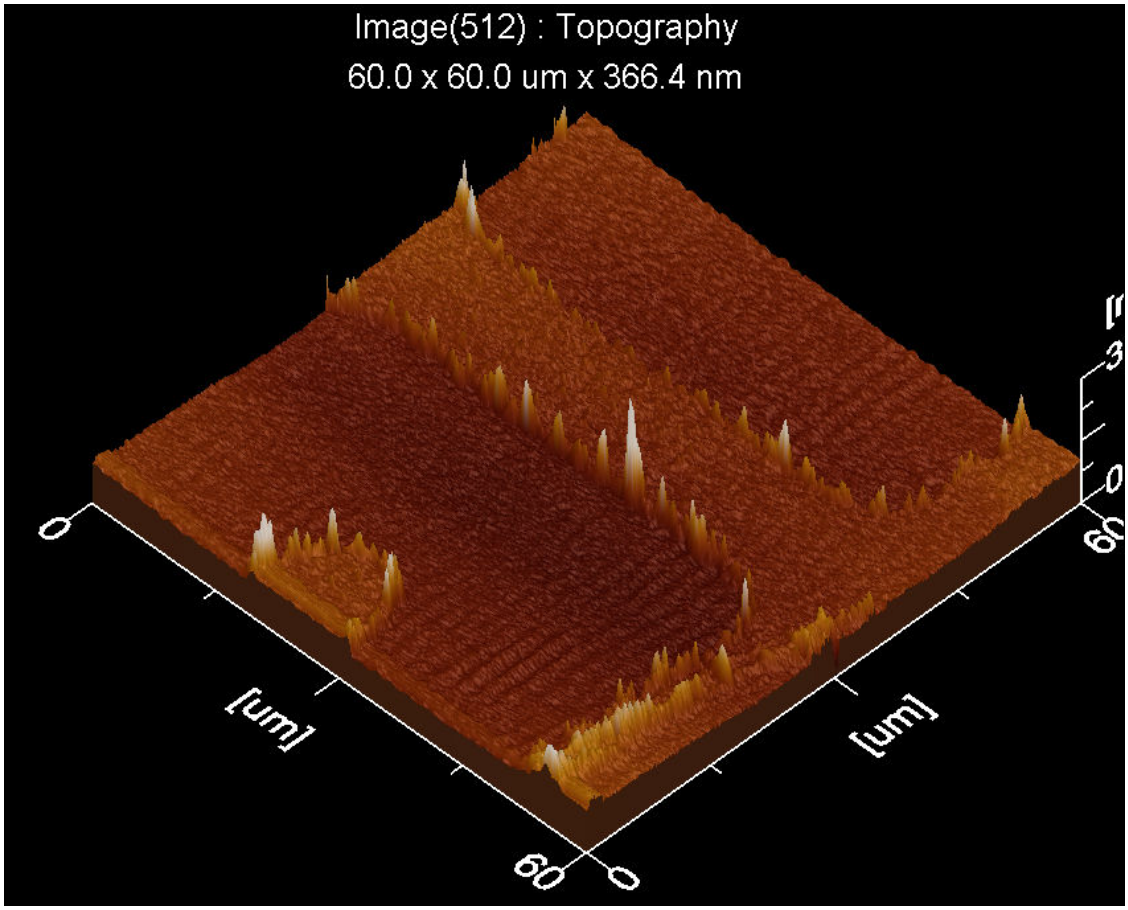

Fig. 106. *3D diagram 2 showing AFM analysis for sample 1 with design 5*

9.1.3. SCANNING ELECTRON MICROSCOPY

9.1.3.1. ADVANCED ELECTRODE DESIGN 2

Scanning electron microscopy was used to obtain more detailed images of the three fully fabricated samples with each individual designs. Tests were conducted regarding electrode rigidness and whether or not we successfully obtained evaporated designs meeting the desired design parameters. 5kV for electron beam and spot size 3 was used for beam parameters.

Fig. 108 shows electrode width is approximately 9.71 μm which is fairly close to our desired 10 μm wide electrodes. The gaps between the electrodes however are a good 1.3 μm away from our desired 10 μm mark. The distance between the nanotips and the main electrode has increased approximately 3.7 μm. This is mainly because the tip is only 6.8 μm and had not fully developed during lithography. This reduction from our 10 μm mark with the length of the tip was added onto the distance.

Regarding electrode rigidness, if we look at Figs. 109 and 110, we can see that smooth straight electrodes have not been achieved. The only main cause for this is the photomask. The best way to maintain this cheap process would be to apply an after-treatment to the sample which etches or smoothens the electrodes.

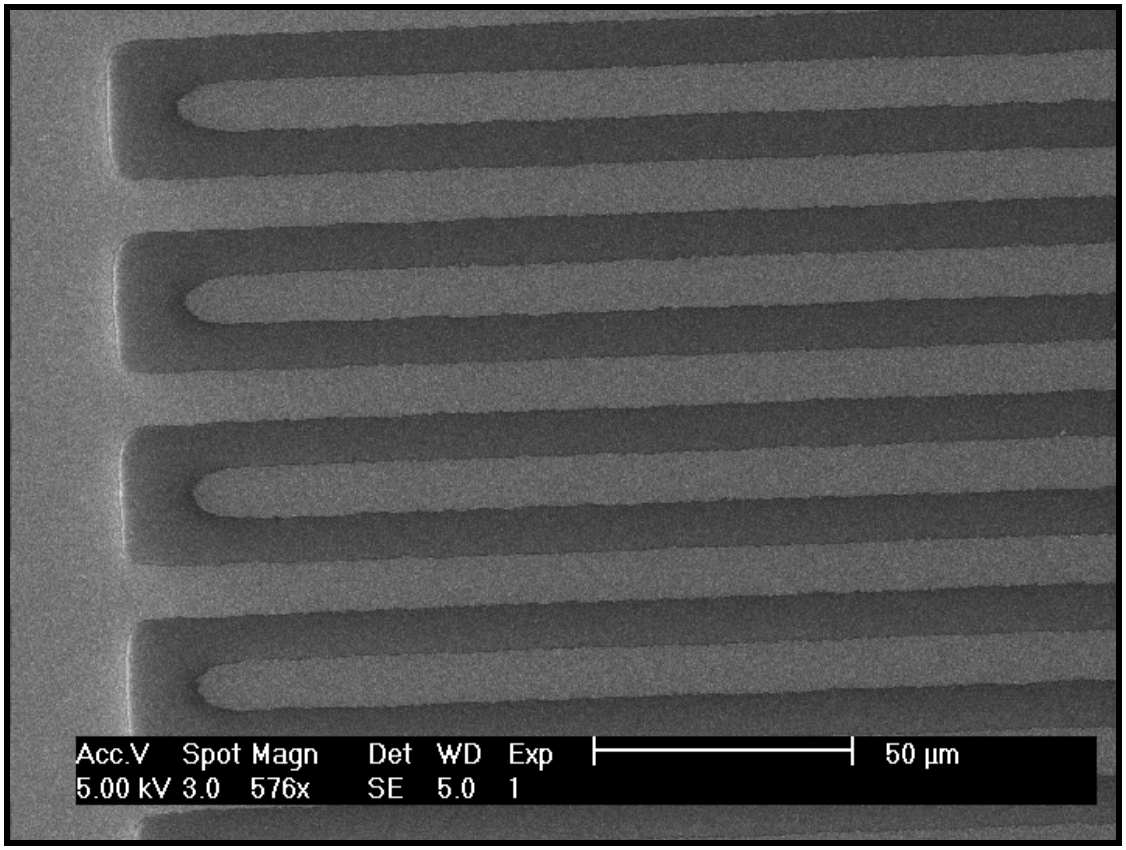

Fig. 107. *SEM image of sample 9 with design 2 for size analysis*

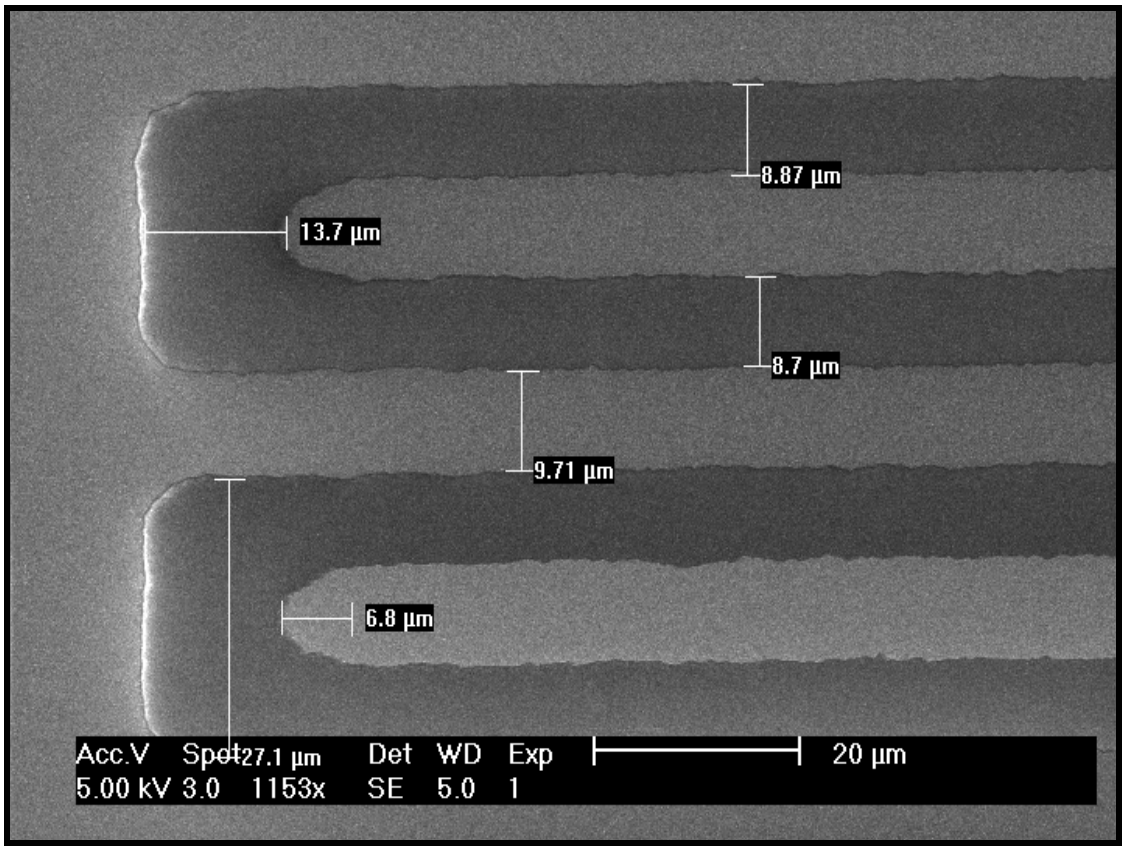

Fig. 108. *SEM image of sample 9 with design 2 for size analysis including measurements*

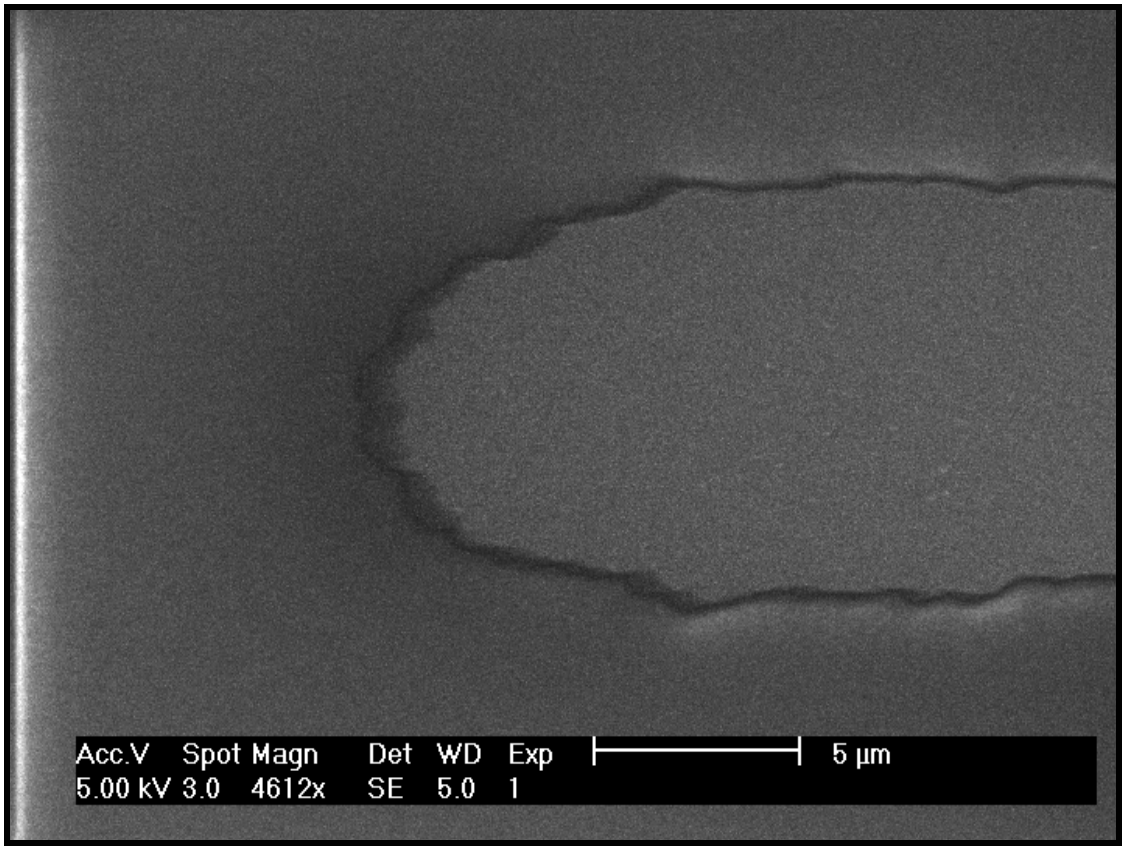

Fig. 109. *Close-up SEM image showing microtip for electrode rigidity*

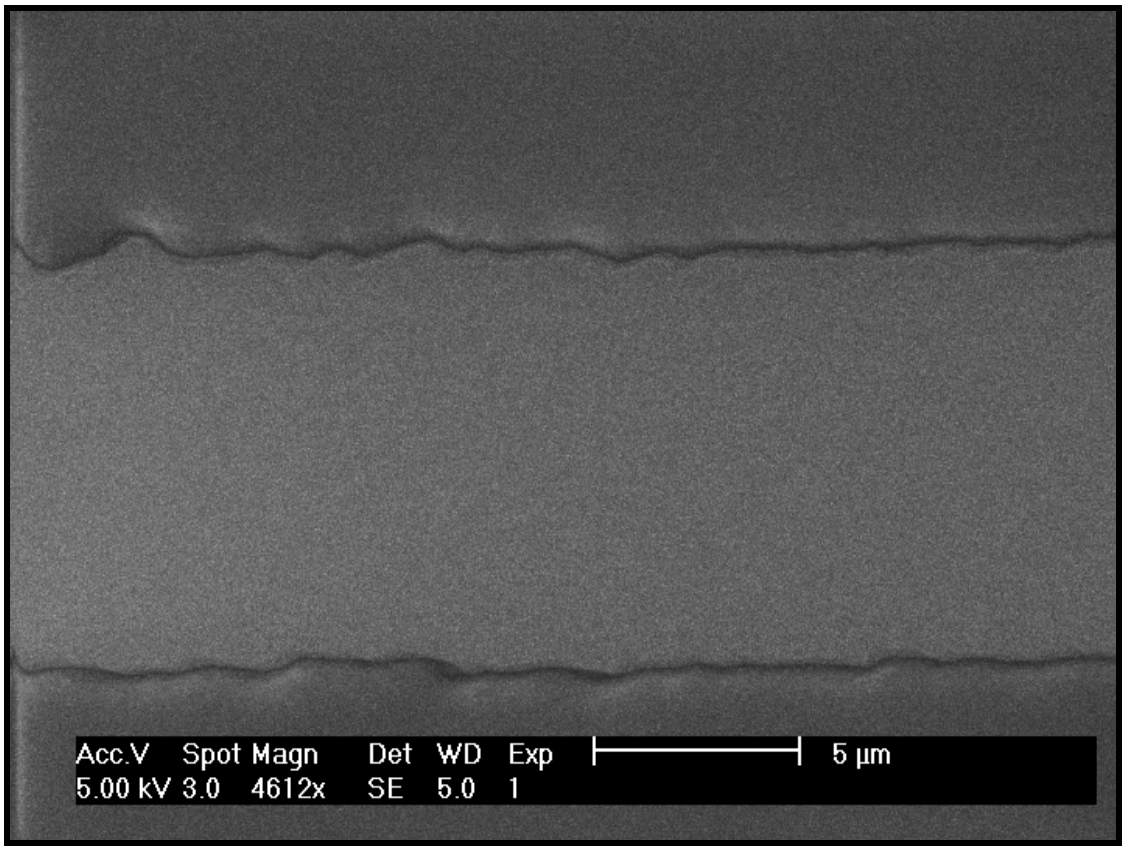

Fig. 110. *Close-up SEM image showing electrode body for electrode rigidity*

9.1.3.2. ADVANCED ELECTRODE DESIGN 4

Tests were conducted, similar to electrode design 2, regarding electrode rigidness and whether or not we successfully obtained evaporated designs meeting the desired design parameters.

Fig. 112 shows electrode width is approximately 24.5 μm which unfortunately is twice the size of our desired 10 μm wide electrodes. The gaps between the electrodes however are a good 26.3 μm, which is an extra 6.3 μm from our desired parameter. This is mainly because as the tips are only approximately 7.54 μm in height, instead of their 10 μm desired parameter, and had not fully developed during lithography. This has increased the width of the electrode as well as the distance between electrodes. Further research and trials need to be conducted to Fig. out how to fully develop these microtips. Once we have perfectly developed these tips then the rest of our desired parameters will perfectly be fabricated too.

Regarding electrode rigidness, if we look at Figs. 113 and 114, we can see that there is rigidity between the electrodes. The only main cause for this is the photomask. The best way to maintain this cheap process would be to apply an after treatment to the sample which etches or smoothes the electrodes.

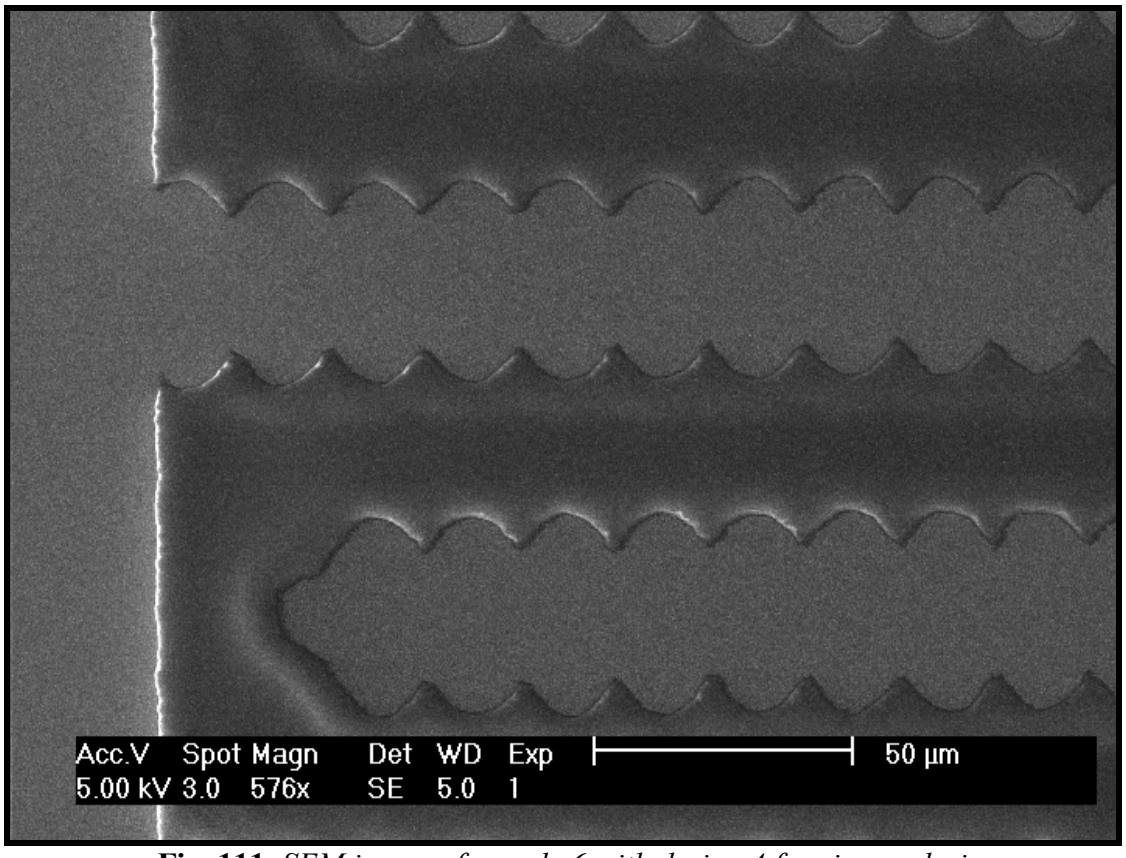

Fig. 111. *SEM image of sample 6 with design 4 for size analysis*

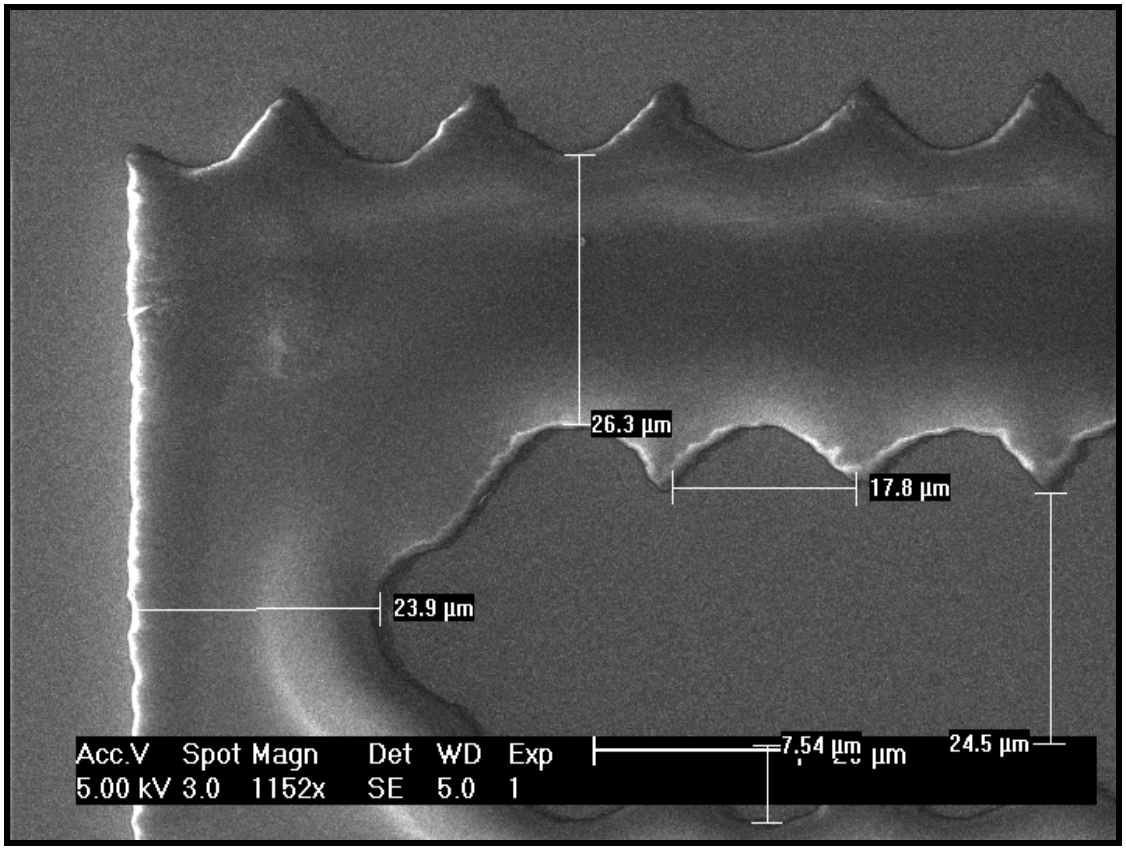

Fig. 112. *SEM image of sample 6 with design 4 for size analysis including measurements*

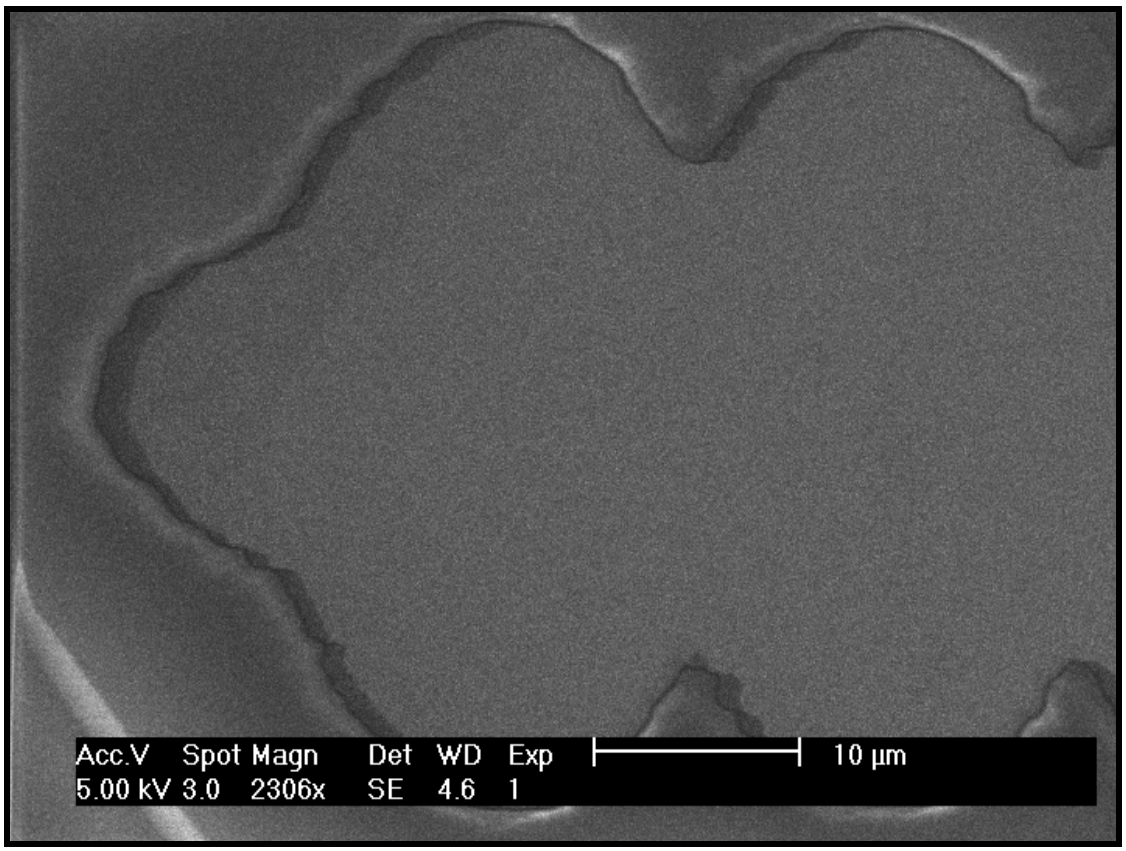

Fig. 113. *Close-up SEM image showing microtip for electrode rigidity*

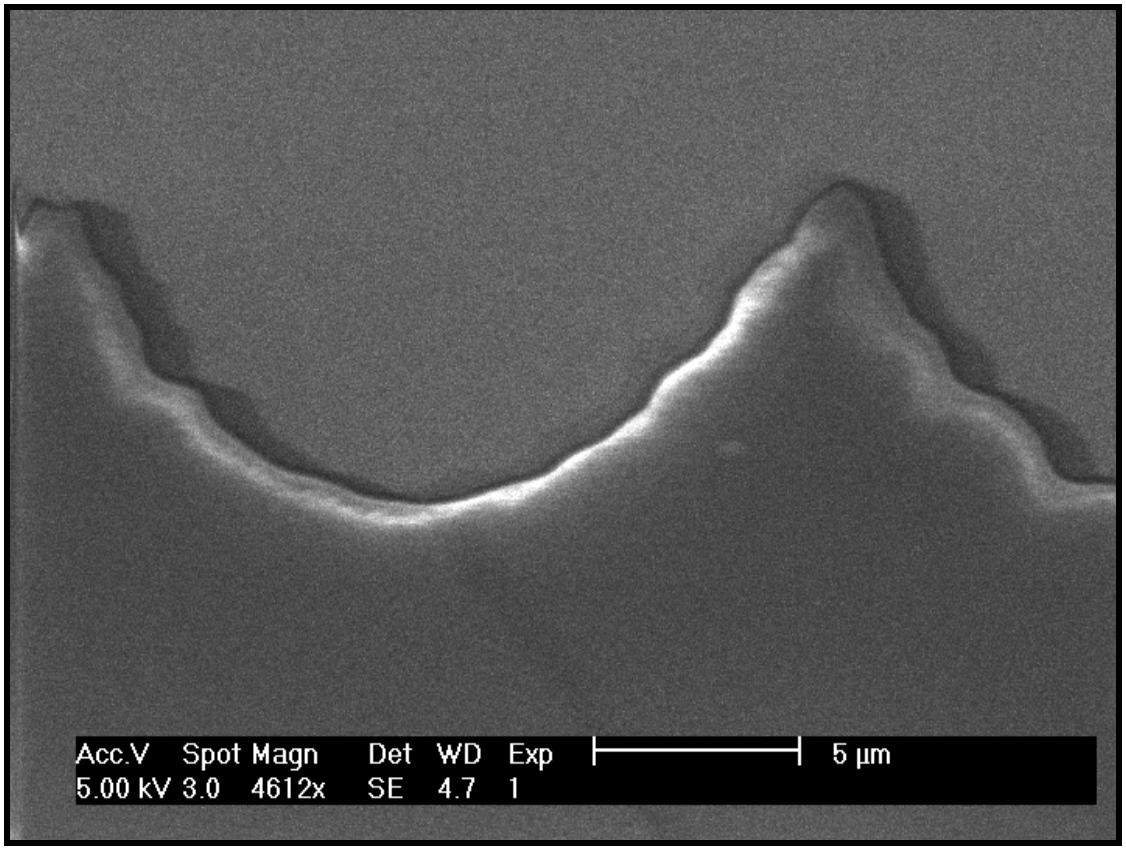

Fig. 114. *Close-up SEM image showing electrode body for electrode rigidity*

9.1.3.3. ADVANCED ELECTRODE DESIGN 5

Tests were conducted, similar to electrode design 2 and 4, regarding electrode rigidness and whether or not we successfully obtained evaporated designs meeting the desired design parameters.

Fig. 116 shows electrode width is approximately 10.3 µm which is an impressive 0.3 µm increase to our desired parameter. The distances between the smaller vertical interdigitated electrodes start off from 16.4 µm to 18.8 µm. Even though these distances should have been 20 µm, they are still surprisingly very close. The distances from the closest vertical electrodes to the main electrode range from 44.1 µm to 46.9 µm which is smaller that the required 50 µm. Surprisingly all the values are smaller compared to the mask that was given. Hence further research must be conducted to see why that is. Maybe reducing developer time during photolithography may stop the development a bit earlier than what is needed.

Regarding electrode rigidness, if we look at Figs. 117 and 118, we can see that there is rigidity between the electrodes. The only main cause for this is the photomask. The best way to maintain this cheap process would be to apply an after treatment to the sample which etches or smoothes the electrodes.

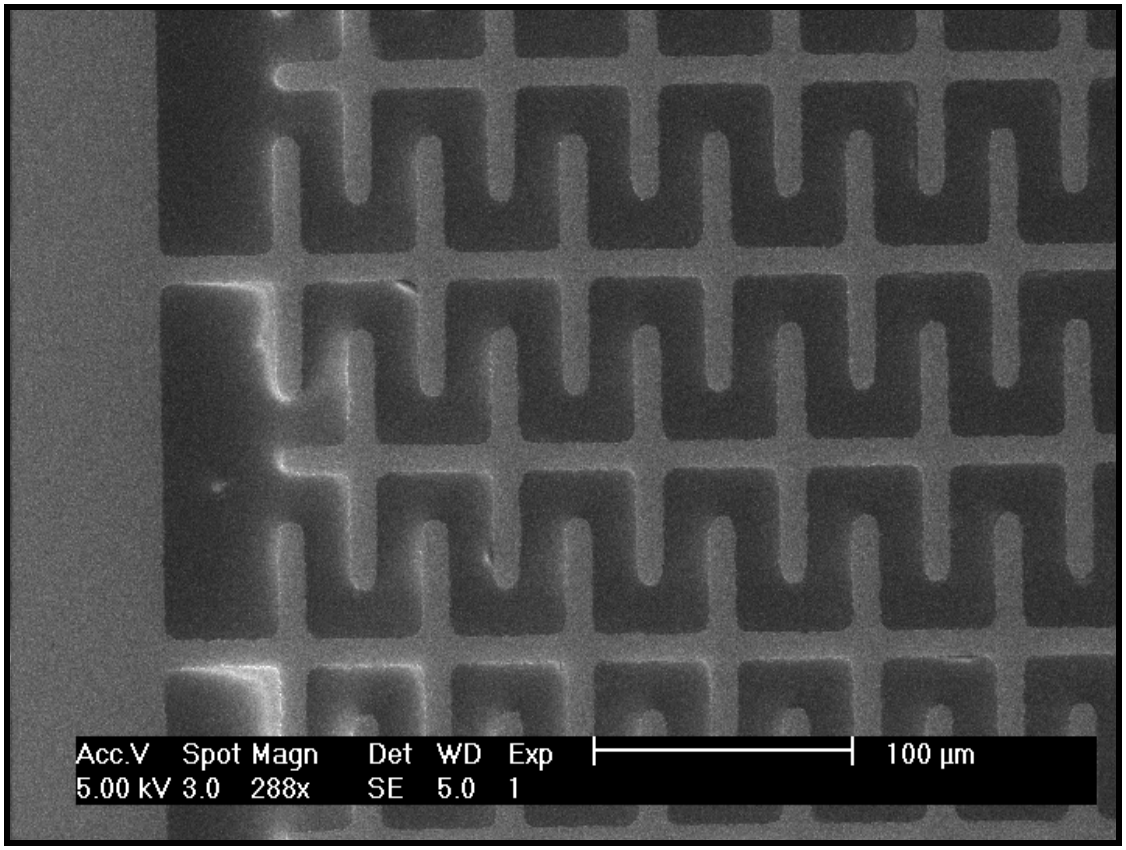

Fig. 115. *SEM image of sample 1 with design 5 for size analysis*

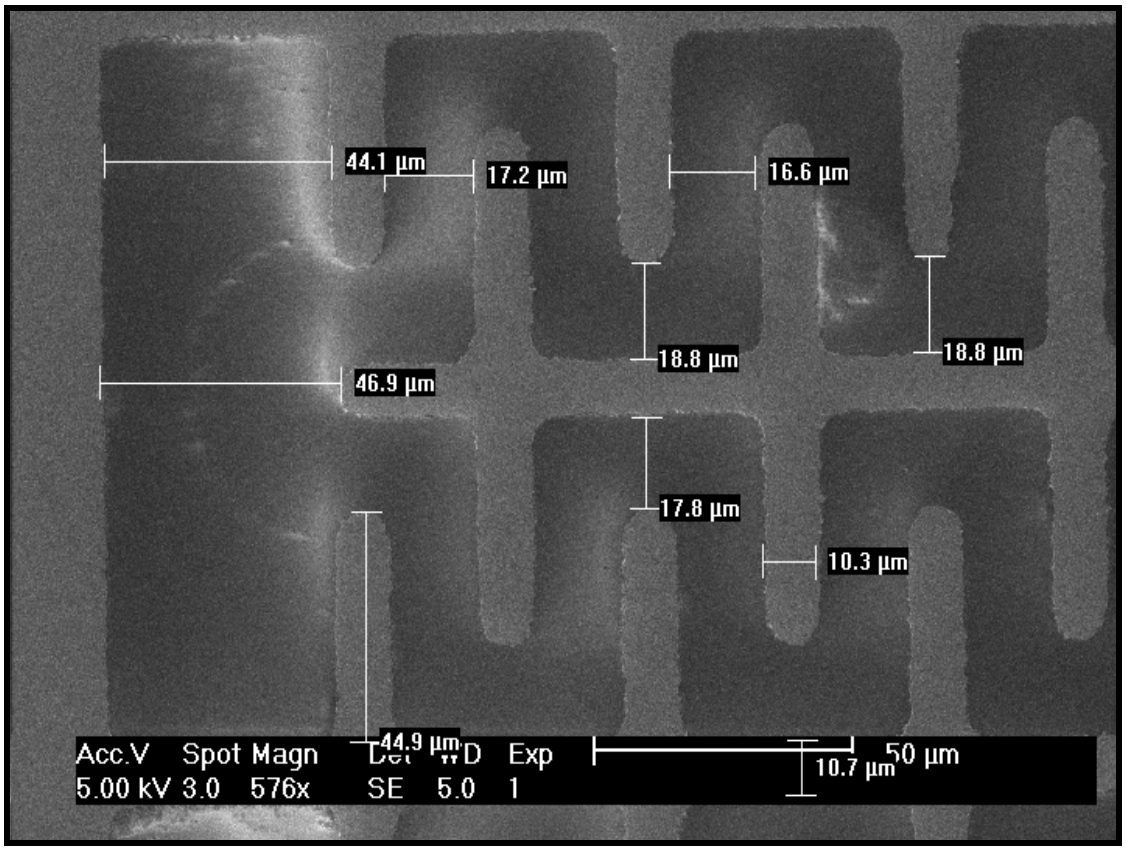

Fig. 116. *SEM image of sample 1 with design 5 for size analysis including measurements*

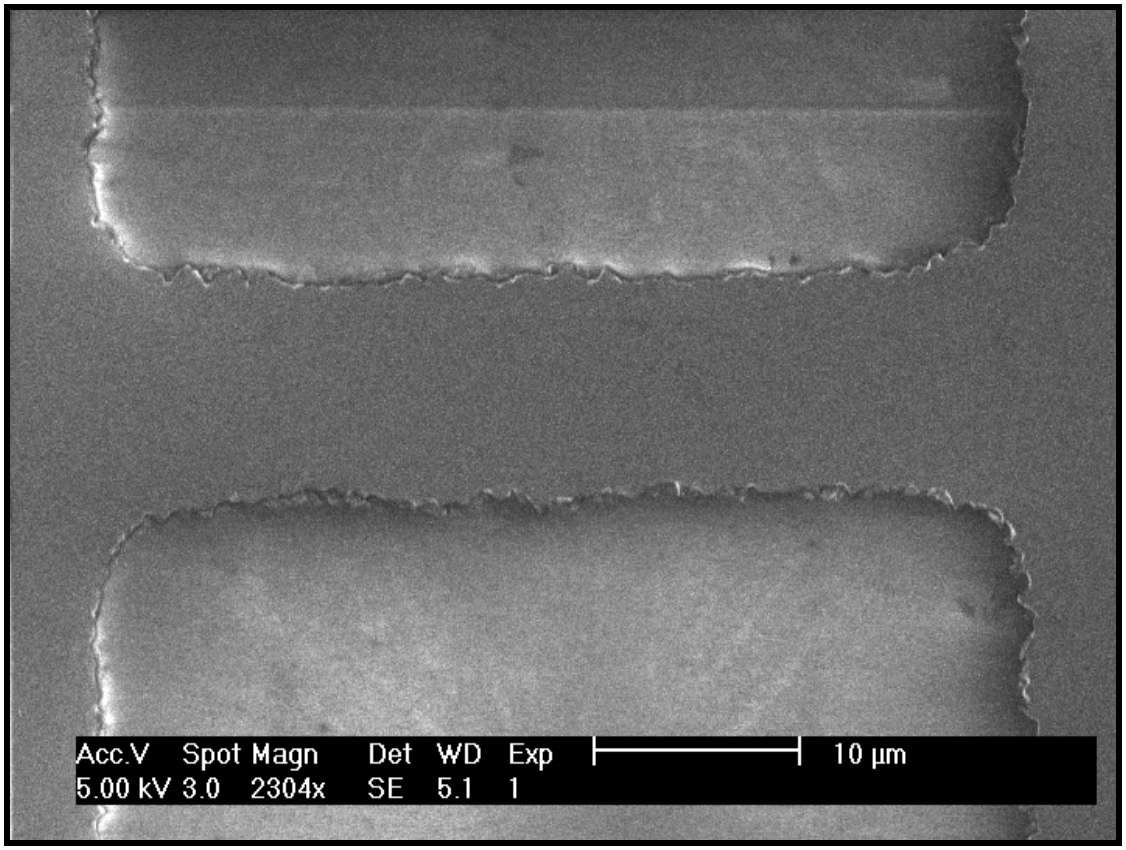

Fig. 117. *Close-up SEM image showing electrode body for electrode rigidity*

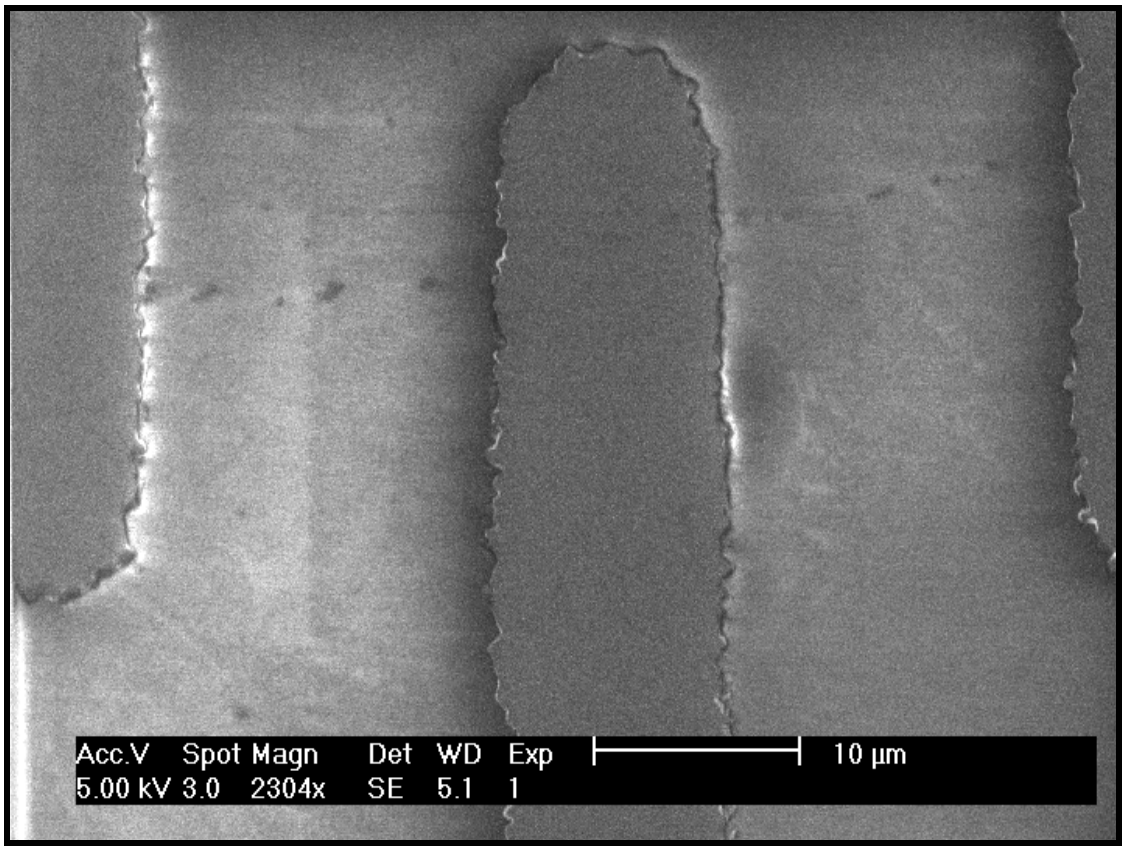

Fig. 118. *Close-up SEM image showing microtip for electrode rigidity*

9.2. COMPONENT 2
9.2.1. SCANNING ELECTRON MICROSCOPY
9.2.1.1. MWNT SIZE AND STATE ANALYSIS

Scanning electron microscopy was used to obtain images regarding the state the MWNTs are in as well as get some diameter sizes.

The MWNTs are intertwined with one another like cotton wool. With diameters of approximately between 20nm to 25nm, according to Figs. 121 and 124 and according to our suppliers notes, their lengths vary from 10 µm to 50 µm. The project requires 500 nm long MWNTs for the nanoelectrode technology and 10 µm for the micro-technology. It can be seen through these images that it will at the moment be hard to obtain single strands of MWNTs in an aqueous solution. Therefore, further experimentation regarding breaking the nanotubes, chemically or mechanically, needs to be conducted and then reviewed again under the electron microscope.

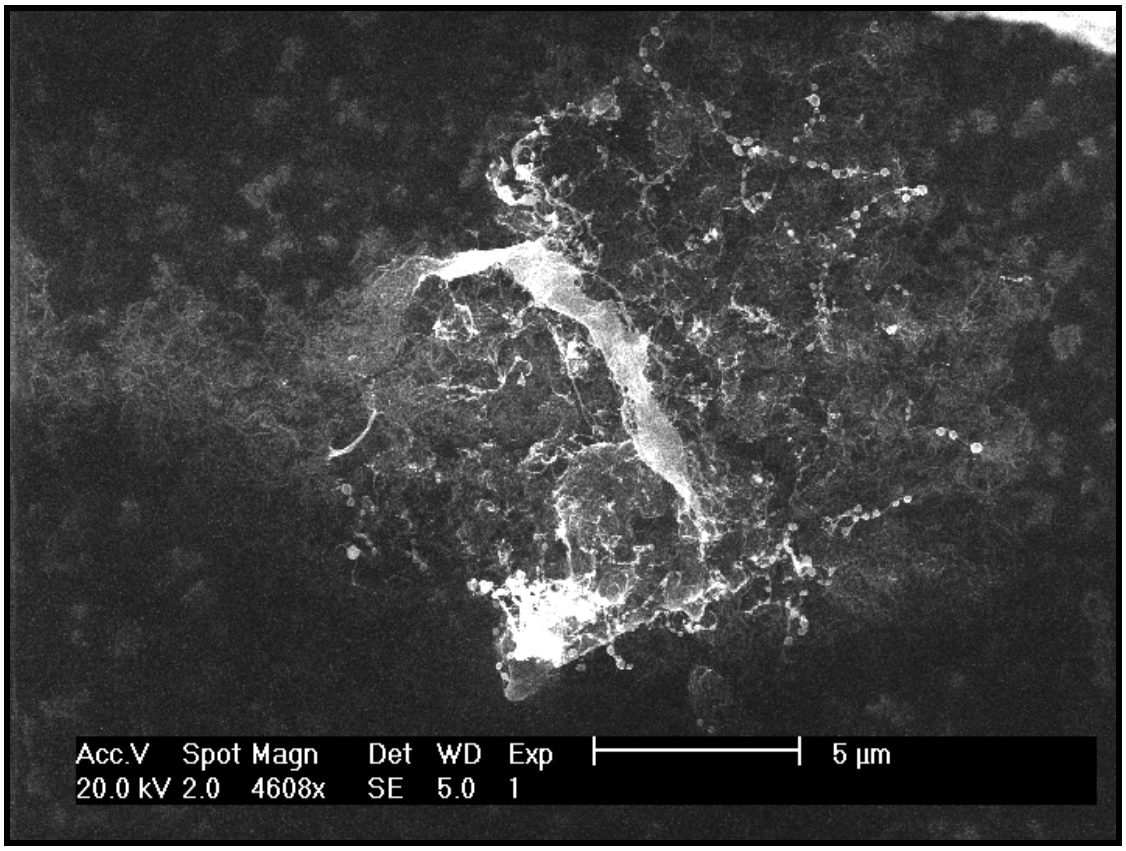

Fig. 119. *SEM image of MWNT area 1 - Close-up 1*

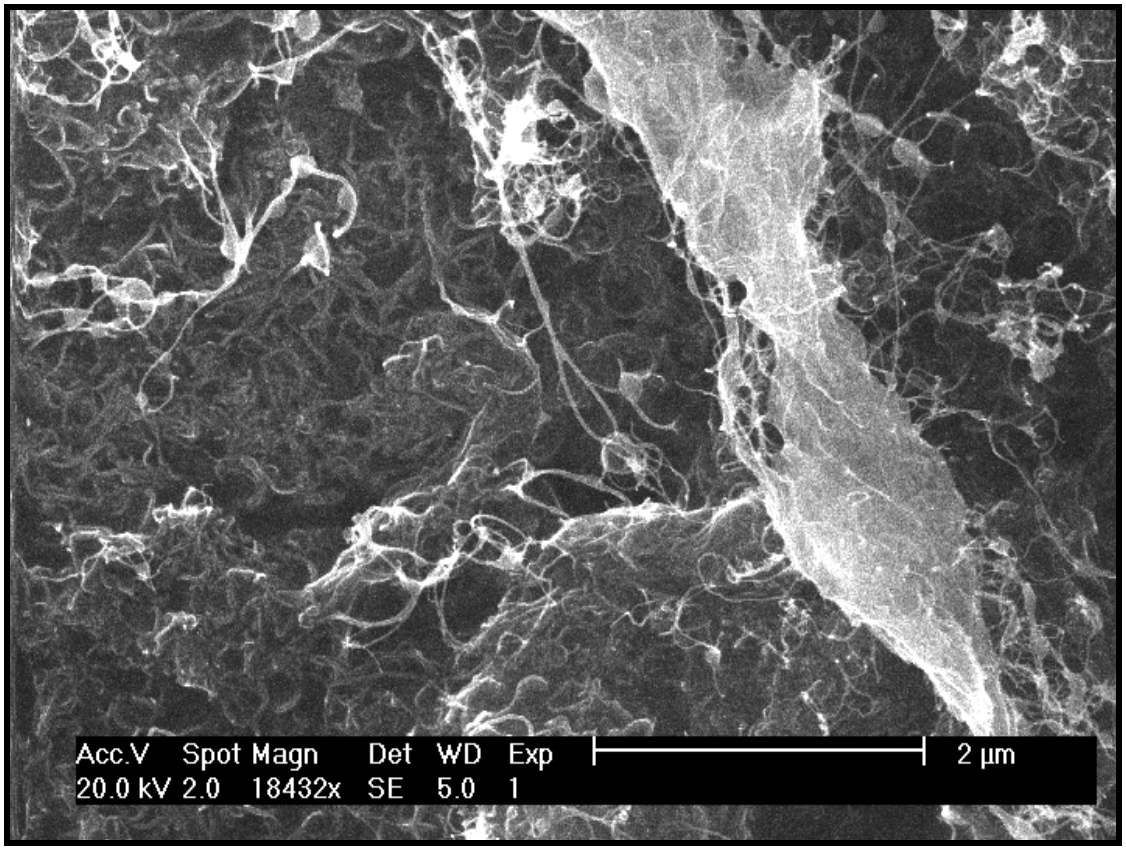

Fig. 120. *SEM image of MWNT area 1 - Close-up 2*

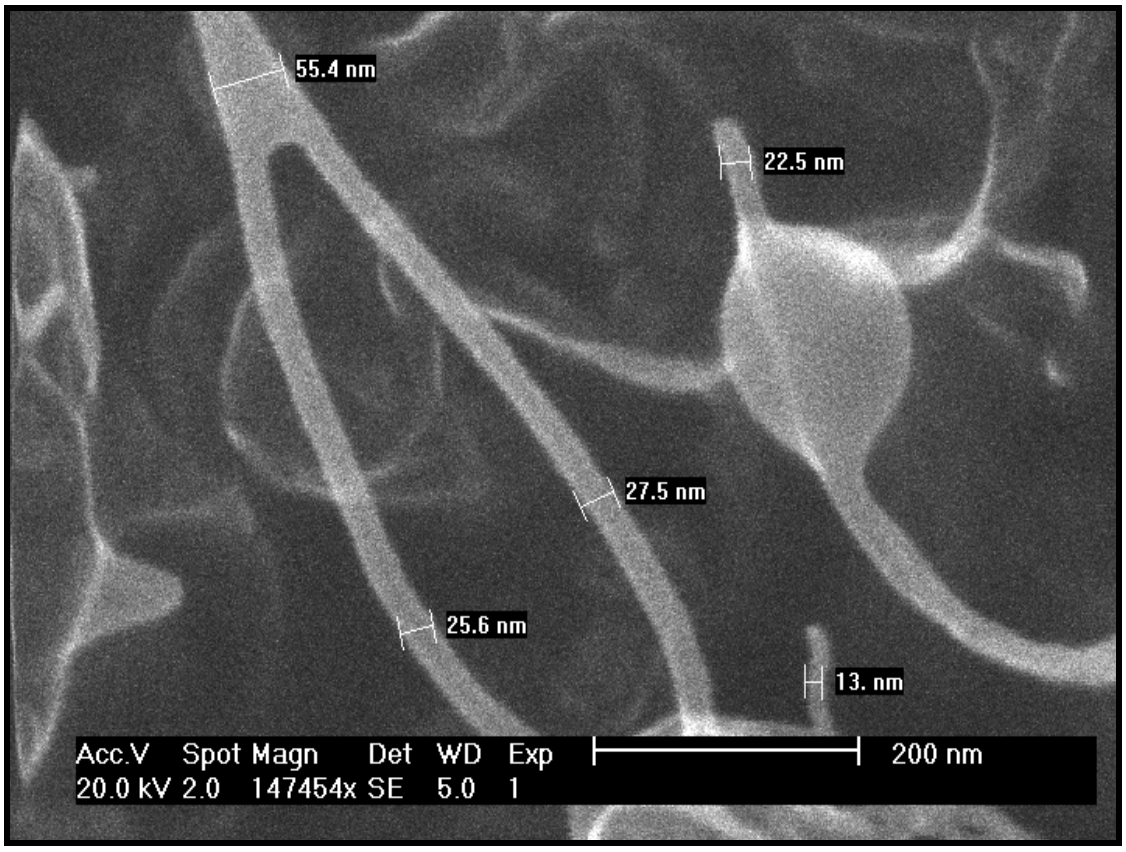

Fig. 121. *SEM image of MWNT area 1 - Close-up 3*

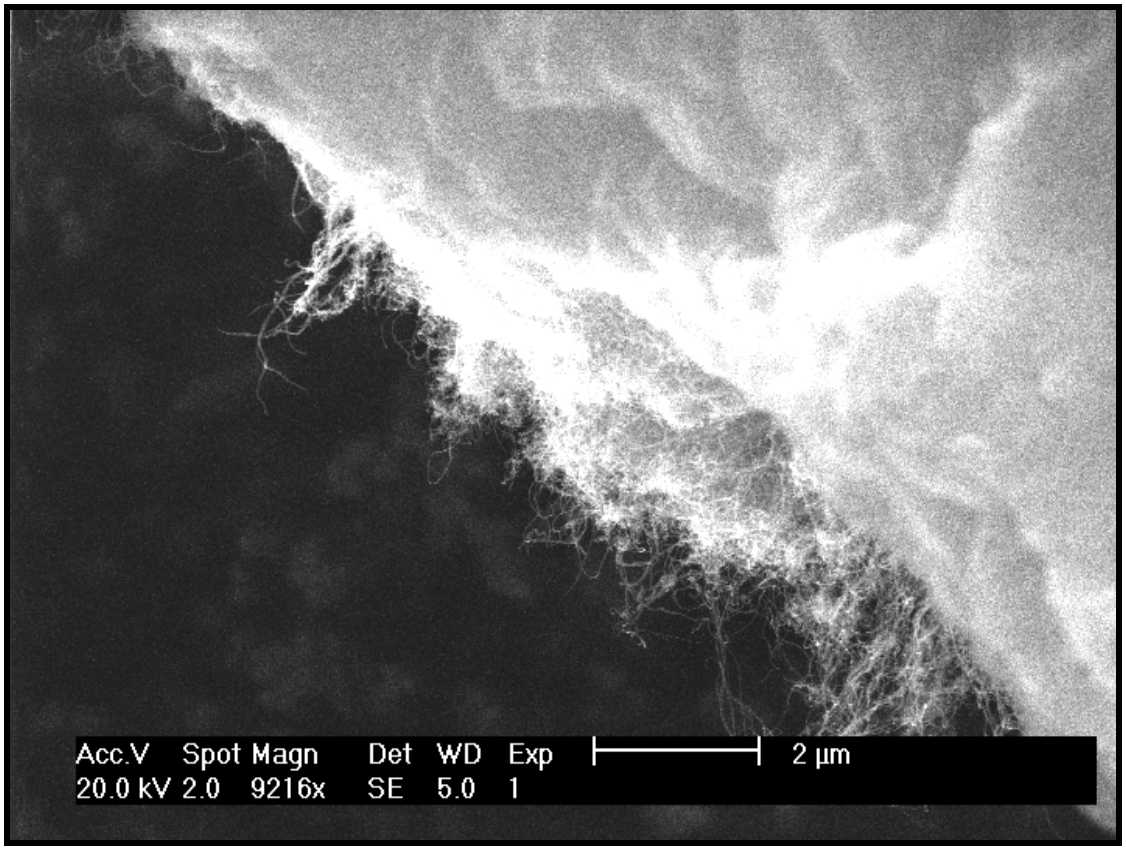

Fig. 122. *SEM image of MWNT area 2 - Close-up 1*

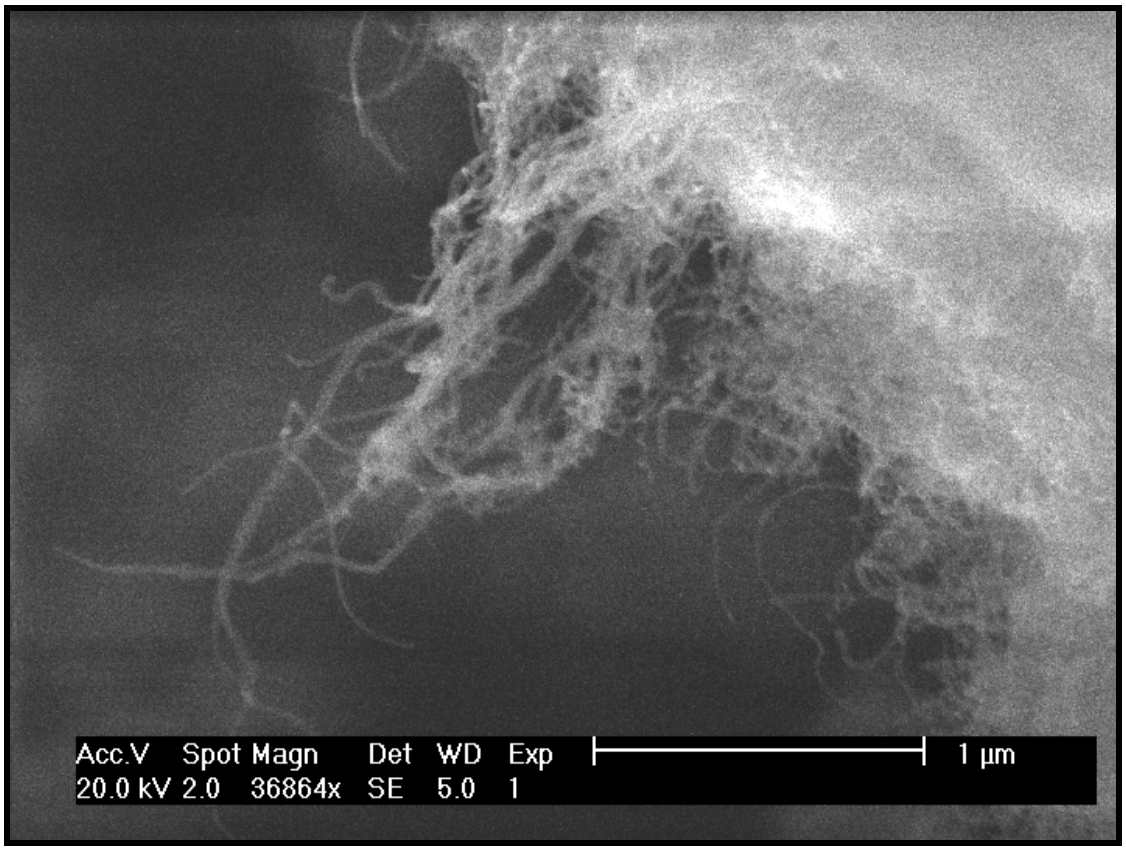

Fig. 123. *SEM image of MWNT area 2 - Close-up 2*

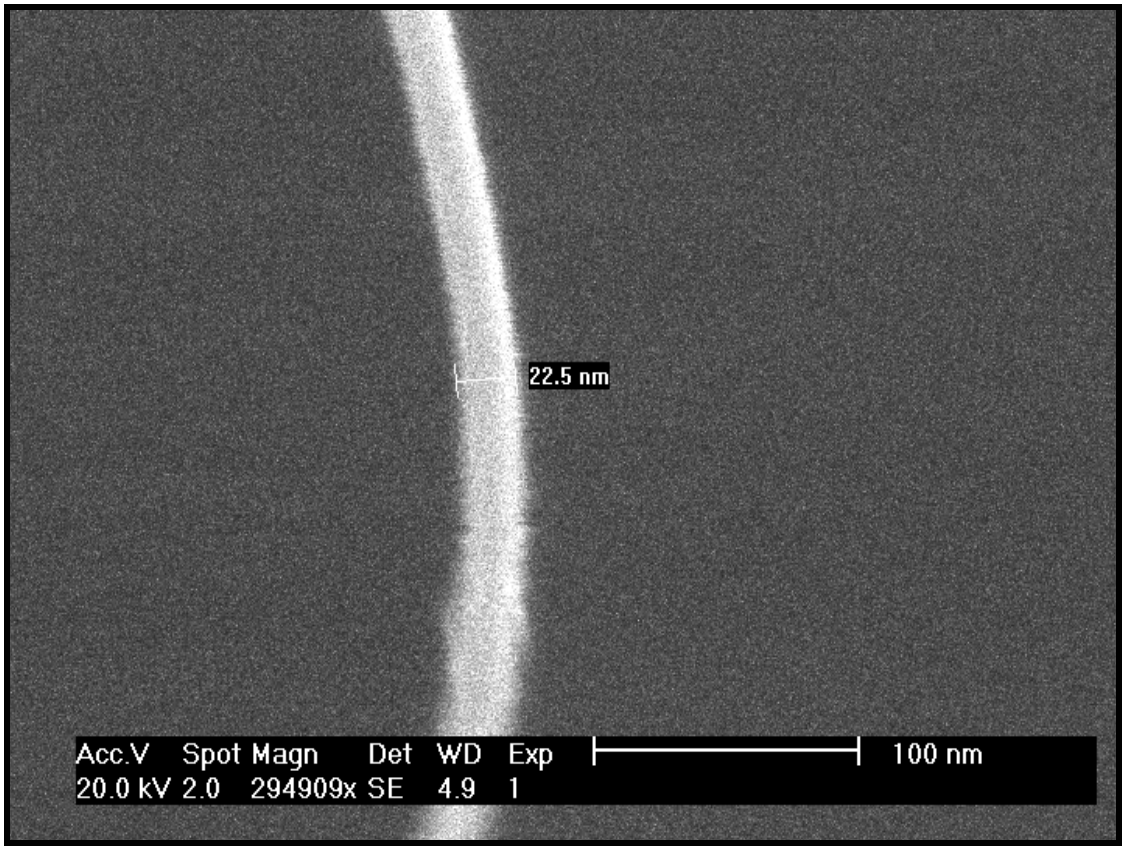

Fig. 124. *SEM image of MWNT area 2 - Close-up 3*

9.3. ISSUES INVOLVED AND POSSIBLE SOLUTIONS

9.3.1. PHOTOLITHOGRAPHY

9.3.1.1. FORCE-GENERATED MASK LIMITS

One of the main disadvantages to contact force mode in photolithography is the gradual deterioration of the mask, once using it a certain number of times. For example during underexposure, the mark would be revealed on the silicon substrate which would cut the electrodes in half and not allow current to go through the electrodes completely.

That is why it is recommended that the same design be printed a few times, so that if one can see that a mask is getting scratches, then it can be replaced with a new one. However, further testing may be needed to Fig. out whether or not it shares the same parameters as its predecessors or then new parameters need to be calculated. Being the cheapest mask in the industry, its main repercussion is time and efficiency.

The five masks, which were used for photolithography, began getting scratches after being used 6 times. This was because the contact force between the photoresist covered sample and photomask was at 1000 g (the highest force), which gradually affected the detail of the mask. We can see in the following images, how underexposure showed the scratches that were present on the mask.

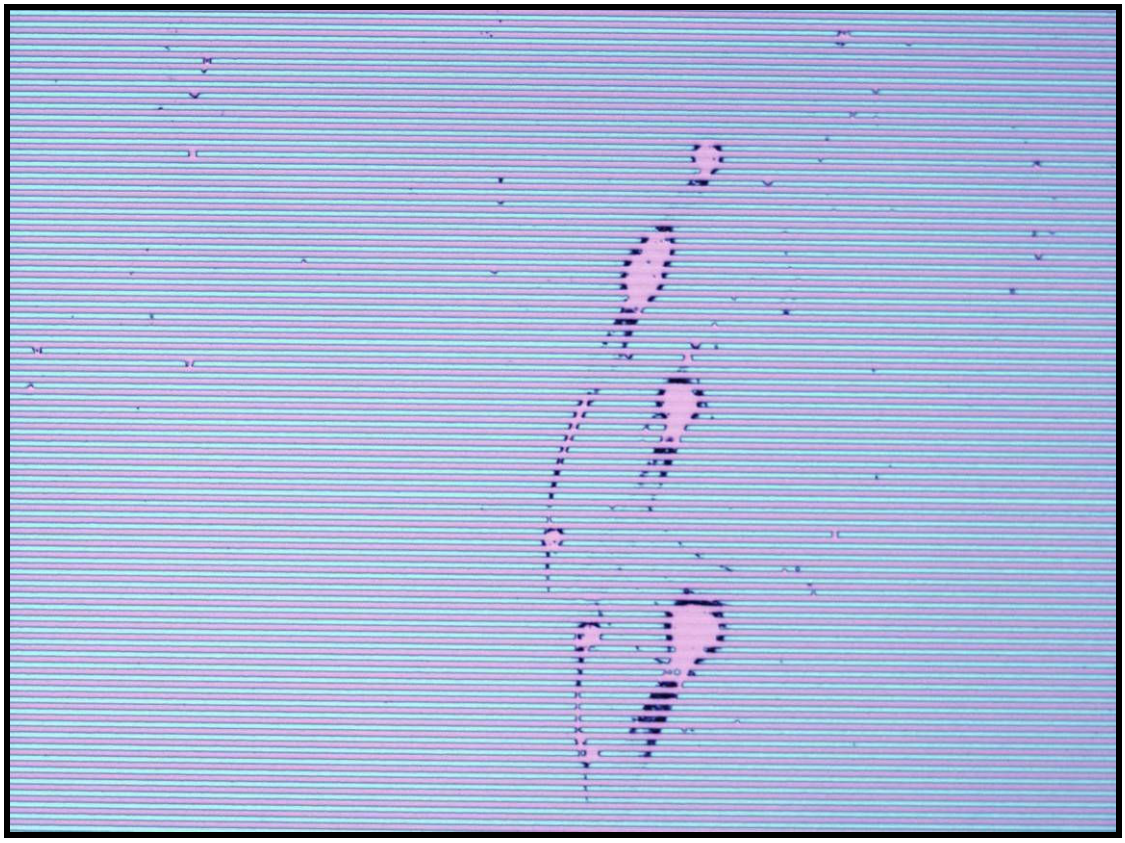

Fig. 125. *Test 31 - Session 10 – Sample 3 – Design 2*
(Example of mask mark print on sample through underexposure)

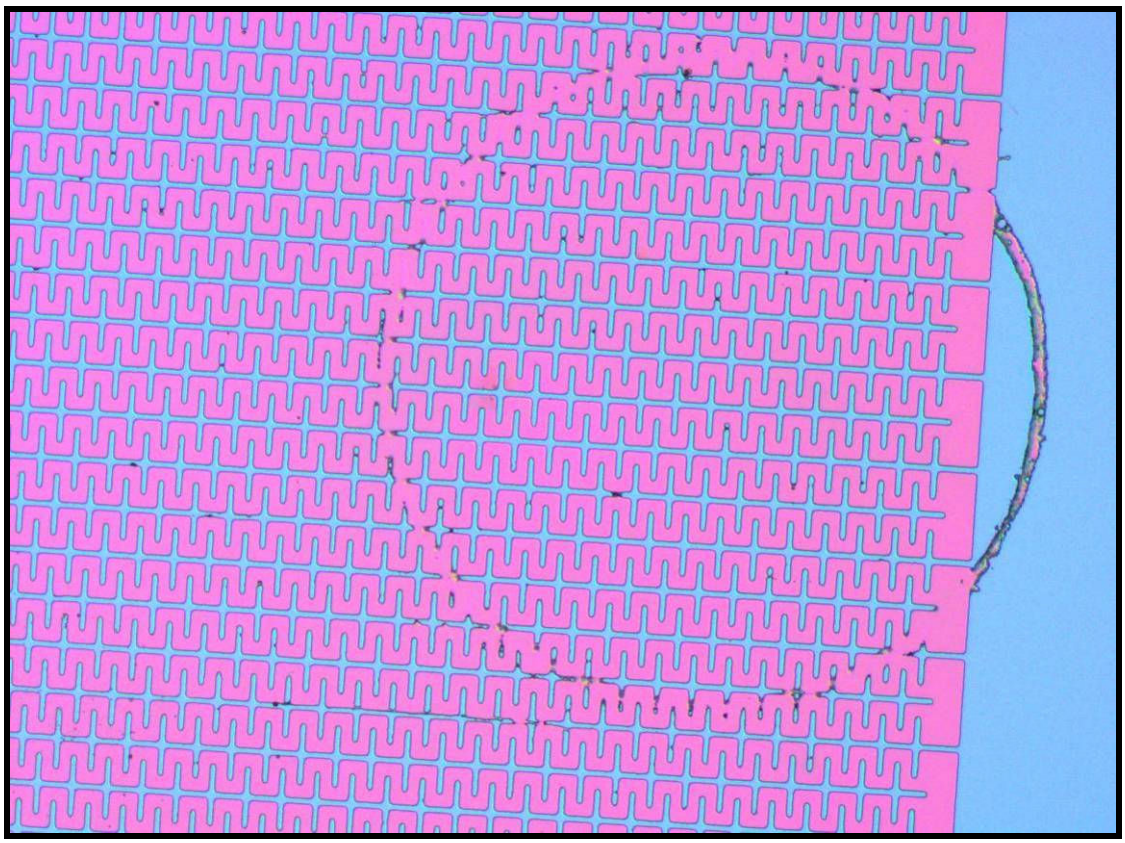

Fig. 126. *Test 10 - Session 4 – Sample 2 – Design 5*
(Example of mask mark print on sample through underexposure)

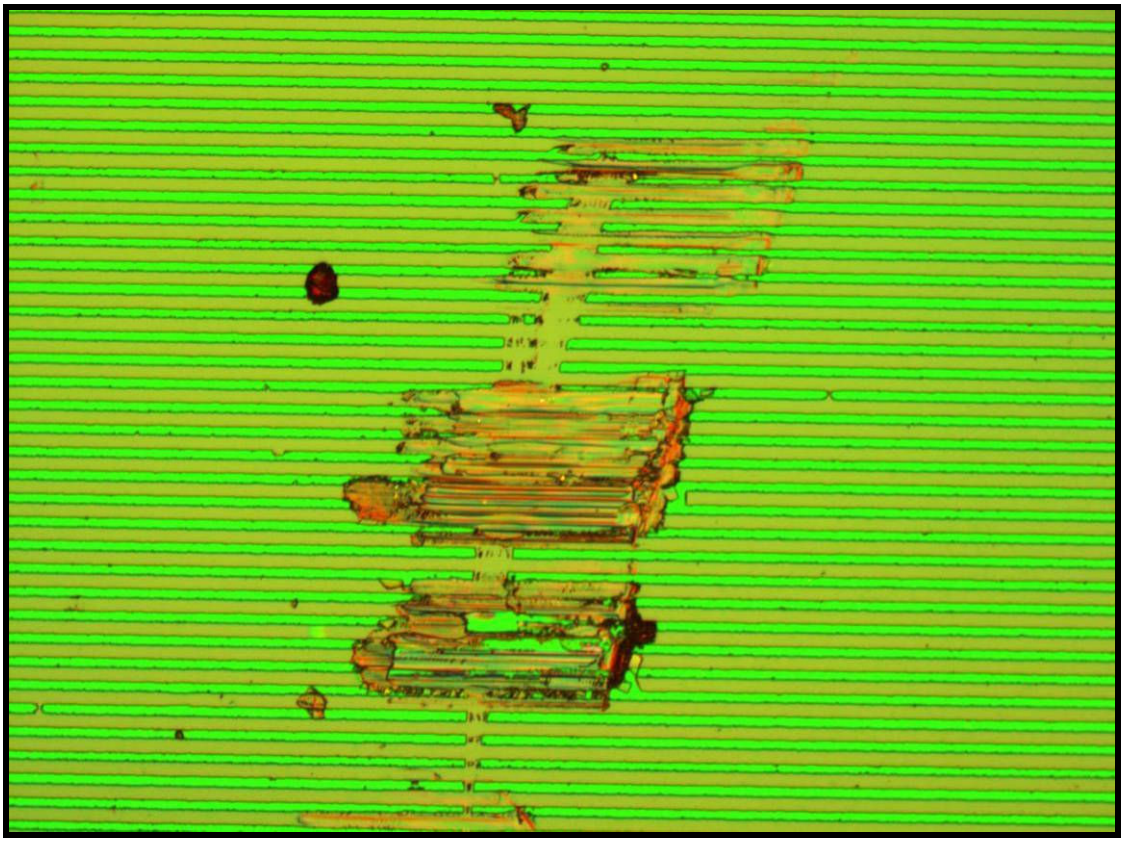

Fig. 127. *Test 1 - Session 1 – Sample 1 – Design 1*
(Example of mask mark print on sample through underexposure)

9.3.1.2. OVEREXPOSURE

Whether it was increasing the exposure time or the developer time, there were several cases where the printed mask on the silicon substrate was overexposed. This formed bridges between the electrodes, causing a short circuit and allowing the current to flow through. This defied the main operation behind component 1 as it was component 2 that would form the bridges, from the electrostatic force, a current to flow through.

We can see from Figs. 128 to 130, that overexposing the silicon substrate when it comes to altering the exposure and developer time, is a sensitive process. It can either overexpose one tiny area creating a bridge, as shown in Fig. 130, or then overexpose the entire mask, as shown in Fig. 129.

The positive side to overexposure is that exposes over the mask markings. If those were present then they would cut off most of the smaller electrodes. But the negative side is that the gaps between the smaller electrodes would significantly be smaller.

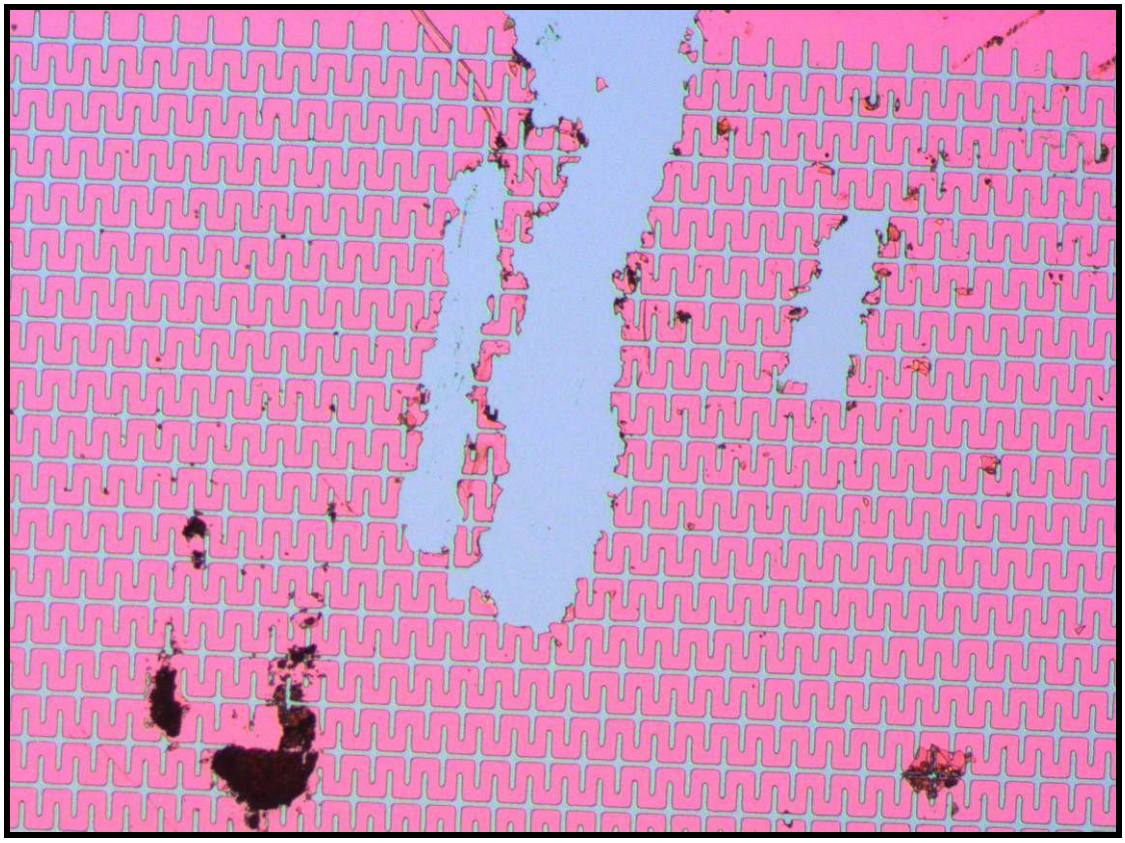

Fig. 128. *Test 5 - Session 2 – Sample 4 – Design 5*
(Example of overexposure creating short circuits)

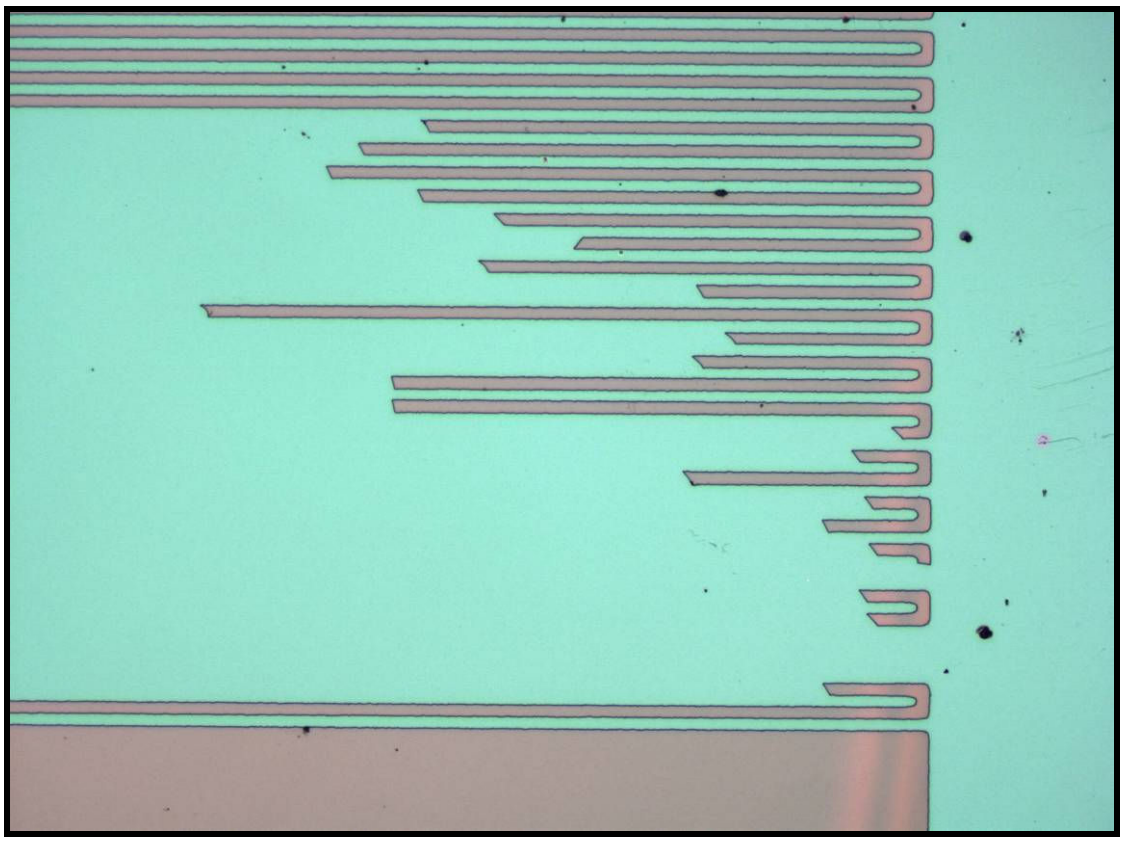

Fig. 129. *Test 17 - Session 6 – Sample 3 – Design 1*
(Example of overexposure creating short circuits)

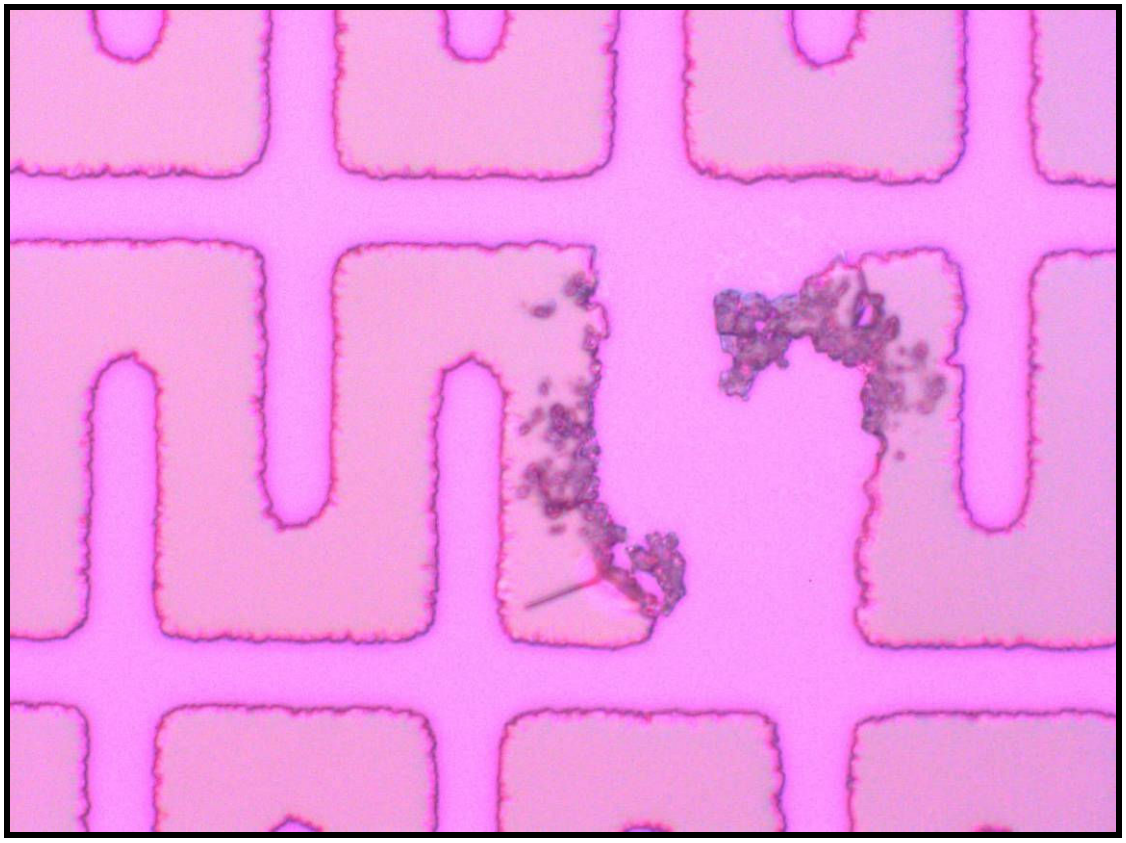

Fig. 130. *Test 15 - Session 5 – Sample 3 – Design 5*
(Example of overexposure creating short circuits)

9.3.1.3. UNDEREXPOSURE

Underexposure usually occurs when the exposure and the developer time are usually decreased. Due to such short times, this under-develops the photo mask and hence the mask markings are vividly exhibited. This can be seen in the Fig. 131.

The main disadvantage of underexposure is when your desired design will not show in your designated area. This affects the evaporation process, as the evaporated metal will lift off the underexposed area. After lift-off, this will affect the efficiency of the device as your desired design was not fully fabricated.

The positive side to underexposure is that the minor gaps in between the smaller electrodes, criss-crossing one another, are a lot wider than those that have been overexposed. Also underexposure can be used to test whether or not there are any markings on the mask, so that you can replace it with a brand new one. This could be a very valuable technique in photolithography, especially when you are using very cheap masks. As the main limitations are time and efficiency, constant check ups of the mask through underexposure can help us improve that.

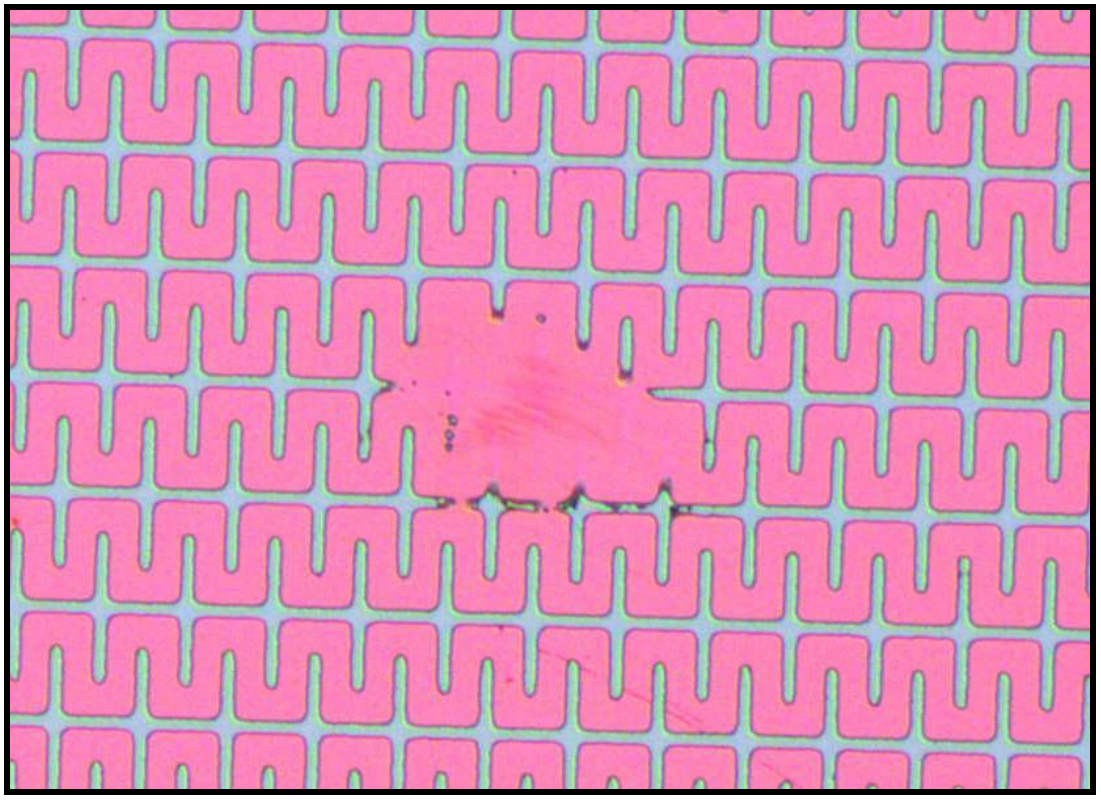

Fig. 131. *Test 5 - Session 2 – Sample 4 – Design 5*
(Example of underexposure cutting off design parameters)

9.3.1.4. ADHESION

Adhesion is when certain dissimilar particles are attached to one another due to the force of attraction. Due to these electrostatic forces, these anomalies can be spotted when the gaps between the smaller electrodes, are curved compared to the usual straight line from the perfectly aligned electrodes.

The usual reason for this is, before they were undergoing the photolithography process, they were not properly prepared when following the experiment in section 7.1.1.2.1. Usually excess ions or residue from the previous photolithography experiments, were accidentally unwashed and left on the surface, causing curved gaps between the smaller electrodes.

Being one of the main problems of photolithography, especially from my experience, constant care needs to go into sample preparation in order to avoid adhesion. As we can see from Figs. 132 to 135 the electrostatic forces could be so strong that they could lift off the entire photoresist image. However luckily, there are smaller cases as shown in Fig. 135 where curved-like anomalies can be seen and could definitely create a short circuit between the electrodes.

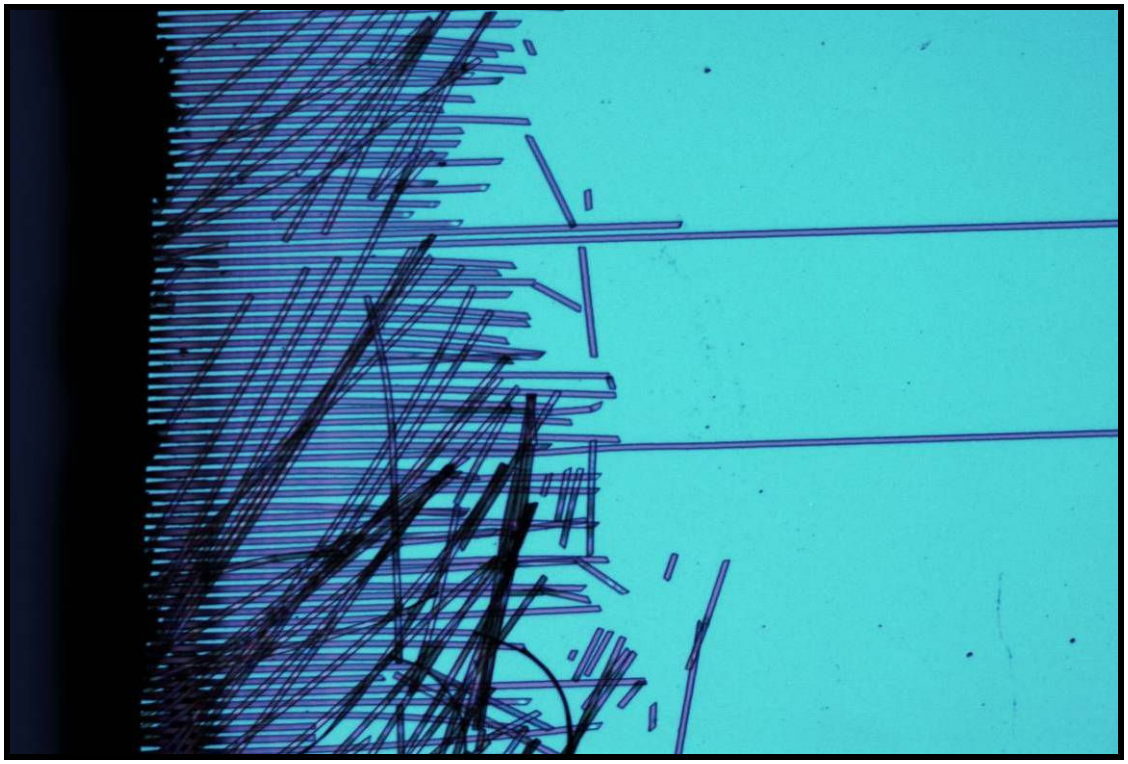

Fig. 132. *Test 20 - Session 8 – Sample 1 – Design 1*
(Example of adhesion)

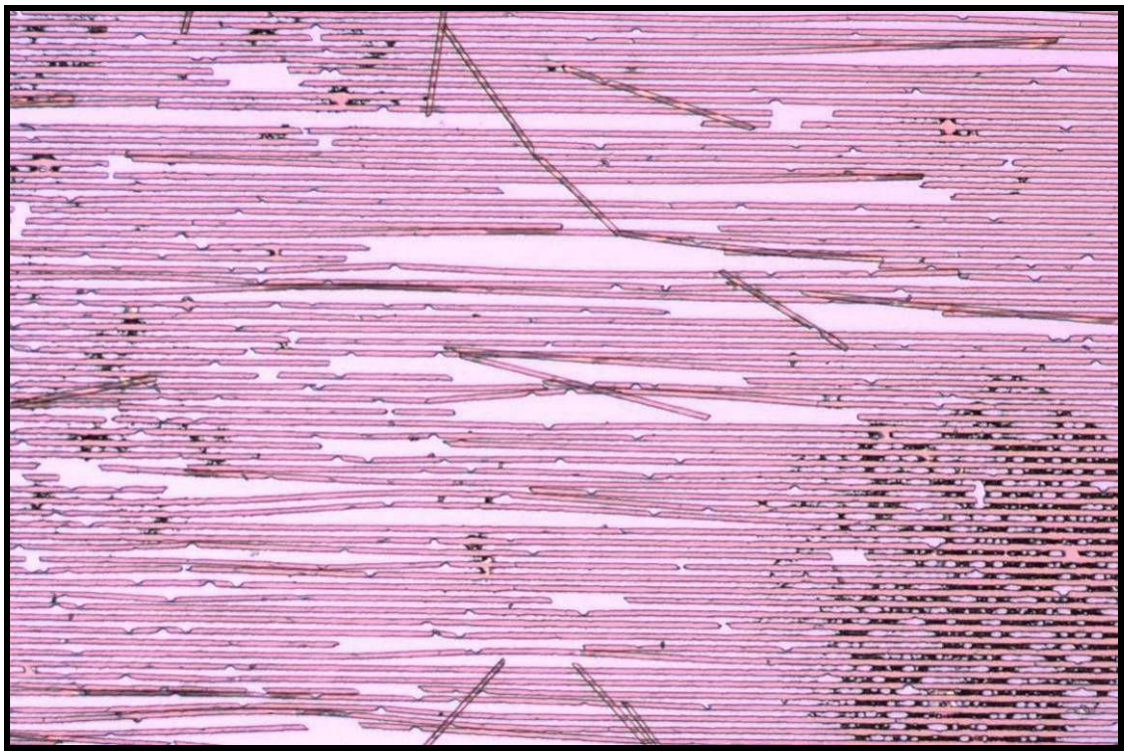

Fig. 133. *Test 18 - Session 7 – Sample 4 – Design 1*
(Example of adhesion)

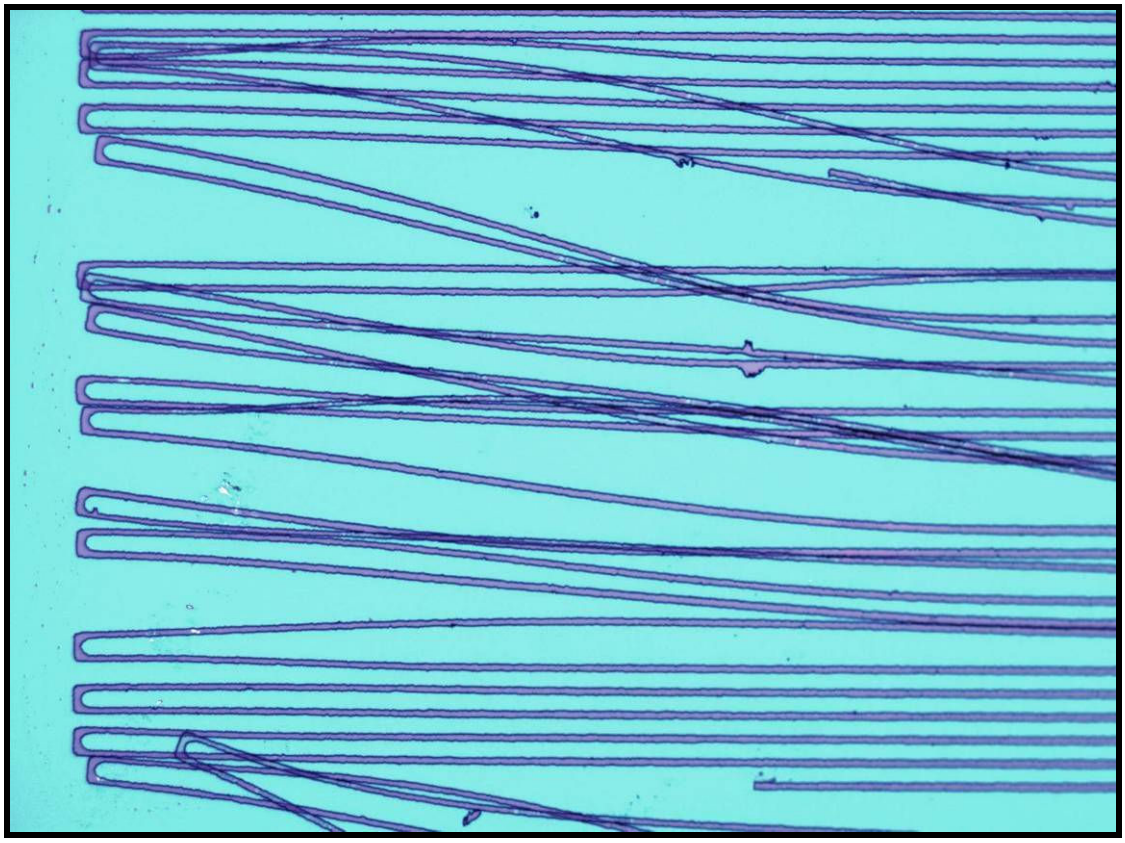

Fig. 134. *Test 17 - Session 6 – Sample 3 – Design 1*
(Example of adhesion)

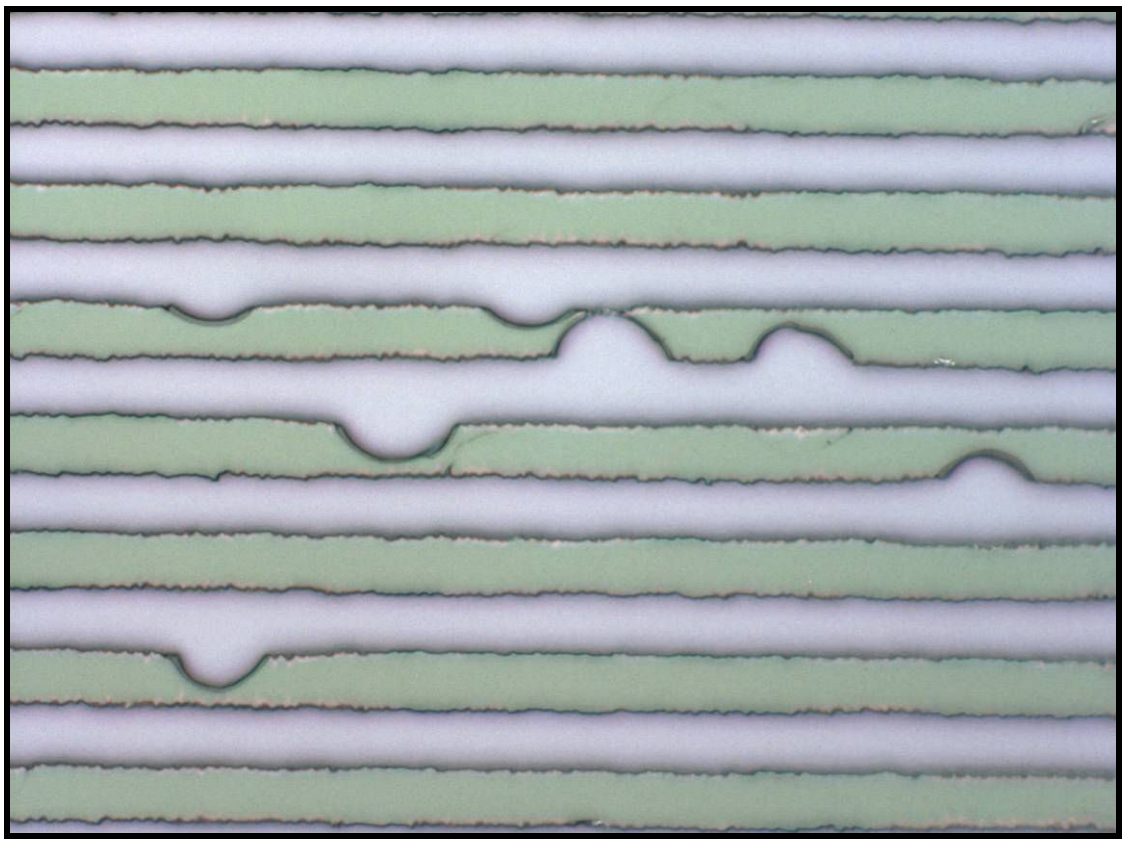

Fig. 135. *Test 18 - Session 8 – Sample 1 – Design 1*
(Example of adhesion)

9.3.1.5. DEBRIS

Debris was a constant issue throughout the entire fabrication process. Those samples, which showed clear signs of debris, were infected by particles either before or after the photoresist process.

Figs. 136 to 138 all show different examples of debris issues. Fig. 138 is your worst case scenario where you entire substrate is covered in debris even if you properly went through the sample preparation process in section 7.1.1.2.1. Fig. 137 is an example of your most popular debris issue, where you have minor particles scattered around the substrate. And if they were on the photoresist then it should not be a problem after evaporation and lift-off as they naturally will come off. However the main issue is when the debris is actually on the electrodes.

Sometimes the silicon preparation process does not wash off all the particles, and other stages may be needed to monitor the presence of debris before it begins the photolithography process. The clean room is supposedly particle-free, however there will always be traces of particles. This may be mainly because the clean room clothes cover the entire body except for the hand and the face. However gloves can be used to cover ones hands and a face mask can be provided for those with beards.

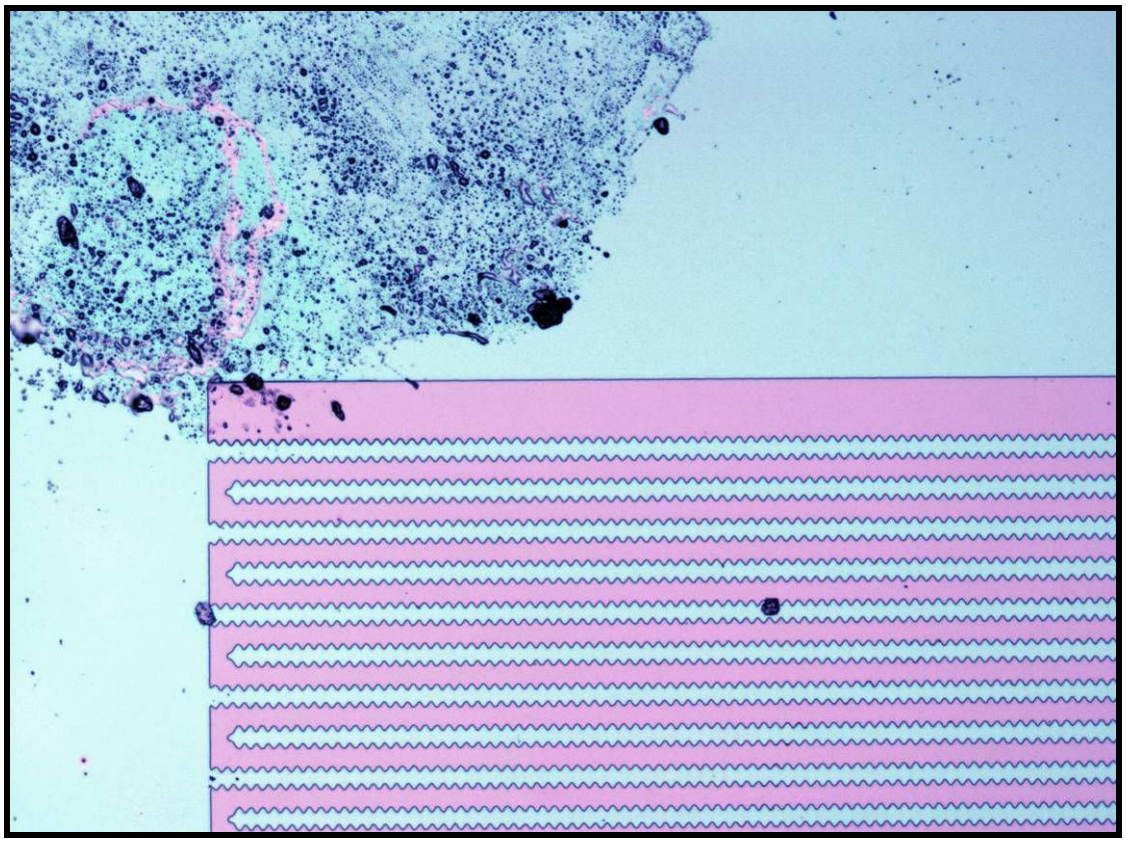

Fig. 136. *Test 24 - Session 9 – Sample 5 – Design 4 (Example of Debris)*

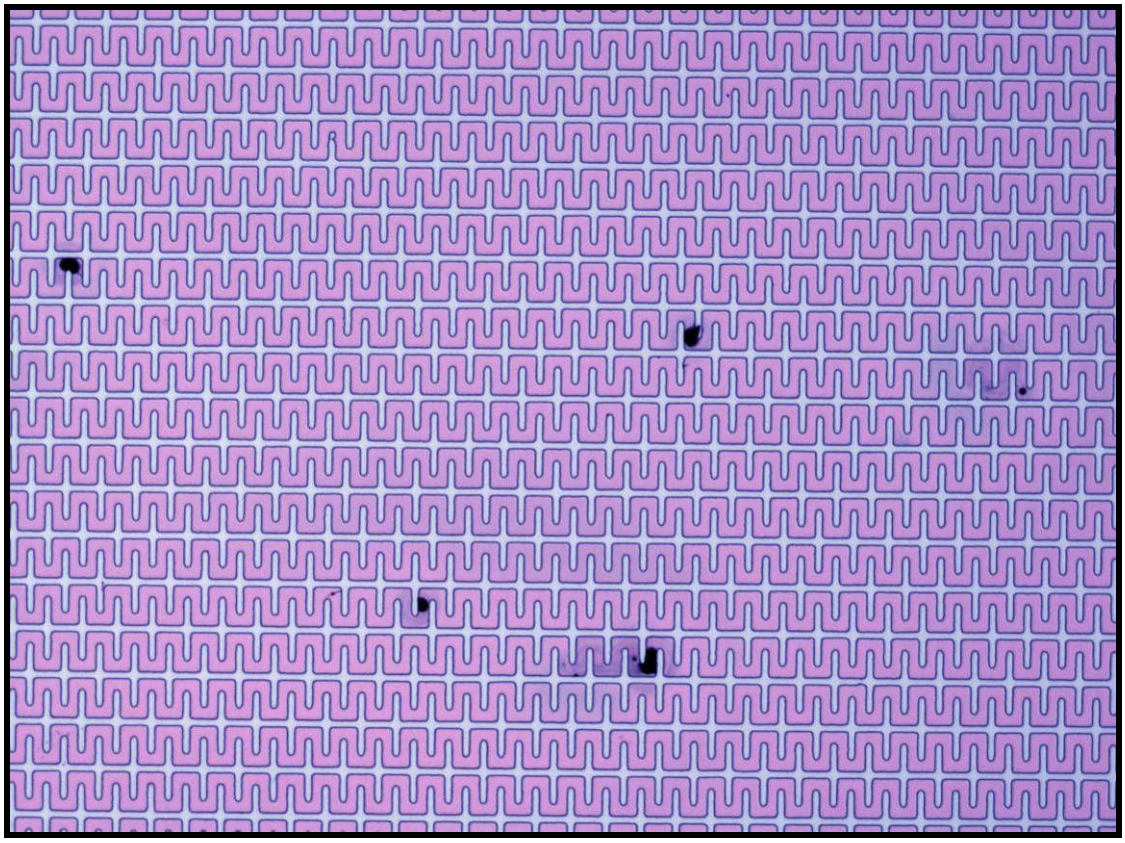

Fig. 137. *Test 35 - Session 11 – Sample 4 – Design 5*
(Example of Debris)

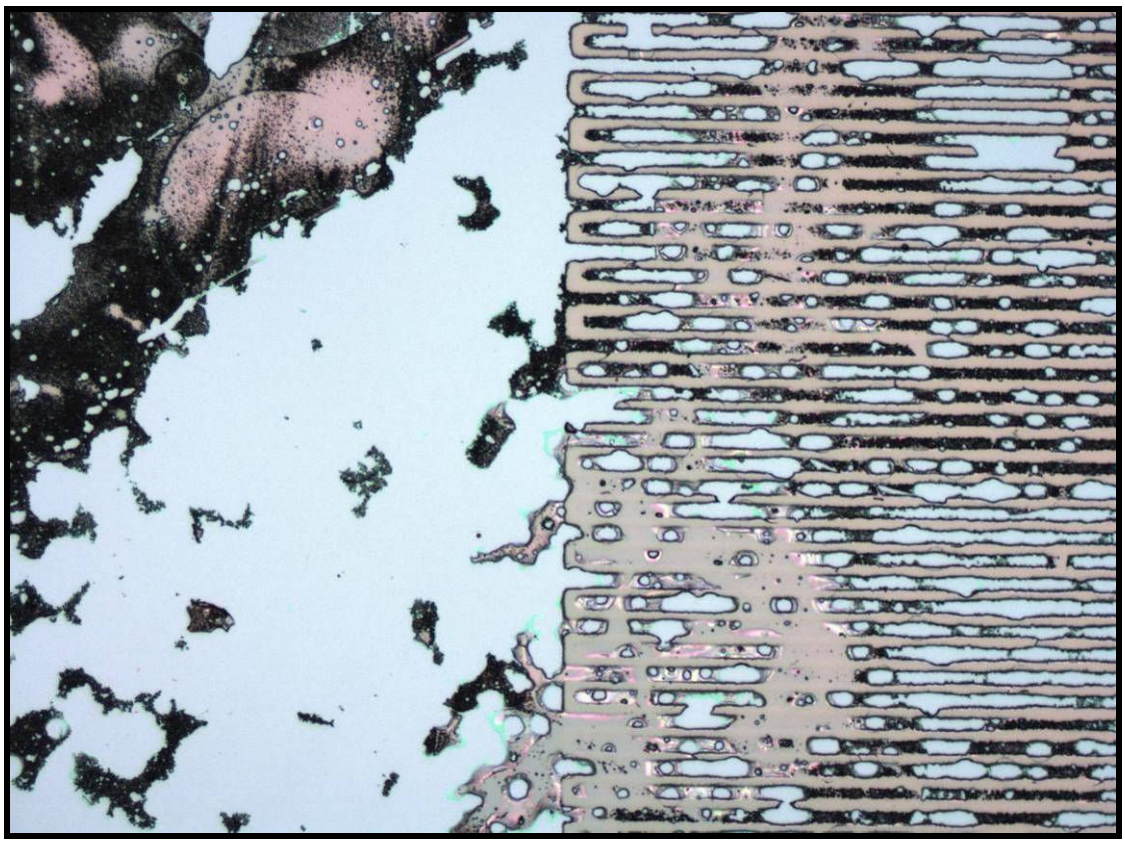

Fig. 138. *Test 18 - Session 7 – Sample 4 – Design 1*
(Example of Debris)

9.3.1.6. LIFTING OFF

The lifting off stage throughout the fabrication process successfully lifted off 20 nm Permealloy and 5 nm Gold from the unexposed areas of many test samples. However there were a few samples that needed more time for lifting off, then the usual. And if that was unsuccessful then certain procedures, with the ultrasonic machine was needed. Usually if the material had not lifted off at a certain time as shown in Figs. 139 and 140 for advanced micro-electrode design 5, then the sample was placed in a beaker with acetone, and then was exposed to 10 – 15 one second bursts in the ultrasonic machine. After then, the remaining material at need to be lifted off successful lifted off.

The main reason why one second bursts where used instead of placing the beaker into the ultrasonic machine for a specific time, is that if we did place it in the machine for a certain time period then all of the evaporated metal, including the electrodes will have come off. Therefore short one second bursts only remove the filament which has already been affected by the acetone that has dissolved the photoresist underneath it.

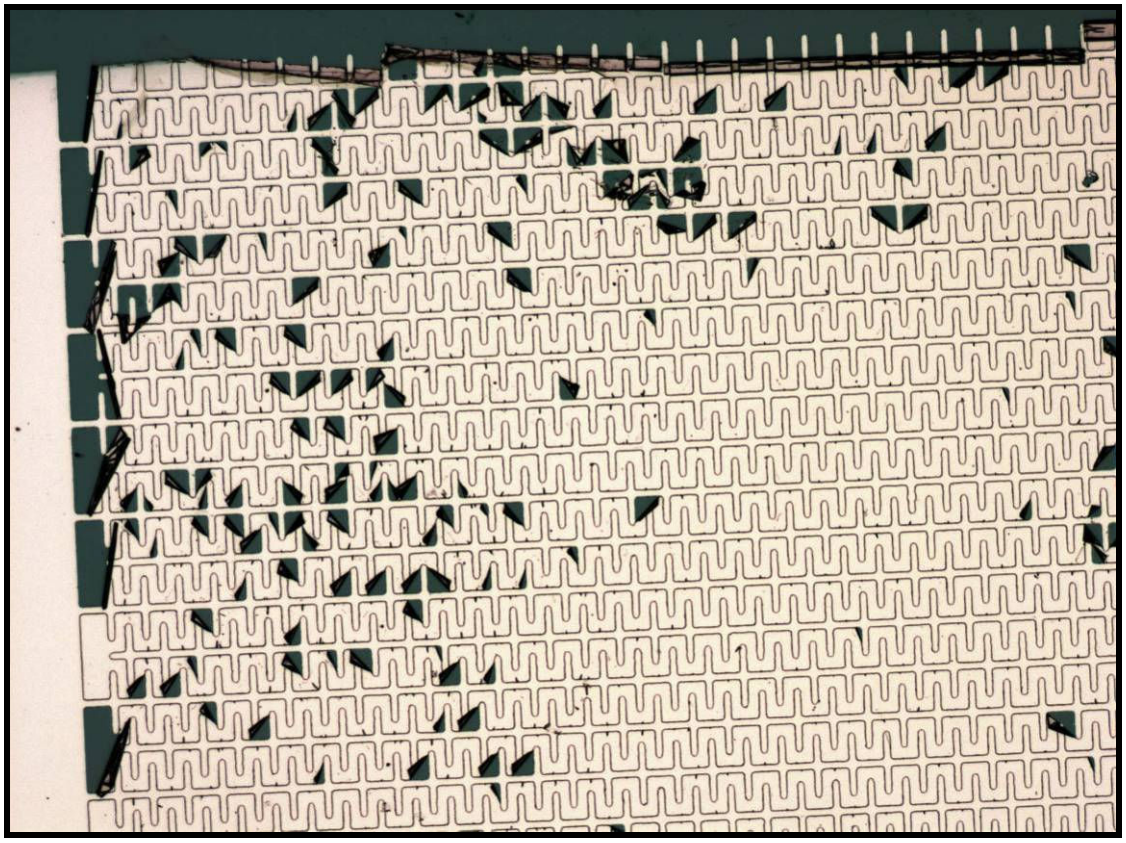

Fig. 139. *Sample 1 – Design 5*
(Example of poor lift off)

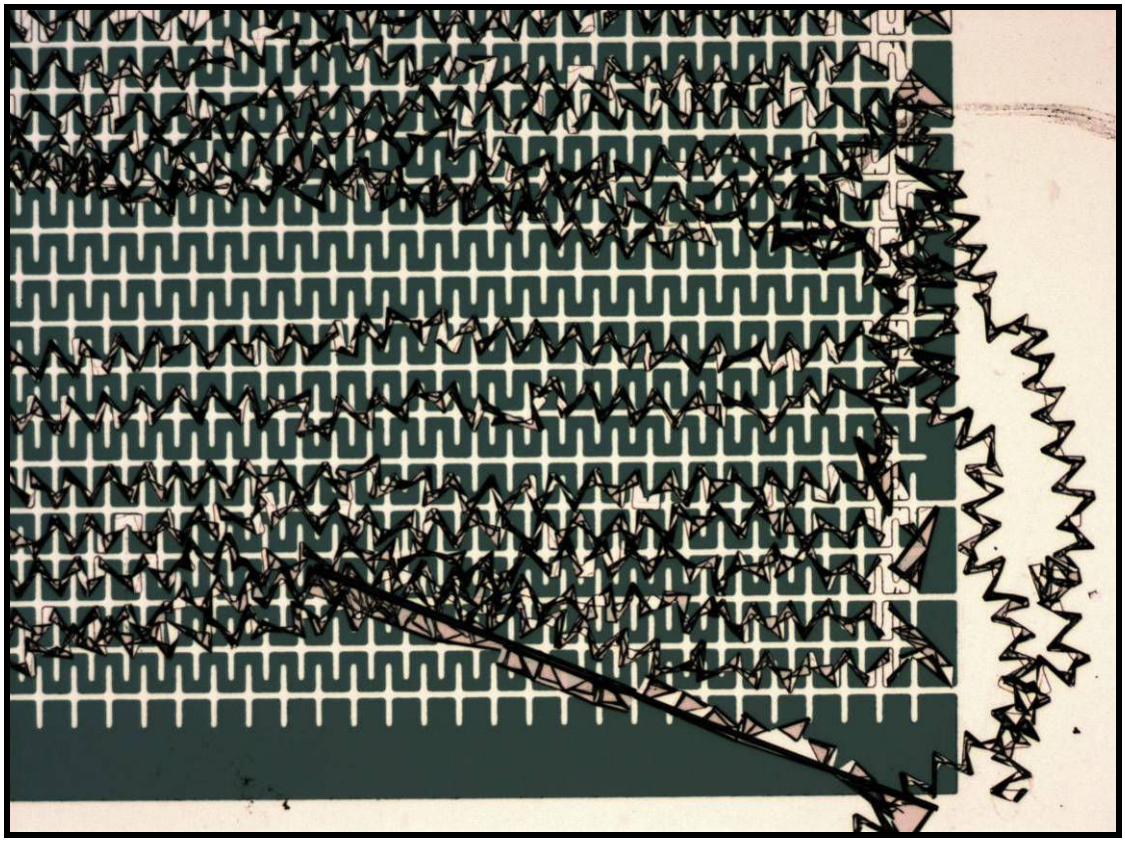

Fig. 140. *Sample 4 – Design 5*
(Example of poor lift off)

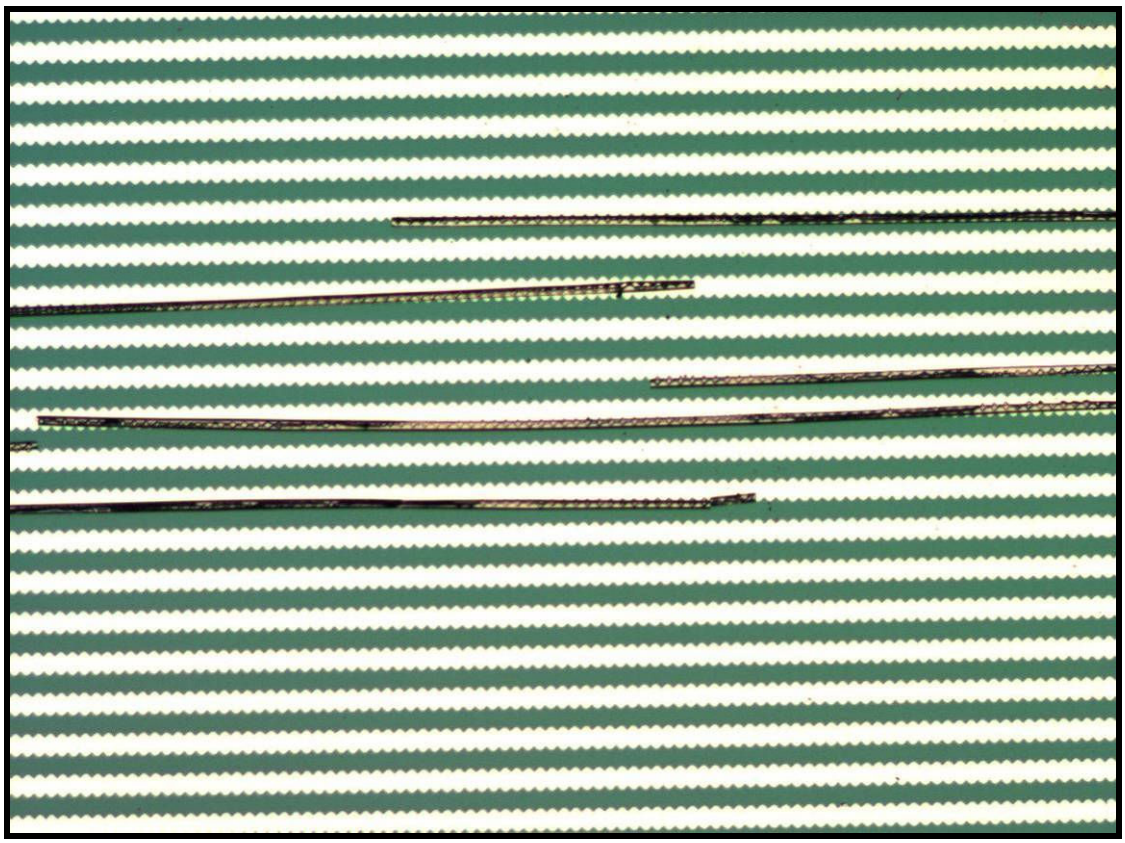

Fig. 141. *Sample 6 – Design 4*
(Example of poor lift off)

10. CONCLUSION & FINAL REMARKS

Due to time and primarily monetary constraints, I was not able to take the project to a PhD level, to fully fabricate and test the microfluidic cancer cell isolation system.

The full year has been spent on literature review and designing the system, learning valuable fabrication and characterization techniques for the project, and recently starting the fabrication and characterization procedure of the micro-electrode version of component 1.

Photolithography resulted in the successful fabrication of 3 out of 5 mask designs. Due to design 1 being faulty and design 3 possessing features less the 10 μm, the mask aligners limit, it was understandable how these designs couldn't get fabricated. Design 2, 4, and 5 were successfully fabricated however characterization through AFM and SEM exhibited issues of size variances, uneven surface, and electrode rigidness.

AFM confirmed the electrode heights to be approximately 25 nm ± 3 nm for all three samples with mask designs 2, 4, and 5, and also confirmed random variations of surface electrode smoothness from ± 5-10 nm for all three samples. It was concluded that the uneven distribution of SiO_2 layer affected the height and smoothness of the electrodes. The main questions however is whether or not there would be a change in performance compared to it being perfectly smooth.

SEM confirmed decent size specifications for mask design 2 and 5, as they followed the desired size specifications in sections 4.1.2. and 4.1.5. However, mask design 4 ended up with electrodes, twice the width of the desired size, that could have been a result of diffraction or mask complexity which thereafter affected the

evaporation process. Further fabrication and characterization sessions are needed to perfectly fabricate component 1, with its desired specifications.

There are several reasons to why the final 3 samples showed issues of electrode rigidity, uneven distribution of metals or SiO_2 layer, and variance in size specifications. The main challenge was to properly utilize one of the cheapest available commercial masks to its maximum potential. The mask designs were printed onto a transparent sheet, which reduced the quality of the mask through electrode rigidity and the slight misprinting of electrodes of equal length and width. The reason for the uneven distribution of evaporated material could mean either an uneven distribution of SiO_2 layer or evaporated material.

The best way to ensure surface smoothness and consistency is to obtain a better way to control the growth of the material and the distribution of the metal through evaporation, for example using Molecular Beam Epitaxy. The best way to improve surface rigidity and achieve desired size specifications would mean that a better material, for the mask, with smaller thickness compared to the plastic film might be more likely to overcome these issues. But if there is a way to smoothen the electrodes, for example chemical etching or using Focus Ion Beam to cut off the edges, then there wouldn't be a need to invest in a better mask.

I still have not yet proven or disproven my hypothesis as more time and money is needed to go into the project. The project, if successful will have huge commercial impact on the biomedical and biotechnology industry, and will provide a more effective in-vitro cancer therapy system, compared to the current most popular ones. This is why the project is currently being patented, as its unique design for in-vitro cancer therapeutics can be protected and worked on in the future.

Several mistakes and issues have been noted down and further improvements have been written in the next section, on what needs to be researched, what needs improvement, and how will that improvement benefit the design and application overall. Further work is also written in the next section and will provide direction towards information about the fabrication, characterization and testing methods for component 2, 3, and the full integration of the technology.

If more time and money is spent on the project, then a successful isolation system, with the desired applications, is could be achievable.

11. FUTURE WORK

Due to time and monetary constraints, all the project goals could not be achieved. Hence therefore with more time and funding, further experimentation can be conducted to improve the bio-sensing system.

11.1. COMPONENT 1: MICRO- AND NANOELECTRODE TECHNOLOGY

- Continue further experimentation for microelectrode photolithography techniques to constitute how many tries it takes before the photomask starts to reduce in quality.
- Research further into chemical and mechanical etching techniques to smoothen rigidity of electrodes after full evaporation of materials. Consider Focused Ion Beam, integrated with Field Emission Scanning Electron Microscopy, for mechanical etching as it was considered to be used to break off any unwanted bridges between the interdigitated electrodes, why not use it to trim off the excess ridges to smoothen the electrodes.
- Continue further experimentation in improving equal distribution or growth of SiO_2 layer under 1200 ^{o}C wet process in the furnace.
- If distribution of SiO_2 layer is still ambiguous and vague variances then consider introducing a silicon nitride layer process using DP80 which performs Cosmo Enhanced Chemical Vapour Deposition (CECVD), to insulate the electrodes.
- Fabricate nanoelectrode technology using electron beam lithography and re-evaluate the full size of 400 µm by 400 µm and try to come of with a design that could fill up the entire 1 cm by 1 cm substrate to properly utilize the areas potential in attracting more nanoparticle hybrids.

- Test conductivity between electrodes to see if current is passing through. If so then use FIB-FESEM to cut them up.
- Perform more conductivity tests with varying thickness of metallic materials to calculate a pattern between whether or not conductivity increase if the materials are thicker.

11.2. COMPONENT 2: MWNT-SPQD-ANTIBODY NANOPARTICLE HYBRID

- Locate a third party supplier for SPQD's or then locate facilities to fabricate SPQD's or equivalents following *Du et al* [9] and *Wang et al's* [11] fabrication and characterization procedures.
- Consider purchasing particles or materials from Invitrogen. Specifically the Dynabeads® for Human Cell Isolation product can be used for the magnetic nanoparticle component, and the Qdot® Nanocrystals product can be used for the quantum dot component. However approximately $1300 will be need to purchase products, so funding will need to be located.
- Retrieve antibodies for specified cancer. These will most likely come with the Invitrogen packages. Decide on bio-conjugation processes between antibodies and SPQD's specifically from what *Huo* [28], *Biju et al* [29], *Smith et al* [30], and *Kerman et al* [32] have been doing. Propose decisions between both biology and bionanotechnology experts for further review and assessment of design and fabrication before testing.
- Attach SPQD-Antibody bio-composite onto MWNT through chemical bio-conjugation. Focus specifically on *Yu et al* [2], *Biju et al* [34], *Pan et al* [35], *Zou* [36], *Heister et al* [37] and *Hu et al* [38] to decide on which attachment method is best. Propose ideas between both biology and bionanotechnology experts for further review and assessment of design and fabrication before testing.
- Obtain a fluorescence microscope that could both excite fluorescent material of the SPQD with UV light and obtain photoluminescence data for comparison to before and after attachment antibody and thereafter to cancerous cells.
- Consider improving the magnetic properties of the MWNT through reviewing *Wang et al* [8] and *Krupskaya et al* [10].

- Consider possibly marking the cancerous cell separately with quantum of another colour, so we can optically see whether or not there is conjugation between the cancerous cell and the nanoparticle hybrid.
- Perform microscopies: SEM, AFM and TEM to obtain images regarding conjugation between particles and how many SPQD's are attached to each individual MWNT, as the desired requirement is 1:1 (SPQD:MWNT)
- Design testing methods to confirm attachment of ONLY nanoparticle hybrid-cancer cell bioconjugates onto component 1.
- Mechanically or chemically shorten 10-50 μm MWNTs to 500 nm according to *Niesz et al* [17]. Research filtration methods to separate 500 nm MWNT.
- Decide and test several MWNT aqueous solutions after been broken down to required lengths. Look at procedures from *Li et al* [12], *Garg et al* [13], *Schierz et al* [14] and *Chun et al* [16] to decide on final procedures for the required aqueous solution.
- Test the dispersion and lengths of these nanoparticle hybrids through SEM.

11.3. COMPONENT 3: MICROFLUIDIC OPERATION CHIP

- Design microfluidic operation with the design requirements of section 4.3.
- Research and review fabrication and characterization techniques, specifically from *Kim et al* [21], *Weigl et al* [22], *Zhang et al* [23] and *Hongbin et al* [24]
- Research and calculate pressures and volumes for solution flow for intake and outtake. Specifically for Stage 5 of the designed cancer cell isolation system, where normal cells are being flushed, and cancerous cells are still attached to nanoparticle hybrids, which are attached to component 1.
- Perform certain tests to confirm solution flow in and out of the component device.
- Decide on which specific type of valve will be used to block the 5 major inlets.
- Perform certain tests to verify that the valves completely block solution from going in and out of the component.

11.4. APPLICATION FOR PATENT

The project shows huge commercial value in the biomedical and bionanotechnology industry regarding in-vitro cancer treatments. If successful in the next 4 years after fabrication and testing it would be good to know the intellectual property is legally

binded to me and the rest of the members who significantly helped with the project. Therefore, an application is currently being written and will be sent off for further process.

12. APPENDIX

12.1. BENG PROJECT

BEng PROJECT OVERVIEW

The project consists of the research and development of a unique two-part bio-sensing system, which successfully improves the major flaws of current Lab-On-A-Chip (LOAC) designs.

The LOAC design, if successful, would be more commercially viable allowing the flexibility of the detection of a number of molecular cancer specimens to be cheaper, faster, and more accurate. Current detection methods today are too detailed, they too are expensive, and take longer to conduct tests. Some machines themselves are not portable. This LOAC design defeats these complications.

Component 1 is an advanced interdigitated electrode design on a silicon substrate, placed onto a chip holder. The electrodes are wire bonded to gold tracks which will be used for testing and experimentation. The research, for this component, hopes to achieve the right electrode design and material needed to magnetically attract component 2 from its EM field generated.

Most lab-on-chip designs consist of just one component, which reduces its applications significantly. The addition of a second component which is equally light and portable, will improve the impedance and amperometric responses of the detection scheme.

Component 2 is the key feature of this system. The complex designed structure of the multi-labelled MWNT device will detect and attach itself to the specified cancer cell, in incubation or under a catalytic process. This will be highly advantageous, as the two attached particles (SuperParamagnetic Quantum Dot (Fe_3O_4 – CdSe), and cancer biomarker (antibody)) will improve on amplification, selectivity and sensitivity of the

specified cell. The research hopes to achieve the following: 1) a strong molecular link between the MWNT hybrid and the cancer cell through the specific biomarker; 2) a strong magnetic attraction between the electrodes and the MWNT hybrid via the SPQD's; 3) a strong fluorescence from the SPQD's before and after attachment with a cancer cell.

The operation of the biosensor is a fairly simple process. At first an aqueous solution of MWNT hybrids are mixed with a blood sample with cancer cells. They are left for a time period under a catalytic process where the MWNT hybrids attach themselves onto the specified cancer cell. A drop of the mixture will be applied onto the electrodes. Once a voltage is applied, the MWNT bioconjugates will align to form bridges between the electrodes, allowing a current to pass from one electrode to the other. Impedance and amperometric responses will be measured using meters and fluorescence change will be viewed and measured through a CCD camera.

BEng PROJECT RESULTS
COMPONENT 1

Several tests were conducted to assess the efficiency and accuracy of component 1. These tests were to ensure the proper operation of the sensor and whether it matched the concluded design specifications. One of the main specifications was that no current is to pass from one electrode to the other. The configured CNTs would provide the bridging between the electrodes, allowing a current to pass from one electrode to the other. A variable pulse was inputted, from the signal generator, and was monitored through the oscilloscope. Resistance measurements of the component, with and without the signal input, were taken to investigate the resistance variance of the silicon substrate. Test results can be seen below:

BEng RESULT GRAPH 1: RESISTANCE RESPONSE FROM VARIANCE IN VOLTAGE OF INDIVIDUAL SENSORS

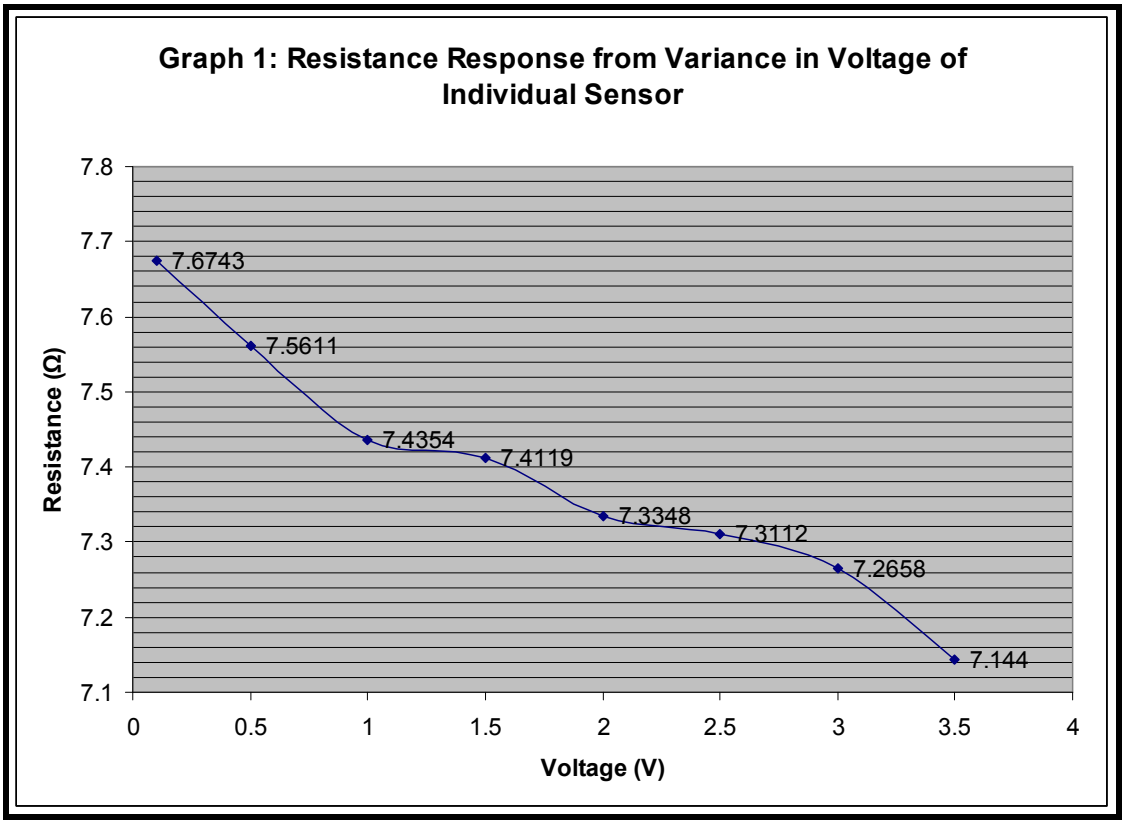

Fig. 142. *Resistance response from variance in voltage of individual sensors*

Voltage	0.1	0.5	1	1.5	2	2.5	3	3.5
Trial 1	7.6743	7.5611	7.4354	7.4119	7.3348	7.3112	7.2658	7.1440

Table 24. *Resistance Response from Variance in Voltage of Individual Sensor (Ω)*

BEng RESULT GRAPH 2: RESISTANCE RESPONSE FROM VARIANCE IN VOLTAGE OF TEST SOLUTION 1 BEFORE TRIAL AND ERROR TESTING

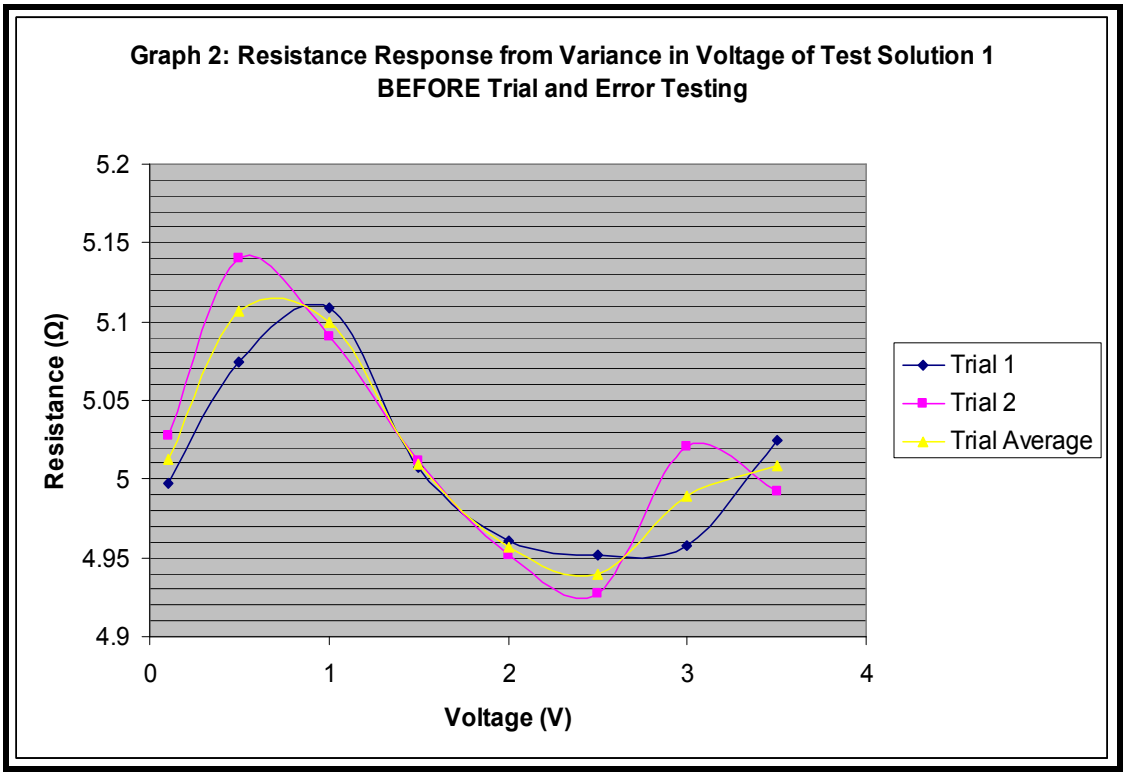

Fig. 143. *Resistance response from variance in voltage of test solution 1 before trail and error testing*

Test Solution 1 contents:

- 5 drops Glycerol
- 45 drops Deionised water

Voltage	0.1	0.5	1	1.5	2	2.5	3	3.5
Trial 1	4.9976	5.0739	5.1091	5.0078	4.9610	4.9515	4.9575	5.0249
Trial 2	5.0273	5.1402	5.0909	5.0112	4.9519	4.9269	5.0207	4.9919
Trial Average	5.01245	5.10705	5.1	5.0095	4.95645	4.9392	4.9891	5.0084

Table 25. *Resistance Response from Variance in Voltage of Test Solution 1 BEFORE Trial and Error Testing (Ω)*

BEng RESULT GRAPH 3: RESISTANCE RESPONSE FROM VARIANCE IN VOLTAGE OF TEST SOLUTION 1 AFTER TRIAL AND ERROR TESTING

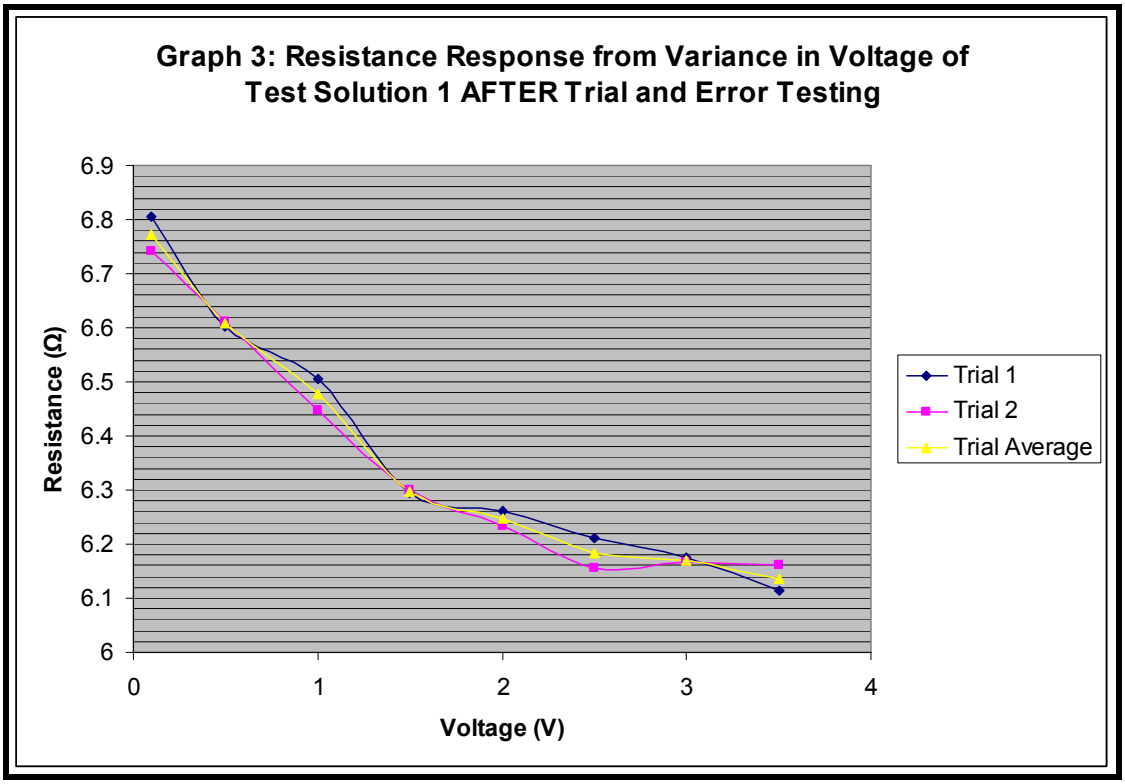

Fig. 144. *Resistance Response from Variance in Voltage of Test Solution 1 AFTER Trial and Error Testing*

Test Solution 1 contents:

- 5 drops Glycerol
- 45 drops Deionised water

Voltage	0.1	0.5	1	1.5	2	2.5	3	3.5
Trial 1	6.8046	6.6033	6.5063	6.2940	6.2609	6.2098	6.1743	6.1140
Trial 2	6.7418	6.6112	6.4473	6.3008	6.2329	6.1564	6.1662	6.1599
Trial Average	6.7732	6.60725	6.4768	6.2974	6.2469	6.1831	6.17025	6.13695

Table 26: *Resistance Response from Variance in Voltage of Test Solution 1 AFTER Trial and Error Testing (Ω)*

BEng RESULT GRAPH 4: RESISTANCE RESPONSE FROM VARIANCE IN VOLTAGE OF TEST SOLUTION 2

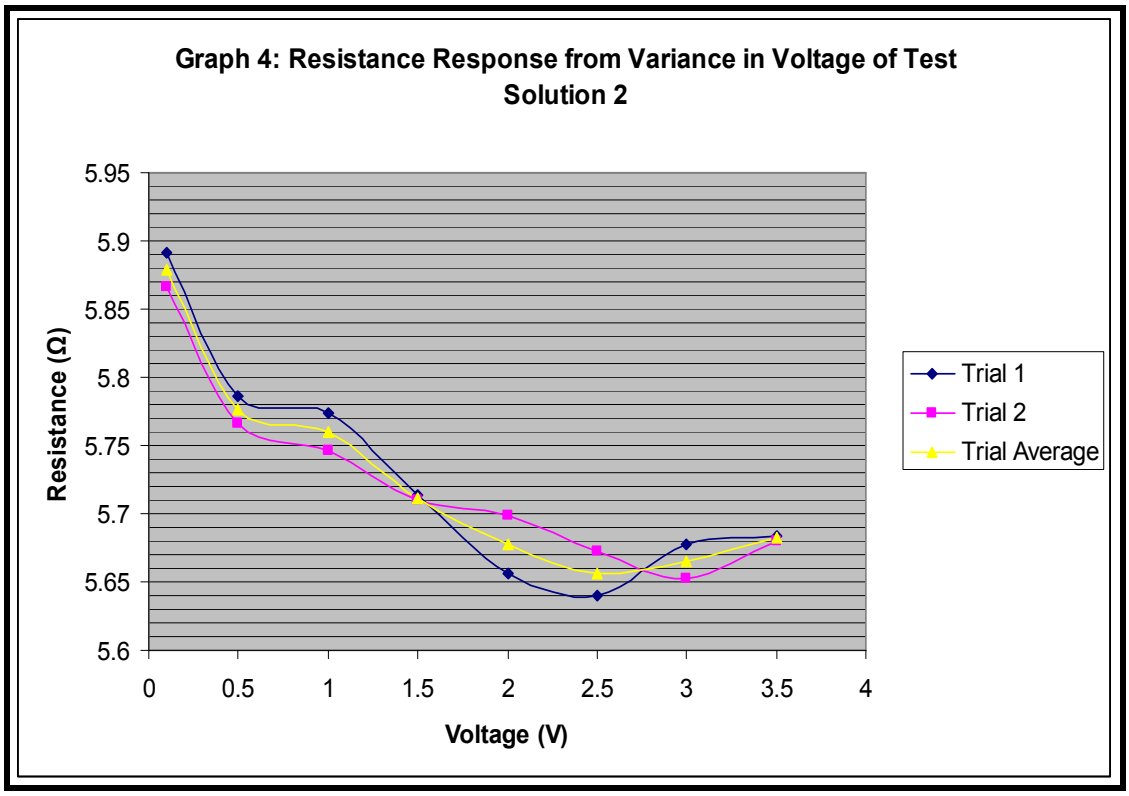

Fig. 145. *Resistance Response from Variance in Voltage of Test Solution 2*

Test Solution 2 (Low Concentration of MWNTs) contents:

- 5 drops Glycerol
- 45 drops Deionised water
- 1 drop of MWNT:Deionised Water solution (1:3)

Voltage	0.1	0.5	1	1.5	2	2.5	3	3.5
Trial 1	5.8908	5.7862	5.7738	5.7135	5.6563	5.6398	5.6771	5.6839
Trail 2	5.8660	5.7657	5.7458	5.7100	5.6992	5.6731	5.6523	5.6799
Trail Average	5.8784	5.77595	5.7598	5.71175	5.67775	5.65645	5.6647	5.6819

Table 27: *Resistance Response from Variance in Voltage of Test Solution 2 (Ω)*

BEng RESULT GRAPH 5: RESISTANCE RESPONSE FROM VARIANCE IN VOLTAGE OF TEST SOLUTION 3

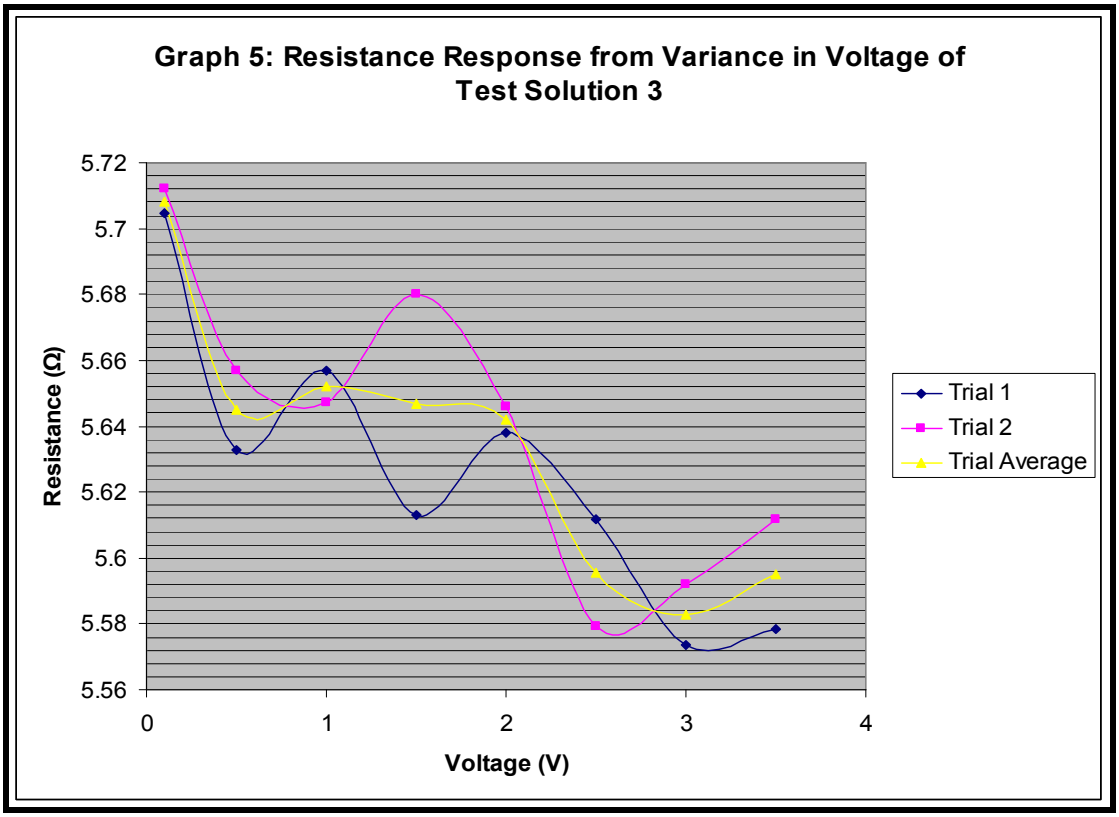

Fig. 146. *Resistance Response from Variance in Voltage of Test Solution 3*

Test Solution 3 (High Concentration of MWNTs) contents:

- 5 drops Glycerol
- 45 drops Deionised water
- 2 drops of MWNT:Deionised Water solution (1:3)

Voltage	**0.1**	**0.5**	**1**	**1.5**	**2**	**2.5**	**3**	**3.5**
Trial 1	5.7046	5.6327	5.6569	5.6130	5.6381	5.6118	5.5737	5.5783
Trail 2	5.7121	5.6570	5.6474	5.6802	5.6460	5.5791	5.5921	5.6117
Trail Average	5.70835	5.64485	5.65215	5.6466	5.64205	5.59545	5.5829	5.595

Table 28: *Resistance Response from Variance in Voltage of Test Solution 3 (Ω)*

Conductivity tests, including a variance in pulse frequencies, unfortunately showed current passing through one set of electrodes to the other. The reasons for this consisted of the following:

- There were bridges, undetected by the eye, between the electrodes during photolithography. This allowed the current to pass through from one electrode to the other. Using the Field Emission Scanning Electron Microscopy machine with an integrated Focused Ion Beam, would allow us to locate the bridge using the FESEM and cut it apart with the FIB.
- The electrostatic force, produced between the electrodes was so strong that it managed to pass a current on the silicon substrate. Hence therefore a substrate with a higher resistance will be needed instead of silicon for future experimentation. To improve on the sensor, a method of insulation of the electrodes will be needed. CECVD has shown successful results. And that method combined with a set of gold electrodes on either glass slides or on quartz could improve the sensors performance significantly.

NANOPARTICLE-ELECTRODE SYSTEM OPERATION

The main testing strategy assessed the operation and interaction of the MWNTs to component 1, and if an electrochemical measurement was produced. Whilst measuring the resistance of several solutions with different concentrations of MWNTs, the interaction of the MWNTs to component 1 was visually investigated under the microscope. It was hypothesized that the electrostatic force from the smaller electrodes will attract individual CNTs to form bridges, which would provide a difference in electrochemical measurements.

The sensor alone had a fairly a smooth linear response with a gradient of $-0.139\ \Omega V^{-1}$ showing a constant reduction of resistance every time the voltage increased. This response would be compared to other responses, when influenced by the test solutions, to see a variance between the electrochemical measurements.

Several tests showed that increasing the concentration of MWNTs in a solution affected the responses. The size of oscillations on these responses increased every time when the concentration of MWNTs increased. However the reasons for these oscillations were still undetermined as visually investigating the interaction under the microscope proved to be difficult. This was due to networks of MWNTs covering up the individual MWNTs, as well as how the optical microscope did not have a stronger

magnification. We can see in the figures below how MWNT networks were floating freely in the solution without any pretreatment.

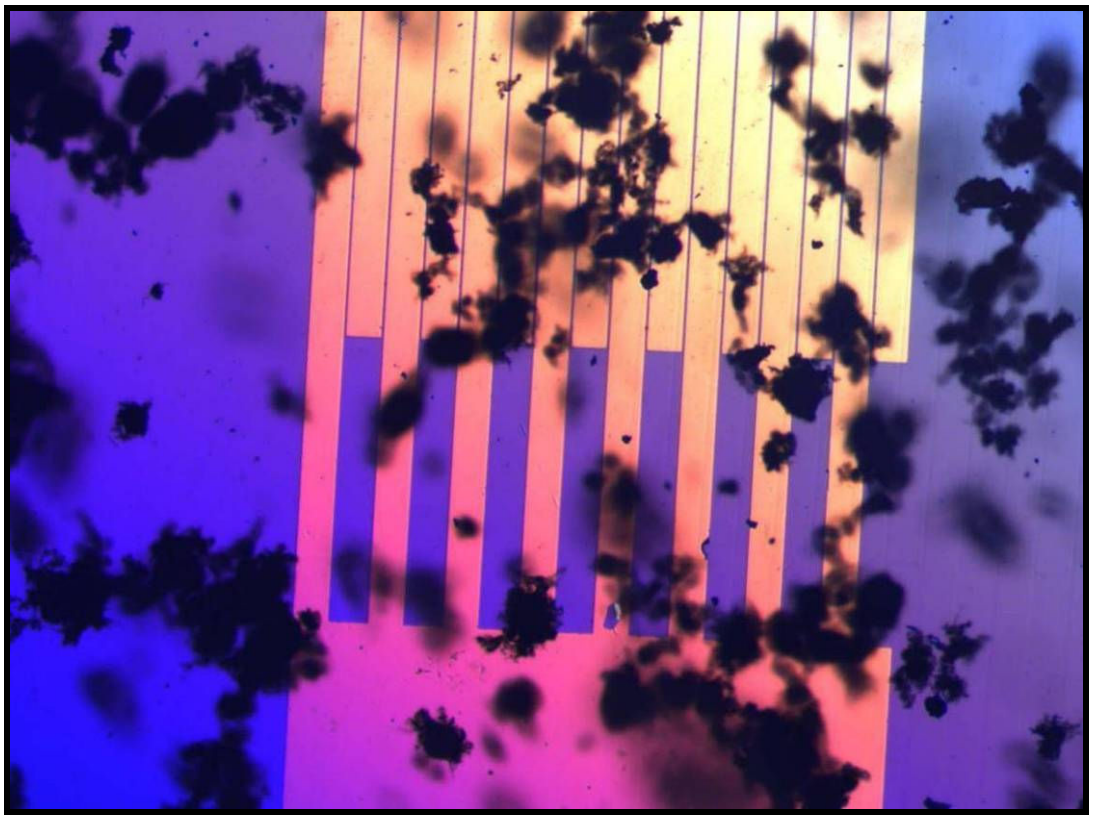

Fig. 147. *Aqueous suspension of small MWNT networks floating over Gold electrodes*

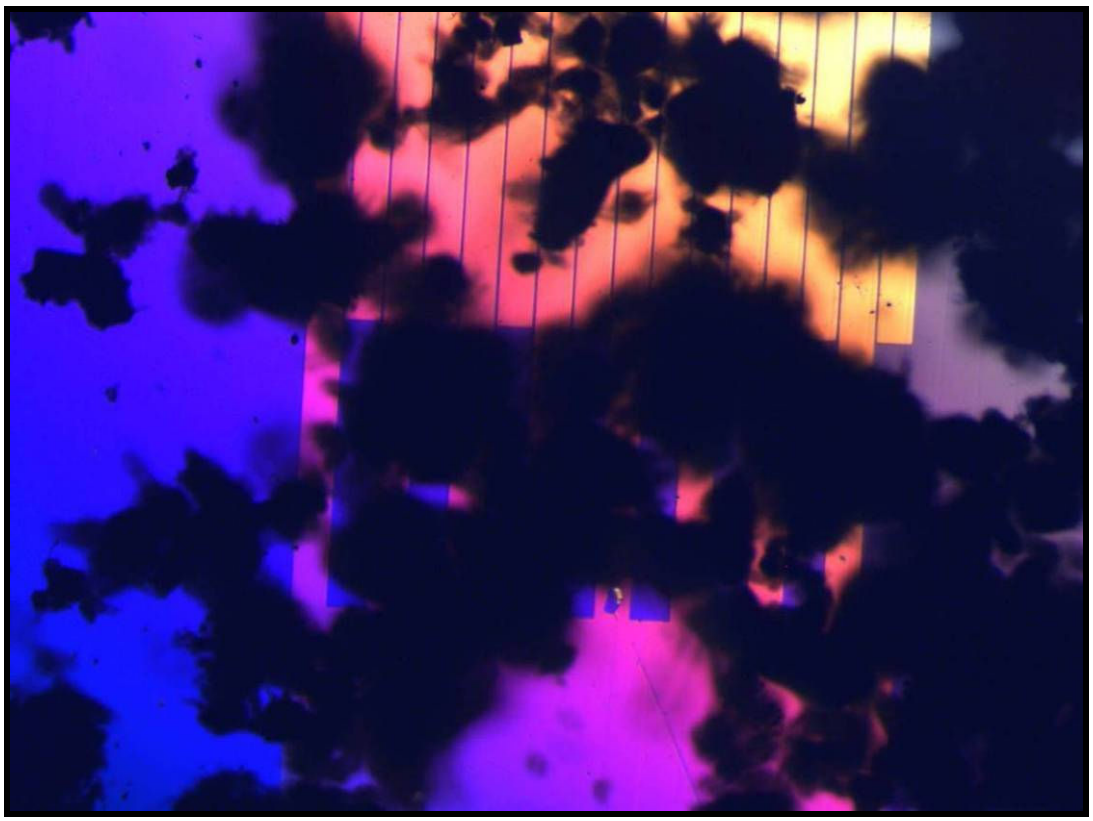

Fig. 148. *Aqueous suspension of large MWNT networks floating over Gold electrodes*

Two reasons were determined for the cause of oscillations in the responses. First, the ambiguous movements of MWNT networks are causing interference to the results. Second, there is some form of oscillation, even if we cant see it, the MWNT networks are reacting to the electrostatic force. They could be moving slightly up and down from the electrodes, which explain the subtle movements and slightly expanding networks from the microscope camera.

BEng PROJECT CONCLUSION & FURTHER IMPROVEMENTS

Due to time and monetary constraints the full desired sensor was not built to prove or disprove the hypothesis. Theoretically, the bio-sensing system would provide a huge commercial impact on the biomedical industry, and will perform well in clinical medicine than current technologies.

FURTHER IMPROVEMENTS ON COMPONENT 1

To reduce or cut off the conductivity between the two electrodes, which was a required specification at the beginning, the following future steps can be taken:

1. Use the same photomask; however introduce a silicon nitride layer process using DP80 which performs Cosmo Enhanced Chemical Vapour Deposition (CECVD), to insulate the electrodes. Insulating the electrodes may reduce conductivity. If the concentration of silicon nitride layer can be controlled then, this can be experimented to completely cut off conductivity between the electrodes. But it needs to be made sure that there will be conductivity between the electrodes when the CNTs are placed between them.
2. Use a glass substrate, instead of the used silicon, the previous tests should be undertaken again using a glass substrate. However if results are still similar to those obtained recently, and a current still flows between the electrodes, then the introduction of the nitride layer would be necessary later on.
3. Design a variety of photo masks, where the gaps between the electrodes are significantly larger. Increasing the gaps between the electrodes can reduce conductivity between them. And when including the silicon nitride process, this could completely cut off the conductivity. Definitely make sure that the gaps between the electrodes can definitely allow a CNT to form a bridge. Hence research the lengths of commercial CNTs and cross link those to the gaps between the electrodes. Longer nanotubes can easily be obtained.

4. The wire bonding process was not successful, due to the malfunctioning equipment that had not been serviced. Or then the right gold and titanium layer thickness, on the electrodes was just not enough. Hence increasing the titanium thickness from 50 nm and the gold thickness from 150 nm would be necessary to produce successful wire bonding, between the electrodes and the larger testing tracks.

FURTHER IMPROVEMENTS ON COMPONENT 2

The CNTs could not be configured with the four particles, because more time and funding was needed to purchase these individual particles and configure them with the CNTs to form the designed hybrid component. Thereafter, testing can commence with a newer and more improved component 1 where the results can be compared to those with the unconfigured CNTs. Once succeeded, further experimentation can improve the technology. Conduct research and experimentation:

- On using SWNTs instead of MWNTs for the CNT platform, and investigate methods of attaching the particles onto the nanotips of both ends.
- On attaching different biomarkers onto the CNTs, to investigate the flexibility of the sensing technology on a range of different biological cells. For example, instead of using antibodies for cancer cell detection, investigate DNA detection and attachment methods.
- On conducting further literature research to find other particles or hybridized particles which may improve on the sensitivity and amplification of the sensing system.
- Conduct further literature research on a solvent for MWNTs, as H_2O makes the MWNTs hydrophobic and form tangled networks between themselves.

12.2. AFM ANALYSIS 1 – SURFACE SMOOTHNESS AFTER SiO_2 GROWTH

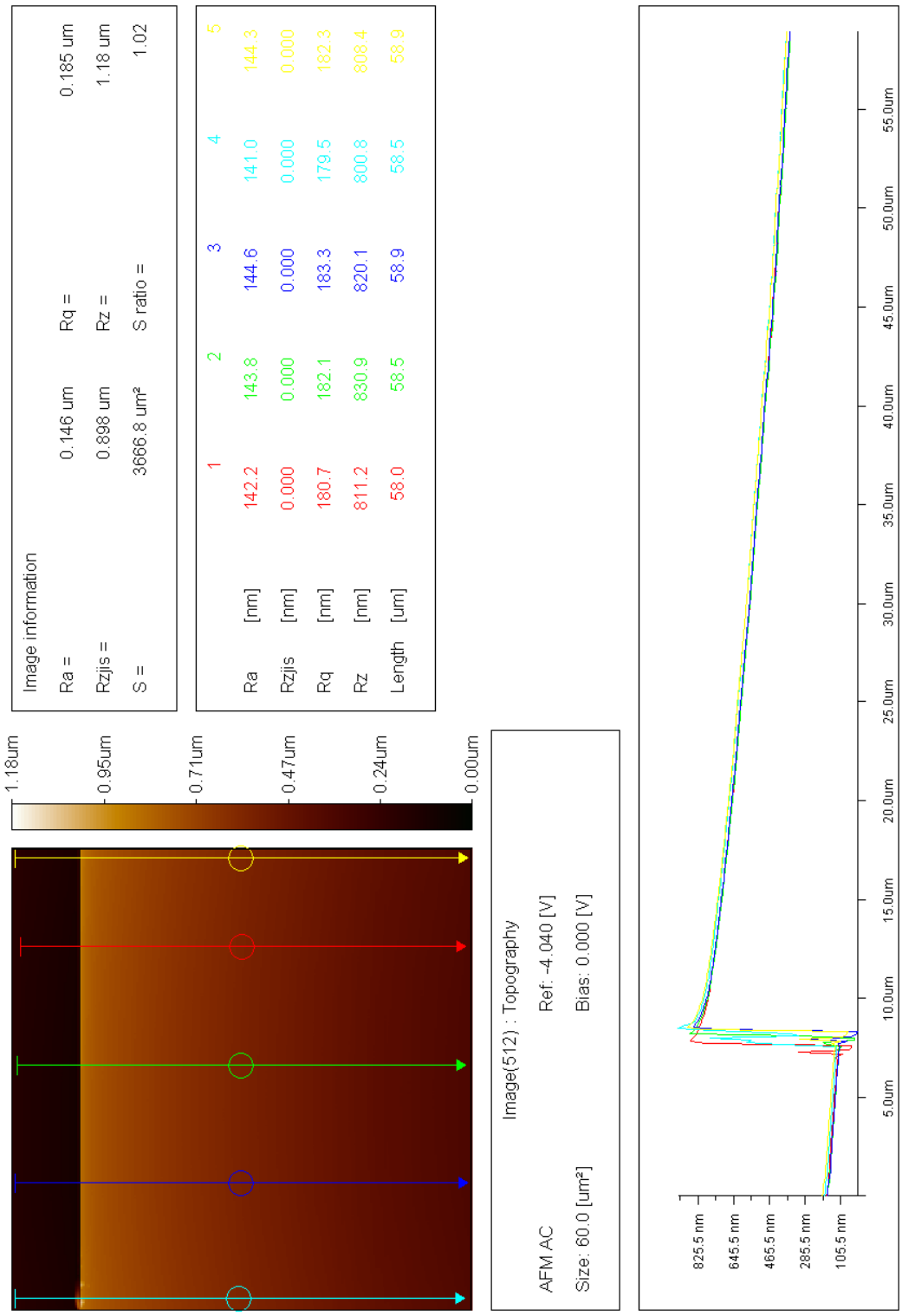

Fig. 149. *AFM Analysis 1 – Surface smoothness after SiO_2 growth*

AFM analysis conducted on a random sample at a random area just to get a generic idea of the surface smoothness of the SiO_2 layer. A layer of 1 µm was grown on the surface and it is hoped to be uniformly flat. However this diagram begs to differ with the massive 700 nm variance.

12.3. AFM ANALYSIS 2 – SURFACE SMOOTHNESS AFTER SiO_2 GROWTH

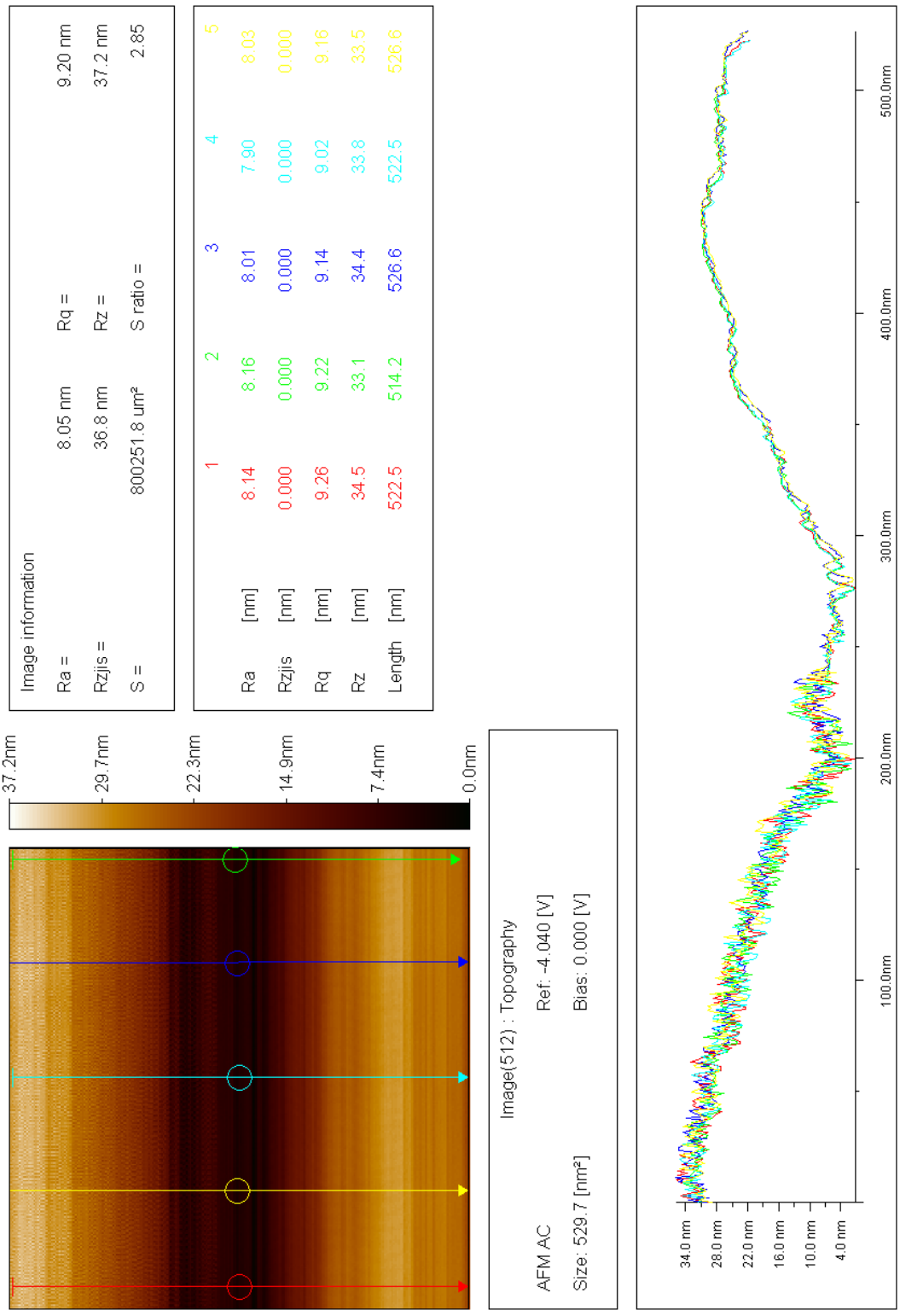

Fig. 150. *AFM Analysis 2 – Surface smoothness after SiO_2 growth*

AFM analysis is conducted on another random sample at another random area and it shows a dip that falls down approximately 20 nm. This also suggests that the grown SiO_2 layer isn't uniform as there are random variances from 20 nm to 700 nm.

12.4. AFM ANALYSIS 1 – FABRICATION OF DESIGN 2 ON SAMPLE 9

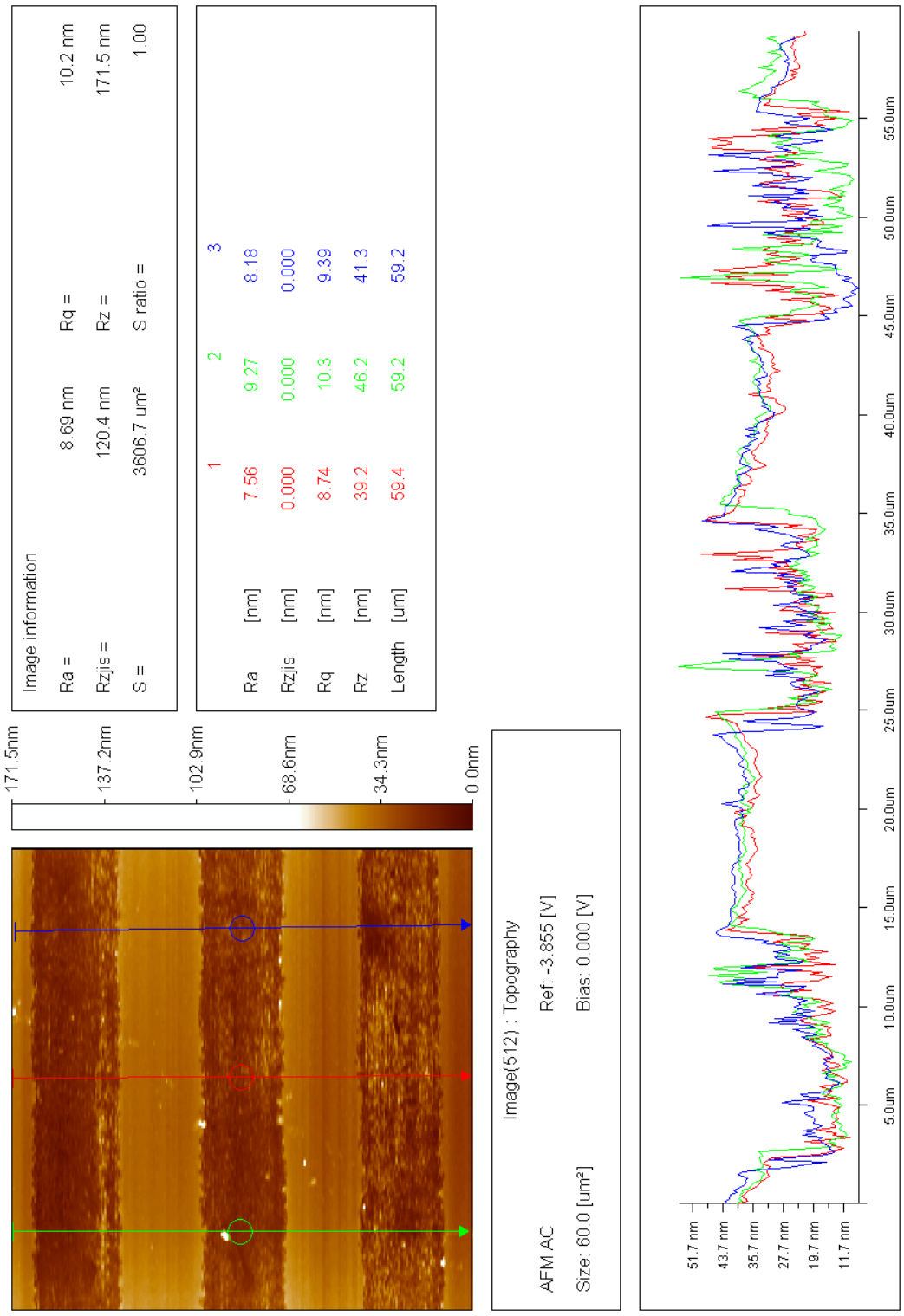

Fig. 151. *AFM Analysis 1 – Fabrication of design 2 on sample 9*

This chart shows topographical analysis for design 2 on sample 9. We can see from the chart the change in height from the sample substrate to the pattern evaporated material. There should be a difference of 25 nm, as that was deposited. And we can confirm this in the diagram, however with a variance of ± 3 nm.

12.5. AFM ANALYSIS 2 – FABRICATION OF DESIGN 2 ON SAMPLE 9

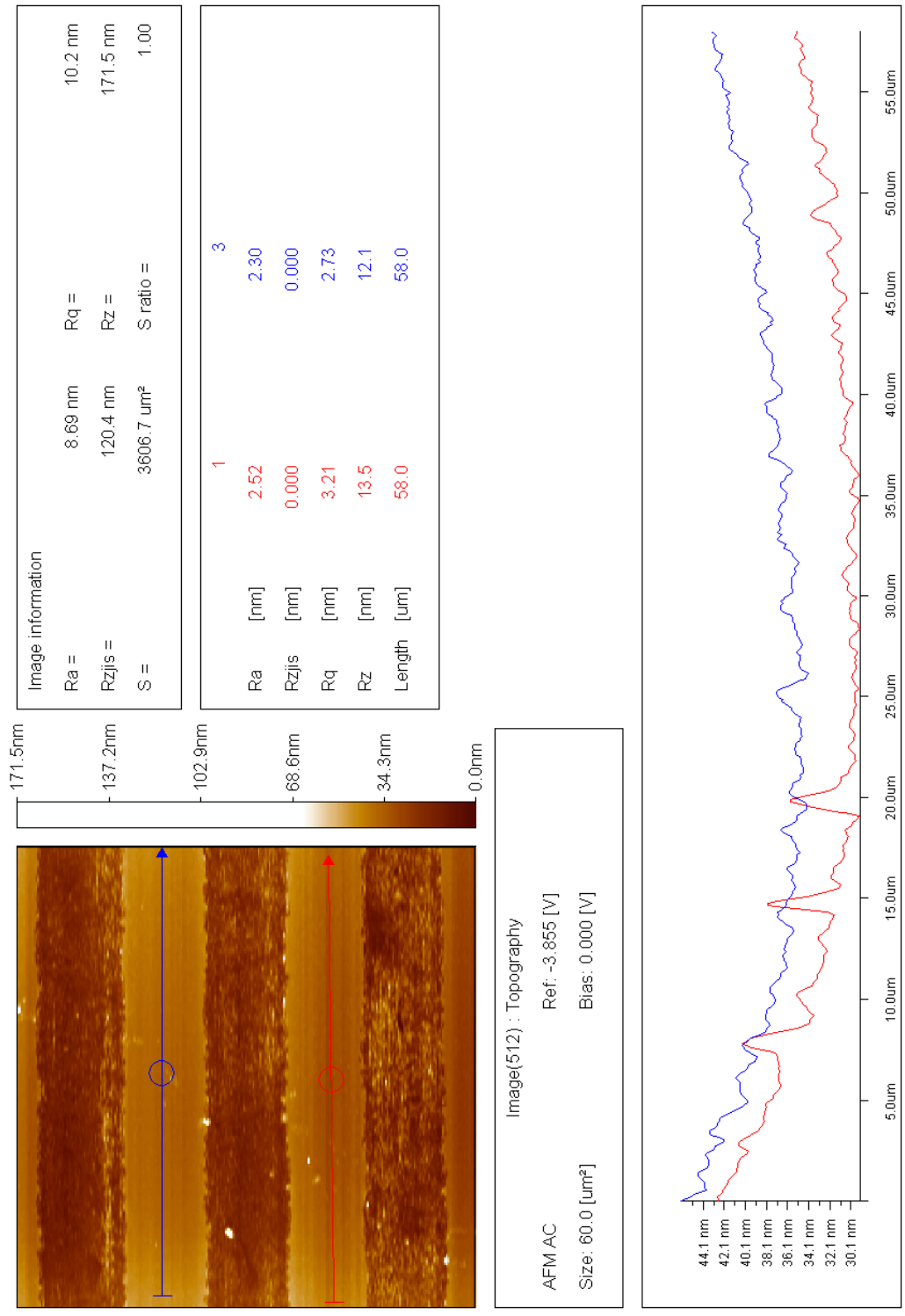

Fig. 152. *AFM Analysis 2 – Fabrication of design 2 on sample 9*

This AFM analysis was for design 2 on sample 9. The topographical chart is used to analyse surface smoothness and see whether or not there is a uniformly flat distribution. As it isn't uniformly flat then this suggests that the evaporating of the material was flawed or then the SiO_2 was unevenly distributed.

12.6. AFM ANALYSIS 1 – FABRICATION OF DESIGN 4 ON SAMPLE 6

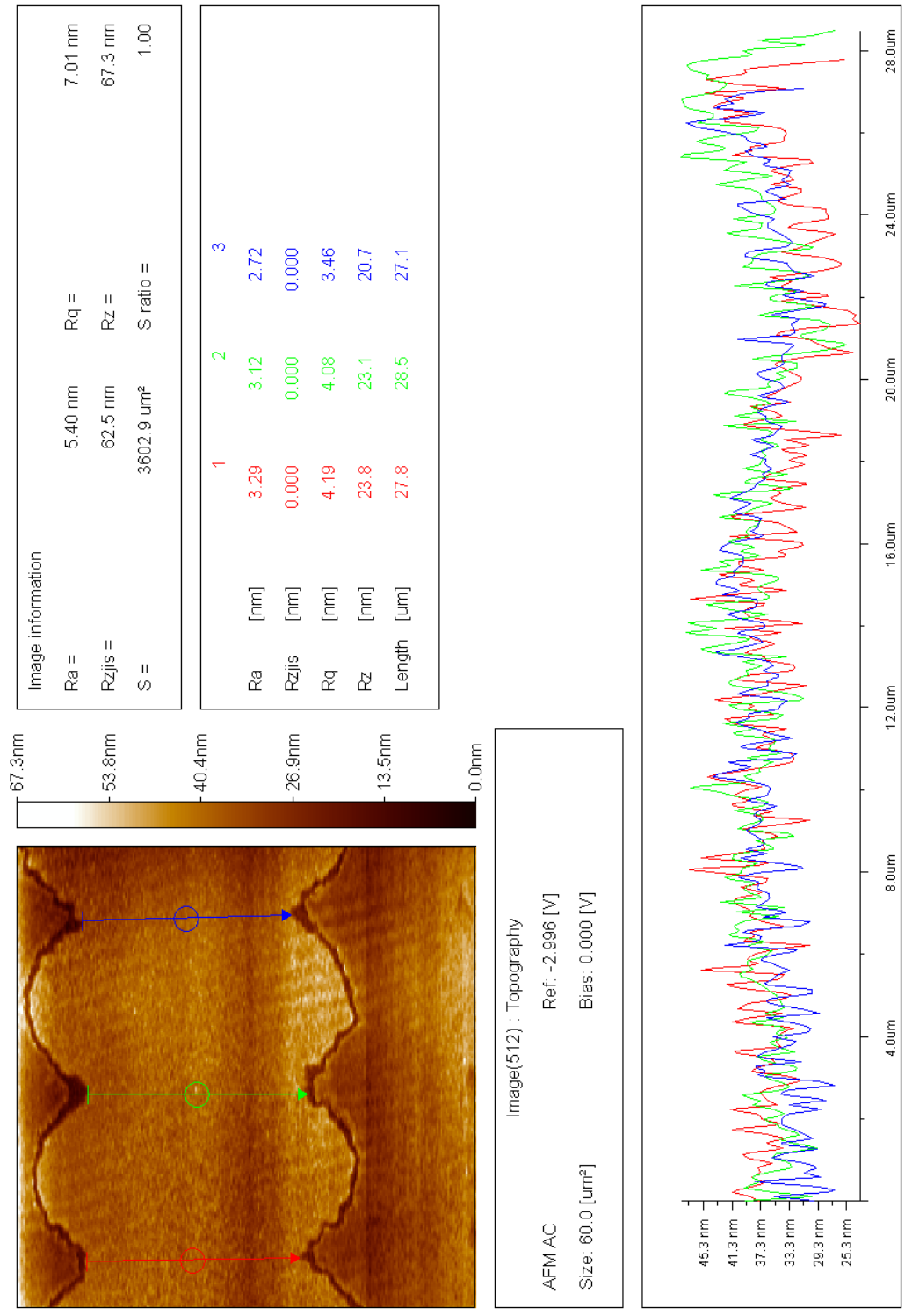

Fig. 153. *AFM Analysis 1 – Fabrication of design 4 on sample 6*

This chart shows topographical analysis for design 4 on sample 6. Surface smoothness was tested and a variation of 10 nm was analyzed confirming the uneven distribution of the evaporated material on top of the SiO_2 layer.

12.7. AFM ANALYSIS 2 – FABRICATION OF DESIGN 4 ON SAMPLE 6

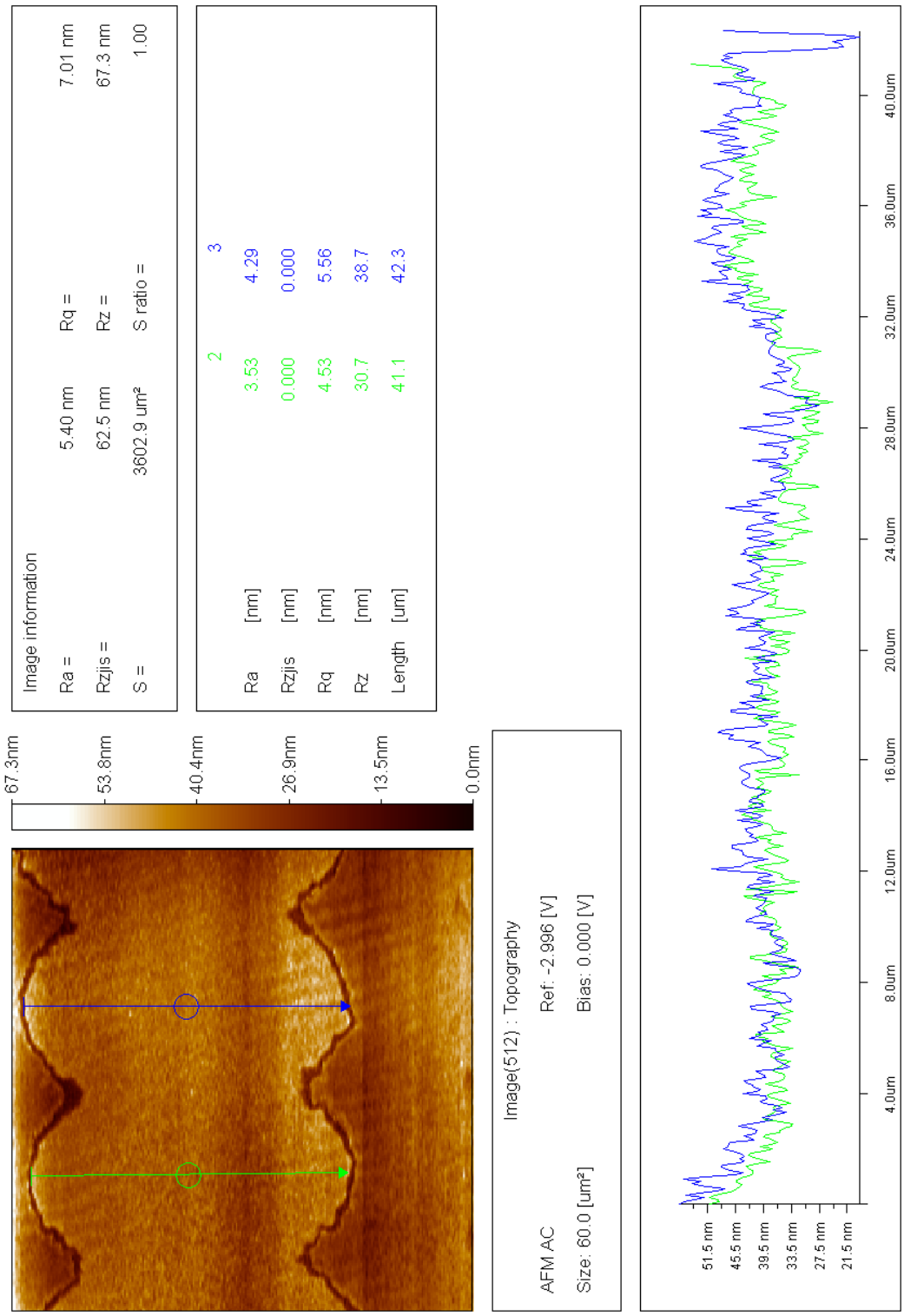

Fig. 154. *AFM Analysis 2 – Fabrication of design 4 on sample 6*

This chart shows topographical analysis for design 4 on sample 6. Surface smoothness was tested and a variation of 15 nm was analyzed confirming the uneven distribution of the evaporated material on top of the SiO_2 layer.

12.8. AFM ANALYSIS 1 – FABRICATION OF DESIGN 5 ON SAMPLE 1

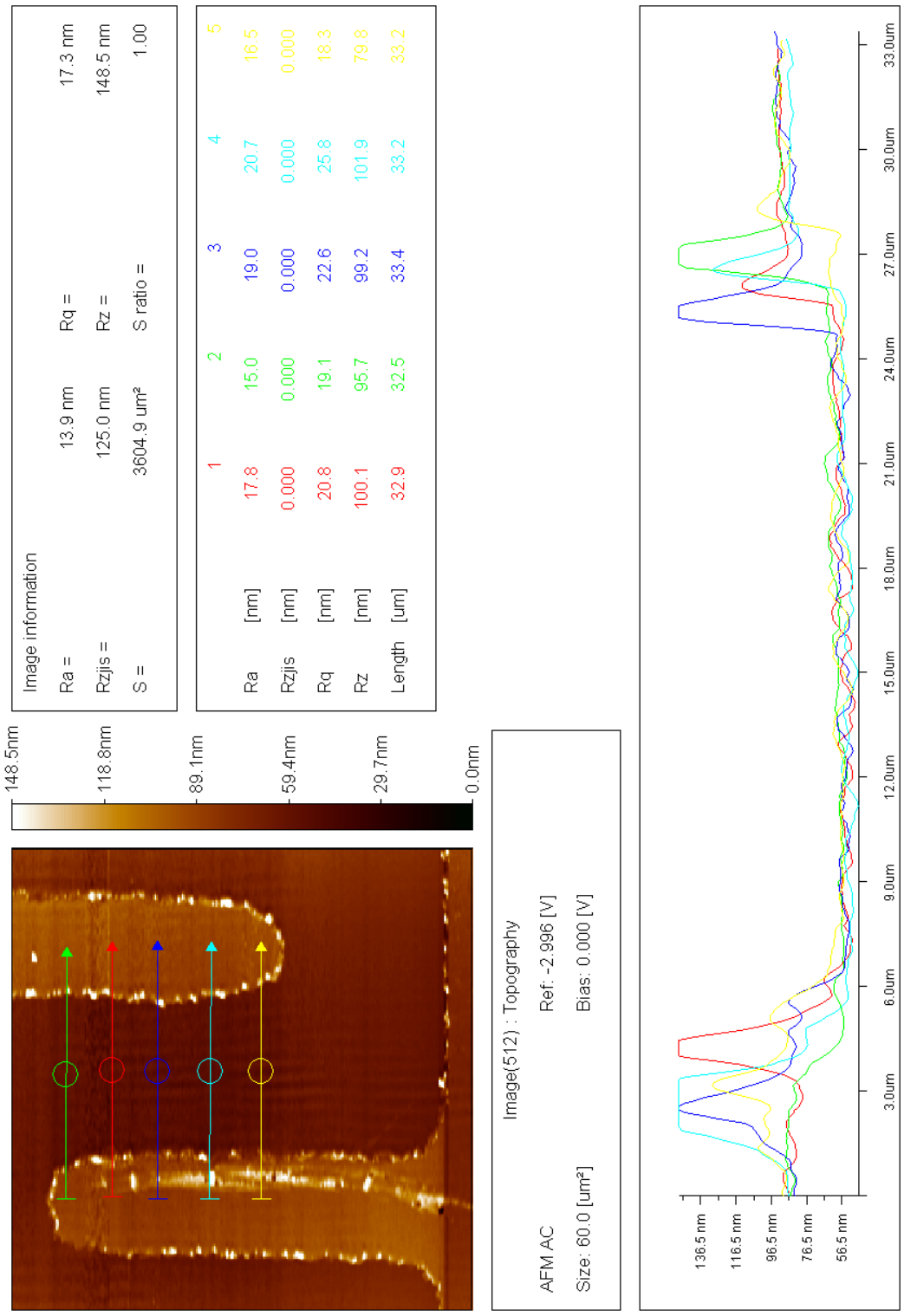

Fig. 155. *AFM Analysis 1 – Fabrication of design 5 on sample 1*

This chart shows topographical analysis for design 5 on sample 1. Electrode height was tested and showed a height difference of 25 nm. Strangely peaks were formed at the edge of the electrodes which are of size 40 nm. This could either be leftover evaporated material or a defect in the analysis.

12.9. AFM ANALYSIS 2 – FABRICATION OF DESIGN 5 ON SAMPLE 1

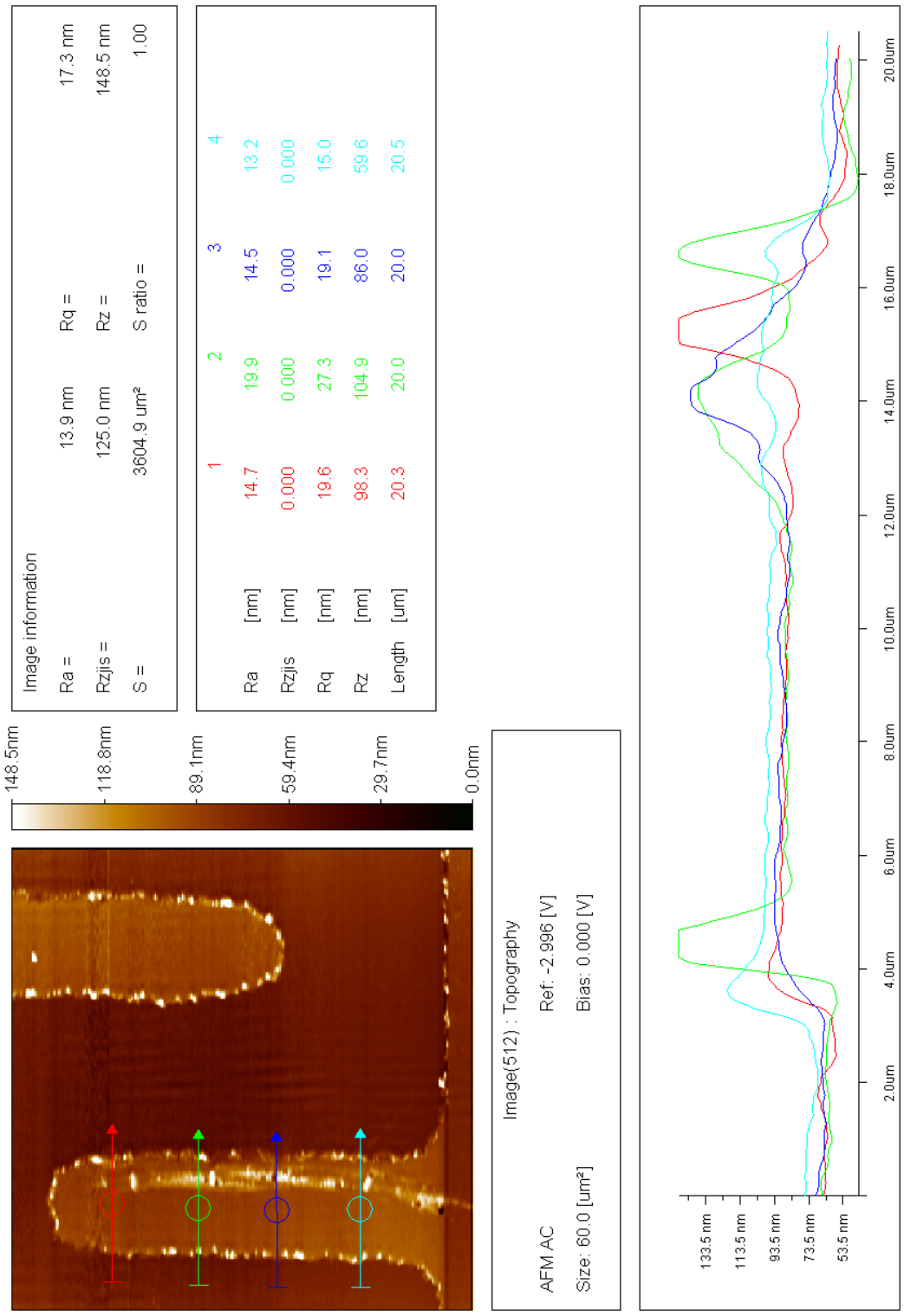

Fig. 156. *AFM Analysis 2 – Fabrication of design 5 on sample 1*

This chart shows topographical analysis for design 5 on sample 1. Electrode height was tested and showed a height difference of 27 nm. Strangely peaks were formed at the edge of the electrodes which are of size 40 nm. This could either be leftover evaporated material or a defect in the analysis.

12.10. AFM ANALYSIS 3 – FABRICATION OF DESIGN 5 ON SAMPLE 1

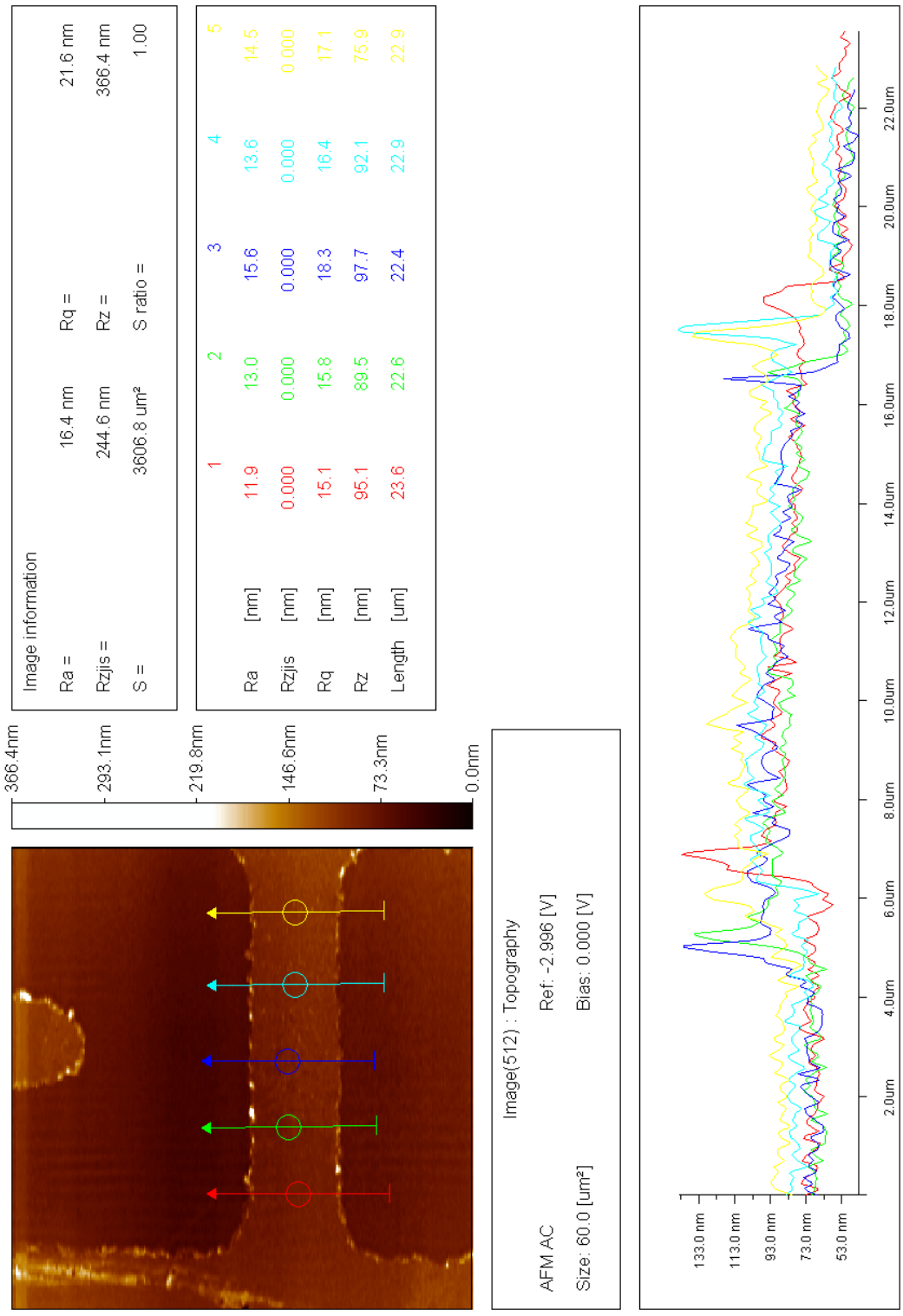

Fig. 156. *AFM Analysis 3 – Fabrication of design 5 on sample 1*

This chart shows topographical analysis for design 5 on sample 1. Electrode height was tested and showed a height difference of 25 nm. Strangely peaks were formed at the edge of the electrodes which are of size 40 nm. Also analysis shows surface smoothness to be non uniform and that the evaporated material or SiO_2 were unevenly distributed.

12.11. RECIPE FOR PHOTOLITHOGRAPHY DEVELOPER

Recipe for 1 litre:

1. Weigh out 5 gm of NaOH into a beaker.
2. Add DI water and stir.
3. Make up to 1 litre in a volumetric flask.

12.12. WET AND DRY SILICON DIOXIDE GROWTH IN REGARDS TO TIME AND TEMPERATURE

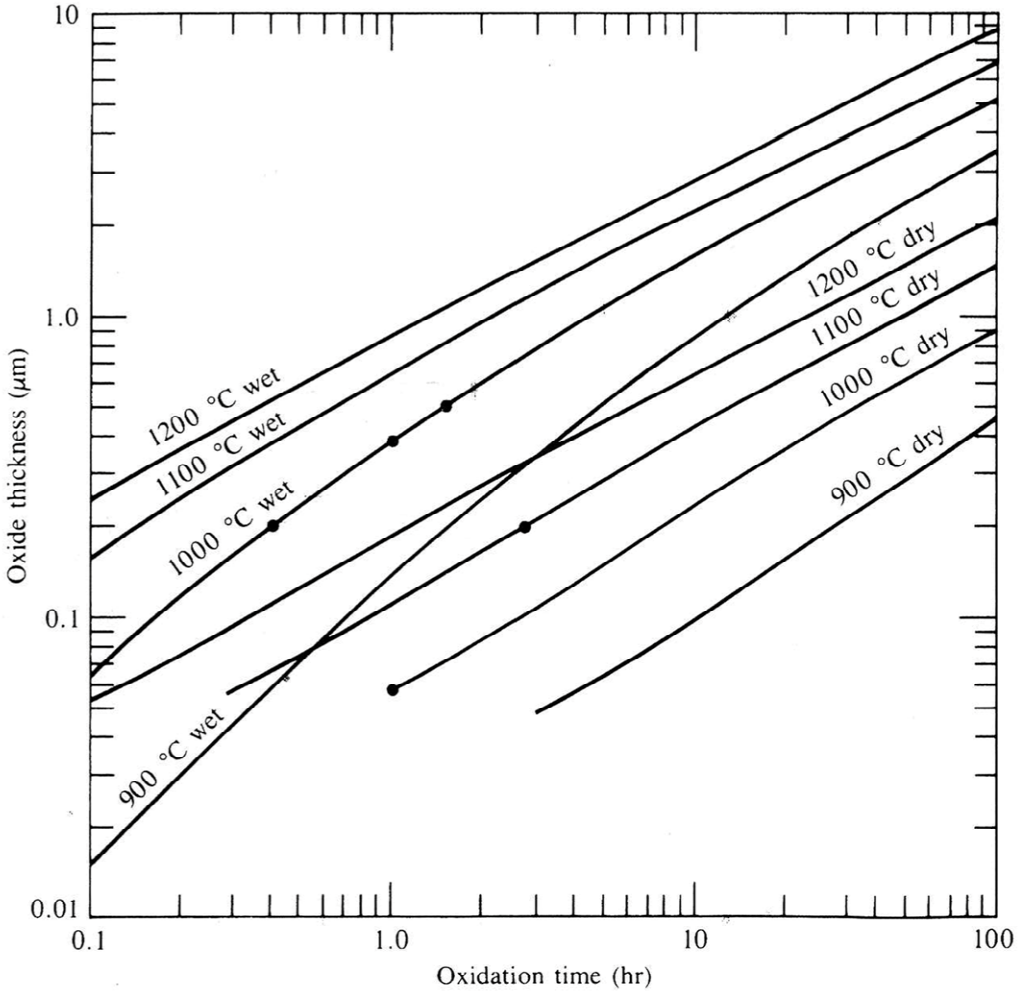

Wet and dry silicon dioxide growth for <100> silicon

Fig. 157. *Wet and dry silicon dioxide growth in regards to time and temperature*[61]

This chart shows the oxidation time required for a certain thickness of silicon dioxide to grow. The chart shows the different temperatures of wet and dry processes.

12.13. PHOTOLITHOGRAPHY EXPERIMENTAL NOTES

SESSION 1

TEST #	NOTES
1	Overall Conclusions and Further Experimentation: • FAIL • Overdevelopment • Excessive rigidness on electrodes. Increase CONTACT TIME and CONTACT FORCE separately to differentiate products. • Signs of defective marks on the mask design 1 • Signs of debris showing poor sample preparation
2	Overall Conclusions and Further Experimentation: • FAIL • Overdevelopment • Less rigidness on electrodes. But rigidness in all of them. Link to sample preparation? • Continuous signs of defective marks on the mask design 1 • Signs of debris showing poor sample preparation

SESSION 2

TEST #	NOTES
3	Overall Conclusions and Further Experimentation: • FAIL • Signs of both over and underdevelopment • Rigidness in electrodes. No smooth lines. Consider increasing CONTACT TIME to improve clarity and smoothness • One defective mark found on the mask design 5 (Underdeveloped) • One short circuit located between opposing electrodes (Overdeveloped) • Smalls signs of debris showing poor sample preparation • The general idea would be to keep the distance between the sample and the mask as small as possible to avoid diffraction and get the electrodes to the correct width. However we didn't want the contact force at its maximum because the general idea would be that the electrodes on the mask could be destroyed due to the amount of force applied. Work down with contact force to see effects.
4	Overall Conclusions and Further Experimentation: • FAIL • Big signs of under and overdevelopment • Rigidness in electrodes. No smooth lines. • Defective mask mark were shown • Big signs of debris showing poor sample preparation • Main cause of failure would have to be poor sample preparation as there were other areas that had very good development even

	though there was rigidness on the electrodes.
5	<u>Overall Conclusions and Further Experimentation:</u> • SEMI-SUCCESS • No sights of over or underdevelopment • Rigidness in electrodes. No smooth lines. Increase CONTACT FORCE to improve clarity and smoothness • Defective mark wasn't shown • Smalls signs of debris showing poor sample preparation • Main issue is the widths of electrodes are larger than the mask and required specifications. Need to reduce this. • This clearly proves that the developer needs to remain at 30 seconds and we need to alter the other two parameters inorder to achieve electrode edge smoothness, without any of the general issues.

SESSION 3

TEST #	NOTES
6	• FAIL • Signs of underdevelopment • Continuous rigidness in electrodes • Signs of debris from poor sample preparation • It can be see the CONTACT FORCE definitely improves on the electrodes smoothness. It also maintains the widths of electrodes with variations up to 1 μm. • Even though there wasn't much of an improvement from 800gram, 1000grams was definitely concluded to be the correct contact force if we want to maximize the masks full potential in obtaining smoother and more defined electrodes. • The mask wasn't affected when applied with this parameter. Hence this shows that we can continuously use this type of mask with the full contact force. • But even though we achieved smooth and defined electrodes, there was a huge issue of overdevelopment. That is why in the next series of tests, Contact Time and Developer Time needs to be altered.

SESSION 4

TEST #	NOTES
7	<u>Overall Conclusions and Further Experimentation:</u> • FAIL • Underdevelopment throughout all the electrodes. Still check if there is a pattern if you reduce developer time. • Continuous excessive rigidness on electrodes. Increase CONTACT TIME and CONTACT FORCE separately to differentiate products. • Signs of debris showing poor sample preparation

	• Repeat same parameters but reduce developer time.
8	<u>Overall Conclusions and Further Experimentation:</u> • FAIL • An increase in underdevelopment throughout all the electrodes. • Continuous excessive rigidness on electrodes. Increase CONTACT TIME and CONTACT FORCE separately to differentiate products. • Signs of debris showing poor sample preparation • Repeat same parameters to double check.
9	<u>Overall Conclusions and Further Experimentation:</u> • FAIL • Double checking confirmed • Signs of debris from poor sample preparation • Continuous excessive rigidness on electrodes. • Signs of overdevelopment in 2 areas. Decrease developer time to see if there is some effect.
10	<u>Overall Conclusions and Further Experimentation:</u> • FAIL • Reduction in developer time increases underdevelopment drastically • Defective marks can be seen. • Debris implies poor sample preparation • Continuous electrode rigidness. • Increase CONTACT FORCE to 1000 and increase developer back to 35
11	<u>Overall Conclusions and Further Experimentation:</u> • FAIL • Decent exposure but still signs of underdevelopment • Debris is shown implying poor sample preparation • This still didn't provide a right solution as reducing the developer time brought back the rigidity as well as increased the sizes of the electrodes by a 2-3 um. • However then it was thought that increasing the exposure time under UV would significantly improve on the smoothness and quality of the electrodes. This is because more electrons will be used to bombarded the mask to make a more detailed electron mask on the sample. So increasing the exposure times significantly were tested afterwards.
12	<u>Overall Conclusions and Further Experimentation:</u> • SEMI-SUCCESS • Decent exposure • Debris is shown implying poor sample preparation • Continuous excessive rigidness on electrodes. • No under or overdevelopment

	• This concludes that we need to further increase the CONTACT TIME in order to bombard more electrons onto the electron mask, giving it a smoother definition.

SESSION 5

TEST #	NOTES
13	Overall Conclusions and Further Experimentation: • FAIL • Decent exposure however there is overdevelopment between the larger electrodes to their closest smaller electrodes. • No debris is shown. Follow same sample preparation method. • Slight improvement on rigidness on electrodes • This concludes that we need to further increase the CONTACT TIME in order to bombard more electrons onto the electron mask, giving it a smoother definition. Increase CONTACT TIME to 30 seconds. If there is still overdevelopment then decrease developer time to 25 seconds.
14	Overall Conclusions and Further Experimentation: • SEMI-SUCCESS • Best exposure for Design 5 however there is overdevelopment between the larger electrodes to their closest smaller electrodes. • No debris is shown. Follow same sample preparation method. • Massive improvement on rigidness on electrodes • Repeat same parameters but decrease developer time to 25 seconds.
15	Overall Conclusions and Further Experimentation: • SEMI-SUCCESS • Best exposure for Design 5. This has reduced the large overdevelopment issues in Test 14. However there is one small short circuit between two opposing electrodes. Repeat step to confirm this or then overcome it. • No debris is shown. Follow same sample preparation method. • Massive improvement on rigidness on electrodes • Repeat same parameters but increase sample preparation. **FINAL PARAMETERS FOR D5:** • CONTACT TIME: 30 seconds • CONTACT FORCE: 1000 gm • DEVELOPER TIME: 25 seconds

SESSION 6

TEST #	NOTES
16	Overall Conclusions and Further Experimentation: • FAIL • Excessive overdevelopment

	• Debris implies poor sample preparation • Electrode rigidness is excessive but this isn't the main concern • Reduce developer time to reduce overdevelopment to 20 sec • Signs of photoresist coming off and being misplaced on the silicon sample. This suggests poor attachment of photoresist onto silicon substrate, which is unusual as the layer or Chlorobenzene definitely should stop this mainly because it's a form of excessive adhesion where the electrostatic forces between the particles are so strong that the photoresist comes off.
17	<u>Overall Conclusions and Further Experimentation:</u> • FAIL • Excessive overdevelopment but improvement from Test 16. • Electrode rigidness is excessive but still isn't the main concern • Reduce developer time to reduce overdevelopment to 10 sec • Photoresist has not come off the silicon substrate however is showing serious cases of adhesion • Debris implies poor sample preparation which has affected development of several groups of electrodes • Mask marks are being shown on the sample • Possibly consider to reduce contact time as excessive electrons aren't needed for a simple design. This could improve the adhesion issue as there will be fever particles that would repel through electrostatic forces.

SESSION 7

TEST #	NOTES
18	<u>Overall Conclusions and Further Experimentation:</u> • FAIL • Excessive overdevelopment but improvement from Test 17. • Excessive electrode rigidness • Reduce contact time to 5 seconds • Excessive signs of adhesion even though electrodes have not come off • Excessive debris implies very poor sample preparation • Excessive mask marks are shown on the sample
19	<u>Overall Conclusions and Further Experimentation:</u> • FAIL • Excessive overdevelopment but improvement from Test 18. • Excessive electrode rigidness • Small signs of adhesion, and how electrodes have come off • Excessive debris implies very poor sample preparation • Excessive mask marks are shown on the sample • Find the right balance between CONTACT TIME and DEVELOPER TIME • Increase CONTACT TIME

SESSION 8

TEST #	NOTES
20	<u>Overall Conclusions and Further Experimentation:</u> • FAIL • Excessive overdevelopment • Excessive electrode rigidness • Excessive signs of adhesion and electrodes have come off at specific areas. • There are areas where the electrodes have perfectly developed and share no problems. (Mask may be faulty) • Small signs of debris but nothing major • Continue to find the right balance between CONTACT TIME and DEVELOPER TIME • Reduce DEVELOPER TIME
21	<u>Overall Conclusions and Further Experimentation:</u> • FAIL however better than test 20 • Areas of over development and underdevelopment • Excessive electrode rigidness • No signs of adhesion • Mask maybe faulty as there are many mask marks shown on the sample as well as both signs of under and overdevelopment on the same mask under the same conditions • Small signs of debris but nothing major • Increase CONTACT TIME to improve electrode rigidness
22	<u>Overall Conclusions and Further Experimentation:</u> • FAIL • Excessive over and underdevelopment and different areas • Excessive electrode rigidness • Excessive signs of adhesion and electrodes have come off at areas. • There are areas where the electrodes have perfectly developed and share no problems. • Mask maybe faulty as there are many mask marks shown on the sample that are both under and overdeveloped under the same conditions • Small signs of debris but nothing major • Reduce DEVELOPER TIME to improve electrode rigidness
23	<u>Overall Conclusions and Further Experimentation:</u> • FAIL but better than Test 22 • Excessive over and underdevelopment and different areas • Excessive electrode rigidness • No signs of adhesion • Mask is faulty due to areas of under and over development • Small signs of debris but nothing major

	• Reduce DEVELOPER TIME to improve electrode rigidness • NO SAMPLES CAN BE MADE WITH THIS MASK. Focus on D2 as it's very similar to D1. **<u>FINAL NOTE:</u> D1 IS A FAULTY MASK**

SESSION 9

TEST #	NOTES
24	<u>Overall Conclusions and Further Experimentation:</u> • SUCCESS • Perfect exposure for Design 4 however tips are a bit curved and electrodes aren't smooth. • No debris is shown. Follow same sample preparation method. • Massive improvement on rigidness on electrodes compared to other designs • Increase DEVELOPER TIME by 5 seconds and CONTACT TIME by 10 seconds
25	<u>Overall Conclusions and Further Experimentation:</u> • SEMI-SUCCESS • Tips are a bit curved and electrodes aren't smooth. No difference regarding increasing CONTACT TIME. • Small signs of debris but nothing major • One short circuit between images but that may be due to poor sample preparation or an issue with the mask. • Repeat parameters to confirm that there is no difference with results compared to test 24
26	<u>Overall Conclusions and Further Experimentation:</u> • SUCCESS • Perfect exposure for Design 4 however tips haven't improved with increasing CONTACT TIME by 10 seconds • Small signs of debris but nothing major • As there isn't any difference on the development of the electrodes by increasing the CONTACT TIME by 10 seconds, its best to go back to 30 seconds to save time and be more efficient with the fabrication process. Consider it. **<u>FINAL PARAMETERS FOR 4:</u>** • CONTACT TIME: 30 seconds • CONTACT FORCE: 1000 g • DEVELOPER TIME: 25 seconds
27	<u>Overall Conclusions and Further Experimentation:</u> • SEMI-SUCCESS • No excessive under or over development • Only small under development at the remaining 0.05 mm of each

	electrodes. The tips begin to breakup implying that not enough development is done. • Small signs of debris but nothing major • Increase CONTACT TIME by 10 seconds and DEVELOPER TIME by 5 seconds to increase number of electrons at the tip to increase detail and improve development
28	<u>Overall Conclusions and Further Experimentation:</u> • SEMI-SUCCESS • The 10 second CONTACT TIME increase and 5 second DEVELOPER TIME increase didn't improve the development of the electrodes, specifically at the final 0.05 mm. • This concludes that this mask design is too defined for this photolithography process and most likely will be hard to develop as the quality of the masks are not the best in the business and the mask aligner can only development designs down to 10 μm and nothing less. **<u>FINAL NOTE:</u>** D3 MASK DESIGN IS UNACHIEVABLE DUE TO MASK ALIGNER RESTRICTIONS.

SESSION 10

TEST #	NOTES
29	<u>Overall Conclusions and Further Experimentation:</u> • SEMI-SUCCESS • No excessive under or over development • But there are two areas that were overdeveloped. • There is a massive scratch (Due to sample falling down) • Debris implies poor sample preparation • Redo experiment but reduce DEVELOPER TIME by 10 seconds
30	<u>Overall Conclusions and Further Experimentation:</u> • SEMI-SUCCESS • No excessive under or over development • Best exposure so far for mask design 2 • No adhesion • Two previous areas that were overdeveloped are perfectly developed • There is only one short circuit involved, however redoing the process with the same parameters should obtain samples without it. Redo experiment but reduce DEVELOPER TIME by 5 seconds
31	<u>Overall Conclusions and Further Experimentation:</u> • SEMI-SUCCESS • Excessive underdevelopment • No adhesion • Underdevelopment throughout the sample which shows mask marks • Redo experiment but reduce DEVELOPER TIME by 5 seconds

	• Redo test 30
32	Overall Conclusions and Further Experimentation: • SUCCESS • No excessive under or over development • Best exposure so far for mask design 2 • No adhesion • No Debris • Redo experiment but reduce DEVELOPER TIME by 5 seconds **FINAL PARAMETERS FOR D2:** • CONTACT TIME: 30 seconds • CONTACT FORCE: 1000 g • DEVELOPER TIME: 15 seconds

SESSION 11

TEST #	NOTES
33	Overall Conclusions and Further Experimentation: • SEMI-SUCCESS • One short circuit created through overdevelopment • No adhesion • Signs of debris
34	Overall Conclusions and Further Experimentation: • SEMI-SUCCESS • No adhesion • Small signs of debris that may affect results • One short circuit created through overdevelopment
35	Overall Conclusions and Further Experimentation: • SEMI-SUCCESS • No adhesion • Small signs of debris that may affect results • One short circuit created through overdevelopment

SESSION 12

TEST #	NOTES
36	Overall Conclusions and Further Experimentation: • SEMI-SUCCESS • One short circuit created through overdevelopment • No adhesion • Signs of debris
37	Overall Conclusions and Further Experimentation: • SEMI-SUCCESS • No adhesion

	• Small signs of debris that may affect results • One short circuit created through overdevelopment
38	<u>Overall Conclusions and Further Experimentation:</u> • SEMI-SUCCESS • No under or over development • No adhesion • Small signs of debris that may affect results • One short circuit created through overdevelopment • Redo process
39	<u>Overall Conclusions and Further Experimentation:</u> • SEMI-SUCCESS • Several groups of electrodes were overdeveloped • No adhesion • Small signs of debris that may affect results • Redo process but reduce DEVELOPER TIME by 5 seconds. **<u>FINAL NOTE:</u>** S6 from test 39 has been chosen for evaporation for D4
40	<u>Overall Conclusions and Further Experimentation:</u> • SUCCESS • No excessive under or over development • No adhesion • Small signs of debris that may affect results • Redo experiment but reduce DEVELOPER TIME by 5 seconds **<u>FINAL PARAMETERS FOR D4:</u>** • CONTACT TIME: 30 seconds • CONTACT FORCE: 1000 g • DEVELOPER TIME: 20 seconds **<u>FINAL NOTE:</u>** S7 from test 40 has been chosen for evaporation for D4
41	<u>Overall Conclusions and Further Experimentation:</u> • SEMI-SUCCESS • Several groups of electrodes were overdeveloped • No adhesion • Small signs of debris that may affect results • Redo process
42	<u>Overall Conclusions and Further Experimentation:</u> • SUCCESS • No excessive under or over development • No adhesion • Small signs of debris that may affect results **<u>FINAL NOTE:</u>** S10 from test 42 has been chosen for evaporation for D2

43	Overall Conclusions and Further Experimentation: • SEMI-SUCCESS • No under or over development • No adhesion • Small signs of debris that may affect results • One short circuit created through overdevelopment **FINAL NOTE:** S4 from test 43 has been chosen for evaporation for D5
44	Overall Conclusions and Further Experimentation: • SEMI - SUCCESS • No excessive under or over development • No adhesion • A variety of debris that may affect results
45	Overall Conclusions and Further Experimentation: • SUCCESS • No excessive under or over development • No adhesion • Small signs of debris that may affect results **FINAL NOTE:** S9 from test 44 has been chosen for evaporation for D2

13. BIBLIOGRAPHY/REFERENCES

1. Natalia C. Tansil, Zhiqiang Gao. "Nanoparticles in biomolecular detection". Nano Today: February 2006, Volume 1, Number 1.

2. Xin Yu, Bernard Munge, Vyomesh Patel, Gary Jensen, Ashwin Bhirde, Joseph D. Gong, Sang N. Kim, John Gillespie, J. Silvio Gutkind, Fotios Papadimitrakopoulos, and James F. Rusling. "Carbon Nanotube Amplification Strategies for Highly Sensitive Immunodetection of Cancer Biomarkers". JACS: Journal of American Chemical Society.

3. Jinhao Gao, Bing Xu. "Applications of nanomaterials inside cells". Nano Today, 4, 37—51, 2009.

4. Avraham Rasooly, James Jacobson. "Development of biosensors for cancer clinical testing". Biosensors and Bioelectronics 21, 1851–1858, 2006.

5. C Srinivasan. "Carbon nanotubes in cancer therapy". Current Science, Vol. 94, No. 3, 10 February 2008.

6. Sheetal J. Patil, Aleksandra Zajac, Tatyana Zhukov, Shekhar Bhansali. "Ultrasensitive electrochemical detection of cytokeratin-7, using Au nanowires based biosensor". Sensors and Actuators B, 859-865, 129, 2008.

7. Shyam Aravamudhan, Niranjan S. Ramgir, Shekhar Bhansali. “Electrochemical biosensor for targeted detection in blood using aligned nanowires”. Sensors and Actuators B, 29-35, 127, 2007.

8. Haitao Wang, Lili Cao, Shancheng Yan, Ningping Huang, Zhongdang Xiao. “An efficient method for decoration of the multiwalled carbon nanotubes with nearly monodispersed magnetite nanoparticles”. Materials Science and Engineering B, 164, 191-194, 2009.

9. Gui Huan Du, Zu Li Liu, Qiang Hua Lu, Xing Xia, Li Hui Jia, Kai Lun Yao, Qian Chu and Su Ming Zhang. “Fe_3O_4/CdSe/ZnS magnetic fluorescent bifunctional nanocomposites”. Nanotechnology, 17, 2850-2854, 2006.

10. Y. Krupskaya, C. Mahn A.Parameswaran, A.Taylor, K.Kramer, S.Hampel, A.Leonhardt, M. Ritschel, B. Buchner, R.Klingeler. “Magnetic study of iron-containing carbon nanotubes: Feasibility for magnetic hyperthermia”. Journal of Magnetism and Magnetic Materials, 321, 4067-4071, 2009.

11. Desheng Wang, Jibao He, Nista Rosenzweig, and Zeev Rosenzweig. “Superparamagnetic Fe_2O_3 Beads-CdSe/ZnS Quantum Dots Core-Shell Nanocomposite Particles for Cell Separation”. Nano Letters, Vol. 4, No. 3, 409-413, 2004.

12. Chia-Chen Li, Jen-Lien Lin, Shu-Jiuan Huang, Jyh-Tsung Lee, Ci-Huei Chen. “A new and acid-exclusive method for dispersing carbon multi-walled nanotubes in aqueous suspensions”. Colloids and Surfaces A: Physicochem. Eng. Aspects , 297, 275-281, 2007.

13. Paritosh Garg, Jorge L. Alvarado, Charles Marsh, Thomas A. Carlson, David A. Kessler, Kalyan Annamalai. “An experimental study on the effect of ultrasonication on viscosity and heat transfer performance of multi-wall carbon nanotube-based aqueous nanofluids”. International Journal of Heat and Mass Transfer, 52, 5090-2101, 2009.

14. A. Schierz, H. Zanker. “Aqueous suspensions of carbon nanotubes: Surface oxidation, colloidal stability and uranium sorption”. Environmental Pollution, 157, 1088-1094, 2009.

15. Kelly Y. Kim. “Nanotechnology platforms and physiological challenges for cancer therapeutics”. Nanomedicine: Nanotechnology, Biology, and Medicine 3, 103-110, 2007.

16. Kyoung-Yong Chun, Sang Kyu Choi, Hyun Jung Kang,Chong Yun Park, Cheol Jin Lee. “Highly dispersed multi-walled carbon nanotubes in ethanol using potassium doping”. Carbon, 44, 1491-1495, 2006.

17. Krisztián Niesz, Andrea Siska, István Vesselényi, Klara Hernadi, Dóra Méhn, Gábor Galbács, Zoltán Kónya, Imre Kiricsi. “Mechanical and chemical breaking of multiwalled carbon nanotubes”. Catalysis Today, 76, 3-10, 2002.

18. Shun-rong Ji, Chen Liu, Bo Zhang, Feng Yang, Jin Xu, Jiang Long, Chen Jin, De-liang Fu, Quan-xing Ni, Xian-jun Yu. “Carbon nanotubes in cancer diagnosis and therapy”. BBA-Reviews on Cancer, 2009.

19. Bin Kang, Yaodong Dai, Shuquan Chang, Da Chen. “Explosion of single-walled carbon nanotubes in suspension induced by a large photoacoustic effect”. Carbon, 46, 974-981, 2008.

20. Hualin Zhang, Zhiqing Chen. “Nanobomb: A potential technique for in vivo imaging and targeted cancer cell destruction”. Correspondence / Medical Hypotheses, 73, 854-865, 2009.

21. Dae Nyun Kim, Yeol Lee,Won-Gun Koh. “Fabrication of microfluidic devices incorporating bead-based reaction and microarray-based detection system for enzymatic assay”. Sensors and Actuators B: Chemical, 137, 305-312, 2009.

22. Bernhard H. Weigl, Ron L. Bardell, Catherine R. Cabrera. “Lab-on-a-chip for drug development”. Advanced Drug Delivery Reviews, 55, 349-377, 2003.

23. Chunsun Zhang, Da Xing, Yuyuan Li. “Micropumps, microvalves, and micromixers within PCR microfluidic chips: Advances and trends”. Biotechnology Advances, 25, 483-514, 2007.

24. Yu Hongbin, Zhou Guangya, Chau Fook Siong,Wang Shouhua, Lee Feiwen. “Novel polydimethylsiloxane (PDMS) based microchannel fabrication method for lab-on-a-chip application”. Sensors and Actuators B: Chemical, 137, 754–761, 2009.

25. Sarbajit Banerjee, Brian E. White, Limin Huang, Blake J. Rego, Stephen O’Brien, and Irving P. Herman. “Precise positioning of single-walled carbon nanotubes by ac dielectrophoresis”. J. Vac. Sci. Technol. B, Vol. 24, No. 6, 2006.

26. Xianming Liu, John L. Spencer, Alan B. Kaiser, W. Mike Arnold. “Selective purification of multiwalled carbon nanotubes by dielectrophoresis within a large array”. Current Applied Physics, 6, 427–431, 2006.

27. Chehung Wei, Ting-You Wei, Cheng-Hao Liang, Fong-Cheng Tai. “The separation of different conducting multi-walled carbon nanotubes by AC dielectrophoresis”. Diamond & Related Materials, 19, 332–336, 2009.

28. Qun Huo. “A perspective on bioconjugated nanoparticles and quantum dots”. Colloids and Surfaces B: Biointerfaces, 59, 1–10, 2007.

29. Vasudevanpillai Biju, Sathish Mundayoor, Ramakrishnapillai V. Omkumar, Abdulaziz Anas, Mitsuru Ishikawa. “Bioconjugated quantum dots for cancer research: Present status, prospects and remaining issues”. Biotechnology Advances, 28, 199–213, 2010.

30. Andrew M. Smith, Hongwei Duan, Aaron M. Mohs, Shuming Nie. “Bioconjugated quantum dots for in vivo molecular and cellular imaging”. Advanced Drug Delivery Reviews, 60, 1226–1240, 2008.

31. Yun Xing and Jianghong Rao. “Quantum dot bioconjugates for in vitro diagnostics & in-vivo imaging”. Cancer Biomarkers, 4, 307–319, 2008.

32. Kagan Kerman, Tatsuro Endo, Masatoshi Tsukamoto, Miyuki Chikae, Yuzuru Takamura, Eiichi Tamiya. “Quantum dot-based immunosensor for the detection of prostate-specific antigen using fluorescence microscopy”. Talanta, 71, 1494–1499, 2007.

33. Karen Grieve, Paul Mulvaney, Franz Grieser. “Synthesis and electronic properties of semiconductor nanoparticles/quantum dots”. Current Opinion in Colloid & Interface Science, 5, 168–172, 2000.

34. Vasudevanpillai Biju, Tamitake Itoh, Yoji Makita, Mitsuru Ishikawa. “Close-conjugation of quantum dots and gold nanoparticles to sidewall functionalized single-walled carbon nanotube templates”. Journal of Photochemistry and Photobiology A: Chemistry, 138, 351–321, 2006.

35. Bifeng Pan, Daxiang Cui, Rong He, Feng Gao, Yafei Zhang. “Covalent attachment of quantum dot on carbon nanotubes”. Chemical Physics Letters, 417, 419–424, 2006.

36. Gui Zheng Zou. “Highly conjugated water soluble CdSe quantum dots to multiwalled carbon nanotubes”. Chinese Chemical Letters, 20, 356–357, 2009.

37. Elena Heister, Vera Neves, Carmen Tılmaciu, Kamil Lipert, Vanesa Sanz Beltran, Helen M. Coley, S. Ravi P. Silva, Johnjoe McFadden. “Triple functionalisation of single-walled carbon nanotubes with doxorubicin, a monoclonal antibody, and a fluorescent marker for targeted cancer therapy”. Carbon, 47, 2152–2160, 2009.

38. Ping An Hu, Takashi Tanii, Guo-Jun Zhang, Takumi Hosaka, Iwao Ohdomari. “Ultrasensitive detection of biomolecules using functionalized multi-walled carbon nanotubes”. Sensors and Actuators B, 124, 161–166, 2007.

39. Invitrogen. *Cell Isolation with Dynabeads® Technology* [online]. Available: http://www.invitrogen.com/site/us/en/home/Products-and-Services/Applications/Cell-and-Tissue-Analysis/Cell-Isolation-and-Expansion/Cell-Isolation.html#Depletion [accessed 10 December 2009]

40. Invitrogen. *DYNAL® Magnetic Beads* [online]. Available: http://www.invitrogen.com/site/us/en/home/brands/Dynal.html?CID=fl-dynal [accessed 10 December 2009]

41. R&D Systems. *PlusCellect™ Cell Selection Kits* [online]. Available: http://www.rndsystems.com/product_detail_objectname_PlusCellectKits.aspx?gclid=CPixoLL_wqMCFeFc4wodMWXYcA [accessed 10 December 2009]

42. MACS Miltenyi Biotec. *MACS® Technology: The gold standard in cell separation* [online]. Available: http://www.miltenyibiotec.com/en/NN_21_MACS_Cell_Separation.aspx [accessed 10 December 2009]

43. Stemcell Technologies. *EasySep®* [online]. Available: http://www.stemcell.com/en/Products/Popular-Product-Lines/EasySep.aspx [accessed 10 December 2009]

44. Invitrogen. *Human Cell Isolation Products* [online]. Available: http://www.invitrogen.com/site/us/en/home/Products-and-Services/Applications/Cell-and-Tissue-Analysis/Cell- Isolation-and-Expansion/Cell-Isolation/Human-Cell-Isolation-Products.html [accessed 10 December 2009]

45. Invitrogen. *Qdot* [online]. Available: http://www.invitrogen.com/site/us/en/home/brands/Molecular-Probes/Key-Molecular-Probes-Products/Qdot.html [accessed 10 December 2009]

46. GX Optical. *Product Price List* [online]. Available: http://www.gxoptical.com/html/xdy1_inverted_fluorescence_mic.html [accessed 13 May 2010]

47. Jeol. *JASM6200 Clairscope* [online]. Available: http://www.jeol.com/PRODUCTS/ElectronOptics/ScanningElectronMicroscopesSEM/HighVacuumLowVaccum/JASM6200ClairScope/tabid/714/Default.asp [accessed 9 June 2010]

48. Precision Photo Mask Service. [online]. Available: http://www.microlitho.co.uk/ [accessed 14 April 2010]

49. http://jnm.snmjournals.org/content/vol48/issue7/images/large/1039fig1.jpeg [accessed 27 July 2010]

50. *Photolithography* [online]. Available: http://www.ece.gatech.edu/research/labs/vc/theory/photolith.html [accessed 03 September 2010]

51. Robert A. Wilson and Heather A. Bullen. *Introduction to Scanning Probe Microscopy (SPM): Basic Theory for Atomic Force Microscopy (AFM)* [online]. Available:http://asdlib.org/onlineArticles/ecourseware/Bullen/SPMModule_BasicTheoryAFM.pdf [accessed 03 September 2010]

52. Nanolab. *Carbon Nanotube Image Gallery* [online]. Available: http://www.nanolab.com/nanotube-image3.html [accessed 28 May 2010]

53. Emmanuel de Chambost, *Everhart-Thornley detector* [online]. Available: http://commons.wikimedia.org/wiki/File:Everhart-Thornley_detector.JPG [accessed 03 September 2010]

54. Central Microscopy of The University of Iowa. *Methodology* [online]. Available: http://www.uiowa.edu/~cemrf/methodology/sem/index.htm [accessed 03 September 2010]

55. Gina S. Fiorini and Daniel T. Chiu. “Disposable microfluidic devices: fabrication, function, and application”. BioTechniques, 38:429-446, March 2005.

56. Shaojun Guo, Shaojun Dong. “Biomolecule-nanoparticle hybrids for electrochemical biosensors”. Trends in Analytical Chemistry, Vol. 28, No.1, 2009.

57. A. Merkoci , M. Aldavert, S. Marın, S. Alegret, “New materials for electrochemical sensing V: Nanoparticles for DNA labeling”. Trends in Analytical Chemistry, Vol. 24, No. 4, 2005.

58. Jeol. *JSPM-5200 Scanning Probe Microscope* [online]. Available: http://www.jeol.com/PRODUCTS/ElectronOptics/ScanningProbeMicroscopesSPM/JSPM5200/tabid/132/Default.aspx [accessed 03 September 2010]

59. The York Jeol Nanocentre. *JSPM 5200* [online]. Available: http://www.york.ac.uk/res/nanocentre/facilities/jspm5200.htm [accessed 03 September 2010]

60. The York Jeol Nanocentre. *FEI Sirion S-FEG FESEM* [online]. Available: http://www.york.ac.uk/res/nanocentre/facilities/fesem.htm [accessed 03 September 2010]

61. Gary S. May, Simon M. Sze. (28 August 2007) *Fundamentals of Semiconductor Fabrication*. John Wiley & Sons.